N°: 7741

**UNIVERSITY PARIS XI**
Faculty of Sciences in Orsay

**CZECH TECHNICAL UNIVERSITY IN PRAGUE**
Faculty of Nuclear Sciences and Physical Engineering

THESIS

presented to obtain the degree of

Doctor of Sciences of the University Paris XI, specialization Mathematics
&
Doctor of the Czech Technical University in Prague, specialization Mathematical Modeling

by

**Martin VOHRALÍK**

---

Title

# NUMERICAL METHODS FOR NONLINEAR ELLIPTIC AND PARABOLIC EQUATIONS

*Application to flow problems in porous and fractured media*

---

Defended on December 9, 2004, before the Thesis Committee:

| | | |
|---|---|---|
| Robert | EYMARD | examiner |
| Miloslav | FEISTAUER | examiner |
| Vivette | GIRAULT | examiner |
| Bernard | HELFFER | chair |
| Danielle | HILHORST | thesis advisor |
| Jiří | MARYŠKA | thesis advisor |
| Marc | BONNET | invited member |

Referees: Miloslav FEISTAUER
Jérôme JAFFRÉ

## Acknowledgements

I would first of all like to express my thanks to my advisors, Professor Danielle Hilhorst and Professor Jiří Maryška. I am very grateful to Professor Hilhorst for being a very responsible thesis advisor. Her experience, availability, and confidence allowed me to see my work through successfully. I owe a lot to Professor Hilhorst also from a personal viewpoint for her warm reception in France. I would also like to give my deep thanks to Professor Maryška, who guided my first scientific steps towards numerical methods in porous media and who integrated me in the French–Czech collaboration which lead to this thesis.

My cordial thanks next go to Professor Robert Eymard for having opened my eyes to the beauty of the finite volume method principles, for letting me share his invaluable knowledge, and for accepting to be a committee member. I would also like to express my gratitude to Mr Marc Bonnet from the HydroExpert company for offering me the opportunity to apply the numerical methods studied theoretically in this thesis to the hydrogeological practice. A note of gratitude finally goes to Doctor Michal Beneš from my home faculty for his constant support and to Professor Christian Grossmann from the Institute of Numerical Mathematics of the Dresden University of Technology for my stay at his institute.

I am especially in debt to Professor Miloslav Feistauer and Professor Jérôme Jaffré, who kindly accepted to be the referees of this thesis. I appreciate deeply their interest in my work as well as their useful comments. I am also very grateful to Professor Bernard Helffer, who agreed to be the committee chief, and to Professor Vivette Girault and Professor Feistauer for accepting to be the committee members.

I value profoundly the fellowship granted by the French Government which allowed me to spend a part of my doctoral studies in France and to discover this beautiful country both scientifically and culturally. I also enjoyed a partial support of the Marie, Zdeňka, and Josef Hlávka Foundation in Prague, which I appreciate very much.

I am very thankful to the whole Department of Numerical Analysis and Partial Differential Equations at Orsay for having received me very warmly.

Finally, my deepest thanks go to my parents and to all my family for their constant support, encouragement, and love. And all this would never be like this without Martina ...

*To my parents*

*To Martina*

# NUMERICAL METHODS FOR NONLINEAR ELLIPTIC AND PARABOLIC EQUATIONS

*Application to flow problems in porous and fractured media*


## Abstract

This thesis deals with numerical methods for the discretization of nonlinear elliptic and parabolic convection–reaction–diffusion partial differential equations. We analyze these methods and apply them to the effective simulation of flow and contaminant transport in porous and fractured media.

In Chapter 1 we propose a scheme allowing for efficient, robust, conservative, and stable discretizations of nonlinear degenerate parabolic convection–reaction–diffusion equations on unstructured grids in two or three space dimensions. We discretize the diffusion term, which generally involves an inhomogeneous and anisotropic diffusion tensor, by means of the nonconforming or mixed-hybrid finite element method and the other terms by means of the finite volume method. The essential part of this chapter is then devoted to showing the existence and uniqueness of a discrete solution and its convergence to a weak solution of the continuous problem. The proofs permit in particular to avoid restrictive hypotheses on the mesh often used in the literature. We finally propose a version of this scheme for nonmatching grids, combining this time the finite volume method with the piecewise linear conforming finite element method. We then apply this version to contaminant transport simulations in porous media.

In Chapter 2 we present a direct proof of the discrete Poincaré–Friedrichs inequalities for a class of nonconforming approximations of the Sobolev space $H^1$, indicate optimal values of the constants in these inequalities, and extend the discrete Friedrichs inequality onto domains only bounded in one direction. The results are important in the analysis of nonconforming numerical methods, such as nonconforming finite element or discontinuous Galerkin methods.

In Chapter 3 we show that the lowest-order Raviart–Thomas mixed finite element method for elliptic problems on simplicial meshes in two or three space dimensions is equivalent to a particular multi-point finite volume scheme. We study this scheme and apply it to the discretization of nonlinear parabolic convection–reaction–diffusion equations. This approach allows significant reduction of the computational time of the mixed finite element method without any loss of its high precision, which is confirmed by numerical experiments.

Finally, in Chapter 4 we propose a version of the lowest-order Raviart–Thomas mixed finite element method for the approximation of elliptic problems on a system of two-dimensional polygons placed in three-dimensional space, prove that it is well-posed, and study its relation to the nonconforming finite element method. These results are finally applied to the simulation of underground water flow through a system of polygons representing a network of fractures that perturbs a rock massif.



**Key words:** Finite volume method – Finite element method – Mixed finite element method – Unstructured grids – Discrete Poincaré–Friedrichs inequalities – Existence and uniqueness – Convergence – Numerical simulations – Degenerate parabolic convection–reaction–diffusion equation – Flow and contaminant transport in porous and fractured media

**AMS subject classifications:** 65M12, 65N30, 76M10, 76M12, 76S05, 35J20, 35K65, 46E35

# METHODES NUMERIQUES POUR DES EQUATIONS ELLIPTIQUES ET PARABOLIQUES NON LINEAIRES

*Application à des problèmes d'écoulement en milieux poreux et fracturés*


**Résumé**

Les travaux de cette thèse portent sur des méthodes numériques pour la discrétisation d'équations aux dérivées partielles elliptiques et paraboliques de convection–réaction–diffusion non linéaires. Nous analysons ces méthodes et nous les appliquons à la simulation effective de l'écoulement et du transport de contaminants en milieux poreux et fracturés.

Au chapitre 1, nous proposons un schéma permettant une discrétisation efficace, robuste, conservative et stable des équations de convection–réaction–diffusion non linéaires paraboliques dégénérées sur des maillages non structurés en dimensions deux ou trois d'espace. Nous discrétisons le terme de diffusion, qui contient en général un tenseur de diffusion inhomogène et anisotrope, par la méthode des éléments finis non conformes ou mixtes-hybrides et les autres termes par la méthode des volumes finis. La partie essentielle du chapitre est ensuite consacrée à montrer l'existence et l'unicité d'une solution discrète et sa convergence vers une solution faible du problème continu. La méthode de démonstration permet en particulier d'éviter des hypothèses restrictives sur le maillage souvent présentes dans la littérature. Nous proposons finalement une variante de ce schéma pour des maillages qui ne se raccordent pas, couplant cette fois la méthode des volumes finis avec celle des éléments finis conformes, et nous l'appliquons à la simulation du transport de contaminants en milieux poreux.

Au chapitre 2, nous présentons une démonstration constructive des inégalités de Poincaré–Friedrichs discrètes pour une classe d'approximations non conformes de l'espace de Sobolev $H^1$, indiquons les valeurs optimales des constantes dans ces inégalités et montrons l'inégalité de Friedrichs discrète pour des domaines bornés dans une direction uniquement. Ces résultats sont importants dans l'analyse de méthodes numériques non conformes, comme les méthodes d'éléments finis non conformes ou de Galerkin discontinu.

Au chapitre 3, nous montrons que la méthode des éléments finis mixtes de Raviart–Thomas de plus bas degré pour des problèmes elliptiques en dimension deux ou trois d'espace est équivalente à un schéma de volumes finis à plusieurs points. Après avoir étudié ce schéma, nous l'appliquons à la discrétisation d'équations de convection–réaction–diffusion paraboliques non linéaires. Cette approche permet de réduire le temps de calcul de la méthode des éléments finis mixtes, tout en conservant sa très grande précision, ce qui est confirmé par les tests numériques.

Enfin, au chapitre 4, nous proposons une version de la méthode des éléments finis mixtes de Raviart–Thomas de plus bas degré pour la résolution de problèmes elliptiques sur un système de polygones bidimensionnels placés dans l'espace tridimensionnel, démontrons qu'elle est bien posée et étudions sa relation avec la méthode des éléments finis non conformes. Ces résultats sont finalement appliqués à la simulation de l'écoulement de l'eau souterraine dans un système de polygones représentant un réseau de fractures perturbant un massif rocheux.



**Mots clés :** Méthodes volumes finis – Méthodes éléments finis – Méthodes éléments finis mixtes – Maillages non structurés – Inégalités de Poincaré–Friedrichs discrètes – Existence et unicité – Convergence – Simulations numériques – Equation de convection–réaction–diffusion parabolique dégénérée – Ecoulement et transport de contaminants en milieux poreux et fracturés

**AMS subject classifications :** 65M12, 65N30, 76M10, 76M12, 76S05, 35J20, 35K65, 46E35

# Table of Contents

# Introduction

Partial differential equations describe a large number of environmental and physical phenomena. Unfortunately, in most cases, it is not possible to find their analytical solutions. To find at least approximate solutions, numerical methods are developed. Nowadays, in the period of computer boom, the interest in their development is still increasing.

The finite element method was developed by engineers in 1950's and studied by mathematicians shortly afterwards. The main works are those of Strang and Fix, Zienkiewicz, and Ciarlet. The finite volume method, again developed by engineers, was studied from the mathematical viewpoint much later, in particular by Eymard, Gallouët, and Herbin. The essential ideas of these two methods appear to be very different: in the finite element one, one minimizes the energy, whereas in the finite volume one, one approaches the flux in an integral formulation. Despite this fact, the discretization of second-order elliptic equations by means of these methods may lead to very close or even identical discrete problems. In particular, in contradiction with what has been claimed for a long time, the finite element method is locally conservative just as the finite volume method, which can be shown by a suitable interpretation of its results. Being very close for the discretization of second-order diffusion terms, these methods are however of a quite different nature for first-order convective or reactive terms or in the discretization of the time derivative. Trying to use the "best of these two worlds" is the motivation for introducing combined finite volume–finite element methods.

The Raviart–Thomas mixed finite element method allows for more precise calculations. One approximates here simultaneously the unknown scalar function and its flux. This method however leads to saddle-point linear systems whose numerical solution may be quite expensive. In order to decrease its computational complexity and to facilitate its implementation, the relations of this method with the nonconforming finite element and finite volume (finite difference) methods have been studied. The results have moreover enabled further progress in the analysis of mixed finite element methods.

In this thesis we study schemes combining the finite volume and finite element methods for the discretization of nonlinear convection–reaction–diffusion problems with inhomogeneous and anisotropic diffusion tensors on very general meshes. We then show that the lowest-order Raviart–Thomas mixed finite element method is equivalent to a particular finite volume scheme. We finally apply these methods to the simulation of problems arising in the environment, namely to the simulation of flow and contaminant transport in porous and fractured media. We also present optimal constants in the discrete Poincaré–Friedrichs inequalities, which are necessary in the analysis of the above numerical schemes. The four chapters of this thesis and Appendix 1.9 may be read independently.

## Chapter 1: Combined finite volume–finite element schemes for degenerate parabolic convection–reaction–diffusion problems

We propose and analyze in this chapter two combined finite volume–finite element schemes enabling an efficient discretization of degenerate parabolic equations on general meshes.

We consider the convection–reaction–diffusion equation

$$\frac{\partial \beta(c)}{\partial t} - \nabla \cdot (\mathbf{S} \nabla c) + \nabla \cdot (c\mathbf{v}) + F(c) = q\,, \tag{1}$$

which describes reactive contaminant transport with equilibrium adsorption reaction in porous media, cf. [19, 81]. Here $c = c(\mathbf{x}, t)$ is the unknown concentration of the contaminant, $\mathbf{v} = \mathbf{v}(\mathbf{x}, t)$ is an external velocity field, $\mathbf{S} = \mathbf{S}(\mathbf{x}, \mathbf{v}, t)$ is the diffusion–dispersion tensor, the function $\beta$ represents time evolution and equilibrium adsorption, the function $F$ represents the changes due to chemical reactions, and finally $q = q(\mathbf{x}, t)$ stands for the sources. The problem is completed by appropriate initial and boundary conditions. The essential difficulties in the numerical approximation of this problem are given by the facts that the equation (1) is degenerate parabolic since $\beta'$ may be unbounded, that it is generally dominated by the convection term, and that it involves the inhomogeneous and anisotropic (nonconstant full-matrix) diffusion–dispersion tensor $\mathbf{S}$.

The finite element method for degenerate parabolic problems has been studied e.g. in [20, 94, 109]. It allows for an easy discretization of the diffusion term with a full tensor and does not impose any restrictions on the meshes. Recall that this method is locally conservative, contrary to what has been claimed for a long time, cf. [68], [61, Section III.12], or [75]. However, it is well-known that numerical instabilities may arise in the convection-dominated case. The cell-centered finite volume method for degenerate parabolic problems has been investigated e.g. in [62, 63]. With an upwind discretization of the convection term, it ensures the stability and is very robust and computationally inexpensive. However, there are restrictions on the mesh for the discretization of the diffusion term and there is also no straightforward way to apply it to problems with anisotropic diffusion tensors. To overcome the weak points of these two classical methods, schemes combining finite elements and finite volumes have been developed, cf. [10, 48, 67, 90]. However, these schemes were only proposed for uniformly parabolic equations and only studied with quite restrictive hypotheses on the mesh.

### A scheme combining the finite volume and nonconforming or mixed-hybrid finite element methods

We consider in this part an unstructured mesh of the space domain consisting of simplices (triangles in space dimension two and tetrahedra in space dimension three). To discretize the equation (1), we were motivated by the method proposed in [10] for fluid mechanics equations.

The scheme reads as follows. We discretize the diffusion term by means of the piecewise linear nonconforming (Crouzeix–Raviart) finite element method on the given grid and the other terms by means of the cell-centered finite volume method on a dual mesh, where the dual volumes are constructed around the sides of the original triangulation. We also alternatively replace the nonconforming finite elements by the mixed-hybrid finite elements, where the only unknowns are the Lagrange multipliers, cf. [15]. In order to adjust the amount of upstream weighting on the basis of the local ratio of convection and diffusion, we propose a numerical flux which takes into account the local Péclet number. We add in this way only the minimal numerical diffusion necessary to stabilize the scheme. Finally, we use a fully implicit time discretization.

We next analyze the scheme. We first show that there exists a unique discrete solution. We then prove that this solution verifies the discrete maximum principle if there are no obtuse angles in the mesh and if the diffusion–dispersion tensor is a scalar function, as well as the local conservativity of the scheme. The subsequent demonstration of a priori estimates and of estimates on differences of time and space translates implies by the Fréchet–Kolmogorov theorem the relative compactness property. We show in this way a strong $L^2$ convergence of a subsequence of approximate solutions towards a weak solution of the continuous problem. Our proofs rely on finite volume tools from [61], which we extend onto schemes with finite element transmissibilities that can be negative (in which case there is no maximum principle) and onto general simplicial meshes. This enables us to generalize the assumptions which were necessary in [10]. In particular, we do not impose any maximal condition on the angles of the mesh and allow its local refinement as well. Finally, we solve the nonlinear systems of algebraic equations for the discrete unknowns corresponding to $\beta(c)$. One can in this way avoid the parabolic regularization (cf. [20]) or perturbation of initial and boundary conditions (cf. [99]), which make the equation uniformly parabolic. Moreover, the resulting matrices are diagonal for the part of the unknowns corresponding to the region where the approximate solution is zero. The proposed scheme allows for efficient, robust, conservative, and stable discretizations of the equation (1), which is finally confirmed by numerical experiments.

This part is summarized in a paper written in collaboration with R. Eymard and D. Hilhorst, submitted for publication in *Numerische Mathematik*. An abbreviated version of this paper was published in the proceedings (peer-reviewed) of the ENUMATH 2003 conference.

### A combined finite volume–finite element scheme for contaminant transport simulation on nonmatching grids

We consider in this part the equation (1) in its precise form describing the reactive miscible displacement of one contaminant in porous media, cf. [25, 123]. We suppose that the mesh is unstructured, composed of polygonal control volumes which are not necessarily convex and which do not necessarily match. We extend on this type of meshes the schemes proposed in [67, 114].

To define the scheme, we first construct a (matching) simplicial grid whose vertices are associated with the control volumes of the given mesh. We next apply the ideas of the previous scheme, combining this time the finite volume method with the piecewise linear conforming finite element method. We generalize the local Péclet numerical flux onto considered meshes and prove that the scheme stays locally conservative and that it satisfies the discrete maximum principle under certain conditions on the simplicial mesh and on the diffusion–dispersion tensor. One could show its convergence using the techniques from the previous part. Our scheme appears much simpler than the other schemes for nonmatching grids, while being very efficient. In particular, we do not introduce any supplementary equations or unknowns on the boundary between the regions with nonmatching grids, nor do we use any interpolation of the discrete solutions on this boundary, cf. [3, 11, 26, 55, 66]. In fact, it could be considered as a consistent version of the scheme proposed in [36]. We finally present the results of the simulation of a model problem with a known analytical solution as well as of a real problem provided by the HydroExpert company, Paris. The proposed scheme has been implemented into the software TALISMAN [104] of this company, which makes use of square grids which can be locally refined and are thus nonmatching.

This part, written in collaboration with R. Eymard and D. Hilhorst, will be submitted for publication in *Transport in Porous Media*.

## Chapter 2: Discrete Poincaré–Friedrichs inequalities

We study in this chapter the discrete versions of the Poincaré–Friedrichs inequalities, which are important in the analysis of nonconforming numerical methods.

The Friedrichs inequality

$$\int_\Omega g^2(\mathbf{x})\,\mathrm{d}\mathbf{x} \le c_F \int_\Omega |\nabla g(\mathbf{x})|^2\,\mathrm{d}\mathbf{x} \qquad \forall g \in H_0^1(\Omega) \tag{2}$$

and the Poincaré inequality

$$\int_\Omega g^2(\mathbf{x})\,\mathrm{d}\mathbf{x} \le c_P \int_\Omega |\nabla g(\mathbf{x})|^2\,\mathrm{d}\mathbf{x} + \tilde{c}_P\Big(\int_\Omega g(\mathbf{x})\,\mathrm{d}\mathbf{x}\Big)^2 \qquad \forall g \in H^1(\Omega) \tag{3}$$

(cf. [91]) play an important role in the theory of partial differential equations. We consider here an open, bounded, and connected polygonal set $\Omega \subset \mathbb{R}^d$, $d = 2, 3$.

Let $\{\mathcal{T}_h\}_h$ be a family of simplicial triangulations of $\Omega$. Let the spaces $W(\mathcal{T}_h)$ be formed by functions locally in $H^1(K)$ on each $K \in \mathcal{T}_h$ such that the mean values of their traces on interior sides coincide. Finally, let $W_0(\mathcal{T}_h) \subset W(\mathcal{T}_h)$ be such that the mean values of the traces on exterior sides of functions from $W_0(\mathcal{T}_h)$ are equal to zero. These spaces are nonconforming approximations of the continuous ones, i.e. $W_0(\mathcal{T}_h) \not\subset H_0^1(\Omega)$ and $W(\mathcal{T}_h) \not\subset H^1(\Omega)$. We investigate in this chapter analogies of (2) and (3) in the forms

$$\int_\Omega g^2(\mathbf{x})\,\mathrm{d}\mathbf{x} \le C_F \sum_{K\in\mathcal{T}_h} \int_K |\nabla g(\mathbf{x})|^2\,\mathrm{d}\mathbf{x} \qquad \forall g \in W_0(\mathcal{T}_h)\,,\ \forall h > 0\,, \tag{4}$$

$$\int_\Omega g^2(\mathbf{x})\,\mathrm{d}\mathbf{x} \le C_P \sum_{K\in\mathcal{T}_h} \int_K |\nabla g(\mathbf{x})|^2\,\mathrm{d}\mathbf{x} + \tilde{C}_P\Big(\int_\Omega g(\mathbf{x})\,\mathrm{d}\mathbf{x}\Big)^2 \qquad \forall g \in W(\mathcal{T}_h)\,,\ \forall h > 0\,. \tag{5}$$

The inequalities (4) and (5) have been studied in [28, 51, 84, 116]. It was shown in [28, 84] that the constants $C_F$, $C_P$ only depend on the domain $\Omega$ and on the shape regularity of the meshes. We establish in this chapter the exact dependence of $C_F$, $C_P$ on these parameters and present an example showing that this dependence is optimal. Finally, the dependence of $C_F$ on $\Omega$ allows us to extend the discrete Friedrichs inequality onto domains which are only bounded in some direction. Our proof of (4) and (5) is constructive and its main idea is to extend the discrete Poincaré–Friedrichs inequalities for piecewise constant functions known from the finite volume methods, see [61]. The results are necessary in the analysis of nonconforming numerical methods, such as nonconforming finite element or discontinuous Galerkin methods.

This chapter has been submitted for publication in *Numerical Functional Analysis and Optimization*.

## Chapter 3: Equivalence between lowest-order mixed finite element and multi-point finite volume methods

We show in this chapter that the lowest-order Raviart–Thomas mixed finite element method for elliptic problems is equivalent to a particular multi-point finite volume scheme and apply consequently this result to the discretization of nonlinear parabolic problems. The purpose is to reduce the computational time of the mixed finite element method without any loss of its high precision.

We first consider the elliptic problem

$$\mathbf{u} = -\mathbf{S}\nabla p \quad \text{in } \Omega\,, \tag{6a}$$

$$\nabla\cdot\mathbf{u} = q \quad \text{in } \Omega\,, \tag{6b}$$

$$p = p_D \quad \text{on } \Gamma_D\,, \quad \mathbf{u}\cdot\mathbf{n} = u_N \quad \text{on } \Gamma_N\,, \tag{6c}$$

where $\Omega \subset \mathbb{R}^d$, $d = 2, 3$, is an open, bounded, and connected polygonal set, $\mathbf{S}$ is a bounded, symmetric, and uniformly positive definite tensor, $p_D \in H^{\frac{1}{2}}(\Gamma_D)$, $u_N \in H^{-\frac{1}{2}}(\Gamma_N)$, and $q \in L_2(\Omega)$. Let $\mathcal{T}_h$ be a simplicial triangulation of $\Omega$. In the lowest-order Raviart–Thomas mixed finite element method [105] for the problem (6a)–(6c) (cf. Nédélec [92] in three space dimensions), one simultaneously seeks the scalar unknowns $P$ associated with the elements of the mesh and the fluxes $U$ through the sides of the mesh. The associated matrix problem is saddle-point and can be written in the form

$$\begin{pmatrix} \mathbb{A} & \mathbb{B}^t \\ \mathbb{B} & 0 \end{pmatrix}\begin{pmatrix} U \\ P \end{pmatrix} = \begin{pmatrix} F \\ G \end{pmatrix}. \tag{7}$$

Following the ideas given in [69], one can decrease the number of unknowns to the Lagrange multipliers associated with the sides and obtain a symmetric and positive definite matrix, cf. [15]. If $\mathbf{S}$ is diagonal, one can eliminate the flux unknowns $U$ using approximate numerical integration, cf. [8, 18, 110]. These ideas can be further extended to the case of general tensors $\mathbf{S}$, cf. [12]. In two space dimensions, the lowest-order Raviart–Thomas mixed finite element method can be reformulated with the aid of a new unknown associated with the elements of the mesh, cf. [37, 121, 122]. To our knowledge, this is the only known exact approach to reduce the number of unknowns of this method to the number of elements.

We present in this chapter a new method which permits to exactly and efficiently reduce the system (7) to a system for the scalar unknowns $P$ only. We show that, under a condition of the invertibility of some local matrices associated with vertices, one can express the flux through a given side using the scalar unknowns, sources, and possibly boundary conditions associated with the elements sharing one of the vertices of this side. Recall that expressing the flux through a given side using the scalar unknowns in neighboring elements is the principle of multi-point finite volume schemes, cf. [1, 44, 65]. Hence the lowest-order Raviart–Thomas mixed finite element method is in the given case equivalent to a particular multi-point finite volume scheme, and this without any numerical integration. We then discuss the modifications of the proposed scheme if the local matrices are not invertible. The elimination leads to a linear system with a sparse but in general nonsymmetric matrix. We prove that this matrix is positive definite under a condition on the mesh and on the tensor $\mathbf{S}$, which can be reduced to a shape criterion allowing for fairly general elements if $\mathbf{S}$ is piecewise constant and scalar. The fulfillment of this condition in particular implies the invertibility of the local matrices discussed above. Finally, the proposed elimination applies in the same way to mixed (cf. [14]) and upwind-mixed (cf. [46, 47, 77]) finite element discretizations of nonlinear parabolic convection–reaction–diffusion problems.

The essential idea of what we propose can be formulated as follows: given a second-order problem, first decompose it into scalar and flux unknowns and guarantee the fulfillment of the inf–sup condition. Then eliminate the added fluxes. One can in this way obtain the precision of the mixed finite element method for the price of the finite volume one, which is confirmed by numerical experiments. Especially for nonlinear parabolic problems, one can reduce the CPU time of standard mixed solution approaches by a factor of 2 to 4. Finally, the proposed

elimination can be easily implemented in a new self-standing code, as well as in existing mixed finite element codes. Extension to higher-order schemes is an ongoing work.

This chapter will be submitted for publication in *M2AN. Mathematical Modelling and Numerical Analysis*. Its abbreviated version was published in *Comptes Rendus de l'Académie des Sciences, Ser. I.*

## Chapter 4: Mixed and nonconforming finite element methods on a fracture network

In this chapter we propose the lowest-order Raviart–Thomas mixed finite element method for elliptic problems on a network of polygons, prove that it is well-posed, and study its relation to the nonconforming finite element method. These results are finally applied to the simulation of underground water flow through a system of polygons representing a network of fractures perturbing a rock massif.

We suppose given a system

$$\mathcal{S} := \bigcup_{\ell \in L} \alpha_\ell \,,$$

where $\alpha_\ell$ is an open two-dimensional polygon placed in three-dimensional space, connected through its edges with other polygons from the system. In contrast to classical planar domains, there can be edges shared by three or more polygons. We consider the elliptic problem on $\mathcal{S}$ to find $p$ and $\mathbf{u}$ such that

$$\begin{aligned} \mathbf{u} &= -\mathbf{K}(\nabla p + \nabla z) \quad \text{in } \alpha_\ell \,, \ell \in L \,, && \text{(8a)} \\ \nabla \cdot \mathbf{u} &= q \quad \text{in } \alpha_\ell \,, \ell \in L \,, && \text{(8b)} \\ p &= p_D \quad \text{on } \Gamma_D \,, \quad \mathbf{u} \cdot \mathbf{n} = u_N \quad \text{on } \Gamma_N \,, && \text{(8c)} \end{aligned}$$

where all the variables are expressed in local coordinates of the appropriate $\alpha_\ell$. Let $f$ be an edge shared by polygons with an index set $I_f$. The system (8a)–(8c) is completed by requiring

$$\begin{aligned} p|_{\overline{\alpha_i}} &= p|_{\overline{\alpha_j}} \quad \text{on } f \qquad \forall i, j \in I_f \,, \\ \sum_{i \in I_f} \mathbf{u}|_{\overline{\alpha_i}} \cdot \mathbf{n}_{f,\alpha_i} &= 0 \quad \text{on } f \end{aligned}$$

for each interior edge $f$, where $\mathbf{n}_{f,\alpha_i}$ is the unit outward normal vector of the edge $f$ with respect to the polygon $\alpha_i$. This relation expresses the continuity of $p$ and the mass balance of $\mathbf{u}$ across $f$. The considered problem describes underground water flow in a fracture network perturbing a rock massif, cf. [5].

We propose in this chapter a mixed finite element method for the above problem. Having first defined function spaces ensuring the appropriate continuity across the interior edges, we prove the existence and uniqueness of a weak mixed solution on a network of polygons. We next consider a triangular discretization of the network and define discrete function spaces, based on the lowest-order Raviart–Thomas mixed finite elements. We then show that this method is well-posed, that is to say that there exists a unique discrete solution. Error estimates then follow from the general theory, cf. [33, 108]. We finally investigate the relation of the hybridization of the lowest-order Raviart–Thomas mixed finite element method to the piecewise linear nonconforming finite element method. We extend the results known in this direction (cf. [15, 38]) onto nonconstant hydraulic conductivity tensors $\mathbf{K}$, inhomogeneous

Dirichlet and Neumann boundary conditions, and onto systems of polygons. This enables in particular an efficient implementation of the mixed finite element method on a system of polygons. We finally present the results of a numerical experiment on a model problem with a known analytical solution and show an application of the proposed method to the simulation of underground water flow in a granitoid massif in Western Bohemia, intended as a nuclear waste repository.

The theoretical results of this chapter are submitted for publication in *Applied Numerical Mathematics*, with the co-authors J. Maryška and O. Severýn. An abbreviated version of this paper was published in *Contemporary Mathematics* (Current Trends in Scientific Computing). A paper with applications, written with the same co-authors, appeared recently in *Computational Geosciences*.

# Chapter 1

# Combined finite volume–finite element schemes for degenerate parabolic convection–reaction–diffusion problems

We propose and analyze in this chapter a numerical scheme for nonlinear degenerate parabolic convection–reaction–diffusion equations in two or three space dimensions. We discretize the diffusion term, which generally involves an inhomogeneous and anisotropic diffusion tensor, over an unstructured simplicial mesh of the space domain by means of the piecewise linear nonconforming (Crouzeix–Raviart) finite element method, or using the stiffness matrix of the hybridization of the lowest-order Raviart–Thomas mixed finite element method. The other terms are discretized by means of a cell-centered finite volume scheme on a dual mesh, where the dual volumes are constructed around the sides of the original mesh. Checking the local Péclet number, we set up the exact necessary amount of upstream weighting to avoid spurious oscillations in the convection-dominated case. This technique also ensures the validity of the discrete maximum principle under some conditions on the mesh and the diffusion tensor. We prove the convergence of the scheme, only supposing the shape regularity condition for the original mesh. We use a priori estimates and the Kolmogorov relative compactness theorem for this purpose. The proposed scheme is robust, only 5-point (7-point in space dimension three), locally conservative, efficient, and stable, which is confirmed by a numerical experiment. We finally propose a version of this scheme for nonmatching grids, combining this time the finite volume method with the piecewise linear conforming finite element method. We then apply this version to contaminant transport simulation in porous media.

## 1.1 Introduction

Degenerate parabolic equations arise in many contexts, such as flow in porous media or free boundary problems. This chapter is motivated by the modeling of contaminant transport in porous media with equilibrium adsorption reaction, see [19, 25], which typically involves a convection–reaction–diffusion equation of the form

$$\frac{\partial \beta(c)}{\partial t} - \nabla \cdot (\mathbf{S} \nabla c) + \mu \nabla \cdot (c\mathbf{v}) + F(c) = q\,, \tag{1.1}$$

where $c$ is the unknown concentration of the contaminant, the function $\beta(\cdot)$ represents time evolution and equilibrium adsorption reaction and is supposed to be continuous and increasing with the growth bounded from below by a positive constant, $\mathbf{S}$ is the diffusion–dispersion tensor, $\mathbf{v}$ is the velocity field in the convection term (given for instance by the Darcy law), the function $F(\cdot)$ represents the changes due to chemical reactions, $q$ stands for the sources, and finally, $\mu$ is a scalar parameter. Equation (1.1) is degenerate parabolic since $\beta'$ may be unbounded, generally dominated by the convection term, and involves inhomogeneous and anisotropic (nonconstant full-matrix) diffusion–dispersion tensor.

A large variety of methods have been proposed for the discretization of degenerate parabolic equations. The conforming piecewise linear finite element method has been studied e.g. in [20, 39, 53, 93, 109], the cell-centered finite volume method in [22, 62, 63], the vertex-centered finite volume method in [6, 96], the finite difference method e.g. in [82], the mixed finite element method in [14, 46, 47], characteristic or Eulerian–Lagrangian methods e.g. in [40, 81], and relaxation schemes have been proposed e.g. in [78]. We shall follow in this chapter the finite element/finite volume approach.

The finite element method allows for an easy discretization of the diffusion term with a full tensor and does not impose any restrictions on the meshes. However, it is well-known that numerical instabilities may arise in the convection-dominated case. Recall that this method is locally conservative, contrary to what has been claimed for a long time, cf. [68, 76, 112], [61, Section III.12], or a detailed analysis given in [75]. The cell-centered finite volume method with an upwind discretization of the convection term ensures the stability and is extremely robust and computationally inexpensive. However, the mesh for the discretization of the diffusion term has to fulfill the following orthogonality property: the line segment relying the emplacement of the unknowns in two neighboring volumes has to be orthogonal to the side (edge in space dimension two and face in space dimension three) between these volumes, cf. [61]. Also, there is no straightforward way to apply this finite volume method to problems with full diffusion tensors. Various "multi-point" schemes where the approximation of the flux through an edge involves several scalar unknowns have been proposed, cf. e.g. [1, 7, 44, 58, 65]. However, such schemes require using more points than the classical 4 points for triangular meshes and 5 points for quadrangular meshes in space dimension two, making the schemes less robust and more susceptible to numerical instabilities. Their extension to three-dimensional unstructured meshes is also not straightforward (with the exception of the scheme proposed in [58]).

A quite intuitive idea is hence to combine a finite element discretization of the diffusion term with a finite volume discretization of the other terms of (1.1), trying to use the "best of both worlds". Schemes combining conforming piecewise linear finite elements on triangles for the diffusion term with $\mathbf{S} = Id$ and finite volumes on dual volumes associated with the vertices, proposed and studied in [48, 67, 90] for fluid mechanics equations, are indeed quite efficient. Our motivation is to extend these ideas to degenerate parabolic problems, to the

combination of the mixed-hybrid finite element and finite volume methods, to inhomogeneous and anisotropic diffusion–dispersion tensors, to space dimension three, and finally to meshes only satisfying the shape regularity condition. We shall also extend such schemes to the case of nonmatching grids in Appendix 1.9.

Let us now introduce the combined scheme that we analyze in this chapter. We consider a triangulation of the space domain consisting of simplices (triangles in space dimension two and tetrahedra in space dimension three). We next construct a dual mesh where the dual volumes are associated with the sides (edges or faces). To construct a dual volume, one connects the barycentres of two neighboring simplices through the vertices of their common side. We finally place the unknowns in the barycentres of the sides. For the discretization of the diffusion term of (1.1), we consider the piecewise linear nonconforming (Crouzeix–Raviart, cf. [45]) finite element method or the mixed-hybrid finite element method where the only unknowns are the Lagrange multipliers, cf. [15, 33, 108]. We recall that the elements of the obtained stiffness matrices naturally express the coefficients for the discrete diffusive fluxes between the unknowns. We obtain the combined scheme by performing a finite volume discretization of (1.1) over the dual mesh and by replacing the finite volume stiffness matrix corresponding to the diffusion term by one of the above finite element stiffness matrices. The combination of finite volumes with nonconforming finite elements was originally proposed and analyzed in [10] as a semi-implicit discretization of a convection–diffusion equation with a nonlinear convection term in space dimension two. As far as we know, the combination of the finite volume method with the mixed-hybrid method is new. However, the two finite element stiffness matrices are very close. For a piecewise constant diffusion tensor, they completely coincide (see [15, 38]), and for a general diffusion tensor, the stiffness matrix of the mixed-hybrid method is the stiffness matrix of the nonconforming method with a piecewise constant diffusion tensor, given as the elementwise harmonic average of the original one (see Lemma 1.8.1 in Appendix 1.8).

We propose the combined scheme for the equation (1.1) in combination with the backward Euler finite difference time stepping. We can mention its following advantages. The scheme is stable since we avoid spurious oscillations in the convection-dominated case by checking the local Péclet number and by adding exactly the necessary amount of upstream weighting. It inherits the diffusion properties of nonconforming/mixed-hybrid finite elements, enabling in particular the use of general meshes and the discretization of anisotropic diffusion tensors. It possesses a discrete maximum principle in the case where all transmissibilities are nonnegative. This happens for instance when the diffusion tensor reduces to a scalar function and when the angles between the outward normal vectors of sides of each simplex in the triangulation are greater or equal to $\pi/2$. The scheme is next locally conservative. It is only 5-point in space dimension two and 7-point in space dimension three. It finally permits to efficiently discretize degenerate parabolic problems: when we search for the discrete unknowns corresponding to $\beta(c)$, the resulting system of nonlinear algebraic equations can be solved by the Newton method without any parabolic regularization (cf. [20]) or perturbation of initial and boundary conditions (cf. [98, 99]), which make the equation uniformly parabolic. Moreover, the resulting matrices are diagonal for the part of the unknowns corresponding to the region where the approximate solution is zero.

Our numerical scheme permits to construct approximate solutions that are piecewise constant on the dual mesh or piecewise linear on the primal simplicial mesh and continuous in the barycentres of the sides of the simplices. We prove the convergence of both these approximations to a weak solution of the continuous problem in this chapter. The methods of proof are based upon the Kolmogorov relative compactness theorem and the finite volume tools from [61]. We extend these tools onto schemes with negative transmissibilities, for cases where

the discrete maximum principle is not satisfied, and for (dual) meshes not necessarily satisfying the orthogonality property. We only need the shape regularity (minimal angle) assumption for the primal triangulation, we require neither the inverse assumption (bounded ratio between the diameters of elements in the primal mesh), nor any maximal angle condition, as it was the case in [10]. We only suppose that $\beta$ is continuous with the growth bounded from below in the case where the discrete maximum principle is satisfied. In the general case we require in addition $\beta$ to be bounded on some interval and Lipschitz-continuous outside this interval. There is no restriction on the maximal time step in the case where $F$ is nondecreasing. If $F$ does not posses this property, we impose an appropriate maximal time step condition. For the sake of simplicity, we only consider the case of a homogeneous Dirichlet boundary condition. Extensions to other types of boundary conditions and to the case where the equation (1.1) involves a nonlinear convection term are possible, using the techniques from [61] and [62].

The rest of the chapter is organized as follows. In Section 1.2 we state the assumptions on the data and present a weak formulation of the continuous problem. In Section 1.3 we define the approximation spaces and introduce the combined finite volume–nonconforming/mixed-hybrid finite element scheme. In Section 1.4 we present some properties of this scheme and prove that it possesses a unique solution, which satisfies a discrete maximum principle under the hypotheses stated above. In Section 1.5 we derive a priori estimates and estimates on differences of time and space translates for the approximate solutions. Finally, in Section 1.6, using the Kolmogorov relative compactness theorem, we prove the convergence of a subsequence of the sequence of approximate solutions to a weak solution of the continuous problem. We present the results of a numerical experiment in Section 1.7 and we give some technical lemmas in Appendix 1.8. Finally, in Appendix 1.9, we propose a version of this scheme for nonmatching grids, combining this time the finite volume method with the piecewise linear conforming finite element method. We then apply this version to contaminant transport simulation in porous media.

## 1.2 The nonlinear degenerate parabolic problem

We consider the equation (1.1) in a polygonal domain (open, bounded, and connected set) $\Omega \subset \mathbb{R}^d$, $d = 2, 3$, with boundary $\partial\Omega$ on the time interval $(0, T)$, $0 < T < \infty$, and denote $Q_T := \Omega \times (0, T)$. We impose the initial condition by

$$c(\cdot, 0) = c_0 \quad \text{in } \Omega \tag{1.2}$$

and the homogeneous Dirichlet boundary condition by

$$c = 0 \quad \text{on } \partial\Omega \times (0, T)\,. \tag{1.3}$$

Let us consider a domain $S \subset \mathbb{R}^d$. We use the standard notation $L^p(S)$ and $\mathbf{L}^p(S) = [L^p(S)]^d$ for the Lebesgue spaces on $S$, $(\cdot,\cdot)_{0,S}$ stands for the $L^2(S)$ or $\mathbf{L}^2(S)$ inner product, and $\|\cdot\|_{0,S}$ for the associated norm. We use $\mathrm{d}\mathbf{x}$ as the integration symbol for the Lebesgue measure on $S$, $\mathrm{d}\gamma(\mathbf{x})$ for the Lebesgue measure on a hyperplane of $S$, and $\mathrm{d}t$ for the Lebesgue measure on $(0, T)$. We denote by $|S|$ the $d$-dimensional Lebesgue measure of $S$, by $|\sigma|$ the $(d-1)$-dimensional Lebesgue measure of $\sigma$, a part of a hyperplane in $\mathbb{R}^d$, and by $|\mathbf{s}|$ the length of a segment $\mathbf{s}$. The diameter of $S$ is the supremum of the lengths of all the line segments $\mathbf{s}$ such that $\mathbf{s} \subset S$. Next, $H^1(S)$ and $H^1_0(S)$ are the Sobolev spaces of functions with square-integrable weak derivatives and $\mathbf{H}(\mathrm{div}, S)$ is the space of vector functions with square-integrable weak divergences, $\mathbf{H}(\mathrm{div}, S) = \{\mathbf{v} \in \mathbf{L}^2(S); \nabla \cdot \mathbf{v} \in L^2(S)\}$. In the subsequent

text we will denote by $C_A$, $c_A$ a constant basically dependent on a quantity $A$ but always independent of the discretization parameters $h$ and $\triangle t$ whose definition we shall give later. We make the following assumption on the data:

*Assumption (A) (Data)*

*(A1)* $\beta \in C(\mathbb{R})$, $\beta(0) = 0$ *is a strictly increasing function such that*

$$|\beta(a) - \beta(b)| \geq c_\beta |a - b|\,, \quad c_\beta > 0$$

*for all* $a, b \in \mathbb{R}$

*or*

*(A2) in addition to (A1), there exists* $P \in \mathbb{R}, P > 0$, *such that* $|\beta(x)| \leq C_\beta$ *in* $[-P, P]$, $C_\beta > 0$, *and* $\beta$ *is Lipschitz-continuous with a constant* $L_\beta$ *on* $(-\infty, -P]$ *and* $[P, +\infty)$;

*(A3)* $\mathbf{S}_{ij} \in L^\infty(Q_T)$, $|\mathbf{S}_{ij}| \leq C_\mathbf{S}/d$ *a.e. in* $Q_T$, $1 \leq i, j \leq d$, $C_\mathbf{S} > 0$, $\mathbf{S}$ *is a symmetric and uniformly positive definite tensor for almost all* $t \in (0, T)$ *with a constant* $c_\mathbf{S} > 0$, *i.e.*

$$\mathbf{S}(\mathbf{x}, t)\boldsymbol{\eta} \cdot \boldsymbol{\eta} \geq c_\mathbf{S}\, \boldsymbol{\eta} \cdot \boldsymbol{\eta} \qquad \forall \boldsymbol{\eta} \in \mathbb{R}^d\,, \text{ for a.e. } (\mathbf{x}, t) \in Q_T\,;$$

*(A4)* $\mathbf{v} \in \mathbf{L}^2(0, T; \mathbf{H}(\mathrm{div}, \Omega)) \cap \mathbf{L}^\infty(Q_T)$ *satisfies* $\nabla \cdot \mathbf{v} = q_S \geq 0$ *a.e. in* $Q_T$, $|\mathbf{v} \cdot \mathbf{n}| \leq C_\mathbf{v}$, $C_\mathbf{v} > 0$, *a.e. on* $l \times (0, T)$ *for each hyperplane* $l \subset \Omega$ *with the normal vector* $\mathbf{n}$;

*(A5)* $\mu \geq 1$;

*(A6)* $F(0) = 0$, $F$ *is a nondecreasing, Lipschitz-continuous function with a constant* $L_F$

*or*

*(A7)* $F(0) = 0$, $F$ *is a Lipschitz-continuous function with a constant* $L_F$ *and* $xF(x) \geq 0$ *for* $x < 0$ *and* $x > M$, $M > 0$;

*(A8)* $q \in L^2(Q_T)$, *where* $q = q_S c_S$ *with* $c_S \in L^\infty(Q_T)$, $0 \leq c_S \leq M$ *a.e. in* $Q_T$;

*(A9)* $c_0 \in L^\infty(\Omega)$, $0 \leq c_0 \leq M$ *a.e. in* $\Omega$.

**Remark 1.2.1. (Hypotheses on $\beta$)** *In contaminant transport problems one typically has* $\beta(c) = c + c^\alpha, \alpha \in (0, 1)$. *Assumption (A1) generalizes this type of functions; we in particular do not limit the number of points where* $\beta'$ *explodes. As we shall see, we will be able to prove the convergence of the combined scheme with this assumption only for the case where the discrete maximum principle holds. In the general case we add Assumption (A2), which is however still satisfied by all realistic functions* $\beta$.

We now give the definition of a weak solution of (1.1)–(1.3), following essentially [83].

**Definition 1.2.2. (Weak solution)** *We say that a function* $c$ *is a weak solution of the problem (1.1)–(1.3) if*

$(i)$ $\quad c \in L^2(0, T; H_0^1(\Omega))\,,$

$(ii)$ $\quad \beta(c) \in L^\infty(0, T; L^2(\Omega))\,,$

$(iii)$ $\quad c$ *satisfies the integral equality*

$$-\int_0^T \int_\Omega \beta(c)\varphi_t \,\mathrm{d}\mathbf{x}\,\mathrm{d}t - \int_\Omega \beta(c_0)\varphi(\cdot, 0)\,\mathrm{d}\mathbf{x} + \int_0^T \int_\Omega \mathbf{S}\nabla c \cdot \nabla\varphi \,\mathrm{d}\mathbf{x}\,\mathrm{d}t -$$

$$-\mu \int_0^T \int_\Omega c\mathbf{v} \cdot \nabla\varphi \,\mathrm{d}\mathbf{x}\,\mathrm{d}t + \int_0^T \int_\Omega F(c)\varphi \,\mathrm{d}\mathbf{x}\,\mathrm{d}t = \int_0^T \int_\Omega q\varphi \,\mathrm{d}\mathbf{x}\,\mathrm{d}t$$

*for all* $\varphi \in L^2(0, T; H_0^1(\Omega))$ *with* $\varphi_t \in L^\infty(Q_T)$, $\varphi(\cdot, T) = 0\,.$

**Remark 1.2.3. (Existence of a weak solution)** *The existence of at least one weak solution is proved in Theorem 1.6.4 below.*

**Remark 1.2.4. (Uniqueness of a weak solution)** *For a slightly more restrictive hypothesis on the data than that given in Assumption (A), the uniqueness of a weak solution given by Definition 1.2.2 is guaranteed by [83]. Namely, no time-dependency of the diffusion–dispersion tensor* $\mathbf{S}$ *is still required in [83].*

## 1.3 Combined finite volume–nonconforming/mixed-hybrid finite element scheme

We will describe the space and time discretizations, define the approximation spaces, and introduce the combined finite volume–finite element scheme in this section.

### 1.3.1 Space and time discretizations

In order to discretize the problem (1.1)–(1.3), we perform a triangulation $\mathcal{T}_h$ of the domain $\Omega$, consisting of closed simplices such that $\overline{\Omega} = \bigcup_{K\in\mathcal{T}_h} K$ and such that if $K, L \in \mathcal{T}_h$, $K \neq L$, then $K \cap L$ is either an empty set or a common face, edge, or vertex of $K$ and $L$. We denote by $\mathcal{E}_h$ the set of all sides, by $\mathcal{E}_h^{\rm int}$ the set of all interior sides, by $\mathcal{E}_h^{\rm ext}$ the set of all exterior sides, and by $\mathcal{E}_K$ the set of all the sides of an element $K \in \mathcal{T}_h$. We define $h := \max_{K\in\mathcal{T}_h} \mathrm{diam}(K)$ and make the following shape regularity assumption on the family of triangulations $\{\mathcal{T}_h\}_h$:

*Assumption (B) (Shape regularity of the space mesh)*

*There exists a positive constant* $\kappa_{\mathcal{T}}$ *such that*

$$\min_{K\in\mathcal{T}_h} \frac{|K|}{\mathrm{diam}(K)^d} \geq \kappa_{\mathcal{T}} \qquad \forall h > 0\,.$$

Assumption *(B)* is equivalent to the more common requirement of the existence of a constant $\theta_{\mathcal{T}} > 0$ such that

$$\max_{K\in\mathcal{T}_h} \frac{\mathrm{diam}(K)}{\rho_K} \leq \theta_{\mathcal{T}} \qquad \forall h > 0\,, \tag{1.4}$$

where $\rho_K$ is the diameter of the largest ball inscribed in the simplex $K$.

We also use a dual partition $\mathcal{D}_h$ of $\Omega$ such that $\overline{\Omega} = \bigcup_{D\in\mathcal{D}_h} D$. There is one dual element $D$ associated with each side $\sigma_D \in \mathcal{E}_h$. We construct it by connecting the barycentres of every $K \in \mathcal{T}_h$ that contains $\sigma_D$ through the vertices of $\sigma_D$. For $\sigma_D \in \mathcal{E}_h^{\rm ext}$, the contour of $D$ is completed by the side $\sigma_D$ itself. We refer to Fig. 1.1 for the two-dimensional case. We denote by $Q_D$ the barycentre of the side $\sigma_D$. As for the primal mesh, we set $\mathcal{F}_h$, $\mathcal{F}_h^{\rm int}$, $\mathcal{F}_h^{\rm ext}$, and $\mathcal{F}_D$ for the dual mesh sides. We denote by $\mathcal{D}_h^{\rm int}$ the set of all interior and by $\mathcal{D}_h^{\rm ext}$ the set of all boundary dual volumes. We finally denote by $\mathcal{N}(D)$ the set of all adjacent volumes to the volume $D$,

$$\mathcal{N}(D) := \left\{E \in \mathcal{D}_h; \exists \sigma \in \mathcal{F}_h^{\rm int} \text{ such that } \sigma = \partial D \cap \partial E\right\}$$

and remark that

$$|K \cap D| = \frac{|K|}{d+1}\,, \tag{1.5}$$

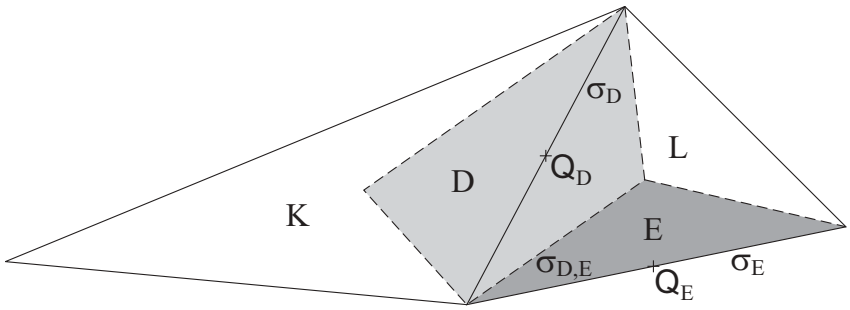


Figure 1.1: Triangles $K, L \in \mathcal{T}_h$ and dual volumes $D, E \in \mathcal{D}_h$ associated with edges $\sigma_D, \sigma_E \in \mathcal{E}_h$

for each $K \in \mathcal{T}_h$ and $D \in \mathcal{D}_h$ such that $\sigma_D \in \mathcal{E}_K$. For $E \in \mathcal{N}(D)$, we also set $d_{D,E} := |Q_E - Q_D|$, $\sigma_{D,E} := \partial D \cap \partial E$, and $K_{D,E}$ the element of $\mathcal{T}_h$ such that $\sigma_{D,E} \subset K_{D,E}$.

We suppose the partition of the time interval $(0,T)$ such that $0 = t_0 < \ldots < t_n < \ldots < t_N = T$ and define $\triangle t_n := t_n - t_{n-1}$ and $\triangle t := \max_{1\le n\le N} \triangle t_n$. In the case where Assumption *(A6)* is satisfied we do not impose any restriction on the time step. When only Assumption *(A7)* is satisfied, we suppose in addition:

*Assumption (C) (Maximum time step for decreasing $F$)*

*The following maximum time step condition is satisfied:*

$$\triangle t < \frac{c_\beta}{L_F}\,.$$

We define the following finite-dimensional spaces:

$$\begin{aligned} X_h &:= \big\{\varphi_h \in L^2(\Omega);\ \varphi_h|_K \text{ is linear } \forall K \in \mathcal{T}_h, \\ &\qquad \varphi_h \text{ is continuous at the points } Q_D, D \in \mathcal{D}_h^{\rm int}\big\}\,, \\ X_h^0 &:= \big\{\varphi_h \in X_h;\ \varphi_h(Q_D) = 0 \quad \forall D \in \mathcal{D}_h^{\rm ext}\big\}\,. \end{aligned}$$

The basis of $X_h$ is spanned by the shape functions $\varphi_D$, $D \in \mathcal{D}_h$, such that $\varphi_D(Q_E) = \delta_{DE}$, $E \in \mathcal{D}_h$, $\delta$ being the Kronecker delta. We recall that the approximations in these spaces are nonconforming since $X_h \not\subset H^1(\Omega)$. We equip $X_h$ with the seminorm

$$\|c_h\|_{X_h}^2 := \sum_{K\in\mathcal{T}_h} \int_K |\nabla c_h|^2 \,\mathrm{d}\mathbf{x}\,,$$

which becomes a norm on $X_h^0$. We have the following lemma:

**Lemma 1.3.1.** *For all $c_h = \sum_{D\in\mathcal{D}_h} c_D\varphi_D \in X_h$, one has*

$$\sum_{\sigma_{D,E}\in\mathcal{F}_h^{\rm int}} \mathrm{diam}(K_{D,E})^{d-2}(c_E - c_D)^2 \;\le\; \frac{d+1}{2d\kappa_{\mathcal{T}}}\|c_h\|_{X_h}^2\,, \tag{1.6}$$

$$\sum_{\sigma_{D,E}\in\mathcal{F}_h^{\rm int}} \frac{|\sigma_{D,E}|}{d_{D,E}}(c_E - c_D)^2 \;\le\; \frac{d+1}{2(d-1)\kappa_{\mathcal{T}}}\|c_h\|_{X_h}^2\,. \tag{1.7}$$

PROOF:
Obviously,

$$d_{D,E} \le \frac{\mathrm{diam}(K_{D,E})}{d}\,, \quad |\sigma_{D,E}| \le \frac{\mathrm{diam}(K_{D,E})^{d-1}}{d-1}\,. \tag{1.8}$$

Thus

$$\sum_{\sigma_{D,E}\in\mathcal{F}_h^{\mathrm{int}}} \mathrm{diam}(K_{D,E})^{d-2}(c_E-c_D)^2 \le \sum_{\sigma_{D,E}\in\mathcal{F}_h^{\mathrm{int}}} \mathrm{diam}(K_{D,E})^{d-2}\left|\nabla c_h|_{K_{D,E}}\right|^2 d_{D,E}^2$$
$$\le \frac{d+1}{2d}\sum_{K\in\mathcal{T}_h} \mathrm{diam}(K)^d\left|\nabla c_h|_K\right|^2 \le \frac{d+1}{2d\kappa_{\mathcal{T}}}\sum_{K\in\mathcal{T}_h}\left|\nabla c_h|_K\right|^2|K| = \frac{d+1}{2d\kappa_{\mathcal{T}}}\|c_h\|_{X_h}^2\,,$$

using the fact that the gradient of $c_h$ is piecewise constant on $\mathcal{T}_h$, (1.8), the fact that each simplex $K\in\mathcal{T}_h$ contains exactly $\binom{d+1}{2} = \frac{(d+1)d}{2}$ dual sides, and Assumption *(B)*. This proves (1.6). Similarly,

$$\sum_{\sigma_{D,E}\in\mathcal{F}_h^{\mathrm{int}}} \frac{|\sigma_{D,E}|}{d_{D,E}}(c_E-c_D)^2 \le \sum_{\sigma_{D,E}\in\mathcal{F}_h^{\mathrm{int}}}\left|\nabla c_h|_{K_{D,E}}\right|^2 d_{D,E}\,|\sigma_{D,E}| \le \frac{d+1}{2(d-1)\kappa_{\mathcal{T}}}\|c_h\|_{X_h}^2\,. \quad \square$$

### 1.3.2 The combined scheme

We are now ready to present the combined scheme.

**Definition 1.3.2. (Combined scheme)** *The fully implicit combined finite volume–nonconforming/mixed-hybrid finite element scheme for the problem (1.1)–(1.3) reads: find the values $c_D^n$, $D\in\mathcal{D}_h$, $n\in\{0,1,\ldots,N\}$, such that*

$$c_D^0 = \frac{1}{|D|}\int_D c_0(\mathbf{x})\,\mathrm{d}\mathbf{x} \qquad D\in\mathcal{D}_h^{\mathrm{int}}\,, \tag{1.9a}$$
$$c_D^n = 0 \qquad D\in\mathcal{D}_h^{\mathrm{ext}},\ n\in\{0,1,\ldots,N\}\,, \tag{1.9b}$$
$$\frac{\beta(c_D^n)-\beta(c_D^{n-1})}{\triangle t_n}|D| - \sum_{E\in\mathcal{D}_h^{\mathrm{int}}}\mathbb{S}_{D,E}^n\,c_E^n + \mu\sum_{E\in\mathcal{N}(D)}\mathbf{v}_{D,E}^n\,\overline{c_{D,E}^n} + F(c_D^n)|D| = q_D^n|D|$$
$$D\in\mathcal{D}_h^{\mathrm{int}}\,,\ n\in\{1,2,\ldots,N\}\,. \tag{1.9c}$$

In (1.9a)–(1.9c) we have denoted

$$\mathbf{v}_{D,E}^n := \frac{1}{\triangle t_n}\int_{t_{n-1}}^{t_n}\int_{\sigma_{D,E}}\mathbf{v}(\mathbf{x},t)\cdot\mathbf{n}_{D,E}\,\mathrm{d}\gamma(\mathbf{x})\,\mathrm{d}t \qquad D\in\mathcal{D}_h^{\mathrm{int}}\,,\ E\in\mathcal{N}(D)\,,\ n\in\{1,2,\ldots,N\}\,,$$

with $\mathbf{n}_{D,E}$ the unit normal vector of the side $\sigma_{D,E}\in\mathcal{F}_D$, outward to $D$, and

$$q_D^n := \frac{1}{\triangle t_n|D|}\int_{t_{n-1}}^{t_n}\int_D q(\mathbf{x},t)\,\mathrm{d}\mathbf{x}\,\mathrm{d}t \qquad D\in\mathcal{D}_h\,,\ n\in\{1,2,\ldots,N\}\,.$$

We refer to the matrix $\mathbb{S}^n$ of the elements $\mathbb{S}_{D,E}^n$, $D,E\in\mathcal{D}_h^{\mathrm{int}}$, at each discrete time $t_n$, $n\in\{1,2,\ldots,N\}$, as to the *diffusion matrix*. This matrix, the stiffness matrix of the nonconforming

or mixed-hybrid finite element method, is defined below. Finally, we define $\overline{c^n_{D,E}}$ for $D \in \mathcal{D}_h^{\rm int}$, $E \in \mathcal{N}(D)$, and $n \in \{1,2,\ldots,N\}$ as follows:

$$\overline{c^n_{D,E}} := \begin{cases} c^n_D + \alpha^n_{D,E}(c^n_E - c^n_D) & \text{if } \mathbf{v}^n_{D,E} \geq 0 \\ c^n_E + \alpha^n_{D,E}(c^n_D - c^n_E) & \text{if } \mathbf{v}^n_{D,E} < 0 \end{cases} . \tag{1.10}$$

Here $\alpha^n_{D,E}$ is the coefficient of the amount of upstream weighting which is defined by

$$\alpha^n_{D,E} := \frac{\max\left\{\min\left\{\mathbb{S}^n_{D,E}, \frac{1}{2}\mu|\mathbf{v}^n_{D,E}|\right\}, 0\right\}}{\mu|\mathbf{v}^n_{D,E}|}, \quad \mathbf{v}^n_{D,E} \neq 0\,. \tag{1.11}$$

We set $\alpha^n_{D,E} := 0$ if $\mathbf{v}^n_{D,E}$=0. We remark that $\overline{c^n_{D,E}} = \widehat{c^n_{D,E}} + \mathrm{sign}(\mathbf{v}^n_{D,E})\alpha^n_{D,E}(c^n_E - c^n_D)$, where $\widehat{c^n_{D,E}}$ stands for full upstream weighting.

**Remark 1.3.3. (Numerical flux)** *We can easily see from (1.11) that $0 \leq \alpha^n_{D,E} \leq 1/2$, i.e. the numerical flux defined by (1.10) ranges from the centered scheme to the full upstream weighting. The amount of upstream weighting is set with respect to the local proportion of convection and diffusion.*

**Remark 1.3.4. (Necessity to construct the dual mesh)** *If we know the values of the fluxes $\mathbf{v}^n_{D,E}$, sources $q^n_D$, and initial conditions $c^0_D$, we have no need to physically construct the dual mesh. Indeed, thanks to (1.5), expressing $|D|$ is immediate.*

We now turn to the definition of the diffusion matrix. To this purpose, we first set

$$\widetilde{\mathbf{S}}^n(\mathbf{x}) := \frac{1}{\triangle t_n}\int_{t_{n-1}}^{t_n} \mathbf{S}(\mathbf{x},t)\,\mathrm{d}t \qquad \mathbf{x} \in \Omega\,,\ n \in \{1,2,\ldots,N\}\,.$$

### Diffusion matrix from the nonconforming method

The diffusion matrix $\mathbb{S}^n$ given by the stiffness matrix $\mathbb{P}^n$ of the nonconforming method writes in the form

$$\mathbb{S}^n_{D,E} := \mathbb{P}^n_{D,E} = -\sum_{K\in\mathcal{T}_h} (\mathbf{S}^n\nabla\varphi_E, \nabla\varphi_D)_{0,K} \qquad D,E \in \mathcal{D}_h\,,\ n \in \{1,2,\ldots,N\}\,, \tag{1.12}$$

where

$$\mathbf{S}^n(\mathbf{x}) = \widetilde{\mathbf{S}}^n(\mathbf{x}) \qquad n \in \{1,2,\ldots,N\}\,,\ \mathbf{x} \in \Omega\,. \tag{1.13}$$

In fact, the members of $\mathbb{S}^n_{D,E}$ for $D \in \mathcal{D}_h^{\rm ext}$ or $E \in \mathcal{D}_h^{\rm ext}$ do not occur in the scheme (1.9a)–(1.9c). It will however show convenient to define these values.

### Diffusion matrix from the mixed-hybrid method

Using the analytic form of the stiffness matrix $\mathbb{M}^n$ of the mixed-hybrid method given in Lemma 1.8.1 in Appendix 1.8, we can define the diffusion matrix $\mathbb{S}^n$ by

$$\mathbb{S}^n_{D,E} := \mathbb{M}^n_{D,E} = -\sum_{K\in\mathcal{T}_h} (\mathbf{S}^n\nabla\varphi_E, \nabla\varphi_D)_{0,K} \qquad D,E \in \mathcal{D}_h\,,\ n \in \{1,2,\ldots,N\}\,, \tag{1.14}$$

where

$$\mathbf{S}^n(\mathbf{y}) = \Big(\frac{1}{|K|}\int_K [\widetilde{\mathbf{S}}^n(\mathbf{x})]^{-1}\,\mathrm{d}\mathbf{x}\Big)^{-1} \qquad \mathbf{y} \in K\,,\ K \in \mathcal{T}_h\,,\ n \in \{1,2,\ldots,N\}\,. \tag{1.15}$$

**Remark 1.3.5. (Stiffness matrices of nonconforming and mixed-hybrid methods)** *We remark that the stiffness matrix of the mixed-hybrid method (1.14) is the stiffness matrix of the nonconforming method (1.12) with a piecewise constant diffusion tensor, given as the inverse of the elementwise average of the inverse of the original one. In particular for an elementwise constant diffusion tensor, the stiffness matrices coincide, whereas for a general diffusion tensor, (1.12) uses its arithmetic and (1.14) its harmonic average.*

**Remark 1.3.6. (Comparison with a pure finite volume scheme)** *Let us consider $\mathcal{T}_h$ consisting of equilateral simplices and $\mathbf{S} = Id$. Then the segments $[Q_D, Q_E]$ are orthogonal to the dual sides $\sigma_{D,E}$ and one has $\mathbb{P}^n_{D,E} = \mathbb{M}^n_{D,E} = \frac{|\sigma_{D,E}|}{d_{D,E}}$, $E \in \mathcal{N}(D)$. Thus, in view of Corollary 1.4.2 below, the pure cell-centered finite volume scheme completely coincides in this case with the combined one. One may regard in this sense the combined scheme as an extension of the pure finite volume scheme to general triangulations and full-matrix diffusion tensors, which does not extend the original 5-point (7-point in space dimension three) stencil.*

**Remark 1.3.7. (Comparison of a combined finite volume–finite element scheme with pure finite volume schemes)** *We recall here that for triangular meshes, the discretization of a Laplacian by the piecewise linear conforming finite element method coincides with that by the vertex-centered finite volume method [6, 96], which is also named the box scheme [17, 71], the finite volume element scheme [35, 56], or control volume finite element scheme [68, 114], see [17, Lemma 3]. Finally, for Delaunay triangulations (the sums of two opposite angles to all edges are less or equal to $\pi$), constructing the control volumes with the aid of orthogonal bisectors, these discretizations are equivalent to that by the cell-centered finite volume method, see [61, Section III.12], cf. also [76, 112]. Hence, when $\mathbf{S} = Id$ and for a Delaunay triangular mesh with the above construction of control volumes, the combined finite volume–finite element scheme [67, 90], the vertex-centered finite volume scheme [6, 96], and the cell-centered finite volume scheme [61, 62] for the discretization of (1.1) coincide.*

In the sequel we shall consider apart the following special case:

*Assumption (D) (Diffusion matrix)*

*All transmissibilities are non-negative, i.e.*

$$\mathbb{S}^n_{D,E} \geq 0 \qquad \forall\, D \in \mathcal{D}_h^{\rm int}\,,\ E \in \mathcal{N}(D) \qquad \forall n \in \{1, 2, \ldots, N\}\,.$$

Since

$$\nabla \varphi_D|_K = \frac{|\sigma_D|}{|K|}\mathbf{n}_{\sigma_D} \qquad K \in \mathcal{T}_h\,,\ \sigma_D \in \mathcal{E}_K \tag{1.16}$$

with $\mathbf{n}_{\sigma_D}$ the unit normal vector of the side $\sigma_D$, outward to $K$, one can immediately see that Assumption *(D)* is satisfied e.g. when the diffusion tensor reduces to a scalar function and when the magnitude of the angles between $\mathbf{n}_{\sigma_D}$, $\sigma_D \in \mathcal{E}_K$, for all $K \in \mathcal{T}_h$ is greater or equal to $\pi/2$.

## 1.4 Existence, uniqueness, and discrete properties

In this section we first present some technical lemmas. We then show the conservativity of the scheme, the coercivity of the bilinear diffusion form corresponding to the diffusion term, and an a priori estimate for an extended scheme, which we shall need later in the proof of the existence of the solution of the discrete problem. Finally, we prove the uniqueness of this solution and the discrete maximum principle when Assumption *(D)* is satisfied.

### 1.4.1 Discrete properties of the scheme

**Lemma 1.4.1.** *For all $D \in \mathcal{D}_h$ and $n \in \{1, 2, \ldots, N\}$, $\mathbb{S}^n_{D,D} = -\sum_{E \in \mathcal{N}(D)} \mathbb{S}^n_{D,E}$.*

Proof:

We will show the assertion for $d = 2$; the case $d = 3$ is similar. We present the proof for the nonconforming method, which in view of Remark 1.3.5 implies the same result for the mixed-hybrid method. Let us consider a fixed dual volume $D \in \mathcal{D}_h$. The edge $\sigma_D$ associated with $D$ is shared by at most two triangles, which we denote by $K$ and $L$. The sum over $K \in \mathcal{T}_h$ in (1.12) for $\mathbb{S}^n_{D,D}$ reduces just to these triangles, considering the definition of the basis function $\varphi_D$. We denote the dual volumes associated with the two other edges of $L$ by $E_1$ and $E_2$. Similarly, the sum over $K \in \mathcal{T}_h$ in (1.12) for $\mathbb{S}^n_{D,E_1}$ and $\mathbb{S}^n_{D,E_2}$ reduces to $L$. Thus it is sufficient to prove that

$$-(\mathbf{S}^n \nabla\varphi_D, \nabla\varphi_D)_{0,L} = (\mathbf{S}^n \nabla\varphi_{E_1}, \nabla\varphi_D)_{0,L} + (\mathbf{S}^n \nabla\varphi_{E_2}, \nabla\varphi_D)_{0,L}\,,$$

since the eventual contribution of the element $K$ is similar. However, this is immediate, since

$$-\varphi_D|_L = (\varphi_{E_1} + \varphi_{E_2})|_L - 1\,. \quad \square$$

**Corollary 1.4.2.** *Using the fact that $\mathbb{S}^n_{D,E} \neq 0$ only if $E \in \mathcal{N}(D)$ or if $E = D$ and Lemma 1.4.1, one has*

$$\sum_{E \in \mathcal{D}_h} \mathbb{S}^n_{D,E}\, c^n_E = \sum_{E \in \mathcal{N}(D)} \mathbb{S}^n_{D,E} c^n_E + \mathbb{S}^n_{D,D} c^n_D = \sum_{E \in \mathcal{N}(D)} \mathbb{S}^n_{D,E}(c^n_E - c^n_D)\,.$$

**Theorem 1.4.3. (Conservativity of the scheme)** *The scheme (1.9a)–(1.9c) is conservative with respect to the dual mesh $\mathcal{D}_h$.*

Proof:

Let us take two fixed neighboring dual volumes $E$ and $D$, $D \in \mathcal{D}_h^{\mathrm{int}}$. Using Corollary 1.4.2 and (1.9b), we can express the discrete diffusive flux from $D$ to $E$ as $-\mathbb{S}^n_{D,E}(c^n_E - c^n_D)$. The discrete diffusive flux from $E$ to $D$ is $-\mathbb{S}^n_{E,D}(c^n_D - c^n_E)$, i.e. we have their equality up to the sign, considering that $\mathbb{S}^n_{D,E} = \mathbb{S}^n_{E,D}$ for all $n \in \{1, 2, \ldots, N\}$, which follows from (1.12) or (1.14) using the symmetry of the tensor $\mathbf{S}$.

For the discrete convective flux from $D$ to $E$, we have $\mu\, \mathbf{v}^n_{D,E}[c^n_D + \alpha^n_{D,E}(c^n_E - c^n_D)]$, supposing $\mathbf{v}^n_{D,E} \geq 0$. For the discrete convective flux from $E$ to $D$, we have $\mu\, \mathbf{v}^n_{E,D}[c^n_D + \alpha^n_{E,D}(c^n_E - c^n_D)]$, i.e. again the equality up to the sign, considering that $\mathbf{v}^n_{D,E} = -\mathbf{v}^n_{E,D}$ and that $\alpha^n_{D,E} = \alpha^n_{E,D}$, which follows from $\mathbb{S}^n_{D,E} = \mathbb{S}^n_{E,D}$. For $\mathbf{v}^n_{D,E} < 0$, the proof is similar. Hence the combined finite volume–finite element scheme is conservative as the pure finite volume is, cf. [61]. $\square$

**Lemma 1.4.4.** *For all $D \in \mathcal{D}_h^{\mathrm{int}}$ and $n \in \{1, 2, \ldots, N\}$,*

$$\sum_{E \in \mathcal{N}(D)} \mathbf{v}^n_{D,E}\, \widehat{c^n_{D,E}} = \sum_{E \in \mathcal{N}(D)} (\mathbf{v}^n_{D,E})^-(c^n_E - c^n_D) + (q_S)^n_D c^n_D |D|\,,$$

*where $(\mathbf{v}^n_{D,E})^- := \min\{\mathbf{v}^n_{D,E}, 0\}$ and*

$$(q_S)^n_D := \frac{1}{\triangle t_n |D|} \int_{t_{n-1}}^{t_n} \int_D q_S(\mathbf{x}, t)\, \mathrm{d}\mathbf{x}\, \mathrm{d}t \qquad \forall D \in \mathcal{D}_h\,,\ \forall n \in \{1, 2, \ldots, N\}\,.$$

PROOF:
Considering that $\mathbf{v}_{D,E}^n = (\mathbf{v}_{D,E}^n)^+ + (\mathbf{v}_{D,E}^n)^-$, where $(\mathbf{v}_{D,E}^n)^+ := \max\{\mathbf{v}_{D,E}^n, 0\}$, we have

$$\begin{aligned}
\sum_{E\in\mathcal{N}(D)} \mathbf{v}_{D,E}^n \widehat{c_{D,E}^n} &= \sum_{E\in\mathcal{N}(D)} (\mathbf{v}_{D,E}^n)^+ c_D^n + \sum_{E\in\mathcal{N}(D)} (\mathbf{v}_{D,E}^n)^- c_E^n \\
&= \sum_{E\in\mathcal{N}(D)} \mathbf{v}_{D,E}^n\, c_D^n + \sum_{E\in\mathcal{N}(D)} (\mathbf{v}_{D,E}^n)^-(c_E^n - c_D^n) \\
&= c_D^n \frac{1}{\triangle t_n} \int_{t_{n-1}}^{t_n} \sum_{E\in\mathcal{N}(D)} \int_{\sigma_{D,E}} \mathbf{v}(\mathbf{x},t)\cdot\mathbf{n}_{D,E}\,\mathrm{d}\gamma(\mathbf{x})\,\mathrm{d}t \\
&\quad + \sum_{E\in\mathcal{N}(D)} (\mathbf{v}_{D,E}^n)^-(c_E^n - c_D^n) = c_D^n \frac{1}{\triangle t_n} \int_{t_{n-1}}^{t_n} \int_D \nabla\cdot\mathbf{v}(\mathbf{x},t)\,\mathrm{d}\mathbf{x}\,\mathrm{d}t \\
&\quad + \sum_{E\in\mathcal{N}(D)} (\mathbf{v}_{D,E}^n)^-(c_E^n - c_D^n) = c_D^n (q_S)_D^n |D| \\
&\quad + \sum_{E\in\mathcal{N}(D)} (\mathbf{v}_{D,E}^n)^-(c_E^n - c_D^n)\,,
\end{aligned}$$

using Assumption *(A4)*. □

**Lemma 1.4.5.** *For all* $c_h = \sum_{D\in\mathcal{D}_h} c_D\varphi_D \in X_h$ *and* $n \in \{1,2,\ldots,N\}$,

$$-\sum_{D\in\mathcal{D}_h} c_D \sum_{E\in\mathcal{D}_h} \mathbb{S}_{D,E}^n c_E \geq c_{\mathbf{S}} \|c_h\|_{X_h}^2\,.$$

PROOF:
We have

$$-\sum_{D\in\mathcal{D}_h} c_D \sum_{E\in\mathcal{D}_h} \mathbb{S}_{D,E}^n c_E = \sum_{K\in\mathcal{T}_h} (\mathbf{S}^n \nabla c_h, \nabla c_h)_{0,K} \geq c_{\mathbf{S}} \|c_h\|_{X_h}^2\,,$$

using (1.12) or (1.14) and Assumption *(A3)* and the subsequent uniform positive definiteness of the diffusion tensors (1.13) and (1.15). □

**Lemma 1.4.6.** *For all* $c_h = \sum_{D\in\mathcal{D}_h} c_D\varphi_D \in X_h$ *and* $n \in \{1,2,\ldots,N\}$,

$$\Big|-\sum_{D\in\mathcal{D}_h} c_D \sum_{E\in\mathcal{D}_h} \mathbb{S}_{D,E}^n c_E\Big| \leq C_{\mathbf{S}} \|c_h\|_{X_h}^2\,. \tag{1.17}$$

*Moreover, for all* $D \in \mathcal{D}_h$, $E \in \mathcal{N}(D)$, *and* $n \in \{1,2,\ldots,N\}$,

$$|\mathbb{S}_{D,E}^n| \leq \frac{C_{\mathbf{S}}}{\kappa_{\mathcal{T}}} \frac{\operatorname{diam}(K_{D,E})^{d-2}}{(d-1)^2}\,. \tag{1.18}$$

PROOF:
We have

$$\Big|-\sum_{D\in\mathcal{D}_h} c_D \sum_{E\in\mathcal{D}_h} \mathbb{S}_{D,E}^n c_E\Big| = \Big|\sum_{K\in\mathcal{T}_h} (\mathbf{S}^n \nabla c_h, \nabla c_h)_{0,K}\Big| \leq C_{\mathbf{S}} \|c_h\|_{X_h}^2\,,$$

using (1.12) or (1.14), Assumption *(A3)*, and (1.13) or (1.15). Considering (1.12) or (1.14), where the sum reduces just to $K_{D,E} \in \mathcal{T}_h$ for $E \in \mathcal{N}(D)$, the equality (1.16), $|\sigma_D|, |\sigma_E| \le \operatorname{diam}(K_{D,E})^{d-1}/(d-1)$, and Assumption *(B)*, we have

$$\begin{aligned} |\mathbb{S}_{D,E}^n| &\le C_{\mathbf{S}} \Big|\nabla\varphi_E|_{K_{D,E}}\Big| \Big|\nabla\varphi_D|_{K_{D,E}}\Big| |K_{D,E}| = C_{\mathbf{S}} \frac{|\sigma_E|}{|K_{D,E}|} \frac{|\sigma_D|}{|K_{D,E}|} |K_{D,E}| \\ &\le C_{\mathbf{S}} \frac{\operatorname{diam}(K_{D,E})^{2d-2}}{(d-1)^2 |K_{D,E}|} \le \frac{C_{\mathbf{S}}}{\kappa_{\mathcal{T}}} \frac{\operatorname{diam}(K_{D,E})^{d-2}}{(d-1)^2}. \quad \square \end{aligned}$$

**Lemma 1.4.7.** *For all values $c_D$, $D \in \mathcal{D}_h$, such that $c_D = 0$ for all $D \in \mathcal{D}_h^{\mathrm{ext}}$ and $n \in \{1, 2, \dots, N\}$,*

$$\sum_{D \in \mathcal{D}_h^{\mathrm{int}}} c_D \sum_{E \in \mathcal{N}(D)} \mathbf{v}_{D,E}^n \, \overline{c_{D,E}} \ge 0 \,.$$

Proof:

We can write

$$\begin{aligned} &\sum_{D \in \mathcal{D}_h^{\mathrm{int}}} c_D \sum_{E \in \mathcal{N}(D)} \mathbf{v}_{D,E}^n \, \overline{c_{D,E}} \\ &= \sum_{\sigma_{D,E} \in \mathcal{F}_h^{\mathrm{int}}, \mathbf{v}_{D,E}^n \ge 0} \mathbf{v}_{D,E}^n \Big( c_D(c_D - c_E) - \alpha_{D,E}^n (c_E - c_D)^2 \Big) \\ &= \frac{1}{2} \sum_{\sigma_{D,E} \in \mathcal{F}_h^{\mathrm{int}}, \mathbf{v}_{D,E}^n \ge 0} \mathbf{v}_{D,E}^n (c_D^2 - c_E^2) + \sum_{\sigma_{D,E} \in \mathcal{F}_h^{\mathrm{int}}} |\mathbf{v}_{D,E}^n| (c_E - c_D)^2 \Big( \frac{1}{2} - \alpha_{D,E}^n \Big) \\ &\ge \frac{1}{2} \sum_{D \in \mathcal{D}_h^{\mathrm{int}}} c_D^2 \sum_{E \in \mathcal{N}(D)} \mathbf{v}_{D,E}^n = \frac{1}{2} \sum_{D \in \mathcal{D}_h^{\mathrm{int}}} c_D^2 (q_S)_D^n |D| \ge 0 \,, \end{aligned}$$

where we have used the fact that $c_D = 0$ for all $D \in \mathcal{D}_h^{\mathrm{ext}}$, the relation $2(a-b)a = (a-b)^2 + a^2 - b^2$, and rewritten the summation over interior dual sides with fixed denotation of the dual volumes sharing given side $\sigma_{D,E}$ such that $\mathbf{v}_{D,E}^n \ge 0$. In the last two estimates we have used, respectively, the fact that $0 \le \alpha_{D,E}^n \le 1/2$, which follows from (1.11), and Assumption *(A4)*. $\square$

**Theorem 1.4.8. (A priori estimate for an extended scheme)** *Let us define an extended scheme by*

$$c_D^0 = \frac{1}{|D|} \int_D c_0(\mathbf{x}) \, \mathrm{d}\mathbf{x} \qquad D \in \mathcal{D}_h^{\mathrm{int}} \,, \tag{1.19a}$$

$$c_D^n = 0 \qquad D \in \mathcal{D}_h^{\mathrm{ext}}, \, n \in \{0, 1, \dots, N\} \,, \tag{1.19b}$$

$$\begin{aligned} &u \frac{\beta(c_D^n) - \beta(c_D^{n-1})}{\triangle t_n} |D| - \sum_{E \in \mathcal{D}_h^{\mathrm{int}}} \mathbb{S}_{D,E}^n \, c_E^n + u \, \mu \sum_{E \in \mathcal{N}(D)} \mathbf{v}_{D,E}^n \, \overline{c_{D,E}^n} + u \, F(c_D^n) |D| \\ &\qquad = u \, q_D^n |D| \qquad D \in \mathcal{D}_h^{\mathrm{int}}, \, n \in \{1, 2, \dots, N\} \end{aligned} \tag{1.19c}$$

*with $u \in [0, 1]$. Let $\delta > 0$ be arbitrary. Then*

$$\sum_{D \in \mathcal{D}_h} (c_D^n)^2 |D| < C_{\mathrm{es}} \qquad \forall n \in \{1, 2, \dots, N\}$$

*with*

$$C_{\rm es} := \frac{4}{c_\beta} M\beta(M)|\Omega| + \frac{4T}{c_\beta^2}\|q\|_{0,Q_T}^2 + \frac{4}{c_\beta} L_F M^2 T|\Omega| + \delta\,.$$

Proof:

We multiply (1.19c) by $\triangle t_n c_D^n$, sum over all $D \in \mathcal{D}_h^{\rm int}$ and $n \in \{1, 2, \ldots, k\}$, and use the fact that $u \geq 0$ and Lemmas 1.4.5 and 1.4.7. Further, for $c_D^n < 0$ or $c_D^n > M$, $F(c_D^n)c_D^n \geq 0$ follows from Assumption *(A6)* or *(A7)*. When $0 \leq c_D^n \leq M$, $-F(c_D^n)c_D^n \leq |F(c_D^n)||c_D^n| \leq L_F M^2$, which altogether yields

$$\begin{aligned} &u\sum_{n=1}^{k}\sum_{D\in\mathcal{D}_h^{\rm int}} [\beta(c_D^n) - \beta(c_D^{n-1})]c_D^n|D| + c_{\mathbf{S}}\sum_{n=1}^{k}\triangle t_n\|c_h^n\|_{X_h}^2 \\ &\leq u\sum_{n=1}^{k}\triangle t_n \sum_{D\in\mathcal{D}_h^{\rm int}} c_D^n q_D^n\ |D| + uL_F M^2\sum_{n=1}^{k}\sum_{D\in\mathcal{D}_h^{\rm int}}\triangle t_n|D| \end{aligned} \tag{1.20}$$

with $c_h^n = \sum_{D\in\mathcal{D}_h} c_D^n\varphi_D$. Let us now introduce a function $B$,

$$B(s) := \beta(s)s - \int_0^s \beta(\tau)\,{\rm d}\tau \qquad s \in \mathbb{R}\,.$$

One then can derive

$$B(c_D^n) - B(c_D^{n-1}) = [\beta(c_D^n) - \beta(c_D^{n-1})]c_D^n - \int_{c_D^{n-1}}^{c_D^n}[\beta(\tau) - \beta(c_D^{n-1})]\,{\rm d}\tau\,.$$

Using that $\beta$ is nondecreasing, one can easily show that

$$\int_{c_D^{n-1}}^{c_D^n}[\beta(\tau) - \beta(c_D^{n-1})]\,{\rm d}\tau \geq 0\,.$$

In view of the two last expressions, one has

$$\sum_{n=1}^{k}\sum_{D\in\mathcal{D}_h^{\rm int}}[B(c_D^n) - B(c_D^{n-1})]|D| \leq \sum_{n=1}^{k}\sum_{D\in\mathcal{D}_h^{\rm int}}[\beta(c_D^n) - \beta(c_D^{n-1})]c_D^n|D|\,,$$

which yields

$$\sum_{D\in\mathcal{D}_h^{\rm int}} B(c_D^k)|D| - \sum_{D\in\mathcal{D}_h^{\rm int}} B(c_D^0)|D| \leq \sum_{n=1}^{k}\sum_{D\in\mathcal{D}_h^{\rm int}}[\beta(c_D^n) - \beta(c_D^{n-1})]c_D^n|D|\,.$$

Using the growth condition on $\beta$ from Assumption *(A1)*, one can derive $B(s) \geq s^2 c_\beta/2$ for all $s \in \mathbb{R}$, see Lemma 1.8.2 in Appendix 1.8. Thus, using in addition Assumption *(A9)*

$$\frac{c_\beta}{2}\sum_{D\in\mathcal{D}_h^{\rm int}}(c_D^k)^2|D| - M\beta(M)|\Omega| \leq \sum_{n=1}^{k}\sum_{D\in\mathcal{D}_h^{\rm int}}[\beta(c_D^n) - \beta(c_D^{n-1})]c_D^n\ |D|\,.$$

We notice that

$$\sum_{n=1}^{N}\sum_{D\in\mathcal{D}_h}\triangle t_n|D|(q_D^n)^2 \le \|q\|_{0,Q_T}^2 \tag{1.21}$$

by the Cauchy–Schwarz inequality. Hence extending the summation over all $n\in\{1,2,\dots,N\}$ and $D\in\mathcal{D}_h$ in the first term of the right-hand side of (1.20) and using the Cauchy–Schwarz and Young inequality, we have

$$\begin{aligned}\sum_{n=1}^{k}\triangle t_n\sum_{D\in\mathcal{D}_h^{\rm int}}c_D^n q_D^n\,|D| &\le \Big(\sum_{n=1}^{N}\triangle t_n\sum_{D\in\mathcal{D}_h}(c_D^n)^2|D|\Big)^{\frac12}\|q\|_{0,Q_T}\\ &\le \frac{\varepsilon}{2}\sum_{n=1}^{N}\triangle t_n\sum_{D\in\mathcal{D}_h}(c_D^n)^2|D| + \frac{1}{2\varepsilon}\|q\|_{0,Q_T}^2\,.\end{aligned}$$

Hence, substituting these estimates into (1.20), we obtain

$$\begin{aligned}&u\frac{c_\beta}{2}\max_{n\in\{1,2,\dots,N\}}\sum_{D\in\mathcal{D}_h}(c_D^n)^2|D| + c_{\mathbf{S}}\sum_{n=1}^{k}\triangle t_n\|c_h^n\|_{X_h}^2 \le uM\beta(M)|\Omega|\\ &+u\frac{\varepsilon}{2}T\max_{n\in\{1,2,\dots,N\}}\sum_{D\in\mathcal{D}_h}(c_D^n)^2|D| + u\frac{1}{2\varepsilon}\|q\|_{0,Q_T}^2 + uL_FM^2T|\Omega|\,,\end{aligned} \tag{1.22}$$

considering also (1.19b) and the fact that $k$ was arbitrarily chosen. We now choose $\varepsilon = c_\beta/(2T)$. When $u\neq 0$, this already yields the assertion of the lemma. When $u=0$, it follows from (1.22) that $c_D^n=0$ for all $D\in\mathcal{D}_h$ and all $n\in\{1,2,\dots,N\}$, since in view of (1.19b), $\|\cdot\|_{X_h}$ is a norm on $X_h$. Thus the assertion of the lemma is trivially satisfied in this case. □

### 1.4.2 Existence, uniqueness, and the discrete maximum principle

**Theorem 1.4.9. (Existence of the solution of the discrete problem)** *The problem (1.9a)–(1.9c) has at least one solution.*

Proof:

The nonlinear system of equations given by (1.9b)–(1.9c) on each discrete time level $t_n$, $n\in\{1,2,\dots,N\}$, can be written as

$$\mathcal{P}(C^n) - \mathbb{S}^nC^n + \mathbb{C}^nC^n + \mathcal{R}(C^n) = \mathcal{P}(C^{n-1}) + Q^n\,, \tag{1.23}$$

where $C^n\in\mathbb{R}^{|\mathcal{D}_h^{\rm int}|}$ ($|\mathcal{D}_h^{\rm int}|$ is the cardinality of the set $\mathcal{D}_h^{\rm int}$) is the vector of discrete unknowns $c_D^n$, $D\in\mathcal{D}_h^{\rm int}$, $\mathbb{S}^n$, the diffusion matrix, and $\mathbb{C}^n$, the discretization of the convective term, are linear mappings from $\mathbb{R}^{|\mathcal{D}_h^{\rm int}|}$ to $\mathbb{R}^{|\mathcal{D}_h^{\rm int}|}$, $\mathcal{P}$ and $\mathcal{R}$ are, due to the continuity of $\beta$ and $F$ following from Assumption *(A1)*, *(A6)*, respectively, continuous mappings from $\mathbb{R}^{|\mathcal{D}_h^{\rm int}|}$ to $\mathbb{R}^{|\mathcal{D}_h^{\rm int}|}$, $Q^n\in\mathbb{R}^{|\mathcal{D}_h^{\rm int}|}$ is a constant vector, and $C^{n-1}\in\mathbb{R}^{|\mathcal{D}_h^{\rm int}|}$ is the vector of discrete values $c_D^{n-1}$ on the previous time step. The vector $C^0$ is given by (1.9a). By Lemma 1.4.5 and (1.9b), $-\mathbb{S}^n$ is a positive definite and consequently invertible matrix. Thus also $\mathbb{S}^n$ is an invertible matrix. Hence, (1.23) is equivalent to

$$C^n = G(C^n) := [\mathbb{S}^n]^{-1}[\mathcal{P}(C^n) + \mathbb{C}^nC^n + \mathcal{R}(C^n) - \mathcal{P}(C^{n-1}) - Q^n]\,. \tag{1.24}$$

Let $H(u, C^n) = u\, G(C^n)$ for $u \in [0,1]$ and $C^n \in \mathbb{R}^{|\mathcal{D}_h^{\rm int}|}$. $H$ is a continuous mapping from $[0,1] \times \mathbb{R}^{|\mathcal{D}_h^{\rm int}|}$ to $\mathbb{R}^{|\mathcal{D}_h^{\rm int}|}$. If we now consider the norm $|C^n| = \sum_{D \in \mathcal{D}_h^{\rm int}} (c_D^n)^2 |D|$ on $\mathbb{R}^{|\mathcal{D}_h^{\rm int}|}$, we have from Theorem 1.4.8 that

$$|C^n| < C_{\rm es} \quad \text{for all } (u, C^n) \in [0,1] \times \mathbb{R}^{|\mathcal{D}_h^{\rm int}|} \text{ such that } C^n = H(u, C^n).$$

Therefore $C^n = H(u, C^n)$ has no solution lying on the boundary of the ball $B_{C_{\rm es}} := \{C^n \in \mathbb{R}^{|\mathcal{D}_h^{\rm int}|}, |C^n| < C_{\rm es}\}$ for $u \in [0,1]$. We thus can define for $u \in [0,1]$ the (Brouwer) topological degree of the application $Id - H(u,\cdot)$ with respect to the ball $B_{C_{\rm es}}$ and right-hand side 0, denoted by $d(Id - H(u,\cdot), B_{C_{\rm es}}, 0)$. Then, the homotopy invariance of the degree ([49], Theorem 3.1 (d3)) leads to

$$d(Id - H(u,\cdot), B_{C_{\rm es}}, 0) = d(Id - H(0,\cdot), B_{C_{\rm es}}, 0)$$

for all $u \in [0,1]$. Since $H(0, C^n)$ is a zero vector for all $C^n \in \mathbb{R}^{|\mathcal{D}_h^{\rm int}|}$, one has $d(Id - H(0,\cdot), B_{C_{\rm es}}, 0) = d(Id, B_{C_{\rm es}}, 0) = 1$, and thus there exists $C^n \in \mathbb{R}^{|\mathcal{D}_h^{\rm int}|}$ such that $C^n - H(1, C^n) = 0$, i.e. $C^n$ is the solution to (1.24). This proves the existence of a solution to (1.9b)–(1.9c) at each discrete time level $t_n$, $n \in \{1, 2, \ldots, N\}$. □

**Theorem 1.4.10. (Uniqueness of the solution of the discrete problem)** *The solution of the problem (1.9a)–(1.9c) is unique.*

Proof:

We will prove the assertion by contradiction. Let us thus suppose that there exists $n \in \{1, 2, \ldots, N\}$ such that $c_D^{n-1} = \tilde{c}_D^{n-1}$ for all $D \in \mathcal{D}_h^{\rm int}$ but $c_D^n \neq \tilde{c}_D^n$ for some $D \in \mathcal{D}_h^{\rm int}$. After subtracting the equation (1.9c) for $c_D^n$ and $\tilde{c}_D^n$ and denoting $s_D^n := c_D^n - \tilde{c}_D^n$, we have

$$\frac{\beta(c_D^n) - \beta(\tilde{c}_D^n)}{\triangle t_n}\, |D| - \sum_{E \in \mathcal{D}_h^{\rm int}} \mathbb{S}_{D,E}^n\, s_E^n + \mu \sum_{E \in \mathcal{N}(D)} \mathbf{v}_{D,E}^n\, \overline{s_{D,E}^n}$$
$$+ F(c_D^n)\, |D| - F(\tilde{c}_D^n)\, |D| = 0 \qquad D \in \mathcal{D}_h^{\rm int}\,.$$

We now multiply the above equality by $s_D^n$ and sum the result over $D \in \mathcal{D}_h^{\rm int}$. This yields, using Lemmas 1.4.5 and 1.4.7,

$$\sum_{D \in \mathcal{D}_h^{\rm int}} [\beta(c_D^n) - \beta(\tilde{c}_D^n)](c_D^n - \tilde{c}_D^n) \frac{|D|}{\triangle t_n} + \sum_{D \in \mathcal{D}_h^{\rm int}} [F(c_D^n) - F(\tilde{c}_D^n)](c_D^n - \tilde{c}_D^n)\, |D| \leq 0\,.$$

When Assumption *(A6)* is satisfied, this is already a contradiction, since from Assumption *(A1)*, $\beta$ is strictly increasing and $F$ is nondecreasing in this case.

When only Assumption *(A7)* is satisfied, we have $|-[F(c_D^n) - F(\tilde{c}_D^n)](c_D^n - \tilde{c}_D^n)| \leq L_F (c_D^n - \tilde{c}_D^n)^2$. In view of Assumption *(A1)*, $[\beta(c_D^n) - \beta(\tilde{c}_D^n)](c_D^n - \tilde{c}_D^n) \geq c_\beta (c_D^n - \tilde{c}_D^n)^2$. Since

$$\sum_{D \in \mathcal{D}_h^{\rm int}} (c_D^n - \tilde{c}_D^n)^2 |D| \neq 0\,,$$

$c_\beta / L_F \leq \triangle t_n$, which is a contradiction with Assumption *(C)* supposed in this case. □

**Theorem 1.4.11. (Discrete maximum principle)** *Under Assumption (D), the solution of the problem (1.9a)–(1.9c) satisfies*

$$0 \le c_D^n \le M$$

*for all* $D \in \mathcal{D}_h$, $n \in \{1, 2, \ldots, N\}$.

Proof:

Setting $\mathbb{T}_{D,E}^n := \mathbb{S}_{D,E}^n - \mu |\mathbf{v}_{D,E}^n| \alpha_{D,E}^n$, $E \in \mathcal{N}(D)$, and using Corollary 1.4.2 and Lemma 1.4.4, we can rewrite (1.9c) as

$$\begin{aligned} &\frac{\beta(c_D^n) - \beta(c_D^{n-1})}{\triangle t_n} |D| - \sum_{E \in \mathcal{N}(D)} \mathbb{T}_{D,E}^n (c_E^n - c_D^n) + \mu \sum_{E \in \mathcal{N}(D)} (\mathbf{v}_{D,E}^n)^- (c_E^n - c_D^n) \\ &+ \mu (q_S)_D^n c_D^n |D| + F(c_D^n) \, |D| = q_D^n \, |D| \qquad D \in \mathcal{D}_h^{\rm int} \,, \, n \in \{1, 2, \ldots, N\} \,. \end{aligned} \tag{1.25}$$

In view of Assumption *(D)* and (1.11), one has $\mathbb{T}_{D,E}^n \ge 0$ for all $D \in \mathcal{D}_h^{\rm int}$, $E \in \mathcal{N}(D)$, and $n \in \{1, 2, \ldots, N\}$. We now make use of an induction argument. We remark that $0 \le c_D^n \le M$ is satisfied for $n = 0$ by Assumption *(A9)* and (1.9a) and (1.9b). Let us suppose that $0 \le c_D^{n-1} \le M$ for all $D \in \mathcal{D}_h^{\rm int}$ and for a fixed $(n-1) \in \{0, 1, \ldots, N-1\}$. Since $|\mathcal{D}_h|$ is finite, there exist $D_0, D_1 \in \mathcal{D}_h$ such that $c_{D_0}^n \le c_D^n \le c_{D_1}^n$ for all $D \in \mathcal{D}_h$. Using a contradiction argument we prove below that $c_{D_0}^n \ge 0$ and $c_{D_1}^n \le M$. Suppose that $c_{D_0}^n < 0$. We remark that $D_0 \in \mathcal{D}_h^{\rm int}$ because of (1.9b). Then, since $\mathbb{T}_{D_0,E}^n \ge 0$ and $-(\mathbf{v}_{D_0,E}^n)^- \ge 0$, we have

$$\sum_{E \in \mathcal{N}(D_0)} \mathbb{T}_{D_0,E}^n (c_E^n - c_{D_0}^n) + \mu \sum_{E \in \mathcal{N}(D_0)} -(\mathbf{v}_{D_0,E}^n)^- (c_E^n - c_{D_0}^n) \ge 0 \,.$$

This yields, using (1.25)

$$\frac{\beta(c_{D_0}^n) - \beta(c_{D_0}^{n-1})}{\triangle t_n} |D_0| + \mu (q_S)_{D_0}^n c_{D_0}^n |D_0| + F(c_{D_0}^n) \, |D_0| - q_{D_0}^n \, |D_0| \ge 0 \,.$$

Now $c_{D_0}^n < 0$ implies $\mu (q_S)_{D_0}^n c_{D_0}^n \le 0$ and $F(c_{D_0}^n) \le 0$ using, respectively, Assumption *(A4)* and *(A5)* and *(A6)* or *(A7)*. Also $-q_{D_0}^n \le 0$, using Assumption *(A8)*. Thus $\beta(c_{D_0}^n) \ge \beta(c_{D_0}^{n-1})$, which is a contradiction, since $\beta$ is strictly increasing from Assumption *(A1)*.

Let us now suppose $c_{D_1}^n > M$. Again $D_1 \in \mathcal{D}_h^{\rm int}$, because of (1.9b). Similarly as in the previous case, one comes to

$$\frac{\beta(c_{D_1}^n) - \beta(c_{D_1}^{n-1})}{\triangle t_n} |D_1| + \mu (q_S)_{D_1}^n c_{D_1}^n |D_1| + F(c_{D_1}^n) \, |D_1| - q_{D_1}^n \, |D_1| \le 0 \,.$$

We can estimate

$$-q_{D_1}^n \, |D_1| \ge -M (q_S)_{D_1}^n |D_1| \ge -\mu M (q_S)_{D_1}^n |D_1|$$

using, respectively, Assumption *(A8)*, *(A4)*, and *(A5)*. It follows from *(A6)* or *(A7)* that $F(c_{D_1}^n) \ge 0$. This implies $\beta(c_{D_1}^n) \le \beta(c_{D_1}^{n-1})$, which is again a contradiction, using Assumption *(A1)*. □

## 1.5 A priori estimates

In this section we give a priori estimates and estimates on differences of time and space translates of the approximate solutions that we shall define.

### 1.5.1 A priori estimates

We now give a priori estimates satisfied by the solution values $c_D^n$, $D \in \mathcal{D}_h$, $n \in \{0, 1, \ldots, N\}$.

**Theorem 1.5.1. (A priori estimates)** *The solution of the combined scheme (1.9a)–(1.9c) satisfies*

$$c_\beta \max_{n\in\{1,2,\ldots,N\}} \sum_{D\in\mathcal{D}_h} (c_D^n)^2 |D| \leq C_{\rm ae}\,, \tag{1.26}$$

$$\max_{n\in\{1,2,\ldots,N\}} \sum_{D\in\mathcal{D}_h} [\beta(c_D^n)]^2 |D| \leq C_{{\rm ae}\beta}\,, \tag{1.27}$$

$$c_{\mathbf{S}} \sum_{n=1}^{N} \triangle t_n \|c_h^n\|_{X_h}^2 \leq C_{\rm ae} \tag{1.28}$$

*with* $c_h^n = \sum_{D\in\mathcal{D}_h} c_D^n \varphi_D$,

$$\begin{aligned} C_{\rm ae} &:= 4M\beta(M)|\Omega| + \frac{4T}{c_\beta}\|q\|_{0,Q_T}^2 + 4L_F M^2 T|\Omega|\,, \\ C_{{\rm ae}\beta} &:= [\beta(M)]^2|\Omega| \end{aligned}$$

*when Assumption (D) is satisfied and only Assumption (A1) holds and*

$$C_{{\rm ae}\beta} := (2C_\beta^2 + 4L_\beta^2 P^2)|\Omega| + \frac{4L_\beta^2}{c_\beta} C_{\rm ae}$$

*when Assumption (D) is not satisfied but Assumption (A2) holds.*

Proof:

The estimates (1.26) and (1.28) follow immediately from (1.22) for $\varepsilon = c_\beta/(2T)$, since for $u = 1$ the extended scheme (1.19a)–(1.19c) completely coincides with the scheme (1.9a)–(1.9c). To see the boundedness of the term on the left-hand side of (1.27) under Assumption *(D)* is immediate, using the discrete maximum principle stated by Theorem 1.4.11. In this case Assumption *(A1)* suffices. In the general case one has to use Assumption *(A2)* to show $[\beta(s)]^2 \leq 2C_\beta^2 + 4L_\beta^2 P^2 + 4L_\beta^2 s^2$, see Lemma 1.8.3 in Appendix 1.8. Hence,

$$\sum_{D\in\mathcal{D}_h} [\beta(c_D^n)]^2 |D| \leq (2C_\beta^2 + 4L_\beta^2 P^2)|\Omega| + 4L_\beta^2 \sum_{D\in\mathcal{D}_h} (c_D^n)^2 |D| \qquad \forall n \in \{1, 2, \ldots, N\}\,. \quad \square$$

**Remark 1.5.2. (Discrete Friedrichs inequality)** *In the proof of Theorem 1.5.1, as well as throughout the whole chapter, we do not make use of the discrete Friedrichs inequality*

$$\|c_h\|_{0,\Omega} \leq C_P \|c_h\|_{X_h} \qquad \forall c_h \in X_h^0\,,\, C_P > 0\,.$$

*This is possible due to the growth condition imposed on $\beta$ in Assumption (A1). However, to prove the convergence of the scheme for an elliptic–parabolic problem or in the stationary case, when Assumption (D) is not satisfied and therefore the discrete maximum principle stated by Theorem 1.4.11 is not valid, the discrete Friedrichs inequality would be necessary. We then refer to [84], [28], or Chapter 2 of this thesis for the proof of this inequality.*

Using the values $c_D^n$, $D \in \mathcal{D}_h$, $n \in \{0, 1, \ldots, N\}$, we now define two approximate solutions.

**Definition 1.5.3. (Approximate solutions)** *Let the values $c_D^n$, $D \in \mathcal{D}_h$, $n \in \{0, 1, \ldots, N\}$, be the solutions to (1.9a)–(1.9c). As the approximate solutions of the problem (1.1)–(1.3) by means of the combined finite volume–nonconforming/mixed-hybrid finite element scheme, we understand:*

*(i) A function $c_{h,\triangle t}$ such that*

$$\begin{aligned} c_{h,\triangle t}(\mathbf{x}, 0) &= c_h^0(\mathbf{x}) \ \text{ for } \ \mathbf{x} \in \Omega\,, \\ c_{h,\triangle t}(\mathbf{x}, t) &= c_h^n(\mathbf{x}) \ \text{ for } \ \mathbf{x} \in \Omega\,,\ t \in (t_{n-1}, t_n] \qquad n \in \{1, \ldots, N\}\,, \end{aligned} \tag{1.29}$$

*where $c_h^n = \sum_{D \in \mathcal{D}_h} c_D^n \varphi_D$;*

*(ii) A function $\tilde{c}_{h,\triangle t}$ such that*

$$\begin{aligned} \tilde{c}_{h,\triangle t}(\mathbf{x}, 0) &= c_D^0 \ \text{ for } \ \mathbf{x} \in D^\circ\,,\ D \in \mathcal{D}_h\,, \\ \tilde{c}_{h,\triangle t}(\mathbf{x}, t) &= c_D^n \ \text{ for } \ \mathbf{x} \in D^\circ\,,\ D \in \mathcal{D}_h\,,\ t \in (t_{n-1}, t_n] \qquad n \in \{1, \ldots, N\}\,. \end{aligned} \tag{1.30}$$

The function $c_{h,\triangle t}$ is piecewise linear and continuous in the barycentres of the interior sides in space and piecewise constant in time; we will call it a *nonconforming finite element solution*. The function $\tilde{c}_{h,\triangle t}$ is given by the values of $c_{h,\triangle t}$ in side barycentres and is piecewise constant on the dual volumes in space and piecewise constant in time; we will call it a *finite volume solution*. The following important relation between $c_{h,\triangle t}$ and $\tilde{c}_{h,\triangle t}$ is valid:

**Lemma 1.5.4.** *There holds*

$$\|c_{h,\triangle t} - \tilde{c}_{h,\triangle t}\|_{0,Q_T} \longrightarrow 0 \ \text{ as } \ h \to 0\,.$$

Proof:

We have

$$\begin{aligned} \|c_{h,\triangle t} - \tilde{c}_{h,\triangle t}\|_{0,Q_T}^2 &= \sum_{n=1}^{N} \triangle t_n \sum_{K \in \mathcal{T}_h} \sum_{\sigma_D \in \mathcal{E}_K} \int_{K \cap D} |c_{h,\triangle t}(\mathbf{x}, t_n) - \tilde{c}_{h,\triangle t}(\mathbf{x}, t_n)|^2 \,\mathrm{d}\mathbf{x} \\ &= \sum_{n=1}^{N} \triangle t_n \sum_{K \in \mathcal{T}_h} \sum_{\sigma_D \in \mathcal{E}_K} \int_{K \cap D} |c_{h,\triangle t}(\mathbf{x}, t_n) - c_{h,\triangle t}(Q_D, t_n)|^2 \,\mathrm{d}\mathbf{x} \\ &= \sum_{n=1}^{N} \triangle t_n \sum_{K \in \mathcal{T}_h} \sum_{\sigma_D \in \mathcal{E}_K} \int_{K \cap D} |\nabla c_{h,\triangle t}(\mathbf{x}, t_n) \cdot (\mathbf{x} - Q_D)|^2 \,\mathrm{d}\mathbf{x} \\ &\le \sum_{n=1}^{N} \triangle t_n \sum_{K \in \mathcal{T}_h} \sum_{\sigma_D \in \mathcal{E}_K} \left| \nabla c_h^n|_K \right|^2 [\mathrm{diam}(D)]^2 |K \cap D| \\ &\le h^2 \sum_{n=1}^{N} \triangle t_n \sum_{K \in \mathcal{T}_h} \left| \nabla c_h^n|_K \right|^2 |K| \le h^2 \sum_{n=1}^{N} \triangle t_n \|c_h^n\|_{X_h}^2 \le h^2 \frac{C_{\mathrm{ae}}}{c_{\mathbf{S}}}\,, \end{aligned}$$

where we have used the definitions of $c_{h,\triangle t}$ and $\tilde{c}_{h,\triangle t}$ and the a priori estimate (1.28). □

**Remark 1.5.5. (Interpretation of the values $c_D^n$)** *We remark that the approximate solutions $c_{h,\triangle t}$, $\tilde{c}_{h,\triangle t}$ are only an interpretation of the values $c_D^n$, $D \in \mathcal{D}_h$, $n \in \{0, 1, \ldots, N\}$. In particular, we may work with $\tilde{c}_{h,\triangle t}$ as in the finite volume method and then use Lemma 1.5.4 to extend the convergence results also to $c_{h,\triangle t}$.*

### 1.5.2 Estimates on differences of time and space translates

Estimates on differences of time and space translates have been used in [63, 64] to prove the relative compactness property of the sequence of approximate solutions. We give below the time translate estimate for $\tilde{c}_{h,\triangle t}$ given by (1.30). We extend the techniques from [63, 64] to the case of negative transmissibilities (which in particular implies that the discrete maximum principle is not satisfied) and to a nonconstant time step.

**Lemma 1.5.6. (Time translate estimate)** *There exists a constant $C_{\rm tt} > 0$ such that*

$$\int_0^{T-\tau} \int_\Omega \Big(\tilde{c}_{h,\triangle t}(\mathbf{x}, t+\tau) - \tilde{c}_{h,\triangle t}(\mathbf{x}, t)\Big)^2 \,\mathrm{d}\mathbf{x}\,\mathrm{d}t \le C_{\rm tt}(\tau + \triangle t)$$

*for all $\tau \in (0, T)$.*

Proof:

We set

$$T_T := \int_0^{T-\tau} \int_\Omega \Big(\tilde{c}_{h,\triangle t}(\mathbf{x}, t+\tau) - \tilde{c}_{h,\triangle t}(\mathbf{x}, t)\Big)^2 \,\mathrm{d}\mathbf{x}\,\mathrm{d}t\,.$$

Using the definition of $\tilde{c}_{h,\triangle t}$ given by (1.30), we can rewrite $T_T$ as

$$T_T = \int_0^{T-\tau} \sum_{D\in\mathcal{D}_h} |D| \Big(c_D^{n_1(t)} - c_D^{n_2(t)}\Big)^2 \,\mathrm{d}t\,,$$

where

$$\begin{aligned} &n_1(t) \in \{1, 2, \ldots, N\} \text{ is such that } t_{n_1-1} < t+\tau \le t_{n_1}\,,\\ &n_2(t) \in \{1, 2, \ldots, N\} \text{ is such that } t_{n_2-1} < t \le t_{n_2}\,. \end{aligned}$$

We now use (1.9b) and the growth condition imposed on $\beta$ in Assumption *(A1)* and estimate

$$\begin{aligned} T_T &\le \frac{1}{c_\beta} \int_0^{T-\tau} \sum_{D\in\mathcal{D}_h^{\rm int}} |D| \Big(c_D^{n_1(t)} - c_D^{n_2(t)}\Big)\Big(\beta\big(c_D^{n_1(t)}\big) - \beta\big(c_D^{n_2(t)}\big)\Big)\,\mathrm{d}t\\ &= \frac{1}{c_\beta} \int_0^{T-\tau} \sum_{D\in\mathcal{D}_h^{\rm int}} |D| \Big(c_D^{n_1(t)} - c_D^{n_2(t)}\Big) \sum_{n=1}^{N} \chi(n,t)\Big(\beta(c_D^n) - \beta(c_D^{n-1})\Big)\,\mathrm{d}t\,, \end{aligned}$$

where the function $\chi(n,t)$ is defined as

$$\chi(n,t) := \begin{cases} 1 & \text{if } t \le t_{n-1} < t+\tau\\ 0 & \text{otherwise} \end{cases}\,.$$

In view of the definition (1.9a)–(1.9c) of the combined scheme and of Corollary 1.4.2, we have

$$\begin{aligned} T_T \le \frac{1}{c_\beta} \sum_{n=1}^{N} \triangle t_n \int_0^{T-\tau} \chi(n,t) \sum_{D\in\mathcal{D}_h^{\rm int}} \Big(c_D^{n_1(t)} - c_D^{n_2(t)}\Big)\Big(\sum_{E\in\mathcal{N}(D)} \mathbb{S}_{D,E}^n (c_E^n - c_D^n)\\ -\mu \sum_{E\in\mathcal{N}(D)} \mathbf{v}_{D,E}^n\, \overline{c_{D,E}^n} - F(c_D^n)\,|D| + q_D^n\,|D|\Big)\,\mathrm{d}t\,. \end{aligned} \tag{1.31}$$

We now estimate each term separately.

### Diffusion term

We set

$$T_D := \sum_{n=1}^{N} \triangle t_n \int_0^{T-\tau} \chi(n,t) \sum_{D\in\mathcal{D}_h} \left(c_D^{n_1(t)} - c_D^{n_2(t)}\right) \sum_{E\in\mathcal{N}(D)} \mathbb{S}_{D,E}^n (c_E^n - c_D^n)\,\mathrm{d}t\,,$$

where we have changed the summation over $D \in \mathcal{D}_h^{\mathrm{int}}$ into the summation over $D \in \mathcal{D}_h$ using (1.9b). This enables us to rewrite $T_D$ as a summation over interior dual sides, since each $\sigma_{D,E} \in \mathcal{F}_h^{\mathrm{int}}$ is in the original sum just twice. This gives

$$\begin{aligned} T_D \;=\; & \sum_{n=1}^{N} \triangle t_n \int_0^{T-\tau} \chi(n,t) \sum_{\sigma_{D,E}\in\mathcal{F}_h^{\mathrm{int}}} \mathbb{S}_{D,E}^n \Big[(c_E^n - c_D^n)\Big(c_D^{n_1(t)} - c_E^{n_1(t)}\Big) \\ & + (c_E^n - c_D^n)\Big(c_E^{n_2(t)} - c_D^{n_2(t)}\Big)\Big]\,\mathrm{d}t\,. \end{aligned}$$

Using the inequality $cab \le |c|a^2/2 + |c|b^2/2$ and the estimate (1.18) on $|\mathbb{S}_{D,E}^n|$, we can write

$$T_D \le T_{D_1} + T_{D_2} + T_{D_3}$$

with

$$\begin{aligned} T_{D_1} &:= \frac{C_{\mathbf{S}}}{\kappa_{\mathcal{T}}} \frac{1}{(d-1)^2} \sum_{n=1}^{N} \triangle t_n \int_0^{T-\tau} \chi(n,t) \sum_{\sigma_{D,E}\in\mathcal{F}_h^{\mathrm{int}}} \mathrm{diam}(K_{D,E})^{d-2} (c_E^n - c_D^n)^2\,\mathrm{d}t\,, \\ T_{D_2} &:= \frac{C_{\mathbf{S}}}{2\kappa_{\mathcal{T}}} \frac{1}{(d-1)^2} \sum_{n=1}^{N} \triangle t_n \int_0^{T-\tau} \chi(n,t) \sum_{\sigma_{D,E}\in\mathcal{F}_h^{\mathrm{int}}} \mathrm{diam}(K_{D,E})^{d-2} \Big(c_E^{n_1(t)} - c_D^{n_1(t)}\Big)^2\,\mathrm{d}t\,, \\ T_{D_3} &:= \frac{C_{\mathbf{S}}}{2\kappa_{\mathcal{T}}} \frac{1}{(d-1)^2} \sum_{n=1}^{N} \triangle t_n \int_0^{T-\tau} \chi(n,t) \sum_{\sigma_{D,E}\in\mathcal{F}_h^{\mathrm{int}}} \mathrm{diam}(K_{D,E})^{d-2} \Big(c_E^{n_2(t)} - c_D^{n_2(t)}\Big)^2\,\mathrm{d}t\,. \end{aligned}$$

We now notice that

$$\int_0^{T-\tau} \chi(n,t)\,\mathrm{d}t \le \tau\,, \tag{1.32}$$

since the function $\chi(n,t)$, for fixed $n$, is nonzero and equal to one just on the interval $(t_{n-1} - \tau, t_{n-1}]$ of length $\tau$. Using this and the a priori estimate (1.28), we have

$$T_{X_1}^* := \sum_{n=1}^{N} \triangle t_n \|c_h^n\|_{X_h}^2 \int_0^{T-\tau} \chi(n,t)\,\mathrm{d}t \le \tau \frac{C_{\mathrm{ae}}}{c_{\mathbf{S}}}\,. \tag{1.33}$$

We now introduce a term $T_{X_3}^*$,

$$T_{X_3}^* := \sum_{n=1}^{N} \triangle t_n \int_0^{T-\tau} \chi(n,t)\,\|c_h^{n_2(t)}\|_{X_h}^2\,\mathrm{d}t$$

and have, using the definition of $n_2(t)$

$$T_{X_3}^* = \sum_{n=1}^{N} \triangle t_n \sum_{m=1}^{N} \int_{t_{m-1}}^{t_m} \chi(n,t) \|c_h^{n_2(t)}\|_{X_h}^2\,\mathrm{d}t = \sum_{m=1}^{N} \|c_h^m\|_{X_h}^2 \sum_{n=1}^{N} \triangle t_n \int_{t_{m-1}}^{t_m} \chi(n,t)\,\mathrm{d}t\,. \tag{1.34}$$

Let us now consider the case where the time step is constant, i.e. $\triangle t_n = \triangle t$ for all $n \in \{1, 2, \ldots, N\}$. We then have, using a simple change of variables and the fact that $t_{m-1} - t_{n-1} = t_m - t_n$,

$$\begin{aligned}\sum_{n=1}^{N} \triangle t_n \int_{t_{m-1}}^{t_m} \chi(n,t)\,\mathrm{d}t &= \sum_{n=1}^{N} \triangle t \int_{t_{m-1}-t_{n-1}}^{t_m - t_{n-1}} \chi(n, s + t_{n-1})\,\mathrm{d}s \\ &= \triangle t \sum_{n=1}^{N} \int_{t_m - t_n}^{t_m - t_{n-1}} 1_{-\tau < s \le 0}\,\mathrm{d}s \le \tau \triangle t\,,\end{aligned}$$

where the function $1_{a<x\le b}$ is equal to 1 on the interval $(a, b]$ and zero otherwise, which we substitute back into (1.34) and use the a priori estimate (1.28) to obtain

$$T^*_{X_3} \le \tau \frac{C_{\mathrm{ae}}}{c_{\mathbf{S}}}\,.$$

Next we consider a nonconstant time step. We have

$$\sum_{n=1}^{N} \triangle t_n \chi(n,t) \le \tau + \triangle t\,,$$

considering that $\chi(n,t)$, for fixed $t$, is nonzero and equal to one just when $t \le t_{n-1} < t + \tau$, i.e. an interval of length $\tau$, and that with each such $n$, we add $\triangle t_n$. Using this, we have

$$T^*_{X_3} \le (\tau + \triangle t) \sum_{m=1}^{N} \|c_h^m\|^2_{X_h} \triangle t_m \le (\tau + \triangle t) \frac{C_{\mathrm{ae}}}{c_{\mathbf{S}}}\,.$$

We next introduce a term $T^*_{X_2}$,

$$T^*_{X_2} := \sum_{n=1}^{N} \triangle t_n \int_0^{T-\tau} \chi(n,t)\, \|c_h^{n_1(t)}\|^2_{X_h}\,\mathrm{d}t\,.$$

Similarly as in the previous case, using the definition of $n_1(t)$, we have

$$\begin{aligned}T^*_{X_2} &\le \sum_{n=1}^{N} \triangle t_n \sum_{m=1}^{N} \int_{t_{m-1}-\tau}^{t_m - \tau} \chi(n,t) \|c_h^{n_1(t)}\|^2_{X_h}\,\mathrm{d}t \\ &= \sum_{m=1}^{N} \|c_h^m\|^2_{X_h} \sum_{n=1}^{N} \triangle t_n \int_{t_{m-1}-\tau}^{t_m - \tau} \chi(n,t)\,\mathrm{d}t\,,\end{aligned}$$

which yields the same estimate for $T^*_{X_2}$ as for $T^*_{X_3}$. We finally introduce

$$T^*_{L_1} := \sum_{n=1}^{N} \triangle t_n \sum_{D \in \mathcal{D}_h} (c_D^n)^2 |D| \int_0^{T-\tau} \chi(n,t)\,\mathrm{d}t \le \tau T \frac{C_{\mathrm{ae}}}{c_\beta}\,, \tag{1.35}$$

which we have estimated using (1.32) and the a priori estimate (1.26), and

$$T^*_{L_i} := \sum_{n=1}^{N} \triangle t_n \int_0^{T-\tau} \chi(n,t) \sum_{D \in \mathcal{D}_h} \left(c_D^{n_{i-1}(t)}\right)^2 |D|\,\mathrm{d}t \qquad i \in \{2, 3\}\,.$$

We shall need $T^*_{L_i}$, $i \in \{1,2,3\}$, for the estimates of the other terms of $T_T$ below. Using the a priori estimate (1.26) and the same techniques as for $T^*_{X_i}$, $i = 2,3$, we altogether come to

$$T^*_{X_i} \le \tau \frac{C_{\mathrm{ae}}}{c_{\mathbf{S}}}, \quad T^*_{L_i} \le \tau T \frac{C_{\mathrm{ae}}}{c_\beta} \qquad i \in \{2,3\} \tag{1.36}$$

for a constant time step and

$$T^*_{X_i} \le (\tau + \triangle t) \frac{C_{\mathrm{ae}}}{c_{\mathbf{S}}}, \quad T^*_{L_i} \le (\tau + \triangle t) T \frac{C_{\mathrm{ae}}}{c_\beta} \qquad i \in \{2,3\} \tag{1.37}$$

for a generally nonconstant time step. Now using (1.6) for $T_{D_1}$, $T_{D_2}$, and $T_{D_3}$, we have

$$T_D \le \frac{C_{\mathbf{S}}}{\kappa_{\mathcal{T}}^2} \frac{d+1}{2d(d-1)^2} \Big( T^*_{X_1} + \frac{1}{2} T^*_{X_2} + \frac{1}{2} T^*_{X_3} \Big) . \tag{1.38}$$

**Convection term**

We will write the convection term as $T_{C_1} + T_{C_2}$, with

$$T_{C_1} := -\mu \sum_{n=1}^{N} \triangle t_n \int_0^{T-\tau} \chi(n,t) \sum_{D \in \mathcal{D}_h} \Big( c_D^{n_1(t)} - c_D^{n_2(t)} \Big) \sum_{E \in \mathcal{N}(D)} \mathbf{v}^n_{D,E} \, \widehat{c^n_{D,E}} \, \mathrm{d}t$$

and

$$T_{C_2} := -\mu \sum_{n=1}^{N} \triangle t_n \int_0^{T-\tau} \chi(n,t) \sum_{D \in \mathcal{D}_h} \Big( c_D^{n_1(t)} - c_D^{n_2(t)} \Big) \sum_{E \in \mathcal{N}(D)} |\mathbf{v}^n_{D,E}| \, \alpha^n_{D,E} (c^n_E - c^n_D) \, \mathrm{d}t ,$$

using the splitting into full upstream weighting and coefficient-centered weighting.

We again rewrite $T_{C_1}$ as the summation over the interior dual sides; we however adjust the denotation of the dual volumes sharing a given side $\sigma_{D,E}$ such that $\mathbf{v}^n_{D,E} \ge 0$. Then, using the definition of the upstream weighting, we have

$$T_{C_1} = \mu \sum_{n=1}^{N} \triangle t_n \int_0^{T-\tau} \chi(n,t) \sum_{\sigma_{D,E} \in \mathcal{F}_h^{\mathrm{int}}, \, \mathbf{v}^n_{D,E} \ge 0} -\mathbf{v}^n_{D,E} c^n_D \Big( c_D^{n_1(t)} - c_E^{n_1(t)} + c_E^{n_2(t)} - c_D^{n_2(t)} \Big) \, \mathrm{d}t .$$

Using $\pm ab \le \varepsilon a^2/2 + b^2/(2\varepsilon)$, $\varepsilon > 0$, where we put $\varepsilon = d_{D,E}$, we come to

$$T_{C_1} \le T_{C_3} + T_{C_4} + T_{C_5}$$

with

$$\begin{aligned}
T_{C_3} &:= \mu \sum_{n=1}^{N} \triangle t_n \int_0^{T-\tau} \chi(n,t) \sum_{\sigma_{D,E} \in \mathcal{F}_h^{\mathrm{int}}, \, \mathbf{v}^n_{D,E} \ge 0} |\mathbf{v}^n_{D,E}| d_{D,E} (c^n_D)^2 \, \mathrm{d}t , \\
T_{C_4} &:= \frac{\mu}{2} \sum_{n=1}^{N} \triangle t_n \int_0^{T-\tau} \chi(n,t) \sum_{\sigma_{D,E} \in \mathcal{F}_h^{\mathrm{int}}} \frac{|\mathbf{v}^n_{D,E}|}{d_{D,E}} \Big( c_E^{n_1(t)} - c_D^{n_1(t)} \Big)^2 \, \mathrm{d}t , \\
T_{C_5} &:= \frac{\mu}{2} \sum_{n=1}^{N} \triangle t_n \int_0^{T-\tau} \chi(n,t) \sum_{\sigma_{D,E} \in \mathcal{F}_h^{\mathrm{int}}} \frac{|\mathbf{v}^n_{D,E}|}{d_{D,E}} \Big( c_E^{n_2(t)} - c_D^{n_2(t)} \Big)^2 \, \mathrm{d}t .
\end{aligned}$$

We have

$$\sum_{\sigma_{D,E}\in\mathcal{F}_h^{\rm int},\,\mathbf{v}_{D,E}^n\geq 0}|\mathbf{v}_{D,E}^n|d_{D,E}(c_D^n)^2\leq C_{\mathbf{v}}\sum_{\sigma_{D,E}\in\mathcal{F}_h^{\rm int},\,\mathbf{v}_{D,E}^n\geq 0}\frac{|K_{D,E}|}{\kappa_{\mathcal{T}}d(d-1)}(c_D^n)^2$$
$$\leq\frac{C_{\mathbf{v}}}{\kappa_{\mathcal{T}}}\frac{d+1}{d-1}\sum_{D\in\mathcal{D}_h}\Big(\frac{|K_D|}{d+1}+\frac{|L_D|}{d+1}\Big)(c_D^n)^2=\frac{C_{\mathbf{v}}}{\kappa_{\mathcal{T}}}\frac{d+1}{d-1}\sum_{D\in\mathcal{D}_h}(c_D^n)^2|D|\,,$$

where we have used Assumption *(A4)*, which implies $|\mathbf{v}_{D,E}^n|\leq C_{\mathbf{v}}|\sigma_{D,E}|$, (1.8), Assumption *(B)*, (1.9b), the fact that each dual volume $D\in\mathcal{D}_h^{\rm int}$ has $d$ dual sides inside a simplex $K_D$ and $d$ dual sides inside a simplex $L_D$ and that $c_D^n$ can appear as an upwind value only at these sides, and (1.5). Thus, we have

$$T_{C_3}\leq\mu\frac{C_{\mathbf{v}}}{\kappa_{\mathcal{T}}}\frac{d+1}{d-1}T_{L_1}^*\,.$$

Using $|\mathbf{v}_{D,E}^n|\leq C_{\mathbf{v}}|\sigma_{D,E}|$ and (1.7), we have

$$T_{C_i}\leq\mu\frac{C_{\mathbf{v}}}{\kappa_{\mathcal{T}}}\frac{d+1}{4(d-1)}T_{X_{i-2}}^*\qquad i\in\{4,5\}\,,$$

which altogether leads to

$$T_{C_1}\leq\mu\frac{C_{\mathbf{v}}}{\kappa_{\mathcal{T}}}\Big(\frac{d+1}{d-1}T_{L_1}^*+\frac{d+1}{4(d-1)}(T_{X_2}^*+T_{X_3}^*)\Big)\,.\tag{1.39}$$

We now consider $T_{C_2}$. We can easily notice that it is almost same as the diffusion term $T_D$, except for $-\mu$ and the term $\mathbb{S}_{D,E}^n$, which is replaced by $|\mathbf{v}_{D,E}^n|\,\alpha_{D,E}^n$. Using $|\mathbf{v}_{D,E}^n|\leq C_{\mathbf{v}}|\sigma_{D,E}|$, $\alpha_{D,E}^n\leq 1/2$, and the estimates (1.6) and (1.8), we easily come to

$$T_{C_2}\leq\mu\frac{C_{\mathbf{v}}}{\kappa_{\mathcal{T}}}h\frac{d+1}{4d(d-1)}\Big(T_{X_1}^*+\frac{1}{2}T_{X_2}^*+\frac{1}{2}T_{X_3}^*\Big)\,.\tag{1.40}$$

**Reaction term**

We denote

$$T_R:=-\sum_{n=1}^{N}\triangle t_n\int_0^{T-\tau}\chi(n,t)\sum_{D\in\mathcal{D}_h}\Big(c_D^{n_1(t)}-c_D^{n_2(t)}\Big)F(c_D^n)|D|\,\mathrm{d}t\,.$$

We estimate

$$-F(c_D^n)(c_D^{n_1}-c_D^{n_2})\leq\frac{(c_D^{n_1}-c_D^{n_2})^2}{2}+\frac{(F(c_D^n))^2}{2}\leq(c_D^{n_1})^2+(c_D^{n_2})^2+\frac{L_F^2(c_D^n)^2}{2}\,,$$

using the inequalities $ab\leq a^2/2+b^2/2$, $(a-b)^2/2\leq a^2+b^2$, the Lipschitz continuity of $F$ with the constant $L_F$, and the fact that $F(0)=0$, following either from Assumption *(A6)* or *(A7)*. This implies

$$T_R\leq\Big(\frac{L_F^2}{2}T_{L_1}^*+T_{L_2}^*+T_{L_3}^*\Big)\,.\tag{1.41}$$

**Sources term**

We denote

$$T_S := \sum_{n=1}^{N} \triangle t_n \int_0^{T-\tau} \chi(n,t) \sum_{D\in\mathcal{D}_h} \left(c_D^{n_1(t)} - c_D^{n_2(t)}\right) q_D^n |D| \,\mathrm{d}t\,.$$

Using the same estimate as for the reaction term, (1.32), and (1.21), we come to

$$T_S \le \frac{1}{2}\tau \|q\|_{0,Q_T}^2 + T_{L_2}^* + T_{L_3}^*\,. \tag{1.42}$$

The assertion of the lemma follows by introducing (1.38), (1.39), (1.40), (1.41), and (1.42) into (1.31), while using the estimates (1.33), (1.35), and (1.37). □

**Remark 1.5.7. (Time translate estimate under Assumption *(D)*)** *If Assumption (D) is valid, the transmissibilities $\mathbb{S}_{D,E}^n$ are non-negative as in the finite volume method. Hence $T_D \le T_{D_1} + T_{D_2} + T_{D_3}$ with*

$$T_{D_1} = \sum_{n=1}^{N} \triangle t_n \int_0^{T-\tau} \chi(n,t) \sum_{\sigma_{D,E}\in\mathcal{F}_h^{\mathrm{int}}} \mathbb{S}_{D,E}^n (c_E^n - c_D^n)^2 \,\mathrm{d}t$$

*and similarly for $T_{D_2}$ and $T_{D_3}$. Thus using*

$$\sum_{\sigma_{D,E}\in\mathcal{F}_h^{\mathrm{int}}} \mathbb{S}_{D,E}^n (c_E^n - c_D^n)^2 = -\sum_{D\in\mathcal{D}_h} c_D \sum_{E\in\mathcal{D}_h} \mathbb{S}_{D,E}^n c_E$$

*and (1.17), $T_D \le C_{\mathbf{S}}(T_{X_1}^* + T_{X_2}^*/2 + T_{X_3}^*/2)$ in this case instead of (1.38).*

**Remark 1.5.8. (Time translate estimate for a constant time step)** *For a constant time step, we have indeed an $O(\tau)$ estimate, using (1.36) instead of (1.37).*

We now give the space translate estimate for $\tilde{c}_{h,\triangle t}$ given by (1.30). Lemma 1.5.9 extends the space translate estimate from [63, 64] to the case of (dual) meshes not necessarily satisfying the orthogonality property.

**Lemma 1.5.9. (Space translate estimate)** *Let us define $\tilde{c}_{h,\triangle t}(\mathbf{x},t)$ by zero outside of $\Omega$. Then there exists a constant $C_{\mathrm{st}} > 0$ such that*

$$\int_0^T \int_\Omega \left(\tilde{c}_{h,\triangle t}(\mathbf{x}+\boldsymbol{\xi},t) - \tilde{c}_{h,\triangle t}(\mathbf{x},t)\right)^2 \mathrm{d}\mathbf{x}\,\mathrm{d}t \le C_{\mathrm{st}}|\boldsymbol{\xi}|(|\boldsymbol{\xi}| + h)$$

*for all $\boldsymbol{\xi} \in \mathbb{R}^d$.*

Proof:

We define a function $\chi_\sigma(\mathbf{x})$ for each $\sigma \in \mathcal{F}_h^{\mathrm{int}}$ by

$$\chi_\sigma(\mathbf{x}) := \begin{cases} 1 & \text{if } \sigma \cap [\mathbf{x}, \mathbf{x}+\boldsymbol{\xi}] \neq \emptyset \\ 0 & \text{if } \sigma \cap [\mathbf{x}, \mathbf{x}+\boldsymbol{\xi}] = \emptyset \end{cases}.$$

A simple geometrical consideration leads to

$$|\tilde{c}_{h,\triangle t}(\mathbf{x}+\boldsymbol{\xi},t) - \tilde{c}_{h,\triangle t}(\mathbf{x},t)| \le \sum_{\sigma_{D,E}\in\mathcal{F}_h^{\mathrm{int}}} |c_E^n - c_D^n| \chi_{\sigma_{D,E}}(\mathbf{x})$$

for a.e. $\mathbf{x} \in \Omega$ and for $t \in (t_{n-1}, t_n]$, considering that $\tilde{c}_{h,\triangle t}$ is piecewise constant on $\mathcal{D}_h$, the Dirichlet boundary condition (1.9b), and the fact that $\tilde{c}_{h,\triangle t}(\mathbf{x}, t)$ is defined by zero outside of $\Omega$. The above inequality is in particular not valid for $\mathbf{x} \in \Omega$ such that the segment $[\mathbf{x}, \mathbf{x} + \boldsymbol{\xi}]$ intersects some vertex of the dual mesh. The Cauchy–Schwarz inequality yields

$$\begin{aligned} &\Big(\tilde{c}_{h,\triangle t}(\mathbf{x}+\boldsymbol{\xi}, t) - \tilde{c}_{h,\triangle t}(\mathbf{x}, t)\Big)^2 \qquad (1.43)\\ \leq &\sum_{\sigma_{D,E} \in \mathcal{F}_h^{\rm int}} \chi_{\sigma_{D,E}}(\mathbf{x}) \mathrm{diam}(K_{D,E}) \sum_{\sigma_{D,E} \in \mathcal{F}_h^{\rm int}} \frac{(c_E^n - c_D^n)^2}{\mathrm{diam}(K_{D,E})} \chi_{\sigma_{D,E}}(\mathbf{x}) \end{aligned}$$

for a.e. $\mathbf{x} \in \Omega$ and for $t \in (t_{n-1}, t_n]$.

The proof of Lemma 2.3.4 from Chapter 2 of this thesis gives

$$\sum_{\sigma_{D,E} \in \mathcal{F}_h^{\rm int}} \chi_{\sigma_{D,E}}(\mathbf{x}) \mathrm{diam}(K_{D,E}) \leq 4(d-1) P \theta_{\mathcal{T}}^{2P} (|\boldsymbol{\xi}| + h)\,, \qquad (1.44)$$

where $P = 2^{d-1}\pi/\phi_{\mathcal{T}}$. Here, the constant $\phi_{\mathcal{T}} > 0$ is such that

$$\min_{K \in \mathcal{T}_h} \phi_K \geq \phi_{\mathcal{T}} \qquad \forall h > 0\,, \qquad (1.45)$$

where $\phi_K$ is the smallest angle of the simplex $K$ (plain angle in radians if $d = 2$ and spheric angle in steradians if $d = 3$). Notice that Assumption *(B)* is equivalent to (1.45). We finally integrate (1.43) over $Q_T$. This gives

$$\begin{aligned} &\int_0^T \int_\Omega \Big(\tilde{c}_{h,\triangle t}(\mathbf{x}+\boldsymbol{\xi}, t) - \tilde{c}_{h,\triangle t}(\mathbf{x}, t)\Big)^2 \,\mathrm{d}\mathbf{x}\,\mathrm{d}t\\ \leq\ &4\frac{(d-1)}{d} P \theta_{\mathcal{T}}^{2P} (|\boldsymbol{\xi}| + h) \sum_{n=1}^N \triangle t_n \sum_{\sigma_{D,E} \in \mathcal{F}_h^{\rm int}} \frac{(c_E^n - c_D^n)^2}{d_{D,E}} \int_\Omega \chi_{\sigma_{D,E}}(\mathbf{x})\,\mathrm{d}\mathbf{x}\,, \end{aligned}$$

using (1.44) and (1.8). Finally, the value $\int_\Omega \chi_{\sigma_{D,E}}(\mathbf{x})\,\mathrm{d}\mathbf{x}$ is the measure of the set of points of $\Omega$ which are located inside a cylinder whose basis is $\sigma_{D,E}$ and generator vector is $-\boldsymbol{\xi}$. Thus

$$\int_\Omega \chi_{\sigma_{D,E}}(\mathbf{x})\,\mathrm{d}\mathbf{x} \leq |\sigma_{D,E}|\,|\boldsymbol{\xi}|\,.$$

Using (1.7) and the a priori estimate (1.28), this yields the assertion of the lemma with

$$C_{\rm st} := 2\frac{(d+1)}{d\kappa_{\mathcal{T}}} P \theta_{\mathcal{T}}^{2P} \frac{C_{\rm ae}}{c_{\mathbf{S}}}\,. \quad \square$$

**Remark 1.5.10. (Constant in the space translate estimate)** *The constant $C_{\rm st}$ in the space translate estimate has the form $C_{\rm st} = C(d, \kappa_{\mathcal{T}}) C_{\rm ae}/c_{\mathbf{S}}$. We recall that for the finite volume mesh satisfying the orthogonality property, this constant equals to $C_{\rm ae}/c_{\mathbf{S}}$, cf. [63, 64]. Hence supposing general unstructured meshes only satisfying the shape regularity Assumption (B) leads to the multiplication by a factor dependent on $d$ and $\kappa_{\mathcal{T}}$. It can be shown (see Chapter 2) that this factor is of the form $C(d)/\kappa_{\mathcal{T}}^2$ for $\{\mathcal{T}_h\}_h$ satisfying the inverse assumption (local refinement not allowed).*

## 1.6 Convergence

Using the a priori estimates of the previous section and the Kolmogorov relative compactness theorem, we show in this section a strong $L^2(Q_T)$ convergence of the approximate solutions to a function $u$ which we prove to be a weak solution of the continuous problem.

### 1.6.1 Strong convergence in $L^2(Q_T)$

**Theorem 1.6.1. (Strong convergence in $L^2(Q_T)$)** *There exist subsequences of $\tilde{c}_{h,\triangle t}$ and $c_{h,\triangle t}$ which converge strongly in $L^2(Q_T)$ to some function $u \in L^2(0,T;H_0^1(\Omega))$.*

Proof:

Let us consider the sequence $\tilde{c}_{h,\triangle t}$. The a priori estimate (1.26) and Lemmas 1.5.6 and 1.5.9 imply that $\tilde{c}_{h,\triangle t}$ satisfies the assumptions of Lemma 1.8.4 in Appendix 1.8. Thus $\tilde{c}_{h,\triangle t}$ verifies the assumptions of the Kolmogorov theorem ([29, Theorem IV.25 ], [61, Theorem 3.9]) and consequently is relatively compact in $L^2(Q_T)$. This implies the existence of a subsequence of $\tilde{c}_{h,\triangle t}$ which converges strongly to some function $u$ in $L^2(Q_T)$. Moreover, due to the space translate estimate of Lemma 1.5.9, [61, Theorem 3.10] gives that $u \in L^2(0,T;H_0^1(\Omega))$. Finally, considering Lemma 1.5.4, $c_{h,\triangle t}$ converges to the same $u$. □

**Remark 1.6.2. (Relative compactness for a constant time step)** *In view of Remark 1.5.8, the a priori estimate (1.26) and Lemmas 1.5.6 and 1.5.9 directly imply that $\tilde{c}_{h,\triangle t}$ verifies the assumptions of the Kolmogorov theorem for a constant time step. Hence, in this case Lemma 1.8.4 is not necessary.*

### 1.6.2 Convergence to a weak solution

We have shown in Theorem 1.6.1 that subsequences of $\tilde{c}_{h,\triangle t}$ and $c_{h,\triangle t}$, which we still denote by $\tilde{c}_{h,\triangle t}$ and $c_{h,\triangle t}$, converge strongly in $L^2(Q_T)$ to some function $u \in L^2(0,T;H_0^1(\Omega))$. We now show that $u$ is a weak solution of the continuous problem. For this purpose, we introduce

$$\Psi := \left\{\psi \in C^{2,1}(\overline{\Omega}\times[0,T]),\ \psi = 0 \text{ on } \partial\Omega\times[0,T],\ \psi(\cdot,T) = 0\right\}. \tag{1.46}$$

We then take an arbitrary $\psi \in \Psi$, multiply (1.9c) by $\triangle t_n\,\psi(Q_D,t_{n-1})$, and sum the result over $D \in \mathcal{D}_h^{\text{int}}$ and $n = 1,\dots,N$. This gives

$$T_T + T_D + T_C + T_R = T_S \tag{1.47}$$

with

$$\begin{aligned}
T_T &:= \sum_{n=1}^{N}\sum_{D\in\mathcal{D}_h}\Big(\beta(c_D^n) - \beta(c_D^{n-1})\Big)\psi(Q_D,t_{n-1})|D|\,,\\
T_D &:= \sum_{n=1}^{N}\triangle t_n \sum_{D\in\mathcal{D}_h}\sum_{E\in\mathcal{D}_h} c_E^n \sum_{K\in\mathcal{T}_h}(\mathbf{S}^n\nabla\varphi_E,\nabla\varphi_D)_{0,K}\,\psi(Q_D,t_{n-1})\,,\\
T_C &:= \mu\sum_{n=1}^{N}\triangle t_n \sum_{D\in\mathcal{D}_h}\sum_{E\in\mathcal{N}(D)} \mathbf{v}_{D,E}^n\,\overline{c_{D,E}^n}\,\psi(Q_D,t_{n-1})\,,\\
T_R &:= \sum_{n=1}^{N}\triangle t_n \sum_{D\in\mathcal{D}_h} F(c_D^n)\,\psi(Q_D,t_{n-1})|D|\,,\\
T_S &:= \sum_{n=1}^{N}\triangle t_n \sum_{D\in\mathcal{D}_h} q_D^n\,\psi(Q_D,t_{n-1})|D|\,,
\end{aligned}$$

using $\psi(Q_D,t_{n-1}) = 0$ for all $D \in \mathcal{D}_h^{\text{ext}}$ and $n = 1,\dots,N$. We now show that each of the above terms converges to its continuous version as $h$ and $\triangle t$ tend to zero.

**Time evolution term**

We use the discrete integration by parts formula and the fact that $\psi(Q_D, t_N) = 0$ for all $D \in \mathcal{D}_h$ to obtain

$$T_T = -\sum_{n=1}^{N} \sum_{D\in\mathcal{D}_h} \beta(c_D^n)\Big(\psi(Q_D, t_n) - \psi(Q_D, t_{n-1})\Big)|D| - \sum_{D\in\mathcal{D}_h} \beta(c_D^0)\psi(Q_D, 0)|D|\,. \tag{1.48}$$

We would now like to show that

$$\sum_{D\in\mathcal{D}_h} \beta(c_D^0)\psi(Q_D, 0)|D| \longrightarrow \int_\Omega \beta(c_0(\mathbf{x}))\psi(\mathbf{x}, 0)\,\mathrm{d}\mathbf{x} \;\text{ as }\; h \to 0\,. \tag{1.49}$$

For this purpose, we introduce

$$T_{T_1} := \sum_{D\in\mathcal{D}_h} \int_D \Big(\beta(c_D^0)\psi(Q_D, 0) - \beta(c_0(\mathbf{x}))\psi(\mathbf{x}, 0)\Big)\,\mathrm{d}\mathbf{x}\,.$$

We add and subtract $\beta(c_D^0)\psi(\mathbf{x}, 0)$ to each term and have

$$T_{T_1} = \sum_{D\in\mathcal{D}_h} \int_D \beta(c_D^0)\Big(\psi(Q_D, 0) - \psi(\mathbf{x}, 0)\Big)\,\mathrm{d}\mathbf{x} + \sum_{D\in\mathcal{D}_h} \int_D \Big(\beta(c_D^0) - \beta(c_0(\mathbf{x}))\Big)\psi(\mathbf{x}, 0)\,\mathrm{d}\mathbf{x}\,.$$

Using the definition of $c_D^0$ given by (1.9a) for $D \in \mathcal{D}_h^{\mathrm{int}}$ and by (1.9b) for $D \in \mathcal{D}_h^{\mathrm{ext}}$, the fact that $\beta$ is increasing by Assumption *(A1)*, and Assumption *(A9)*, we have that $|\beta(c_D^0)| \le \beta(M)$ for all $D \in \mathcal{D}_h$. Due to the boundedness of $|\psi|$ by $C_{1,\psi}$, we come to

$$|T_{T_1}| \le \beta(M) \sum_{D\in\mathcal{D}_h} \int_D |\psi(Q_D, 0) - \psi(\mathbf{x}, 0)|\,\mathrm{d}\mathbf{x} + C_{1,\psi} \sum_{D\in\mathcal{D}_h} \int_D |\beta(c_D^0) - \beta(c_0(\mathbf{x}))|\,\mathrm{d}\mathbf{x}\,. \tag{1.50}$$

Since $\psi \in C^{2,1}(\overline{\Omega} \times [0, T])$, we have

$$|\psi(Q_D, 0) - \psi(\mathbf{x}, 0)| \le C_{2,\psi}|Q_D - \mathbf{x}| \le C_{2,\psi} h$$

for all $\mathbf{x} \in D$, and thus the first term of (1.50) tends to 0 as $h \to 0$. We now consider the second term of (1.50). We have, for boundary dual volumes,

$$\sum_{D\in\mathcal{D}_h^{\mathrm{ext}}} \int_D |c_D^0 - c_0(\mathbf{x})|\,\mathrm{d}\mathbf{x} \le M \sum_{D\in\mathcal{D}_h^{\mathrm{ext}}} |D| \le M|\partial\Omega|h\,,$$

using (1.9b) and Assumption *(A9)*. Considering in addition the definition of $\tilde{c}_{h,\triangle t}$ by (1.30) and (1.9a) for interior dual volumes, $\tilde{c}_{h,\triangle t}(\mathbf{x}, 0)$ converges to $c_0(\mathbf{x})$ in $\Omega$ in the $L^1$ sense as $h \to 0$. Hence at least a subsequence of $\tilde{c}_{h,\triangle t}(\mathbf{x}, 0)$, which we still denote by $\tilde{c}_{h,\triangle t}(\mathbf{x}, 0)$, converges to $c_0(\mathbf{x})$ pointwise a.e. in $\Omega$. Thus also $\beta(\tilde{c}_{h,\triangle t}(\mathbf{x}, 0)) \to \beta(c_0(\mathbf{x}))$ a.e. in $\Omega$, using the continuity of $\beta$. Further, using that $\beta$ is increasing from Assumption *(A1)*, we have $|\beta(\tilde{c}_{h,\triangle t}(\mathbf{x}, 0))| \le \beta(M)$. Hence the Lebesgue dominated convergence theorem implies

$$\sum_{D\in\mathcal{D}_h} \int_D |\beta(c_D^0) - \beta(c_0(\mathbf{x}))|\,\mathrm{d}\mathbf{x} = \int_\Omega |\beta(\tilde{c}_{h,\triangle t}(\mathbf{x}, 0)) - \beta(c_0(\mathbf{x}))|\,\mathrm{d}\mathbf{x} \longrightarrow 0 \;\text{ as }\; h \to 0\,,$$

which can be by repetition extended onto whole $\tilde{c}_{h,\triangle t}(\mathbf{x}, 0)$. Thus $T_{T_1} \to 0$ as $h \to 0$ and consequently (1.49) is fulfilled.

Now we intend to prove that

$$\sum_{n=1}^{N}\sum_{D\in\mathcal{D}_h}\beta(c_D^n)\Big(\psi(Q_D,t_n)-\psi(Q_D,t_{n-1})\Big)|D| \longrightarrow \int_0^T\int_\Omega \beta(u(\mathbf{x},t))\psi_t(\mathbf{x},t)\,\mathrm{d}\mathbf{x}\,\mathrm{d}t \tag{1.51}$$

as $h,\triangle t\to 0$. We set

$$T_{T_2}:=\sum_{n=1}^{N}\sum_{D\in\mathcal{D}_h}\Big[\beta(c_D^n)\Big(\psi(Q_D,t_n)-\psi(Q_D,t_{n-1})\Big)|D|-\int_{t_{n-1}}^{t_n}\int_D\beta(u(\mathbf{x},t))\psi_t(\mathbf{x},t)\,\mathrm{d}\mathbf{x}\,\mathrm{d}t\Big].$$

We add and subtract $\displaystyle\int_{t_{n-1}}^{t_n}\int_D\beta(c_D^n)\psi_t(\mathbf{x},t)\,\mathrm{d}\mathbf{x}\,\mathrm{d}t$ in each term of $T_{T_2}$ to obtain

$$\begin{aligned}T_{T_2} &= \sum_{n=1}^{N}\sum_{D\in\mathcal{D}_h}\beta(c_D^n)\int_{t_{n-1}}^{t_n}\int_D\Big(\frac{\partial\psi}{\partial t}(Q_D,t)-\frac{\partial\psi}{\partial t}(\mathbf{x},t)\Big)\,\mathrm{d}\mathbf{x}\,\mathrm{d}t \\ &\quad+\int_0^T\int_\Omega\Big(\beta(\tilde{c}_{h,\triangle t}(\mathbf{x},t))-\beta(u(\mathbf{x},t))\Big)\psi_t(\mathbf{x},t)\,\mathrm{d}\mathbf{x}\,\mathrm{d}t\,.\end{aligned} \tag{1.52}$$

We have, for all $\mathbf{x}\in D$, for all $D\in\mathcal{D}_h$, and all $h>0$,

$$\Big|\frac{\partial\psi}{\partial t}(Q_D,t)-\frac{\partial\psi}{\partial t}(\mathbf{x},t)\Big|\le f(h)\,,$$

where the function $f$ satisfies $f(h)>0$ and $f(h)\to 0$ as $h\to 0$. This follows by the fact that $\partial\psi/\partial t\in C(\overline{\Omega})$ from (1.46) and hence is uniformly continuous on $\overline{\Omega}$. Thus the first term of (1.52) is bounded by

$$\begin{aligned}f(h)\sum_{n=1}^{N}\sum_{D\in\mathcal{D}_h}|\beta(c_D^n)|\triangle t_n|D| &\le f(h)T^{\frac12}|\Omega|^{\frac12}\Big(\sum_{n=1}^{N}\sum_{D\in\mathcal{D}_h}(\beta(c_D^n))^2\triangle t_n|D|\Big)^{\frac12} \\ &\le f(h)T|\Omega|^{\frac12}C_{\mathrm{ae}\beta}^{\frac12}\,,\end{aligned}$$

using the Cauchy–Schwarz inequality and the a priori estimate (1.27). Further, $|\psi_t(\mathbf{x},t)|\le C_{4,\psi}$, and thus we can estimate $T_{T_2}$ by

$$|T_{T_2}|\le f(h)T|\Omega|^{\frac12}C_{\mathrm{ae}\beta}^{\frac12}+C_{4,\psi}\int_0^T\int_\Omega|\beta(\tilde{c}_{h,\triangle t}(\mathbf{x},t))-\beta(u(\mathbf{x},t))|\,\mathrm{d}\mathbf{x}\,\mathrm{d}t\,. \tag{1.53}$$

We now use that $\tilde{c}_{h,\triangle t}\to u$ strongly in $L^2(Q_T)$ as $h,\triangle t\to 0$, due to Theorem 1.6.1. There exists at least a subsequence of $\tilde{c}_{h,\triangle t}$, which we still denote $\tilde{c}_{h,\triangle t}$, such that $\tilde{c}_{h,\triangle t}(\mathbf{x},t)\to u(\mathbf{x},t)$ a.e. in $Q_T$. Thus, using the continuity of $\beta(\cdot)$, $\beta(\tilde{c}_{h,\triangle t}(\mathbf{x},t))\to\beta(u(\mathbf{x},t))$ a.e. in $Q_T$. Now under Assumption *(D)*, which implies the discrete maximum principle stated by Theorem 1.4.11, and using that $\beta$ is increasing, $|\beta(\tilde{c}_{h,\triangle t}(\mathbf{x},t))|\le\beta(M)$, and thus we can use the Lebesgue dominated convergence theorem to conclude the convergence of the second term of (1.53) and thus of (1.53) to 0 as $h,\triangle t\to 0$. In this case Assumption *(A1)* suffices.

In the general case we use Assumption *(A2)*. We decompose the function $\beta$ as $\beta_1+\beta_2$,

$$\begin{aligned}&\beta_1(x):=\beta(x)\ \text{ on }\ [-P,P]\,,\quad \beta_1(x):=0\ \text{ on }\ (-\infty,-P)\cup(P,+\infty)\,,\\ &\beta_2(x):=0\ \text{ on }\ [-P,P]\,,\quad \beta_2(x):=\beta(x)\ \text{ on }\ (-\infty,-P)\cup(P,+\infty)\,.\end{aligned}$$

We further introduce a function $y$ linearly connecting the points $[-P,\beta(-P)]$ and $[P,\beta(P)]$ and zero otherwise,

$$y(x) := \frac{\beta(P)-\beta(-P)}{2P}x + \frac{\beta(P)+\beta(-P)}{2} \text{ on } [-P,P]\,, \quad y(x) := 0 \text{ on } (-\infty,-P)\cup(P,+\infty)\,.$$

We finally define $\tilde\beta_1 := \beta_1 - y$ and $\tilde\beta_2 := \beta_2 + y$ and remark that $\beta = \tilde\beta_1 + \tilde\beta_2$. Clearly, $\tilde\beta_1$ is continuous on $\mathbb{R}$ and satisfies $|\tilde\beta_1(x)| \le 2C_\beta$ on $\mathbb{R}$ and $\tilde\beta_2$ is Lipschitz-continuous on $\mathbb{R}$ with $\max\{L_\beta, [\beta(P)-\beta(-P)]/(2P)\}$. We now estimate

$$\begin{aligned}\int_0^T\int_\Omega |\beta(\tilde c_{h,\triangle t}(\mathbf{x},t)) - \beta(u(\mathbf{x},t))|\,\mathrm{d}\mathbf{x}\,\mathrm{d}t \;\le\; &\int_0^T\int_\Omega |\tilde\beta_1(\tilde c_{h,\triangle t}(\mathbf{x},t)) - \tilde\beta_1(u(\mathbf{x},t))|\,\mathrm{d}\mathbf{x}\,\mathrm{d}t\\ &+\int_0^T\int_\Omega |\tilde\beta_2(\tilde c_{h,\triangle t}(\mathbf{x},t)) - \tilde\beta_2(u(\mathbf{x},t))|\,\mathrm{d}\mathbf{x}\,\mathrm{d}t\,.\end{aligned}$$

The first term of the above expression converges to zero using the Lebesgue dominated convergence theorem as in the previous case. For the second term, it suffices to use the Lipschitz continuity of $\tilde\beta_2$ and the strong convergence of $\tilde c_{h,\triangle t}$ to $u$ in $L^2(Q_T)$. Thus (1.51) is satisfied. Combining (1.49) and (1.51), we have

$$T_T \longrightarrow -\int_0^T\int_\Omega \beta(u(\mathbf{x},t))\psi_t(\mathbf{x},t)\,\mathrm{d}\mathbf{x}\,\mathrm{d}t - \int_\Omega \beta(c_0(\mathbf{x}))\psi(\mathbf{x},0)\,\mathrm{d}\mathbf{x} \tag{1.54}$$

as $h, \triangle t \to 0$.

### Diffusion term

We rewrite $T_D$ as

$$T_D = \sum_{n=1}^N \triangle t_n \sum_{K\in\mathcal{T}_h}\int_K \mathbf{S}^n\nabla c_h^n(\mathbf{x})\cdot\nabla\Big(\sum_{D\in\mathcal{D}_h}\psi(Q_D,t_{n-1})\varphi_D(\mathbf{x})\Big)\,\mathrm{d}\mathbf{x}\,,$$

using the definition of $c_h^n \in X_h$, and define

$$\mathbf{S}_{\triangle t}(\mathbf{x},t) := \mathbf{S}^n(\mathbf{x}) \text{ for } \mathbf{x}\in\Omega\,,\ t\in(t_{n-1},t_n] \qquad n\in\{1,\dots,N\}\,, \tag{1.55}$$

where $\mathbf{S}^n$ is given by (1.13) for the nonconforming method and by (1.15) for the mixed-hybrid method. We will show the validity of two passages to the limit. We begin by showing that

$$\begin{aligned}&\sum_{n=1}^N \triangle t_n \sum_{K\in\mathcal{T}_h}\int_K \mathbf{S}^n\nabla c_h^n(\mathbf{x})\cdot\nabla\Big(\sum_{D\in\mathcal{D}_h}\psi(Q_D,t_{n-1})\varphi_D(\mathbf{x})\Big)\,\mathrm{d}\mathbf{x}\\ &-\sum_{n=1}^N \triangle t_n \sum_{K\in\mathcal{T}_h}\int_K \mathbf{S}^n\nabla c_h^n(\mathbf{x})\cdot\nabla\psi(\mathbf{x},t_{n-1})\,\mathrm{d}\mathbf{x}\longrightarrow 0 \text{ as } h\to 0\,.\end{aligned} \tag{1.56}$$

We set

$$I_\psi(\cdot,t_{n-1}) := \sum_{D\in\mathcal{D}_h}\psi(Q_D,t_{n-1})\varphi_D$$

and

$$T_{D_1} := \sum_{n=1}^N \triangle t_n \sum_{K\in\mathcal{T}_h}\int_K \mathbf{S}^n\nabla c_h^n(\mathbf{x})\cdot\nabla\Big(I_\psi(\mathbf{x},t_{n-1}) - \psi(\mathbf{x},t_{n-1})\Big)\,\mathrm{d}\mathbf{x}\,.$$

We then estimate

$$|T_{D_1}| \le C_{\mathbf{S}} \sum_{n=1}^{N} \triangle t_n \|c_h^n\|_{X_h} \|I_\psi(\cdot, t_{n-1}) - \psi(\cdot, t_{n-1})\|_{X_h} ,$$

using the Cauchy–Schwarz inequality. Next we use the interpolation estimate

$$\begin{aligned} \|I_\psi(\cdot, t_{n-1}) - \psi(\cdot, t_{n-1})\|_{X_h} &= \Big( \sum_{K \in \mathcal{T}_h} \int_K \Big| \nabla \big( I_\psi(\cdot, t_{n-1}) - \psi(\cdot, t_{n-1}) \big) \Big|^2 \,\mathrm{d}\mathbf{x} \Big)^{\frac{1}{2}} \\ &\le C_I \theta_{\mathcal{T}} h \Big( \sum_{K \in \mathcal{T}_h} |\psi(\cdot, t_{n-1})|_{2,K}^2 \Big)^{\frac{1}{2}} \le C_I \theta_{\mathcal{T}} C_{5,\psi} h , \end{aligned}$$

where $\theta_{\mathcal{T}}$ is given by the consequence (1.4) of Assumption *(B)*, $C_I$ does not depend on $h$ (nor on $\triangle t$), and $|\cdot|_{2,K}$ denotes the $H^2$ seminorm, see for instance [41, Theorem 15.3]. Finally, the Cauchy–Schwarz inequality yields

$$|T_{D_1}| \le C_{\mathbf{S}} C_I \theta_{\mathcal{T}} C_{5,\psi} h \Big( \sum_{n=1}^{N} \triangle t_n \|c_h^n\|_{X_h}^2 \Big)^{\frac{1}{2}} \Big( \sum_{n=1}^{N} \triangle t_n \Big)^{\frac{1}{2}} = C_{\mathbf{S}} C_I \theta_{\mathcal{T}} C_{5,\psi} T^{\frac{1}{2}} \Big( \frac{C_{\mathrm{ae}}}{c_{\mathbf{S}}} \Big)^{\frac{1}{2}} h ,$$

using the a priori estimate (1.28). Hence (1.56) is fulfilled.

We next show that

$$\sum_{n=1}^{N} \triangle t_n \sum_{K \in \mathcal{T}_h} \int_K \mathbf{S}^n \nabla c_h^n(\mathbf{x}) \cdot \nabla \psi(\mathbf{x}, t_{n-1}) \,\mathrm{d}\mathbf{x} \longrightarrow \int_0^T \int_\Omega \mathbf{S} \nabla u(\mathbf{x}, t) \cdot \nabla \psi(\mathbf{x}, t) \,\mathrm{d}\mathbf{x} \,\mathrm{d}t \tag{1.57}$$

as $h, \triangle t \to 0$. We see that both $c_h^n(\mathbf{x})$ and $\psi(\mathbf{x}, t_{n-1})$ are constant in time, so that we can easily introduce an integral with respect to time into the first term of (1.57). We further add and subtract $\displaystyle\sum_{n=1}^{N} \int_{t_{n-1}}^{t_n} \int_\Omega \mathbf{S}^n \nabla c_h^n(\mathbf{x}) \nabla \psi(\mathbf{x}, t) \,\mathrm{d}\mathbf{x} \,\mathrm{d}t$ and introduce

$$\begin{aligned} T_{D_2} &:= \sum_{n=1}^{N} \int_{t_{n-1}}^{t_n} \sum_{K \in \mathcal{T}_h} \int_K \mathbf{S}^n \nabla c_h^n(\mathbf{x}) \cdot \Big( \nabla \psi(\mathbf{x}, t_{n-1}) - \nabla \psi(\mathbf{x}, t) \Big) \,\mathrm{d}\mathbf{x} \,\mathrm{d}t , \\ T_{D_3} &:= \int_0^T \sum_{K \in \mathcal{T}_h} \int_K \mathbf{S}_{\triangle t} \nabla c_{h,\triangle t}(\mathbf{x}, t) \cdot \nabla \psi(\mathbf{x}, t) \,\mathrm{d}\mathbf{x} \,\mathrm{d}t - \int_0^T \int_\Omega \mathbf{S} \nabla u(\mathbf{x}, t) \cdot \nabla \psi(\mathbf{x}, t) \,\mathrm{d}\mathbf{x} \,\mathrm{d}t , \end{aligned}$$

where $c_{h,\triangle t}$ is given by (1.29). Clearly, (1.57) is valid when $T_{D_2}$ and $T_{D_3}$ tend to zero as $h, \triangle t \to 0$. We first estimate $T_{D_2}$. We have, for $t \in (t_{n-1}, t_n]$,

$$|\nabla \psi(\mathbf{x}, t_{n-1}) - \nabla \psi(\mathbf{x}, t)| \le g(\triangle t) ,$$

where $g$ satisfies $g(\triangle t) > 0$ and $g(\triangle t) \to 0$ as $\triangle t \to 0$. Thus

$$|T_{D_2}| \le C_{\mathbf{S}} g(\triangle t) \sum_{n=1}^{N} \triangle t_n \sum_{K \in \mathcal{T}_h} \Big| \nabla c_h^n |_K \Big| |K| \le C_{\mathbf{S}} g(\triangle t) \Big( \frac{C_{\mathrm{ae}}}{c_{\mathbf{S}}} \Big)^{\frac{1}{2}} T^{\frac{1}{2}} |\Omega|^{\frac{1}{2}} ,$$

using the Cauchy–Schwarz inequality and the a priori estimate (1.28).

We now turn to $T_{D_3}$. We will show later that

$$T'_{D_3} := \int_0^T \sum_{K\in\mathcal{T}_h} \int_K \Big(\nabla c_{h,\triangle t}(\mathbf{x},t) - \nabla u(\mathbf{x},t)\Big)\cdot \mathbf{w}(\mathbf{x},t)\,\mathrm{d}\mathbf{x}\,\mathrm{d}t \longrightarrow 0 \tag{1.58}$$

as $h, \triangle t \to 0$ for all $\mathbf{w} \in [C^\infty(\overline{Q_T})]^d$. Using the density of the set $[C^\infty(\overline{Q_T})]^d$ in $[L^2(Q_T)]^d$, we will conclude a weak convergence of $\nabla c_{h,\triangle t}$ (piecewise constant function is space and time) to $\nabla u$. Next, $(\mathbf{S}_{\triangle t})_{i,j}$, $1 \le i,j \le d$, converge strongly in $L^1(Q_T)$ to $\mathbf{S}_{i,j}$ by its definition (1.55). Using the boundedness of $\mathbf{S}_{\triangle t}$ and $\mathbf{S}$ given by Assumption *(A3)*, we have also strong $L^2(Q_T)$ convergence. Hence it suffices to apply Lemma 1.8.5 from Appendix 1.8 to conclude that $T_{D_3} \to 0$ as $h, \triangle t \to 0$, provided that (1.58) is satisfied.

To show (1.58), we first rewrite $T'_{D_3}$ as

$$T'_{D_3} = \sum_{n=1}^N \int_{t_{n-1}}^{t_n} \sum_{K\in\mathcal{T}_h} \int_K \nabla c_h^n(\mathbf{x})\cdot\mathbf{w}(\mathbf{x},t)\,\mathrm{d}\mathbf{x}\,\mathrm{d}t + \int_0^T\int_\Omega u(\mathbf{x},t)\nabla\cdot\mathbf{w}(\mathbf{x},t)\,\mathrm{d}\mathbf{x}\,\mathrm{d}t\,,$$

where we have used the Green theorem for $u$ (recall that $u \in L^2(0,T;H_0^1(\Omega))$ by Theorem 1.6.1) and $\mathbf{w}$. We easily notice that we cannot use the Green theorem for $c_h^n$ on $\Omega$, since $c_h^n \notin H^1(\Omega)$. We are thus forced to apply it on each $K \in \mathcal{T}_h$.

We rewrite the first term of $T'_{D_3}$ as

$$\sum_{n=1}^N \int_{t_{n-1}}^{t_n} \sum_{K\in\mathcal{T}_h} \int_K -c_h^n(\mathbf{x})\nabla\cdot\mathbf{w}(\mathbf{x},t)\,\mathrm{d}\mathbf{x}\,\mathrm{d}t + \sum_{n=1}^N \int_{t_{n-1}}^{t_n} \sum_{K\in\mathcal{T}_h} \int_{\partial K} c_h^n(\mathbf{x})\mathbf{w}(\mathbf{x},t)\cdot\mathbf{n}\,\mathrm{d}\gamma(\mathbf{x})\,\mathrm{d}t\,.$$

We next consider the term

$$T''_{D_3} := \sum_{n=1}^N \int_{t_{n-1}}^{t_n} \sum_{K\in\mathcal{T}_h} \int_{\partial K} c_h^n\mathbf{w}\cdot\mathbf{n}\,\mathrm{d}\gamma(\mathbf{x})\,\mathrm{d}t\,. \tag{1.59}$$

Reordering the summation by sides, we come to

$$\begin{aligned} T''_{D_3} \;=\; & \sum_{n=1}^N \int_{t_{n-1}}^{t_n} \Big( \sum_{\sigma_{K,L}\in\mathcal{E}_h^{\mathrm{int}}} \int_{\sigma_{K,L}} (c_h^n|_K - c_h^n|_L)\mathbf{w}\cdot\mathbf{n}_{K,L}\,\mathrm{d}\gamma(\mathbf{x}) \\ & + \sum_{\sigma_K\in\mathcal{E}_h^{\mathrm{ext}}} \int_{\sigma_K} c_h^n|_K\mathbf{w}\cdot\mathbf{n}_K\,\mathrm{d}\gamma(\mathbf{x})\Big)\,\mathrm{d}t\,, \end{aligned}$$

where we have used $\mathbf{w}\cdot\mathbf{n}_{K,L} = -\mathbf{w}\cdot\mathbf{n}_{L,K}$ following from $\mathbf{w} \in [C^\infty(\overline{Q_T})]^d$. The functions $c_h^n|_K - c_h^n|_L$ or $c_h^n|_K$ restricted to a side $\sigma_{K,L} \in \mathcal{E}_h^{\mathrm{int}}$ or $\sigma_K \in \mathcal{E}_h^{\mathrm{ext}}$, respectively, are first-order polynomials, vanishing in the barycentre $Q_D$ of this side. For $\sigma_{K,L} \in \mathcal{E}_h^{\mathrm{int}}$, this follows from the continuity requirement given in the definition of $X_h$ and for $\sigma_K \in \mathcal{E}_h^{\mathrm{ext}}$ from the zero Dirichlet boundary condition imposed by (1.9b). Hence

$$\int_{\sigma_{K,L}} \Big(c_h^n|_K(\mathbf{x}) - c_h^n|_L(\mathbf{x})\Big)\,\mathrm{d}\gamma(\mathbf{x}) = 0\,, \quad \int_{\sigma_K} c_h^n|_K(\mathbf{x})\,\mathrm{d}\gamma(\mathbf{x}) = 0 \tag{1.60}$$

for all $\sigma_{K,L} \in \mathcal{E}_h^{\mathrm{int}}$ and $\sigma_K \in \mathcal{E}_h^{\mathrm{ext}}$, since the quadrature formula using the value in the barycentre of a segment ($d=2$) or a triangle ($d=3$) is precise for linear functions. We further estimate

$$\Big|c_h^n|_K(\mathbf{x})\Big| = \Big|c_h^n|_K(\mathbf{x}) - c_h^n|_K(Q_D)\Big| \le \Big|\nabla c_h^n|_K\Big|\,|\mathbf{x}-Q_D| \le \Big|\nabla c_h^n|_K\Big|\frac{\mathrm{diam}(\sigma_K)}{4-d}\,,$$

with $\mathbf{x} \in \sigma_K \in \mathcal{E}_h^{\rm ext}$, where we have used $|\mathbf{x} - Q_D| \le \mathrm{diam}(\sigma_K)/2$ for $d = 2$ but only $|\mathbf{x} - Q_D| \le \mathrm{diam}(\sigma_K)$ for $d = 3$. Similarly,

$$\left|c_h^n|_K(\mathbf{x}) - c_h^n|_L(\mathbf{x})\right| \le \left|\nabla c_h^n|_K\right| \frac{\mathrm{diam}(\sigma_{K,L})}{4-d} + \left|\nabla c_h^n|_L\right| \frac{\mathrm{diam}(\sigma_{K,L})}{4-d} \qquad \mathbf{x} \in \sigma_{K,L} \in \mathcal{E}_h^{\rm int}\,.$$

We have from the smoothness of $\mathbf{w}$

$$\mathbf{w} \cdot \mathbf{n}_{\sigma_D}(\mathbf{x}) = \mathbf{w} \cdot \mathbf{n}_{\sigma_D}(Q_D) + f(\boldsymbol{\xi})|Q_D - \mathbf{x}| \qquad \mathbf{x} \in \sigma_D \in \mathcal{E}_h\,,\ \boldsymbol{\xi} \in [Q_D, \mathbf{x}]$$

with $|f(\boldsymbol{\xi})| \le C_{\mathbf{w}}$. Thus

$$\int_{\sigma_K} c_h^n|_K(\mathbf{x}) f(\mathbf{x}) |Q_D - \mathbf{x}| \,\mathrm{d}\gamma(\mathbf{x}) \le C_{\mathbf{w}} \Big(\frac{\mathrm{diam}(\sigma_K)}{4-d}\Big)^2 \left|\nabla c_h^n|_K\right| |\sigma_K|$$

for an exterior side $\sigma_K$ and similarly

$$\int_{\sigma_{K,L}} \Big(c_h^n|_K(\mathbf{x}) - c_h^n|_L(\mathbf{x})\Big) f(\boldsymbol{\xi}) |Q_D - \mathbf{x}| \,\mathrm{d}\gamma(\mathbf{x}) \le C_{\mathbf{w}} \Big(\frac{\mathrm{diam}(\sigma_{K,L})}{4-d}\Big)^2 \Big(\left|\nabla c_h^n|_K\right| + \left|\nabla c_h^n|_L\right|\Big) |\sigma_{K,L}|$$

for an interior side $\sigma_{K,L}$. Using these estimates, we immediately come to

$$\begin{aligned} |T''_{D_3}| &\le C_{\mathbf{w}} \frac{h}{(4-d)^2} \frac{d+1}{d-1} \sum_{n=1}^{N} \int_{t_{n-1}}^{t_n} \sum_{K \in \mathcal{T}_h} \left|\nabla c_h^n|_K\right| \mathrm{diam}(K)^d \,\mathrm{d}t \\ &\le \frac{C_{\mathbf{w}}}{\kappa_{\mathcal{T}}} \frac{h}{(4-d)^2} \frac{d+1}{d-1} \sum_{n=1}^{N} \triangle t_n \sum_{K \in \mathcal{T}_h} \left|\nabla c_h^n|_K\right| |K| \le \frac{C_{\mathbf{w}}}{\kappa_{\mathcal{T}}} \frac{h}{(4-d)^2} \frac{d+1}{d-1} \Big(\frac{C_{\rm ae}}{c_{\mathbf{S}}}\Big)^{\frac{1}{2}} T^{\frac{1}{2}} |\Omega|^{\frac{1}{2}}\,, \end{aligned}$$

using the fact that each $\nabla c_h^n|_K$ is in the summation over all sides just $(d+1)$-times, $|\sigma_D| \le \mathrm{diam}(K)^{d-1}/(d-1)$ and $\mathrm{diam}(\sigma_D) \le \mathrm{diam}(K) \le h$ for all $\sigma_D \in \mathcal{E}_K$, Assumption *(B)*, the Cauchy–Schwarz inequality, and the a priori estimate (1.28). Thus $T''_{D_3} \to 0$ as $h \to 0$.

To conclude that $T'_{D_3} \to 0$ as $h, \triangle t \to 0$, it remains to show that

$$-\sum_{n=1}^{N} \int_{t_{n-1}}^{t_n} \sum_{K \in \mathcal{T}_h} \int_K c_h^n(\mathbf{x}) \nabla \cdot \mathbf{w}(\mathbf{x}, t) \,\mathrm{d}\mathbf{x}\,\mathrm{d}t + \int_0^T \int_\Omega u(\mathbf{x}, t) \nabla \cdot \mathbf{w}(\mathbf{x}, t) \,\mathrm{d}\mathbf{x}\,\mathrm{d}t \longrightarrow 0\,.$$

This is however immediate, since we can rewrite it as

$$\int_0^T \int_\Omega (u(\mathbf{x}, t) - c_{h,\triangle t}(\mathbf{x}, t)) \nabla \cdot \mathbf{w}(\mathbf{x}, t) \,\mathrm{d}\mathbf{x}\,\mathrm{d}t \longrightarrow 0\,,$$

which is a consequence of the strong $L^2(Q_T)$ convergence of $c_{h,\triangle t}$ to $u$. Thus $T'_{D_3} \to 0$ and consequently $T_{D_3} \to 0$ as $h, \triangle t \to 0$.

Using (1.56) and (1.57), we see that

$$T_D \longrightarrow \int_0^T \int_\Omega \mathbf{S} \nabla u(\mathbf{x}, t) \cdot \nabla \psi(\mathbf{x}, t) \,\mathrm{d}\mathbf{x}\,\mathrm{d}t \ \text{ as } \ h, \triangle t \to 0\,. \tag{1.61}$$

**Remark 1.6.3. (Nonconforming approximation)** *The fact that $T''_{D_3}$ given by (1.59) is not immediately equal to zero is the consequence of the nonconforming-type approximation. However, since the approximation is continuous in the barycentres of interior sides and equal to zero in the barycentres of exterior sides, (1.60) is fulfilled and consequently $T''_{D_3}$ is of order $h$, which suffices for the convergence.*

**Convection term**

We begin by denoting

$$\mathbf{v}^n(\mathbf{x}) := \frac{1}{\triangle t_n}\int_{t_{n-1}}^{t_n} \mathbf{v}(\mathbf{x},t)\,\mathrm{d}t \qquad n\in\{1,2,\ldots,N\}\,,\ \mathbf{x}\in\Omega\,. \tag{1.62}$$

We now show the validity of two passages to the limit. First, we intend to show that

$$\mu\sum_{n=1}^{N}\triangle t_n\sum_{D\in\mathcal{D}_h}\sum_{E\in\mathcal{N}(D)}\mathbf{v}^n_{D,E}\,\overline{c^n_{D,E}}\,\psi(Q_D,t_{n-1})+\mu\sum_{n=1}^{N}\triangle t_n\sum_{D\in\mathcal{D}_h}c^n_D\sum_{E\in\mathcal{N}(D)} \tag{1.63}$$
$$\int_{\sigma_{D,E}}\mathbf{v}^n(\mathbf{x})\cdot\mathbf{n}_{D,E}\,\psi(\mathbf{x},t_{n-1})\,\mathrm{d}\gamma(\mathbf{x})-\mu\sum_{n=1}^{N}\triangle t_n\sum_{D\in\mathcal{D}_h}c^n_D\int_D\nabla\cdot\mathbf{v}^n(\mathbf{x})\psi(\mathbf{x},t_{n-1})\,\mathrm{d}\mathbf{x}\longrightarrow 0$$

as $h\to 0$. We add and subtract the terms $c^n_D\psi(Q_D,t_{n-1})\mathbf{v}^n_{D,E}$ and $\overline{c^n_{D,E}}\int_{\sigma_{D,E}}\mathbf{v}^n(\mathbf{x})\cdot\mathbf{n}_{D,E}\,\psi(\mathbf{x},t_{n-1})\,\mathrm{d}\gamma(\mathbf{x})$ to each term of the left-hand side of (1.63). We denote

$$\begin{aligned}
T_{C_1} &:= \mu\sum_{n=1}^{N}\triangle t_n\sum_{D\in\mathcal{D}_h}\sum_{E\in\mathcal{N}(D)}(\overline{c^n_{D,E}}-c^n_D)\Big(\psi(Q_D,t_{n-1})\mathbf{v}^n_{D,E}\\
&\quad-\int_{\sigma_{D,E}}\mathbf{v}^n(\mathbf{x})\cdot\mathbf{n}_{D,E}\,\psi(\mathbf{x},t_{n-1})\,\mathrm{d}\gamma(\mathbf{x})\Big)\,,\\
T_{C_2} &:= \mu\sum_{n=1}^{N}\triangle t_n\sum_{D\in\mathcal{D}_h}\sum_{E\in\mathcal{N}(D)}\overline{c^n_{D,E}}\int_{\sigma_{D,E}}\mathbf{v}^n(\mathbf{x})\cdot\mathbf{n}_{D,E}\,\psi(\mathbf{x},t_{n-1})\,\mathrm{d}\gamma(\mathbf{x})\,,\\
T_{C_3} &:= \mu\sum_{n=1}^{N}\triangle t_n\sum_{D\in\mathcal{D}_h}c^n_D\psi(Q_D,t_{n-1})\sum_{E\in\mathcal{N}(D)}\mathbf{v}^n_{D,E}\,,\\
T_{C_4} &:= \mu\sum_{n=1}^{N}\triangle t_n\sum_{D\in\mathcal{D}_h}c^n_D\int_D\nabla\cdot\mathbf{v}^n(\mathbf{x})\psi(\mathbf{x},t_{n-1})\,\mathrm{d}\mathbf{x}\,.
\end{aligned}$$

One can easily verify that (1.63) is satisfied when $T_{C_1}\to 0$, $T_{C_2}\to 0$, and $(T_{C_3}-T_{C_4})\to 0$ as $h\to 0$.

We begin with $T_{C_2}$. We denote

$$\mathbf{v}^n_{\psi;D,E} := \int_{\sigma_{D,E}}\mathbf{v}^n(\mathbf{x})\cdot\mathbf{n}_{D,E}\,\psi(\mathbf{x},t_{n-1})\,\mathrm{d}\gamma(\mathbf{x})\,.$$

Since the summation in $T_{C_2}$ is over all $D\in\mathcal{D}_h$ and all its neighbors, each interior dual side is in the summation just twice. We consider one fixed interior dual side $\sigma_{D,E}$, where we have denoted $D$ and $E$ such that $\mathbf{v}^n_{D,E}\ge 0$, and have

$$\Big(c^n_D+\alpha^n_{D,E}(c^n_E-c^n_D)\Big)\mathbf{v}^n_{\psi;D,E}+\Big(c^n_D+\alpha^n_{D,E}(c^n_E-c^n_D)\Big)\mathbf{v}^n_{\psi;E,D}=0\,,$$

considering the definition of the local Péclet upstream weighting (1.10) and $\mathbf{v}^n_{\psi;D,E}=-\mathbf{v}^n_{\psi;E,D}$. Thus $T_{C_2}=0$.

Next we consider $T_{C_3}$ and $T_{C_4}$. We immediately have that

$$\sum_{E\in\mathcal{N}(D)}\mathbf{v}^n_{D,E}=\int_D\nabla\cdot\mathbf{v}^n(\mathbf{x})\,\mathrm{d}\mathbf{x}\qquad\forall D\in\mathcal{D}_h^{\mathrm{int}}\,,$$

using the definition of $\mathbf{v}_{D,E}^n$. We further estimate

$$\begin{aligned}
|T_{C_3} - T_{C_4}| &= \Big|\mu \sum_{n=1}^{N} \triangle t_n \sum_{D\in\mathcal{D}_h^{\mathrm{int}}} c_D^n \int_D \nabla\cdot\mathbf{v}^n(\mathbf{x})\Big(\psi(Q_D,t_{n-1}) - \psi(\mathbf{x},t_{n-1})\Big)\,\mathrm{d}\mathbf{x}\Big| \\
&\le C_{2,\psi} h\mu \sum_{n=1}^{N}\sum_{D\in\mathcal{D}_h} |c_D^n| \int_{t_{n-1}}^{t_n}\int_D q_S(\mathbf{x},t)\,\mathrm{d}\mathbf{x}\,\mathrm{d}t \qquad (1.64)\\
&\le C_{2,\psi} h\mu \Big(\sum_{n=1}^{N}\sum_{D\in\mathcal{D}_h} \triangle t_n |D| (c_D^n)^2\Big)^{\frac12} \left(\sum_{n=1}^{N}\sum_{D\in\mathcal{D}_h} \frac{\Big(\int_{t_{n-1}}^{t_n}\int_D q_S(\mathbf{x},t)\,\mathrm{d}\mathbf{x}\,\mathrm{d}t\Big)^2}{\triangle t_n |D|}\right)^{\frac12} \\
&\le C_{2,\psi} h\mu \Big(\frac{C_{\mathrm{ae}}}{c_\beta} T\Big)^{\frac12} \|q_S\|_{0,Q_T}\,,
\end{aligned}$$

considering the boundary condition $c_D^n = 0$ for all $D \in \mathcal{D}_h^{\mathrm{ext}}$,

$$|\psi(Q_D,t_{n-1}) - \psi(\mathbf{x},t_{n-1})| \le C_{2,\psi} h \qquad (1.65)$$

for all $\mathbf{x} \in D$,

$$\int_D |\nabla\cdot\mathbf{v}^n(\mathbf{x})|\,\mathrm{d}\mathbf{x} = \frac{1}{\triangle t_n}\int_D\int_{t_{n-1}}^{t_n} \nabla\cdot\mathbf{v}(\mathbf{x},t)\,\mathrm{d}t\,\mathrm{d}\mathbf{x} = \frac{1}{\triangle t_n}\int_D\int_{t_{n-1}}^{t_n} q_S(\mathbf{x},t)\,\mathrm{d}t\,\mathrm{d}\mathbf{x}\,,$$

which follows from Assumption *(A4)*, the Cauchy–Schwarz inequality, and the a priori estimate (1.26). Thus $(T_{C_3} - T_{C_4}) \to 0$ as $h \to 0$.

We finally turn to $T_{C_1}$. We first define

$$T_{C_5} := \sum_{n=1}^{N} \triangle t_n \sum_{D\in\mathcal{D}_h}\sum_{E\in\mathcal{N}(D)} \mathrm{diam}(K_{D,E})^{d-2} (\overline{c_{D,E}^n} - c_D^n)^2\,.$$

We have

$$(\overline{c_{D,E}^n} - c_D^n)^2 = \Big(\alpha_{D,E}^n (c_E^n - c_D^n)\Big)^2 \le \frac14 (c_E^n - c_D^n)^2$$

when $\mathbf{v}_{D,E}^n \ge 0$, considering the definition of the local Péclet upstream weighting (1.10) and Remark 1.3.3, which gives $0 \le \alpha_{D,E}^n \le 1/2$. Similarly, when $\mathbf{v}_{D,E}^n < 0$, we come to

$$(\overline{c_{D,E}^n} - c_D^n)^2 = \Big((c_E^n - c_D^n)(1-\alpha_{D,E}^n)\Big)^2 \le (c_E^n - c_D^n)^2\,.$$

We have

$$\begin{aligned}
T_{C_5} &\le 2\sum_{n=1}^{N} \triangle t_n \sum_{\sigma_{D,E}\in\mathcal{F}_h^{\mathrm{int}}} \mathrm{diam}(K_{D,E})^{d-2} (c_E^n - c_D^n)^2 \\
&\le \frac{d+1}{d\kappa_{\mathcal{T}}} \sum_{n=1}^{N} \triangle t_n \|c_h^n\|_{X_h}^2 \le \frac{d+1}{d\kappa_{\mathcal{T}}} \frac{C_{\mathrm{ae}}}{c_{\mathbf{S}}}\,,
\end{aligned}$$

noticing that each interior dual side is in the original summation just twice, using the estimate (1.6) and the a priori estimate (1.28). We next define

$$\begin{aligned}
T_{C_6} := \sum_{n=1}^{N} \triangle t_n \sum_{D\in\mathcal{D}_h}\sum_{E\in\mathcal{N}(D)} &\frac{1}{\mathrm{diam}(K_{D,E})^{d-2}} \\
&\Big(\int_{\sigma_{D,E}} \mathbf{v}^n(\mathbf{x})\cdot\mathbf{n}_{D,E}\Big(\psi(Q_D,t_{n-1}) - \psi(\mathbf{x},t_{n-1})\Big)\,\mathrm{d}\gamma(\mathbf{x})\Big)^2
\end{aligned}$$

and estimate

$$\begin{aligned}|T_{C_6}| &\le C_{2,\psi}^2 h^2 C_{\mathbf{v}}^2 \sum_{n=1}^{N} \triangle t_n \sum_{D\in\mathcal{D}_h} \sum_{E\in\mathcal{N}(D)} \frac{1}{\operatorname{diam}(K_{D,E})^{d-2}} |\sigma_{D,E}|^2 \\ &\le C_{2,\psi}^2 h^2 C_{\mathbf{v}}^2 \frac{(d+1)d}{(d-1)^2} \sum_{n=1}^{N} \triangle t_n \sum_{K\in\mathcal{T}_h} \operatorname{diam}(K)^d \le C_{2,\psi}^2 h^2 \frac{C_{\mathbf{v}}^2}{\kappa_{\mathcal{T}}} \frac{(d+1)d}{(d-1)^2} |\Omega| T\,,\end{aligned}$$

using (1.65), $|\mathbf{v}_{D,E}^n| \le C_{\mathbf{v}} |\sigma_{D,E}|$ following from Assumption *(A4)*, (1.8), noticing that each interior dual side is in the original summation just twice and that each $K \in \mathcal{T}_h$ contains exactly $\binom{d+1}{2} = \dfrac{(d+1)d}{2}$ dual sides, and finally Assumption *(B)*. We now notice that

$$T_{C_1}^2 \le \mu^2 T_{C_5} T_{C_6}\,,$$

using the Cauchy–Schwarz inequality, and hence $T_{C_1} \to 0$ as $h \to 0$. Thus (1.63) is satisfied.

Using the Green theorem and considering $c_D^n = 0$ for all $D \in \mathcal{D}_h^{\mathrm{ext}}$, we easily come to

$$\begin{aligned}&\mu \sum_{n=1}^{N} \triangle t_n \sum_{D\in\mathcal{D}_h} c_D^n \sum_{E\in\mathcal{N}(D)} \int_{\sigma_{D,E}} \mathbf{v}^n(\mathbf{x}) \cdot \mathbf{n}_{D,E}\, \psi(\mathbf{x}, t_{n-1})\, \mathrm{d}\gamma(\mathbf{x}) \triangle t_n \qquad (1.66)\\ = \;& \mu \sum_{n=1}^{N} \sum_{D\in\mathcal{D}_h} c_D^n \int_D \mathbf{v}^n(\mathbf{x}) \nabla\psi(\mathbf{x}, t_{n-1})\, \mathrm{d}\mathbf{x} + \mu \sum_{n=1}^{N} \triangle t_n \sum_{D\in\mathcal{D}_h} c_D^n \int_D \nabla\cdot\mathbf{v}^n(\mathbf{x}) \psi(\mathbf{x}, t_{n-1})\, \mathrm{d}\mathbf{x}\,.\end{aligned}$$

We will now demonstrate that

$$\begin{aligned}&\mu \sum_{n=1}^{N} \triangle t_n \sum_{D\in\mathcal{D}_h} c_D^n \int_D \mathbf{v}^n(\mathbf{x}) \cdot \nabla\psi(\mathbf{x}, t_{n-1})\, \mathrm{d}\mathbf{x} \qquad (1.67)\\ \longrightarrow \;& \mu \int_0^T \int_\Omega u(\mathbf{x}, t) \mathbf{v}(\mathbf{x}, t) \cdot \nabla\psi(\mathbf{x}, t)\, \mathrm{d}\mathbf{x}\, \mathrm{d}t \;\text{ as }\; h, \triangle t \to 0\,.\end{aligned}$$

We introduce

$$\begin{aligned}T_{C_7} &:= \mu \sum_{n=1}^{N} \int_{t_{n-1}}^{t_n} \int_\Omega \tilde{c}_{h,\triangle t}(\mathbf{x}, t) \mathbf{v}^n(\mathbf{x}) \cdot \Big(\nabla\psi(\mathbf{x}, t_{n-1}) - \nabla\psi(\mathbf{x}, t)\Big)\, \mathrm{d}\mathbf{x}\, \mathrm{d}t\,,\\ T_{C_8} &:= \mu \sum_{n=1}^{N} \int_{t_{n-1}}^{t_n} \int_\Omega \Big(\tilde{c}_{h,\triangle t}(\mathbf{x}, t) - u(\mathbf{x}, t)\Big) \mathbf{v}^n(\mathbf{x}) \cdot \nabla\psi(\mathbf{x}, t)\, \mathrm{d}\mathbf{x}\, \mathrm{d}t\,,\\ T_{C_9} &:= \mu \sum_{n=1}^{N} \int_{t_{n-1}}^{t_n} \int_\Omega u(\mathbf{x}, t) \Big(\mathbf{v}^n(\mathbf{x}) - \mathbf{v}(\mathbf{x}, t)\Big) \cdot \nabla\psi(\mathbf{x}, t)\, \mathrm{d}\mathbf{x}\, \mathrm{d}t\,.\end{aligned}$$

We have

$$|\nabla\psi(\mathbf{x}, t_{n-1}) - \nabla\psi(\mathbf{x}, t)| \le g(\triangle t)$$

for $t \in (t_{n-1}, t_n]$ and thus

$$|T_{C_7}| \le g(\triangle t)\mu \sum_{n=1}^{N} \sum_{D\in\mathcal{D}_h} |c_D^n| \int_D \int_{t_{n-1}}^{t_n} |\mathbf{v}(\mathbf{x}, t)|\, \mathrm{d}\mathbf{x}\, \mathrm{d}t \le g(\triangle t)\mu \Big(\frac{C_{\mathrm{ae}}}{c_\beta} T\Big)^{\frac{1}{2}} \|\mathbf{v}\|_{0,Q_T}\,,$$

using the same estimate as in (1.64). Thus $T_{C_7} \to 0$ as $\triangle t \to 0$. It is immediate that $T_{C_8} \to 0$ as $h, \triangle t \to 0$, using the strong (and consequently weak) convergence of $\tilde{c}_{h,\triangle t}$ to $u$. By Assumption *(A4)* and (1.62) $\mathbf{v}$ and $\mathbf{v}^n$ are bounded, and hence the piecewise constant in time approximation given by $\mathbf{v}^n$ converges strongly in $\mathbf{L}^2(Q_T)$ to $\mathbf{v}$ as $\triangle t \to 0$. Since $|\nabla\psi| \le C_{2,\psi}$ and $u \in L^2(Q_T)$, it suffices to use the Cauchy–Schwarz inequality to conclude that $T_{C_9} \to 0$ as $\triangle t \to 0$. Thus (1.67) is fulfilled. Finally, using (1.63), (1.66), and (1.67), we see that

$$T_C \longrightarrow -\mu \int_0^T \int_\Omega u(\mathbf{x},t)\mathbf{v}(\mathbf{x},t)\cdot\nabla\psi(\mathbf{x},t)\,\mathrm{d}\mathbf{x}\,\mathrm{d}t \;\text{ as }\; h,\triangle t \to 0\,. \tag{1.68}$$

### Reaction term

We would now like to show that

$$T_R \longrightarrow \int_0^T \int_\Omega F(u(\mathbf{x},t))\psi(\mathbf{x},t)\,\mathrm{d}\mathbf{x}\,\mathrm{d}t \;\text{ as }\; h,\triangle t \to 0\,. \tag{1.69}$$

For this purpose, we introduce

$$\begin{aligned} T_{R_1} &:= \sum_{n=1}^N \sum_{D\in\mathcal{D}_h} F(c_D^n) \int_{t_{n-1}}^{t_n} \int_D \Big(\psi(Q_D,t_{n-1}) - \psi(\mathbf{x},t)\Big)\,\mathrm{d}\mathbf{x}\,\mathrm{d}t\,,\\ T_{R_2} &:= \sum_{n=1}^N \sum_{D\in\mathcal{D}_h} \int_{t_{n-1}}^{t_n} \int_D \Big(F(c_D^n) - F(u(\mathbf{x},t))\Big)\psi(\mathbf{x},t)\,\mathrm{d}\mathbf{x}\,\mathrm{d}t\,. \end{aligned}$$

We have

$$|\psi(Q_D,t_{n-1}) - \psi(\mathbf{x},t)| \le C_{3,\psi}(h+\triangle t) \tag{1.70}$$

for all $\mathbf{x} \in D$ and $t \in (t_{n-1}, t_n]$, and thus

$$|T_{R_1}| \le C_{3,\psi}L_F(h+\triangle t)\sum_{n=1}^N \sum_{D\in\mathcal{D}_h} \triangle t_n |D||c_D^n| \le C_{3,\psi}L_F(h+\triangle t)\Big(\frac{C_{\mathrm{ae}}}{c_\beta}T\Big)^{\frac{1}{2}}|\Omega|^{\frac{1}{2}}T^{\frac{1}{2}}\,,$$

using the Lipschitz continuity of $F$, following either from Assumption *(A6)* or *(A7)*, the Cauchy–Schwarz inequality, and the a priori estimate (1.26). Hence, $T_{R_1} \to 0$ as $h, \triangle t \to 0$. We have

$$|T_{R_2}| \le C_{1,\psi}L_F \int_0^T \int_\Omega |\tilde{c}_{h,\triangle t}(\mathbf{x},t) - u(\mathbf{x},t)|\,\mathrm{d}\mathbf{x}\,\mathrm{d}t\,,$$

which tends to 0 because of the strong $L^2(Q_T)$ convergence of $\tilde{c}_{h,\triangle t}$ to $u$. Thus, (1.69) is fulfilled.

### Sources term

We finally show that

$$T_S \longrightarrow \int_0^T \int_\Omega q(\mathbf{x},t)\psi(\mathbf{x},t)\,\mathrm{d}\mathbf{x}\,\mathrm{d}t \;\text{ as }\; h,\triangle t \to 0\,. \tag{1.71}$$

We set

$$T_{S_1} := \sum_{n=1}^{N} \sum_{D\in\mathcal{D}_h} q_D^n \int_{t_{n-1}}^{t_n} \int_D \Big(\psi(Q_D, t_{n-1}) - \psi(\mathbf{x}, t)\Big) \,\mathrm{d}\mathbf{x}\,\mathrm{d}t\,,$$
$$T_{S_2} := \sum_{n=1}^{N} \sum_{D\in\mathcal{D}_h} \int_{t_{n-1}}^{t_n} \int_D \Big(q_D^n - q(\mathbf{x}, t)\Big)\psi(\mathbf{x}, t) \,\mathrm{d}\mathbf{x}\,\mathrm{d}t\,.$$

We have

$$|T_{S_1}| \le C_{3,\psi}(h + \triangle t) \sum_{n=1}^{N} \sum_{D\in\mathcal{D}_h} \int_{t_{n-1}}^{t_n} \int_D |q(\mathbf{x}, t)| \,\mathrm{d}\mathbf{x}\,\mathrm{d}t \le C_{3,\psi}(h + \triangle t)\|q\|_{0,Q_T}|\Omega|^{\frac{1}{2}}T^{\frac{1}{2}}\,,$$

using (1.70) and the Cauchy–Schwarz inequality. Finally,

$$|T_{S_2}| \le C_{1,\psi} \sum_{n=1}^{N} \sum_{D\in\mathcal{D}_h} \int_{t_{n-1}}^{t_n} \int_D |q_D^n - q(\mathbf{x}, t)| \,\mathrm{d}\mathbf{x}\,\mathrm{d}t\,,$$

which tends to 0 as $h, \triangle t \to 0$ because of the $L^1$ convergence of the piecewise constant approximation $q_D^n$ to $q$. Thus (1.71) is satisfied.

We are now ready to give the final theorem of this chapter:

**Theorem 1.6.4. (Convergence to a weak solution)** *There exist subsequences of $\tilde{c}_{h,\triangle t}$ and $c_{h,\triangle t}$, the approximate solutions of the problem (1.1)–(1.3) by means of the combined finite volume–nonconforming/mixed-hybrid finite element scheme (1.9a)–(1.9c) given by Definition 1.5.3, which converge strongly in $L^2(Q_T)$ to a weak solution of the problem (1.1)–(1.3) given by Definition 1.2.2. If the weak solution is unique, then the whole sequences $\tilde{c}_{h,\triangle t}$, $c_{h,\triangle t}$ converge to the weak solution.*

Proof:

We have from Theorem 1.6.1 that subsequences of $\tilde{c}_{h,\triangle t}$ and $c_{h,\triangle t}$ converge strongly in $L^2(Q_T)$ to some function $u \in L^2(0, T; H_0^1(\Omega))$. The function $u$ satisfies

$$\begin{aligned}
&-\int_0^T \int_\Omega \beta(u(\mathbf{x}, t))\psi_t(\mathbf{x}, t) \,\mathrm{d}\mathbf{x}\,\mathrm{d}t - \int_\Omega \beta(c_0(\mathbf{x}))\psi(\mathbf{x}, 0) \,\mathrm{d}\mathbf{x} \\
&+\int_0^T \int_\Omega \mathbf{S}(\mathbf{x}, t)\nabla u(\mathbf{x}, t) \cdot \nabla\psi(\mathbf{x}, t) \,\mathrm{d}\mathbf{x}\,\mathrm{d}t - \mu \int_0^T \int_\Omega u(\mathbf{x}, t)\mathbf{v}(\mathbf{x}, t) \cdot \nabla\psi(\mathbf{x}, t) \,\mathrm{d}\mathbf{x}\,\mathrm{d}t \\
&+\int_0^T \int_\Omega F(u(\mathbf{x}, t))\psi(\mathbf{x}, t) \,\mathrm{d}\mathbf{x}\,\mathrm{d}t = \int_0^T \int_\Omega q(\mathbf{x}, t)\psi(\mathbf{x}, t) \,\mathrm{d}\mathbf{x}\,\mathrm{d}t
\end{aligned}$$

for all test functions $\psi \in \Psi$, given by (1.46). This follows from (1.54), (1.61), (1.68), (1.69), (1.71), and (1.47). In addition, $\beta(u) \in L^\infty(0, T; L^2(\Omega))$, which follows from (1.27). Thus $u$ is a weak solution of the problem (1.1)–(1.3), because of the density of the set $\Psi$ in the set $\{\varphi;\, \varphi \in L^2(0, T; H_0^1(\Omega)),\, \varphi_t \in L^\infty(Q_T),\, \varphi(\cdot, T) = 0\}$. If the weak solution given by Definition 1.2.2 is unique, then by contradiction the convergence statement is valid for the whole sequences $\tilde{c}_{h,\triangle t}$ and $c_{h,\triangle t}$. □

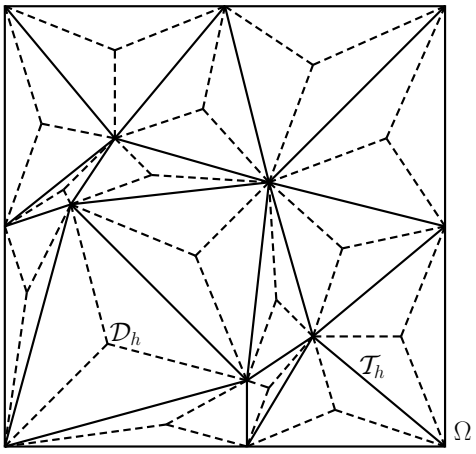


Figure 1.2: Initial space mesh $\mathcal{T}_h$ (solid) and its dual mesh $\mathcal{D}_h$ (dashed)

## 1.7 Numerical experiment

We present the results of a numerical experiment in this section. The computations were done in double precision on a notebook with Intel Pentium 4-M 1.8 GHz processor and MS Windows XP operating system. Machine precision was in power of $10^{-16}$.

We test a model degenerate parabolic convection–diffusion problem with a known traveling wave solution (cf. [81]). In particular, we consider the equation (1.1) for $\Omega = (0,1) \times (0,1)$ and $T = 1$ with

$$\begin{aligned} \beta(c) &= c^{\frac{1}{2}} \text{ for } c \geq 0\,, \\ \mathbf{S} &= \delta \begin{pmatrix} 1 & 0 \\ 0 & 1 \end{pmatrix}, \\ \mathbf{v} &= (v, 0)\,, \\ \mu &= 1\,,\ F(c) = 0\,,\ q = 0\,. \end{aligned}$$

Here, $\delta > 0$ and $v > 0$ are parameters. We fix $v$ to 0.8 and let $\delta$ vary: for large values of $\delta$, diffusion dominates over convection and conversely for small values of $\delta$. The initial and Dirichlet boundary conditions are given by the exact solution

$$c(x,y,t) = \left(1 - e^{\frac{v}{2\delta}(x - vt - p)}\right)^2 \text{ for } x \leq vt + p\,, \quad c(x,y,t) = 0 \text{ for } x \geq vt + p\,.$$

The shift $p$ defines the position of the front of the wave at $t = 0$ and is set to 0.2. Note that the problem is degenerate parabolic since $\beta'(0) = +\infty$ and the solution takes the value of 0.

We perform the simulations on an unstructured triangular mesh of the space domain; the initial mesh is given in Figure 1.2. The initial time step is $T/2$. We refine the space mesh by dividing each triangle regularly into four subtriangles. Each time the space mesh is refined, the time step is divided by two. We define the Péclet number by $\mathrm{Pe} := h\,v/\delta$. The initial conditions are the values of the exact solution for $t = 0$ at the midpoints of triangle edges. The boundary conditions are given similarly. The simulated problem is only one-dimensional. We use this fact to test the performance of the numerical scheme that we propose for strongly irregular two-dimensional meshes. The case where the triangular mesh contains angles greater than $\pi/2$ is similar to the case where the diffusion tensor is anisotropic: in both cases the

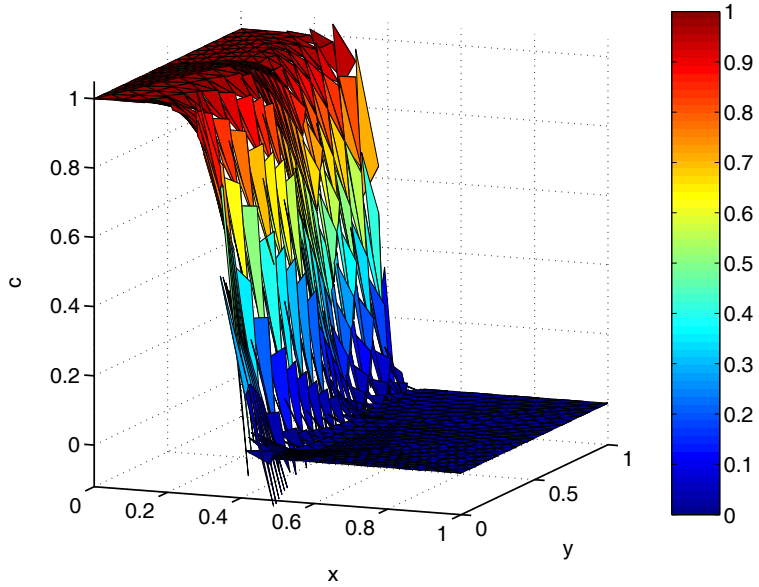


Figure 1.3: Approximate solution at $t = 0.25$, $\delta = 0.01$, $r = 3$

discrete maximum principle is not necessarily satisfied (recall that this principle holds under Assumption *(D)*, cf. Theorem 1.4.11). Hence we need to define the function $\beta(c)$ for $c < 0$. To fulfill Assumptions *(A1)* and *(A2)*, we set $\beta(c) := -\beta(-c)$ for $c < 0$.

At each discrete time level, we have to solve the nonlinear system of algebraic equations given by (1.9a)–(1.9c). Since $\beta'(0) = +\infty$ and since the solution takes the value of 0, we cannot directly apply the Newton method for this purpose. The traditional finite element technique to overcome this difficulty consists in regularization (approximation of $\beta$ by functions with bounded slope), cf. [20]. Another method, applicable however only when the discrete maximum principle holds, consists in perturbing the initial and boundary conditions so that all the values that the scheme works with were strictly positive (the problem is no more degenerate parabolic), see [98, 99]. We use here a method which has been used in the field of the finite volume method (cf. [61]): we introduce new unknowns $u_D^n = \beta(c_D^n)$ and rewrite the system of equations (1.9a)–(1.9c) for these new unknowns. We believe that this approach is advantageous for the following reasons: (i) There is no need to regularize the problem or to perturb the data (now $[\beta^{-1}]'(0) = 0$); (ii) One can directly apply the Newton method to linearize the problem; (iii) The resulting matrices are diagonal for the part of the unknowns corresponding to the region where the concentration is zero. Indeed, on the step $k$ of the linearization at time $t_n$, we approximate $c_E^{n,k} = \beta^{-1}(u_E^{n,k}) \approx \beta^{-1}(u_E^{n,k-1}) + (\beta^{-1})'(u_E^{n,k-1})(u_E^{n,k} - u_E^{n,k-1})$, which vanishes in view of $\beta^{-1}(0) = (\beta^{-1})'(0) = 0$. Let $\{u_D^{n,k}\}_{D\in\mathcal{D}_h^{\rm int}}$ be the solution vector on the step $k$. The linearization is terminated whenever

$$\Big(\sum_{D\in\mathcal{D}_h^{\rm int}} (u_D^{n,k} - u_D^{n,k-1})^2\Big)^{\frac12} \Big/ \Big(\sum_{D\in\mathcal{D}_h^{\rm int}} (u_D^{n,k})^2\Big)^{\frac12} \le \text{1e-10}\,.$$

The bi-conjugate gradients stabilized method (Bi-CGStab) [103, 117], preconditioned by the LU incomplete factorization with drop tolerance 1e-3, cf. [111], is used for the solution of the associated linear systems. The iterations were stopped whenever the relative residual decreased below 1e-10.

| Ref. | T. st. | Unkn. | $\mathrm{Pe}_{\delta=0.05}$ | $t_{\delta=0.05}$ | $\mathrm{Pe}_{\delta=0.01}$ | $t_{\delta=0.01}$ | $\mathrm{Pe}_{\delta=0.0001}$ | $t_{\delta=0.0001}$ |
|---|---|---|---|---|---|---|---|---|
| 1 | 4 | 88 | 4.56 | 0:01 | 22.80 | 0:01 | 2280.0 | 0:01 |
| 3 | 16 | 1504 | 1.14 | 0:16 | 5.70 | 0:15 | 570.0 | 0:11 |
| 5 | 64 | 24448 | 0.29 | 19:11 | 1.43 | 17:49 | 142.5 | 9:51 |

Table 1.1: Number of refinements, number of time steps, number of unknowns, Péclet number, and computational times in min:sec for $\delta = 0.05$, 0.01, and 0.0001, respectively

We consider three values of $\delta$: 0.05, 0.01, and 0.0001. The number of refinements is $r = 1, 3$, and 5 ($r = 0$ corresponds to the initial mesh). We refer to Table 1.1 for the number of unknowns, Péclet numbers, and computational times. For the finest meshes, there were up to 15 Newton steps necessary in the first iteration. This number then decreased to approx. 7 per time step. We can see the approximate solution for $\delta = 0.01$ and $r = 3$ at $t = 0.25$ in Figure 1.3. We give the profiles of approximate solutions in $y = 0.5$ for the different values of $\delta$ and $r$ in Figures 1.4 and 1.5. The profile in $y = 0.5$ is defined by all the calculated values $c_D$ such that $Q_D$ (the midpoint of the edge $\sigma_D$ associated with the dual volume $D$) satisfies $|Q_D - l_{0.5}| \leq 0.25$ for $r = 1$, $|Q_D - l_{0.5}| \leq 0.08$ for $r = 3$, and $|Q_D - l_{0.5}| \leq 0.02$ for $r = 5$, where $l_{0.5}$ is the line $y = 0.5$.

We finally give some comments on the results. First, the scheme works easily for the given irregular mesh, which would not be possible with the standard finite volume method, cf. [61]. This irregularity (angles greater than $\pi/2$) on the other hand causes the violation of the discrete maximum principle. However, this violation is only noticeable for the coarsest meshes ($r = 0, 1$, in power of 1e-3) and disappears with the refinement of the meshes. The scheme naturally works with negative values due to the appropriate definition of $\beta(c)$ for $c < 0$. We remark that the negative values of the approximation that are visible in Figure 1.3 have no relation to the discrete maximum principle; they are only a consequence of a piecewise linear interpretation of the (positive) values $c_D^n$. The influence of unsuitable shapes of the elements is also visible in Figures 1.4 and 1.5—notice the local fluctuations in the profiles for $r = 1$ and 3. This influence is however only because of the finite volume part of the scheme, which can be easily verified by considering a pure hyperbolic problem. Next, the local Péclet upstream weighting reduces the numerical diffusion of full upstream weighting to the amount exactly necessary to ensure the stability of the scheme. In particular, the coefficients $\alpha_{D,E}^n$ given by (1.11) automatically increase with $r$. Moreover, the different values of these parameters for different dual sides of the mesh reflect the local ratio of the diffusion and convection fluxes (recall that e.g. for a dual side parallel with $\mathbf{v}$, the flux of $\mathbf{v}$ through this side is zero). This numerical flux would be still more efficient for a problem where the ratio of $v$ and $\delta$ is not uniform over $\Omega$. Finally, precise approximation of realistic convection-dominated problems on fixed grids with the proposed scheme may still be expensive in terms of the computational cost. A local refinement strategy as that proposed in [95, 96] would then be necessary.

## 1.8 Appendix A: Technical lemmas

We give here some technical lemmas that were needed in this chapter.

**Lemma 1.8.1.** *Let us consider the elliptic problem*

$$-\nabla \cdot (\mathbf{S}\nabla p) = q \quad \text{in } \Omega, \tag{1.72a}$$

$$p = 0 \quad \text{on } \partial\Omega, \tag{1.72b}$$

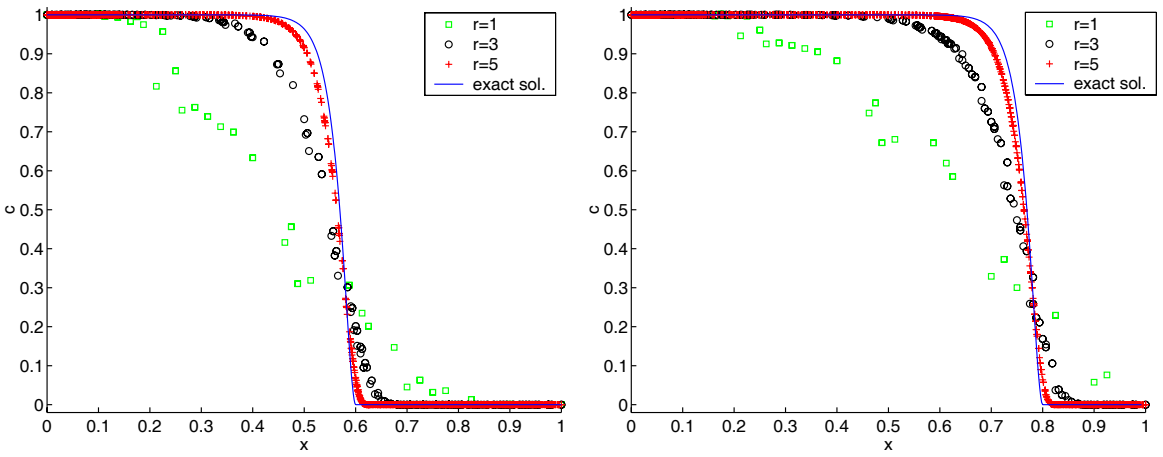


Figure 1.4: Solution profiles for $y = 0.5$ and $\delta = 0.01$, at $t = 0.5$ (left) and at $t = 0.75$ (right)

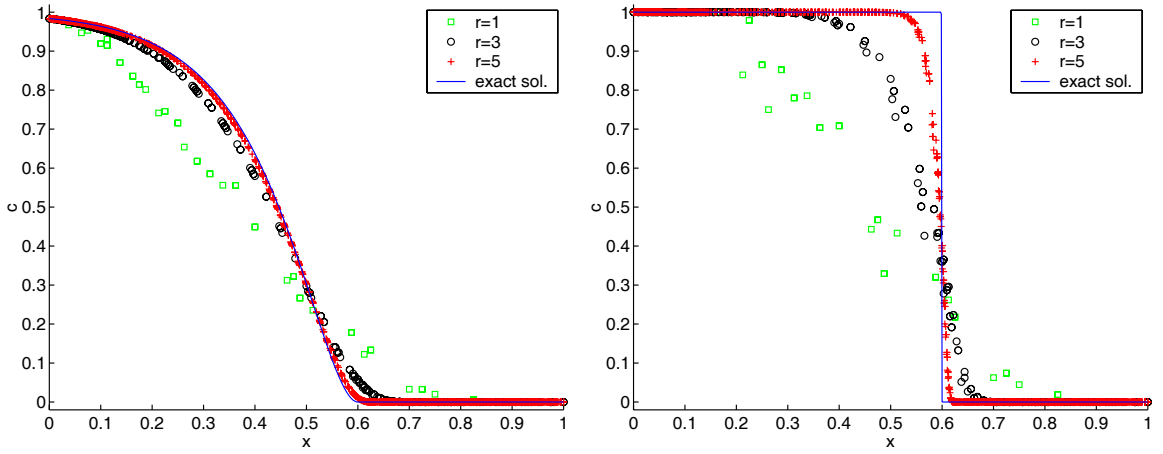


Figure 1.5: Solution profiles for $y = 0.5$ at $t = 0.5$, $\delta = 0.05$ (left) and $\delta = 0.0001$ (right)

*where $q \in L^2(\Omega)$. Then the stiffness matrix for the Lagrange multipliers of the hybridization of the lowest-order Raviart–Thomas mixed finite element method on the simplicial mesh $\mathcal{T}_h$ has the form*

$$\mathbb{M}_{D,E} = -\sum_{K\in\mathcal{T}_h} (\mathbf{S}_K \nabla\varphi_E, \nabla\varphi_D)_{0,K} \qquad D, E \in \mathcal{D}_h^{\mathrm{int}}\,, \tag{1.73}$$

*where*

$$\mathbf{S}_K = \Big(\frac{1}{|K|}\int_K \mathbf{S}^{-1}\,\mathrm{d}\mathbf{x}\Big)^{-1} \qquad \forall K \in \mathcal{T}_h\,. \tag{1.74}$$

Proof:

The hybridization of the lowest-order Raviart–Thomas mixed finite element method for the problem (1.72a)–(1.72b) reads (cf. [33, Section V.1.2]): find $\mathbf{u}_h \in \mathbf{V}_h$, $p_h \in \Phi_h$, and $\lambda_h \in \Lambda_h$

such that

$$\sum_{K\in\mathcal{T}_h}\left\{(\mathbf{S}^{-1}\mathbf{u}_h,\mathbf{v}_h)_{0,K}-(\nabla\cdot\mathbf{v}_h,p_h)_{0,K}+\langle\mathbf{v}_h\cdot\mathbf{n},\lambda_h\rangle_{\partial K}\right\}=0\qquad\forall\,\mathbf{v}_h\in\mathbf{V}_h\,,\quad(1.75a)$$

$$-\sum_{K\in\mathcal{T}_h}(\nabla\cdot\mathbf{u}_h,\phi_h)_{0,K}=-(q,\phi_h)_{0,\Omega}\qquad\forall\phi_h\in\Phi_h\,,\quad(1.75b)$$

$$\sum_{K\in\mathcal{T}_h}\langle\mathbf{u}_h\cdot\mathbf{n},\mu_h\rangle_{\partial K}=0\qquad\forall\mu_h\in\Lambda_h\,.\quad(1.75c)$$

Here, $\mathbf{V}_h$ is the space of elementwise linear vector functions such that $\mathbf{u}_h\in\mathbf{V}_h$ satisfies $\mathbf{u}_h|_K=(a_K+d_Kx,\,b_K+d_Ky)$ if $d=2$ and $\mathbf{u}_h|_K=(a_K+d_Kx,\,b_K+d_Ky,\,c_K+d_Kz)$ if $d=3$ for all $K\in\mathcal{T}_h$, $\Phi_h$ is the space of elementwise constant scalar functions, and $\Lambda_h$ is the space of sidewise constant scalar Lagrange multipliers. For all $D\in\mathcal{D}_h$, we denote $\lambda_h|_{\sigma_D}$ by $\lambda_D$ and require $\lambda_D=0$ for all $D\in\mathcal{D}_h^{\rm ext}$. We now extend the ideas of [38], where the tensor $\mathbf{S}$ is supposed piecewise constant on $\mathcal{T}_h$.

Let us set $\tilde\lambda_h:=\sum_{D\in\mathcal{D}_h}\lambda_D\varphi_D$. Using (1.16), we have

$$\sum_{\sigma_D\in\mathcal{E}_K}\lambda_D|\sigma_D|\mathbf{n}_{\sigma_D}=|K|\sum_{\sigma_D\in\mathcal{E}_K}\lambda_D\nabla\varphi_D|_K=|K|\,\nabla\tilde\lambda_h|_K\,.$$

Then denoting the unit coordinate vectors as $\mathbf{e}_i$ and taking, respectively, $\mathbf{v}_h=\mathbf{e}_i$ in $K$, $1\le i\le d$, $\mathbf{v}_h=0$ otherwise as the test functions in (1.75a), we come to

$$\int_K\mathbf{S}^{-1}\mathbf{u}_h\,\mathrm{d}\mathbf{x}+|K|\,\nabla\tilde\lambda_h|_K=0\qquad\forall K\in\mathcal{T}_h\,.$$

Next we notice that the stiffness matrix does not depend on $q$ and hence we can pose $q=0$. Considering $\phi_h=1$ on $K$ and zero otherwise in (1.75b), this yields $d_K=0$ for all $K\in\mathcal{T}_h$. Hence $\mathbf{u}_h|_K=-\mathbf{S}_K\nabla\tilde\lambda_h|_K$ with $\mathbf{S}_K$ given by (1.74). It now suffices to substitute this into (1.75c) to obtain a system for the Lagrange multipliers $\lambda_D$, $D\in\mathcal{D}_h^{\rm int}$, with the matrix given by (1.73). □

**Lemma 1.8.2.** *Let us consider the function $B(s)$, $s\in\mathbb{R}$, $B(s)=\beta(s)s-\int_0^s\beta(\tau)\,\mathrm{d}\tau$, with $\beta$ satisfying Assumption (A1). Then $B(s)\ge s^2c_\beta/2$ for all $s\in\mathbb{R}$.*

Proof:

Let us first consider a given $s\ge0$. We then have for each $h>0$

$$\frac{B(s+h)-B(s)}{h}=\frac{\beta(s+h)-\beta(s)}{h}s+\beta(s+h)-\frac1h\int_s^{s+h}\beta(\tau)\,\mathrm{d}\tau\,.$$

This gives, using that $\beta(s+h)-\beta(s)\ge c_\beta h$, which follows from Assumption *(A1)*, and the continuity of $\beta$

$$\liminf_{h\to0^+}\frac{B(s+h)-B(s)}{h}\ge c_\beta s\,.$$

Hence, using the fact that $B(0)=0$ and that $s^2c_\beta/2=0$ for $s=0$, we have $B(s)\ge s^2c_\beta/2$ for all $s\ge0$. The proof for $s<0$ proceeds similarly. □

**Lemma 1.8.3.** *Let $\beta$ satisfy Assumption (A2). Then $[\beta(s)]^2\le2C_\beta^2+4L_\beta^2P^2+4L_\beta^2s^2$ for all $s\in\mathbb{R}$.*

PROOF:
If $s \in [-P, P]$, the assertion of the lemma is trivially satisfied, since by Assumption *(A2)*, $|\beta(s)| \leq C_\beta$. If $s > P$, then using the Lipschitz continuity of $\beta$ on $[P, +\infty)$, one has

$$\beta(s) = \beta(P) + \beta(s) - \beta(P) \leq \beta(P) + L_\beta(s - P)$$

and similarly for $s < -P$. Thus, using the inequality $(a \pm b)^2 \leq 2(a^2 + b^2)$ and $|\beta(\pm P)| \leq C_\beta$, one has, for $|s| > P$,

$$[\beta(s)]^2 \leq 2C_\beta^2 + 4L_\beta^2 P^2 + 4L_\beta^2 s^2 \,. \quad \square$$

**Lemma 1.8.4.** *Let $\Omega \subset \mathbb{R}^p$, $p > 1$, be an open bounded set, $\{a_n, n \in \mathbb{N}\}$ a sequence of functions from $L^2(\Omega)$, defined by zero on $\mathbb{R}^p \setminus \Omega$, $h_n$ a sequence of non-negative real values with $\lim_{n\to\infty} h_n = 0$, and $C > 0$. Let the functions $a_n$ satisfy*

$$\int_\Omega \Big(a_n(\mathbf{x} + \boldsymbol{\eta}) - a_n(\mathbf{x})\Big)^2 \,\mathrm{d}\mathbf{x} \leq C|\boldsymbol{\eta}| + h_n \qquad \forall \boldsymbol{\eta} \in \mathbb{R}^p \,, \forall\, n \in \mathbb{N} \,. \tag{1.76}$$

*Then*

$$\forall \varepsilon > 0 \quad \exists \zeta > 0 \quad \forall \boldsymbol{\eta} \in \mathbb{R}^p, |\boldsymbol{\eta}| < \zeta \quad \forall n \in \mathbb{N} \quad \int_\Omega \Big(a_n(\mathbf{x} + \boldsymbol{\eta}) - a_n(\mathbf{x})\Big)^2 \,\mathrm{d}\mathbf{x} \leq \varepsilon \,. \tag{1.77}$$

PROOF:
Let us consider a fixed $\varepsilon > 0$. Let $n_0$ be such that $\forall n > n_0$, $|h_n| < \varepsilon/2$. The continuity in mean of the functions $a_1, \ldots, a_{n_0}$ implies

$$\int_{\mathbb{R}^p} \Big(a_i(\mathbf{x} + \boldsymbol{\eta}) - a_i(\mathbf{x})\Big)^2 \,\mathrm{d}\mathbf{x} \longrightarrow 0 \ \text{ as } \ |\boldsymbol{\eta}| \to 0 \qquad \forall i \in \{1, \ldots, n_0\} \,,$$

or, more precisely,

$$\begin{gathered} \forall i \in \{1, \ldots, n_0\} \quad \forall \varepsilon^* > 0 \quad \exists \zeta_i^* > 0 \quad \forall \boldsymbol{\eta}^* \in \mathbb{R}^p, |\boldsymbol{\eta}^*| < \zeta_i^* \\ \int_{\mathbb{R}^p} \Big(a_i(\mathbf{x} + \boldsymbol{\eta}^*) - a_i(\mathbf{x})\Big)^2 \,\mathrm{d}\mathbf{x} \leq \varepsilon^* \,. \end{gathered} \tag{1.78}$$

We set $\varepsilon^* = \varepsilon$ in (1.78) and define $\zeta^* := \min_{i=1,\ldots,n_0} \zeta_i^*$. Since $n_0 < \infty$, $\zeta^* > 0$. It is finally enough to choose

$$\zeta = \min\left\{\zeta^*, \frac{\varepsilon}{2C}\right\} \,.$$

Indeed, for $n < n_0$, estimate (1.77) is valid due to (1.78). For $n > n_0$, (1.76) and the fact that $|h_n| < \varepsilon/2$ yields the assertion of the lemma. $\square$

**Lemma 1.8.5.** *Let $\Omega \subset \mathbb{R}^p$, $p \geq 1$, be an open bounded set and let $d \geq 1$. Let the vector-valued functions $\mathbf{u}^n \in [L^2(\Omega)]^d$ such that $\int_\Omega \mathbf{u}^n \cdot \mathbf{u}^n \,\mathrm{d}\mathbf{x} \leq U^2$, $U > 0$, converge weakly in $[L^2(\Omega)]^d$ to some function $\mathbf{u} \in [L^2(\Omega)]^d$. Let the matrix-valued functions $\mathbf{M}^n$, $\mathbf{M}^n_{i,j} \in L^2(\Omega)$, $1 \leq i, j \leq d$, converge elementwise strongly in $L^2(\Omega)$ to some function $\mathbf{M}$. Then*

$$\int_\Omega \mathbf{M}^n \mathbf{u}^n \cdot \psi \,\mathrm{d}\mathbf{x} \to \int_\Omega \mathbf{M}\mathbf{u} \cdot \psi \,\mathrm{d}\mathbf{x}$$

*for all $\psi \in [C(\overline{\Omega})]^d$.*

PROOF:
We have

$$\begin{aligned}\int_\Omega (\mathbf{M}^n\mathbf{u}^n - \mathbf{M}\mathbf{u})\cdot\psi\,\mathrm{d}\mathbf{x} &= \sum_{i=1}^d\sum_{j=1}^d \int_\Omega (\mathbf{M}_{i,j}^n\mathbf{u}_j^n - \mathbf{M}_{i,j}\mathbf{u}_j)\psi_i\,\mathrm{d}\mathbf{x}\\ &= \sum_{i=1}^d\sum_{j=1}^d \Big(\int_\Omega (\mathbf{M}_{i,j}^n - \mathbf{M}_{i,j})\mathbf{u}_j^n\psi_i\,\mathrm{d}\mathbf{x} + \int_\Omega (\mathbf{u}_j^n - \mathbf{u}_j)\mathbf{M}_{i,j}\psi_i\,\mathrm{d}\mathbf{x}\Big).\end{aligned}$$

The first term is bounded by

$$C_\psi \sum_{i=1}^d\sum_{j=1}^d \Big(\int_\Omega (\mathbf{M}_{i,j}^n - \mathbf{M}_{i,j})^2\,\mathrm{d}\mathbf{x}\Big)^{\frac{1}{2}}\Big(\int_\Omega (\mathbf{u}_j^n)^2\,\mathrm{d}\mathbf{x}\Big)^{\frac{1}{2}} \le C_\psi U \sum_{i=1}^d\sum_{j=1}^d \Big(\int_\Omega (\mathbf{M}_{i,j}^n - \mathbf{M}_{i,j})^2\,\mathrm{d}\mathbf{x}\Big)^{\frac{1}{2}},$$

using the fact that $|\psi_i| \le C_\psi$, $1 \le i \le d$, $C_\psi > 0$, and the Cauchy–Schwarz inequality, and thus converges to zero using the strong convergence of $\mathbf{M}_{i,j}^n$ to $\mathbf{M}_{i,j}$, $1 \le i,j \le d$. The second term converges to zero by the definition of the weak convergence of $\mathbf{u}^n$ to $\mathbf{u}$. □

## 1.9 Appendix B: A combined finite volume–finite element scheme for contaminant transport simulation on nonmatching grids

We present in this appendix a variant of the scheme from the first part of the chapter for nonmatching grids and apply it to contaminant transport simulation in porous media.

### 1.9.1 Introduction

We consider in this appendix the equation (1.1) in its precise form describing the reactive miscible displacement of one contaminant in porous media. We suppose that a domain $\Omega \subset \mathbb{R}^d$, $d = 2, 3$, is discretized into a nonoverlapping nonmatching grid possibly containing nonconvex elements, as that given in Figure 1.6 below by the dashed line.

The discretization methods for nonmatching grids represent a very active area of research. They are usually proposed in the context of domain decomposition methods, cf. [102]. The mortar method was developed for elliptic problems discretized by the finite element or spectral methods in [26]. This approach has been later extended to mixed finite element methods [11, 120], finite volume element methods [55], and cell-centered finite volume methods [3, 66]. A nonconsistent but simple, stable, and efficient (see the comparative tests in [66]) cell-centered finite volume scheme for nonoverlapping nonmatching grids has been proposed in [36].

We apply here the ideas of combined finite volume–finite element schemes (cf. [67, 114]) and in particular a variant of the scheme proposed and studied in the first part of this chapter to the discretization of (1.1) on the given grids. We are motivated by the following consideration: the mesh can be nonmatching and can contain nonconvex control volumes for a pure cell-centered finite volume discretization of the equation (1.1) without the diffusion term, cf. [61, Chapter VI]. The mesh is required to match along hyperplanes of $\mathbb{R}^d$ and to consist of convex control volumes only when the diffusion term is present, cf. [61, Chapter III]. We however notice that given a set of points, we can always construct a simplicial mesh (consisting of triangles if $d = 2$ and of tetrahedra if $d = 3$) with vertices given by this set of points. Hence an intuitive idea

is as follows: given a nonmatching mesh with possibly nonconvex elements and with a set of points associated with these elements, construct a simplicial mesh having this set of points as vertices. Then consider a finite element discretization of the diffusion term of (1.1) on the simplicial mesh and a finite volume discretization of the other terms of (1.1) on the original mesh.

We believe that the proposed approach to the discretization of the equation (1.1) on nonmatching grids is in some sense the simplest, yet (at least in our opinion) very efficient. In particular, we do not introduce any supplementary equations or unknowns on the boundary between the regions with nonmatching grids, nor do we use any interpolation of the discrete solutions on this boundary. There is no need for this for the finite volume part and the finite element part uses a conforming mesh. The proposed scheme is similar to that from [36]. The essential difference is that we replace the finite volume diffusion fluxes by the finite element ones. This is very important in the present case, since the diffusion fluxes through the interfaces between the subdomains with nonmatching grids of the scheme proposed in [36] are not consistent, whereas our discrete diffusion fluxes are consistent. Next, the scheme is stable since we avoid spurious oscillations in the convection-dominated case by checking the local Péclet number and by adding exactly the necessary amount of upstream weighting and it possesses a discrete maximum principle under some conditions on the simplicial mesh and on the tensor $\mathbf{S}$. The scheme can finally be easily implemented in any finite volume code, in order to permit a (nonmatching) local refinement of the mesh and an easy discretization of inhomogeneous and anisotropic tensors, a highly desirable feature in contaminant transport modeling. This was in fact our original motivation.

This appendix is organized as follows. We describe in Section 1.9.2 the problem of reactive transport with equilibrium adsorption in porous media. We propose in Section 1.9.3 a combined finite volume–finite element scheme with the backward Euler finite difference time stepping for the discretization of this problem. We prove in Section 1.9.4 the local conservativity of the scheme and the discrete maximum principle under appropriate conditions on the simplicial mesh and on the tensor $\mathbf{S}$. Its convergence could be proved using the techniques from the first part of this chapter. Finally, in Section 1.9.5 we demonstrate the performances of the proposed scheme on some model as well as real problems and in Section 1.9.6 we give some concluding remarks.

### 1.9.2 The contaminant transport problem

Let $(0,T)$ be a time interval, $0 < T < +\infty$. We consider a reactive miscible displacement with equilibrium adsorption of one contaminant in $\Omega$, described by

$$\begin{aligned}
\frac{\partial(\theta c)}{\partial t} + \rho_b \frac{\partial w(c)}{\partial t} - \nabla\cdot(\mathbf{S}\nabla c) + \nabla\cdot(c\mathbf{v}) & \\
+\lambda\,(\theta c + \rho_b w(c)) - q_{\text{out}} c &= q_{\text{in}} c_s \quad \text{in } \Omega\times(0,T)\,, && \text{(1.79a)}\\
c(\cdot,0) &= c_0 \quad \text{in } \Omega\,, && \text{(1.79b)}\\
c &= g \quad \text{on } \partial\Omega\times(0,T)\,. && \text{(1.79c)}
\end{aligned}$$

The problem (1.79a)–(1.79c) falls into the frame of the problem (1.1)–(1.3) studied in the first part of this chapter, with an additional sink term and an inhomogeneous Dirichlet boundary condition. Neumann or Robin boundary conditions can also be considered. In (1.79a)–(1.79c) $c = c(\mathbf{x},t)$ is the unknown concentration of the dissolved contaminant ($[\mathrm{ML}^{-d}]$), $\theta = \theta(\mathbf{x},t)$ is the water content ([-]) (we shall hereafter denote by $\theta_s$ the saturated water content and by $\theta_r$ the residual water content), $\rho_b = \rho_b(\mathbf{x})$ is the bulk density of the porous medium

($[\mathrm{ML}^{-d}]$), and $w : \mathbb{R} \to \mathbb{R}$ is the equilibrium adsorption function. We suppose that adsorption is sufficiently fast in comparison with the speed of the displacement of the contaminant so that the concentration of the dissolved contaminant $c$ and the concentration ratio of the immobilized contaminant $w(c)$ ([-]) are in equilibrium. In particular, we shall consider, for $c \geq 0$, $w(c) = \mu_1 c^{\mu_2}$, where $\mu_1$ and $\mu_2$ are positive constants, in the case of the Freundlich isotherm and $w(c) = \nu_1\nu_2 c/(1+\nu_2 c)$, where $\nu_1$ and $\nu_2$ are positive constants, in the case of the Langmuir isotherm. We suppose that the velocity field $\mathbf{v} = \mathbf{v}(\mathbf{x}, t)$ ($[\mathrm{LT}^{-1}]$) is given by the Darcy law

$$\mathbf{v} = -\mathbf{K}(p)\nabla(p+z)\,, \tag{1.80}$$

where $\mathbf{K} = \mathbf{K}(\mathbf{x}, p)$ is the hydraulic conductivity tensor ($[\mathrm{LT}^{-1}]$), $z = z(\mathbf{x})$ is the elevation, the upward vertical coordinate ([L]), and $p = p(\mathbf{x}, t)$, the pressure head ([L]), is the solution of the Richards problem, which describes two-phase water–air flow in the subsurface,

$$\begin{aligned}
\frac{\partial\theta(p)}{\partial t} - \nabla\cdot\mathbf{K}(p)\nabla(p+z) &= q_{\mathrm{out}} + q_{\mathrm{in}} \quad \text{in } \Omega\times(0,T)\,, && \text{(1.81a)}\\
p(\cdot,0) &= p_0 \quad \text{in } \Omega\,, && \text{(1.81b)}\\
p &= p_D \quad \text{on } \Gamma_D\times(0,T)\,, && \text{(1.81c)}\\
-\mathbf{K}(p)\nabla(p+z)\cdot\mathbf{n} &= u_N \quad \text{on } \Gamma_N\times(0,T)\,. && \text{(1.81d)}
\end{aligned}$$

Here $\overline{\Gamma_D}\cup\overline{\Gamma_N} = \partial\Omega$, $\Gamma_D\cap\Gamma_N = \emptyset$, $|\Gamma_D| \neq 0$. The dependence of $\theta$ and $\mathbf{K}$ on $p$ is given for example by the van Genuchten law, see [118]. We suppose that the diffusion–dispersion tensor $\mathbf{S} = \mathbf{S}(\mathbf{x}, \mathbf{v})$ ($[\mathrm{L}^2\mathrm{T}^{-1}]$) is given by

$$\begin{aligned}
\mathbf{S}_{ii} &= \alpha_T|\mathbf{v}| + (\alpha_L - \alpha_T)\frac{\mathbf{v}_i^2}{|\mathbf{v}|} + \sigma \qquad i = 1,\dots,d\,,\\
\mathbf{S}_{ij} = \mathbf{S}_{ji} &= (\alpha_L - \alpha_T)\frac{\mathbf{v}_i\mathbf{v}_j}{|\mathbf{v}|} \qquad i,j = 1,\dots,d\,,
\end{aligned}$$

where $\mathbf{v}_i$ are the components of the velocity vector $\mathbf{v}$ and $|\mathbf{v}|$ is its length, $\alpha_L = \alpha_L(\mathbf{x})$ is the longitudinal dispersivity ([L]), $\alpha_T = \alpha_T(\mathbf{x})$ is the transverse dispersivity ([L]), and finally $\sigma = \sigma(\mathbf{x})$ is the molecular diffusion coefficient ($[\mathrm{L}^2\mathrm{T}^{-1}]$). We consider first-order irreversible reactions such as radioactive decay, hydrolysis, and some forms of biodegradation, where $\lambda$ is the reaction rate constant ($[\mathrm{T}^{-1}]$). Finally, $q_{\mathrm{in}} = q_{\mathrm{in}}(\mathbf{x}, t)$, $q_{\mathrm{in}} \geq 0$, denotes the sources per unit volume ($[\mathrm{T}^{-1}]$). In the case of a source, we have to specify the concentration of the entering dissolved contaminant $c_s$. In contrast, the concentration of the leaving dissolved contaminant due to the sinks per unit volume $q_{\mathrm{out}} = q_{\mathrm{out}}(\mathbf{x}, t)$ ($[\mathrm{T}^{-1}]$), $q_{\mathrm{out}} \leq 0$, is given by the unknown concentration $c$. We refer to [19, 25, 79, 123] for more details.

### 1.9.3 Combined finite volume–finite element scheme

We define in this section the space and time discretizations and introduce the combined finite volume–finite element scheme.

#### Space and time discretizations

We suppose a generally nonconstant time step for the time discretization. We split up the time interval $(0,T)$ such that $0 = t_0 < \ldots < t_n < \ldots < t_N = T$ and define $\triangle t_n := t_n - t_{n-1}$, $n \in \{1, 2, \ldots, N\}$. We next describe the space discretization.

As a *primal grid* of $\Omega$, we understand a partition $\mathcal{D}_h$ of $\Omega$ into closed polygons such that $\overline{\Omega} = \bigcup_{D\in\mathcal{D}_h} D$ and such that the intersection of interiors of two different polygons is empty. We

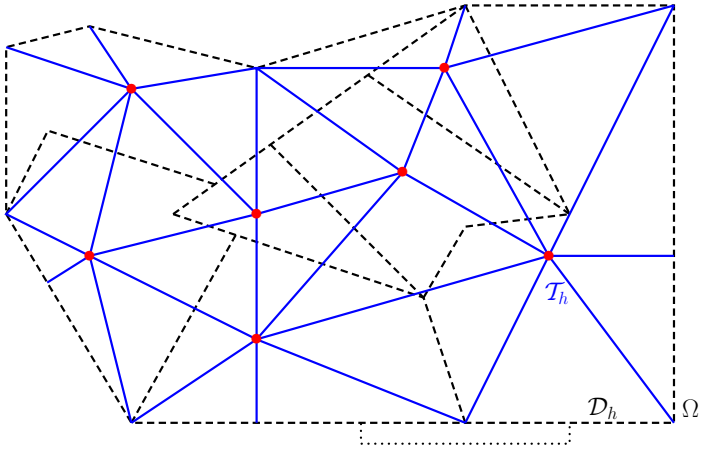


Figure 1.6: Primal nonmatching grid $\mathcal{D}_h$ (dashed) and dual triangular grid $\mathcal{T}_h$ (solid)

in particular admit nonmatching grids, i.e. the case where there exist two different polygons $D, E \in \mathcal{D}_h$ such that their intersection is not an empty set but it is not a common vertex, edge, or side (edge if $d = 2$, face if $d = 3$) of $D$ and $E$. An example of an admissible primal grid is given in Figure 1.6 by the dashed line. We suppose that there exists a family of points $\mathcal{P}_h$ such that there is one point $V_D$ in the interior of $D$ associated with each $D \in \mathcal{D}_h$.

A *dual grid* of $\Omega$ is a partition $\mathcal{T}_h$ of $\Omega$ into closed simplices which satisfies the following properties: (i) The set of points $\mathcal{P}_h$ is contained in the set of vertices of $\mathcal{T}_h$, denoted by $\mathcal{V}_h$; (ii) The vertices from $\mathcal{V}_h \setminus \mathcal{P}_h$ lie on the boundary of $\Omega$; (iii) $\mathcal{T}_h$ is conforming, i.e. the intersection of two different simplices is either an empty set or their common vertex, edge, or face; (iv) $\overline{\Omega} = \bigcup_{K \in \mathcal{T}_h} K$. This definition is not unique: we have a choice in connecting the different points $V_D \in \mathcal{P}_h$ and also a choice in the definition of the vertices on the boundary. The general intention is to find a triangulation such that the transmissibilities $\mathbb{S}^n_{D,E}$ defined below by (1.83) were non-negative, since this implies the discrete maximum principle, cf. Theorem 1.9.4 and Remarks 1.9.5 and 1.9.6 below. An example of a dual grid to a primal nonmatching grid is given in Figure 1.6 by the solid line.

In order to simplify the notation in the next sections, we define still a *fictitious boundary grid* $\mathcal{D}_h^{\mathrm{ext}}$. We associate a fictitious control volume $D$ with each vertex $V \in \mathcal{V}_h$ lying on the boundary $\partial\Omega$. We define $D$ in such way that $D \cap \Omega = \emptyset$, $D \cap \overline{\Omega} \subset \partial\Omega$, and $V \in D \cap \overline{\Omega}$. We finally require that the boundaries of $D$, $D \in \mathcal{D}_h^{\mathrm{ext}}$, halve the segments of $\partial\Omega$ between the boundary vertices, so that $\cup_{D \in \mathcal{D}_h^{\mathrm{ext}}} \{D \cap \overline{\Omega}\} = \partial\Omega$. An example of $D \in \mathcal{D}_h^{\mathrm{ext}}$ is given in Figure 1.6 by the dotted line. We shall use the notation $V_D$ for the vertex associated with $D \in \mathcal{D}_h^{\mathrm{ext}}$, as for the vertices from $\mathcal{P}_h$ and control volumes from $\mathcal{D}_h$.

We next denote by $\mathcal{N}(D)$ the set of all neighbors of a control volume $D \in \mathcal{D}_h$, i.e. the set of $E \in \mathcal{D}_h \cup \mathcal{D}_h^{\mathrm{ext}}$ such that $D \cap E$ has a positive $(d-1)$-dimensional measure. In particular, using the above definition of the set $\mathcal{D}_h^{\mathrm{ext}}$, we can easily write the integral over $\partial D$ as $\sum_{E \in \mathcal{N}(D)} \int_{\partial D \cap \partial E} \mathrm{d}\gamma(\mathbf{x})$. Similarly, for a vertex $V_D \in \mathcal{P}_h$, we denote by $\mathcal{M}(V_D)$ the set of all vertices $V_E \in \mathcal{V}_h$ such that there exists an edge between $V_D$ and $V_E$.

### The combined scheme

The combined scheme is obtained by the discretization of the diffusion term of (1.79a) by means of the piecewise linear conforming finite element method on $\mathcal{T}_h$, the discretization of

the other terms of (1.79a) by means of the cell-centered finite volume method on $\mathcal{D}_h$, and using a finite difference time stepping.

**Definition 1.9.1. (Combined scheme)** *The fully implicit combined finite volume–finite element scheme for the problem (1.79a)–(1.79c) reads: find the values $c_D^n$, $D \in \mathcal{D}_h$, $n \in \{0, 1, \ldots, N\}$, such that*

$$c_D^0 = \frac{1}{|D|} \int_D c_0(\mathbf{x})\, \mathrm{d}\mathbf{x} \qquad D \in \mathcal{D}_h\,, \tag{1.82a}$$

$$c_D^n = g(V_D, t_n) \qquad D \in \mathcal{D}_h^{\mathrm{ext}}\,,\ n \in \{1, 2, \ldots, N\}\,, \tag{1.82b}$$

$$\frac{\theta_D^n c_D^n - \theta_D^{n-1} c_D^{n-1}}{\triangle t_n} |D| + (\rho_b)_D \frac{w(c_D^n) - w(c_D^{n-1})}{\triangle t_n}\, |D| - \sum_{V_E \in \mathcal{M}(V_D)} \mathbb{S}_{D,E}^n (c_E^n - c_D^n)$$
$$+ \sum_{E \in \mathcal{N}(D)} \mathbf{v}_{D,E}^n\, \overline{c_{D,E}^n} + \lambda[\theta_D^n c_D^n + (\rho_b)_D w(c_D^n)]|D| - (q_{\mathrm{out}})_D^n c_D^n |D| = (q_{\mathrm{in}} c_s)_D^n |D|$$
$$D \in \mathcal{D}_h\,,\ n \in \{1, 2, \ldots, N\}\,. \tag{1.82c}$$

In the above definition we have used

$$\begin{aligned}
\theta_D^n &:= \frac{1}{|D|} \int_D \theta(\mathbf{x}, t_n) \qquad D \in \mathcal{D}_h\,,\ n \in \{0, 1, \ldots, N\}\,,\\
(\rho_b)_D &:= \frac{1}{|D|} \int_D \rho_b(\mathbf{x}) \qquad D \in \mathcal{D}_h\,,\\
(q_{\mathrm{out}})_D^n &:= \frac{1}{\triangle t_n |D|} \int_{t_{n-1}}^{t_n} \int_D q_{\mathrm{out}}(\mathbf{x}, t)\, \mathrm{d}\mathbf{x}\, \mathrm{d}t \qquad D \in \mathcal{D}_h\,,\ n \in \{1, 2, \ldots, N\}\,,\\
(q_{\mathrm{in}} c_s)_D^n &:= \frac{1}{\triangle t_n |D|} \int_{t_{n-1}}^{t_n} \int_D q_{\mathrm{in}}(\mathbf{x}, t) c_s(\mathbf{x}, t)\, \mathrm{d}\mathbf{x}\, \mathrm{d}t \qquad D \in \mathcal{D}_h\,,\ n \in \{1, 2, \ldots, N\}
\end{aligned}$$

and we have denoted the flux of $\mathbf{v}$ between $D \in \mathcal{D}_h$ and $E \in \mathcal{N}(D)$ for $n \in \{1, 2, \ldots, N\}$ by

$$\mathbf{v}_{D,E}^n := \frac{1}{\triangle t_n} \int_{t_{n-1}}^{t_n} \int_{\partial D \cap \partial E} \mathbf{v}(\mathbf{x}, t) \cdot \mathbf{n}_{D,E}\, \mathrm{d}\gamma(\mathbf{x})\, \mathrm{d}t\,,$$

where $\mathbf{n}_{D,E}$ is the unit normal vector of the side $\partial D \cap \partial E$ between $D$ and $E$, outward to $D$. For the notational convenience, we define $\mathbf{v}_{D,E}^n$ by 0 if $E \notin \mathcal{N}(D)$. We suppose that the functions $g$ and $\theta$ are sufficiently smooth in order to define $c_D^n$, $D \in \mathcal{D}_h^{\mathrm{ext}}$, and $\theta_D^n$. In analogy with the first part of this chapter, we first define

$$\widetilde{\mathbf{S}}^n(\mathbf{x}) := \frac{1}{\triangle t_n} \int_{t_{n-1}}^{t_n} \mathbf{S}(\mathbf{x}, t)\, \mathrm{d}t \qquad \mathbf{x} \in \Omega\,,\ n \in \{1, 2, \ldots, N\}\,.$$

The transmissibility between $V_D$ and $V_E$, $D \in \mathcal{D}_h$, $E \in \mathcal{D}_h \cup \mathcal{D}_h^{\mathrm{ext}}$, is then given by

$$\mathbb{S}_{D,E}^n := -\int_\Omega \mathbf{S}^n \nabla\varphi_E \cdot \nabla\varphi_D\, \mathrm{d}\mathbf{x} \qquad n \in \{1, 2, \ldots, N\}\,, \tag{1.83}$$

where we have again two choices of the definition of $\mathbf{S}^n$. We can either use directly $\mathbf{S}^n = \widetilde{\mathbf{S}}^n$, or define a piecewise constant tensor

$$\mathbf{S}^n(\mathbf{y}) = \Big(\frac{1}{|K|} \int_K [\widetilde{\mathbf{S}}^n(\mathbf{x})]^{-1}\, \mathrm{d}\mathbf{x}\Big)^{-1} \qquad \mathbf{y} \in K\,,\ K \in \mathcal{T}_h\,,\ n \in \{1, 2, \ldots, N\}\,.$$

These two choices correspond, respectively, to the arithmetic or harmonic average of the diffusion–dispersion tensor.

Finally, again in analogy with the first part of this chapter, we define the value $\overline{c^n_{D,E}}$ for $D \in \mathcal{D}_h$ , $E \in \mathcal{N}(D)$, and $n \in \{1, 2, \ldots, N\}$ as follows:

$$\overline{c^n_{D,E}} := \begin{cases} c^n_D + \alpha^n_{D,E}(c^n_E - c^n_D) & \text{if } \mathbf{v}^n_{D,E} \geq 0 \\ c^n_E + \alpha^n_{D,E}(c^n_D - c^n_E) & \text{if } \mathbf{v}^n_{D,E} < 0 \end{cases} .$$

Here $\alpha^n_{D,E}$ is the coefficient of the amount of upstream weighting which is defined by

$$\alpha^n_{D,E} := \frac{\max\left\{\min\left\{\mathbb{S}^n_{D,E}, \frac{1}{2}|\mathbf{v}^n_{D,E}|\right\}, 0\right\}}{|\mathbf{v}^n_{D,E}|}, \quad \mathbf{v}^n_{D,E} \neq 0 . \tag{1.84}$$

We set $\alpha^n_{D,E} := 0$ if $\mathbf{v}^n_{D,E}$=0. We remark that in the scheme studied in the first part of this chapter, there can be nonzero convective and diffusive fluxes between $D$ and $E$ only if $D$ and $E$ neighbors. This is however not the case with the scheme (1.82a)–(1.82c): there can be nonzero convective flux between $D$ and $E$ only if $D$ and $E$ neighbors, but there can be nonzero diffusive flux between $D$ and $E$ even if $D$ and $E$ are not neighbors (because the transmissibility between $D$ and $E$ is given by the grid $\mathcal{T}_h$). However, as we shall see in Theorem 1.9.4, the local Péclet upstream weighting still guarantees, adding minimal numerical diffusion, the stability of the scheme.

### 1.9.4 Discrete properties of the scheme

We show in this section two essential properties of the scheme proposed in this appendix. The ideas follow those introduced in [61] for finite volume schemes and extended onto combined finite volume–finite element schemes in the first part of this chapter.

**Theorem 1.9.2. (Conservativity of the scheme)** *The scheme (1.82a)–(1.82c) is conservative with respect to the primal mesh $\mathcal{D}_h$.*

Proof:

Let us take two fixed dual volumes $E \in \mathcal{D}_h$ and $D \in \mathcal{D}_h$. The discrete diffusive flux from $D$ to $E$ is given by $-\mathbb{S}^n_{D,E}(c^n_E - c^n_D)$. The discrete diffusive flux from $E$ to $D$ is given by $-\mathbb{S}^n_{E,D}(c^n_D - c^n_E)$, i.e. we have their equality up to the sign, considering that $\mathbb{S}^n_{D,E} = \mathbb{S}^n_{E,D}$ for all $n \in \{1, 2, \ldots, N\}$, which follows from (1.83) using the symmetry of the tensor $\mathbf{S}$.

For the discrete convective flux from $D$ to $E$, we have $\mathbf{v}^n_{D,E}[c^n_D + \alpha^n_{D,E}(c^n_E - c^n_D)]$, supposing $\mathbf{v}^n_{D,E} \geq 0$. For the discrete convective flux from $E$ to $D$, we have $\mathbf{v}^n_{E,D}[c^n_D + \alpha^n_{E,D}(c^n_E - c^n_D)]$, i.e. again the equality up to the sign, considering that $\mathbf{v}^n_{D,E} = -\mathbf{v}^n_{E,D}$ and that $\alpha^n_{D,E} = \alpha^n_{E,D}$, which follows from $\mathbb{S}^n_{D,E} = \mathbb{S}^n_{E,D}$. For $\mathbf{v}^n_{D,E} < 0$, the proof is similar. Hence the combined finite volume–finite element scheme is conservative as the pure finite volume is, cf. [61]. □

It follows from (1.80) and (1.81a) that $\nabla \cdot \mathbf{v} = q_{\text{out}} + q_{\text{in}} - \partial\theta/\partial t$. This property implies the following lemma:

**Lemma 1.9.3.** *For all $D \in \mathcal{D}_h$ and $n \in \{1, 2, \ldots, N\}$,*

$$\begin{aligned} \sum_{E \in \mathcal{N}(D)} \mathbf{v}^n_{D,E}\, \widehat{c^n_{D,E}} \;=\; & \sum_{E \in \mathcal{N}(D)} (\mathbf{v}^n_{D,E})^-(c^n_E - c^n_D) + (q_{\text{in}})^n_D c^n_D |D| \\ & + (q_{\text{out}})^n_D c^n_D |D| - \Big(\frac{\theta^n_D - \theta^{n-1}_D}{\triangle t_n}\Big) c^n_D |D| , \end{aligned}$$

*where $(\mathbf{v}^n_{D,E})^- := \min\{\mathbf{v}^n_{D,E}, 0\}$ and where the definition of $(q_{\text{in}})^n_D$ is as that of $(q_{\text{out}})^n_D$.*

PROOF:

Considering that $\mathbf{v}_{D,E}^n = (\mathbf{v}_{D,E}^n)^+ + (\mathbf{v}_{D,E}^n)^-$, where $(\mathbf{v}_{D,E}^n)^+ := \max\{\mathbf{v}_{D,E}^n, 0\}$, and the definition of the upstream weighting, we have

$$\begin{aligned}
\sum_{E\in\mathcal{N}(D)} \mathbf{v}_{D,E}^n \, \widehat{c_{D,E}^n} &= \sum_{E\in\mathcal{N}(D)} (\mathbf{v}_{D,E}^n)^+ c_D^n + \sum_{E\in\mathcal{N}(D)} (\mathbf{v}_{D,E}^n)^- c_E^n \\
&= \sum_{E\in\mathcal{N}(D)} \mathbf{v}_{D,E}^n \, c_D^n + \sum_{E\in\mathcal{N}(D)} (\mathbf{v}_{D,E}^n)^- (c_E^n - c_D^n) \\
&= c_D^n \frac{1}{\triangle t_n} \int_{t_{n-1}}^{t_n} \int_D \nabla\cdot\mathbf{v}(\mathbf{x},t)\,\mathrm{d}\mathbf{x}\,\mathrm{d}t + \sum_{E\in\mathcal{N}(D)} (\mathbf{v}_{D,E}^n)^- (c_E^n - c_D^n) \\
&= c_D^n (q_{\mathrm{in}})_D^n |D| + c_D^n (q_{\mathrm{out}})_D^n |D| + \sum_{E\in\mathcal{N}(D)} (\mathbf{v}_{D,E}^n)^- (c_E^n - c_D^n) \\
&\quad - \Big(\frac{\theta_D^n - \theta_D^{n-1}}{\triangle t_n}\Big) c_D^n |D| \,. \quad \square
\end{aligned}$$

We now give an important theorem, guaranteeing that under certain conditions on $\mathcal{T}_h$ and $\mathbf{S}$, we obtain physically correct results.

**Theorem 1.9.4. (Discrete maximum principle)** *Let $\mathbb{S}_{D,E}^n \geq 0$ for all $D \in \mathcal{D}_h$, $V_E \in \mathcal{M}(V_D)$, and all $n \in \{1,2,\ldots,N\}$. Let the initial, sources, and Dirichlet boundary concentrations satisfy $0 \leq c_0 \leq M$, $0 \leq c_s \leq M$, and $0 \leq g \leq M$, respectively. Let finally the adsorption function $w$ be nondecreasing and such that $w(0) = 0$ and let $\lambda \geq 0$. Then the solution of the problem (1.82a)–(1.82c) satisfies*

$$0 \leq c_D^n \leq M$$

*for all $D \in \mathcal{D}_h$, $n \in \{1,2,\ldots,N\}$.*

PROOF:

Setting $\mathbb{T}_{D,E}^n := \mathbb{S}_{D,E}^n - |\mathbf{v}_{D,E}^n|\alpha_{D,E}^n$, $D \in \mathcal{D}_h$, $E \in \mathcal{L}(D)$, where $E \in \mathcal{L}(D)$ if $E \in \mathcal{N}(D)$ or if $V_E \in \mathcal{M}(V_D)$, and using Lemma 1.9.3, we can rewrite the scheme (1.82a)–(1.82c) as

$$\begin{aligned}
&\frac{\theta_D^{n-1} c_D^n - \theta_D^{n-1} c_D^{n-1}}{\triangle t_n} |D| + (\rho_b)_D \frac{w(c_D^n) - w(c_D^{n-1})}{\triangle t_n} |D| - \sum_{E\in\mathcal{L}(D)} \mathbb{T}_{D,E}^n (c_E^n - c_D^n) \\
&+ \sum_{E\in\mathcal{N}(D)} (\mathbf{v}_{D,E}^n)^- (c_E^n - c_D^n) + \lambda[\theta_D^n c_D^n + (\rho_b)_D w(c_D^n)]|D| = (q_{\mathrm{in}} c_s)_D^n |D| - c_D^n (q_{\mathrm{in}})_D^n |D| \\
&\qquad D \in \mathcal{D}_h \,,\, n \in \{1,2,\ldots,N\} \,.
\end{aligned}$$

In view of the definition of $\mathbb{T}_{D,E}^n$ and of (1.84), one has $\mathbb{T}_{D,E}^n \geq 0$ for all $D \in \mathcal{D}_h$, $E \in \mathcal{L}(D)$, and $n \in \{1,2,\ldots,N\}$. We now make use of an induction argument. We remark that $0 \leq c_D^n \leq M$ is satisfied for $n = 0$, using the assumption on $c_0$. Let us suppose that $0 \leq c_D^{n-1} \leq M$ for all $D \in \mathcal{D}_h$ for a fixed $(n-1) \in \{0,1,\ldots,N-1\}$. Since the set $\mathcal{D}_h \cup \mathcal{D}_h^{\mathrm{ext}}$ is finite, there exist $D_0, D_1 \in \mathcal{D}_h \cup \mathcal{D}_h^{\mathrm{ext}}$ such that $c_{D_0}^n \leq c_D^n \leq c_{D_1}^n$ for all $D \in \mathcal{D}_h \cup \mathcal{D}_h^{\mathrm{ext}}$. Using a contradiction argument we prove below that $c_{D_0}^n \geq 0$ and $c_{D_1}^n \leq M$. Suppose that $c_{D_0}^n < 0$. We remark that $D_0 \in \mathcal{D}_h$, using the assumption on the Dirichlet boundary condition $g$. Then, since $\mathbb{T}_{D_0,E}^n \geq 0$ and $-(\mathbf{v}_{D_0,E}^n)^- \geq 0$, we have

$$\sum_{E\in\mathcal{L}(D_0)} \mathbb{T}_{D_0,E}^n (c_E^n - c_{D_0}^n) + \sum_{E\in\mathcal{N}(D_0)} -(\mathbf{v}_{D_0,E}^n)^- (c_E^n - c_{D_0}^n) \geq 0 \,.$$

This yields

$$\frac{\theta_{D_0}^{n-1}c_{D_0}^n-\theta_{D_0}^{n-1}c_{D_0}^{n-1}}{\triangle t_n}|D_0|+(\rho_b)_{D_0}\frac{w(c_{D_0}^n)-w(c_{D_0}^{n-1})}{\triangle t_n}\,|D_0|$$
$$+\lambda[\theta_{D_0}^n c_{D_0}^n+(\rho_b)_{D_0}w(c_{D_0}^n)]|D_0|-(q_{\rm in}c_s)_{D_0}^n|D_0|+c_{D_0}^n(q_{\rm in})_{D_0}^n|D_0|\geq 0\,.$$

Now $c_{D_0}^n<0$ implies $c_{D_0}^n(q_{\rm in})_{D_0}^n\leq 0$ and one also has $-(q_{\rm in}c_s)_{D_0}^n\leq 0$. Using the fact that $\theta\geq\theta_s>0$ and that $w$ is nondecreasing and satisfies $w(0)=0$, $\theta_{D_0}^n c_{D_0}^n+(\rho_b)_{D_0}w(c_{D_0}^n)\leq 0$ follows. Finally, $w(c_{D_0}^n)-w(c_{D_0}^{n-1})\leq 0$, using that $w$ is nondecreasing. Thus $c_{D_0}^n\geq c_{D_0}^{n-1}$, which is a contradiction.

Let us now suppose that $c_{D_1}^n>M$. In view of the Dirichlet boundary condition, $D_1$ again necessarily lies in $\mathcal{D}_h$. Similarly as in the previous case, one comes to

$$\frac{\theta_{D_1}^{n-1}c_{D_1}^n-\theta_{D_1}^{n-1}c_{D_1}^{n-1}}{\triangle t_n}|D_1|+(\rho_b)_{D_1}\frac{w(c_{D_1}^n)-w(c_{D_1}^{n-1})}{\triangle t_n}\,|D_1|$$
$$+\lambda[\theta_{D_1}^n c_{D_1}^n+(\rho_b)_{D_1}w(c_{D_1}^n)]|D_1|-(q_{\rm in}c_s)_{D_1}^n|D_1|+c_{D_1}^n(q_{\rm in})_{D_1}^n|D_1|\leq 0\,.$$

We can estimate

$$-(q_{\rm in}c_s)_{D_1}^n\geq -M(q_{\rm in})_{D_1}^n\geq -c_{D_1}^n(q_{\rm in})_{D_1}^n\,.$$

Simply $\theta_{D_1}^n c_{D_1}^n+(\rho_b)_{D_1}w(c_{D_1}^n)\geq 0$ and $w(c_{D_1}^n)-w(c_{D_1}^{n-1})\geq 0$. This implies $c_{D_1}^n\leq c_{D_1}^{n-1}$, which is again a contradiction. □

**Remark 1.9.5. (Discrete maximum principle)** *We see that the discrete maximum principle holds as soon as the transmissibilities $\mathbb{S}_{D,E}^n$ defined by (1.83) are non-negative. This is e.g. the case, in two space dimensions, when* **S** *reduces to a constant scalar function and when $\mathcal{T}_h$ is Delaunay, that is the circumcircle of each triangle does not contain any vertex in its interior, and under the additional condition that no circumcenters of boundary triangles lie outside the domain, cf. [80, 100]. Remark that given a set of points, we can always construct a Delaunay triangulation. In three space dimensions, however, a Delaunay tetrahedral mesh in general does not guarantee the non-negativity of the finite element transmissibilities, cf. [86, 100]. We refer to Remark 1.9.7 for the modification of the proposed scheme, which guarantees the discrete maximum principle in both two and three space dimensions under the condition that* **S** *is a constant scalar function.*

**Remark 1.9.6. (Dual Delaunay triangulation for a locally refined square grid)** *Let us consider a locally refined square grid, where a square is refined into 9 subsquares and where the difference of levels of refinement of two neighboring squares is at most one, such as that given in Figure 1.7 by the dashed line. Then an example of a dual Delaunay triangulation is given in Figure 1.7 by the solid line.*

**Remark 1.9.7. (A two-grid finite volume scheme verifying the discrete maximum principle for S constant and scalar)** *When* **S** *is a constant scalar function, we can replace the discretization of the diffusion term by the finite element method on a dual simplicial grid by a finite volume discretization on a Voronoï grid given by the points from $\mathcal{V}_h$. Recall that in two space dimensions, this would lead to the same scheme for the Voronoï mesh dual to a Delaunay triangulation, cf. [61, Section III.12.2]. The interest in it is that in three space dimensions, the finite volume discretization of a Laplacian on a Voronoï grid still leads to positive transmissibilities; compare this with Remark 1.9.5.*

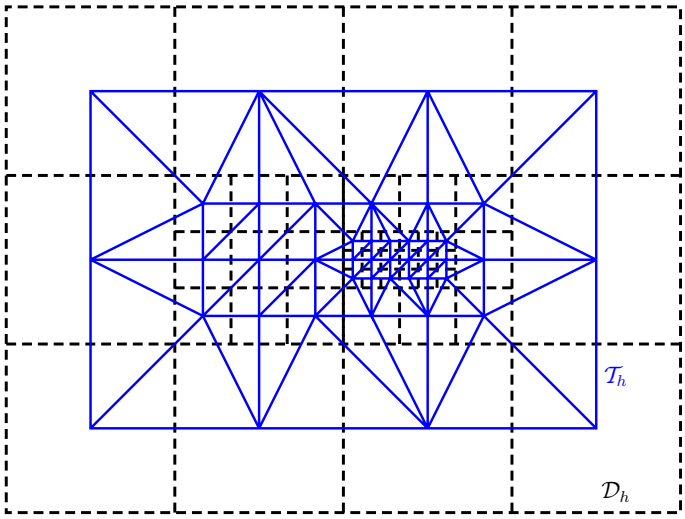


Figure 1.7: Primal locally refined square grid $\mathcal{D}_h$ (dashed) and dual triangular grid $\mathcal{T}_h$ (solid)

### 1.9.5 Numerical simulations

We present here the results of two numerical experiments in space dimension two.

#### Model problem with a known analytical solution

The purpose of this problem is to test the proposed scheme on nonmatching grids. Let us consider a linear model problem of the type (1.79a)–(1.79c) with constant coefficients given by

$$\theta = 1\,,\ w = 0\,,$$
$$\mathbf{S} = \delta \begin{pmatrix} 1 & 0 \\ 0 & 1 \end{pmatrix}\,,\ \mathbf{v} = (v_1, v_2)\,,$$
$$\lambda = 0\,,\ q_{\text{out}} = 0\,,\ q_{\text{in}} = 0\,.$$

The initial and boundary conditions are given by the exact solution

$$c(x,y,t) = \frac{1}{200\nu t + 1} e^{-50\frac{(x-x_0-v_1 t)^2 + (y-y_0-v_2 t)^2}{200\nu t + 1}}$$

representing a Gaussian peak starting at the point $(x_0, y_0)$, being transported by the convective field $\mathbf{v}$, and diffusing. Let us in particular consider

$$\Omega = (0,3) \times (0,3)\,,\ T = 2\,,$$
$$v_1 = 0.8\,,\ v_2 = 0.4\,,\ x_0 = 0.5\,,\ y_0 = 1.35\,.$$

We consider the discretization of the domain $\Omega$ into $N^2$ squares with $N = 10, 20, 40$, and 80. We shall call these grids in the following as unrefined grids. We next consider local refinements and uniform refinements of these grids, where one square is refined into 9 subsquares. We never refine twice along a given edge. An example of a locally refined grid and the appropriate dual triangular grid is given in Figure 1.7. In view of Remark 1.9.6, the scheme (1.82a)–(1.82c) for the considered problem satisfies the discrete maximum principle. We divide the time interval $(0,T)$ into $1.6N$ time steps and consider two values of the parameter $\delta$: for $\delta = 0.1$, the problem is diffusion-dominated, and for $\delta = 0.001$, the problem is convection-dominated.

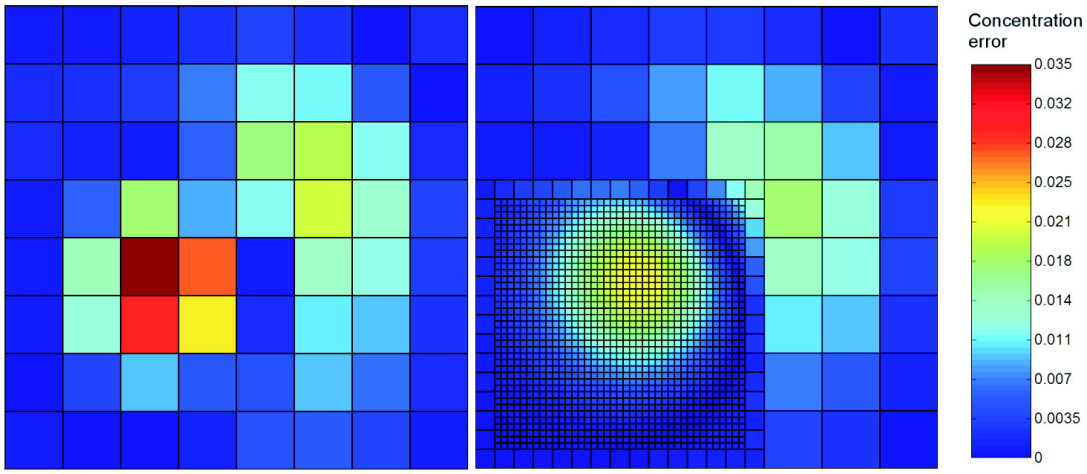


Figure 1.8: Errors of the approximate solutions on unrefined $20 \times 20$ (left) and locally refined (right) grids for $\delta = 0.1$ at $t = 3/8$, cut of the domain

| N | T. st. | Unkn. | $\|c_h - c\|_{0,h,\Omega}$ | Unkn. | $\|c_h - c\|_{0,h,\Omega}$ | Unkn. | $\|c_h - c\|_{0,h,\Omega}$ |
|---|---|---|---|---|---|---|---|
| 10 | 16 | 100 | 0.01277 | 316 | 0.00547 | 900 | 0.00491 |
| 20 | 32 | 400 | 0.00354 | 1264 | 0.00301 | 3600 | 0.00270 |
| 40 | 64 | 1600 | 0.00173 | 5056 | 0.00158 | 14400 | 0.00143 |
| 80 | 128 | 6400 | 0.00086 | 20224 | 0.00080 | 57600 | 0.00074 |

Table 1.2: N, number of time steps, number of unknowns, and discrete $L^2(\Omega)$ errors for $\delta = 0.1$ at $t = 2$ for unrefined, locally refined, and uniformly refined square grids, respectively

| N | T. st. | Unkn. | $\|c_h - c\|_{0,h,\Omega}$ | Unkn. | $\|c_h - c\|_{0,h,\Omega}$ | Unkn. | $\|c_h - c\|_{0,h,\Omega}$ |
|---|---|---|---|---|---|---|---|
| 10 | 16 | 100 | 0.1419 | 316 | 0.1347 | 900 | 0.1347 |
| 20 | 32 | 400 | 0.1364 | 1264 | 0.1222 | 3600 | 0.1222 |
| 40 | 64 | 1600 | 0.1249 | 5056 | 0.1032 | 14400 | 0.1031 |
| 80 | 128 | 6400 | 0.1064 | 20224 | 0.0777 | 57600 | 0.0777 |

Table 1.3: N, number of time steps, number of unknowns, and discrete $L^2(\Omega)$ errors for $\delta = 0.001$ at $t = 2$ for unrefined, locally refined, and uniformly refined square grids, respectively

We first perform a simple test. We consider $\delta = 0.1$, the time step of length $1/16$, a $20 \times 20$ grid of $\Omega$, and its local refinement in a part of the subdomain where $c$ is nonzero. The pointwise errors in centers of the cells at $t = 3/8$ are given in Figure 1.8. We can see that we have decreased the error in the refined part, whereas in the unrefined part, the error almost does not change. In particular, we do not produce any error around the interface between the refined and unrefined subdomains.

We next consider the whole time interval $(0, 2)$. During this interval, the peak of the exact solution moves from the point $(0.5, 1.35)$ to the point $(2.1, 2.15)$. We consider the unrefined, locally refined, and uniformly refined grids; the locally refined subdomain can be seen in

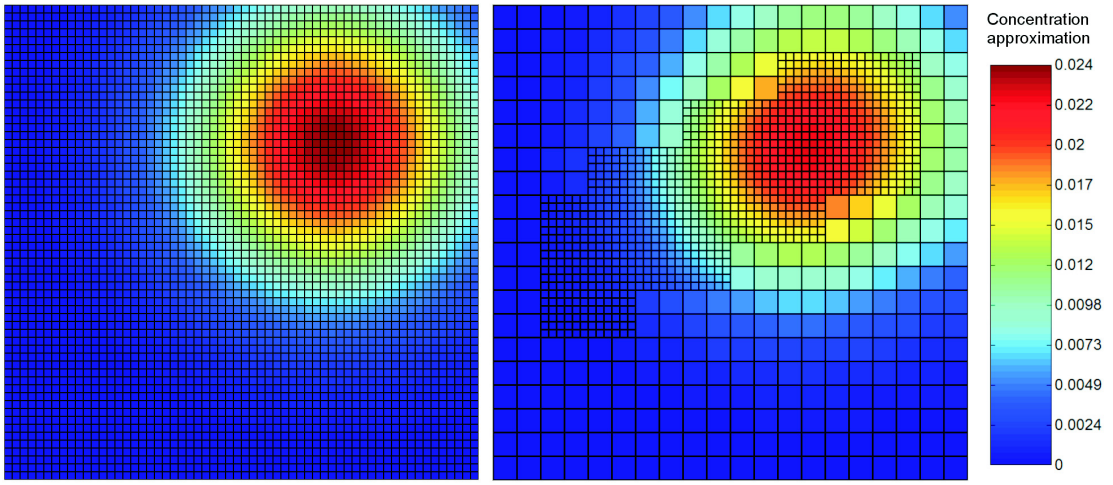


Figure 1.9: Exact solution (left) and approximate solution on a locally refined grid (right) for $\delta = 0.1$ at $t = 2$

Figure 1.9. We give the discrete $L^2(\Omega)$ errors at time $t = 2$ for $\delta = 0.1$ in Table 1.2 and for $\delta = 0.001$ in Table 1.3. The discrete norm $\|c_h - c\|_{0,h,\Omega}$ is the $L^2(\Omega)$ norm of the difference of the piecewise constant solution on the square grid and the exact solution, evaluated with a quadrature formula. We can see an expected linear convergence in the diffusion-dominated case. The error is significantly decreased by refining the grid locally around the region where $c$ is nonzero. An example of the solution on a locally refined grid at $t = 2$ for $\delta = 0.1$ is given in Figure 1.9, together with the exact solution on the same grid refined uniformly. In the convection-dominated case, however, the error of the approximate solution is significant. The one-level local refinement is not sufficient in this case.

### Real problem

We simulate in this section a real flow–transport problem provided by the HydroExpert company, Paris. We use for this purpose the software program TALISMAN of this company, cf. [104]. The combined scheme on a grid represented in Figure 1.7 is implemented in this code.

The domain $\Omega \in \mathbb{R}^3$ is an aquifer with bottom coordinate $z_b = z_b(x, y)$, top coordinate $z_t = z_t(x, y)$, and aperture $e = z_t - z_b = e(x, y)$, see Figure 1.10. We consider the Dupuit approximation of the Richards equation in $\Omega$, consisting in integrating the Richards equation over the aquifer aperture $e$ under the assumption that the flow is only horizontal, cf. [23]. We consider in addition the effect of water compressibility and a nonlinear discharge function. Let us denote by $\Omega'$ the horizontal plane of $\Omega$, cf. Figure 1.10, and by $\Gamma'_D$ and $\Gamma'_N$ the Dirichlet and Neumann boundaries of $\Omega'$, respectively. The flow problem then reads

$$\frac{\partial \tilde{\theta}(h)}{\partial t} - \nabla \cdot \tilde{\mathbf{K}}(h) \nabla h + Q_d(h) = \tilde{q}_{\text{out}} + \tilde{q}_{\text{in}} \quad \text{in } \Omega' \times (0,T)\,, \tag{1.85a}$$

$$h(\cdot, 0) = h_0 \quad \text{in } \Omega'\,, \tag{1.85b}$$

$$h = h_D \quad \text{on } \Gamma'_D \times (0,T)\,, \tag{1.85c}$$

$$-\tilde{\mathbf{K}}(h) \nabla h \cdot \mathbf{n} = 0 \quad \text{on } \Gamma'_N \times (0,T)\,, \tag{1.85d}$$

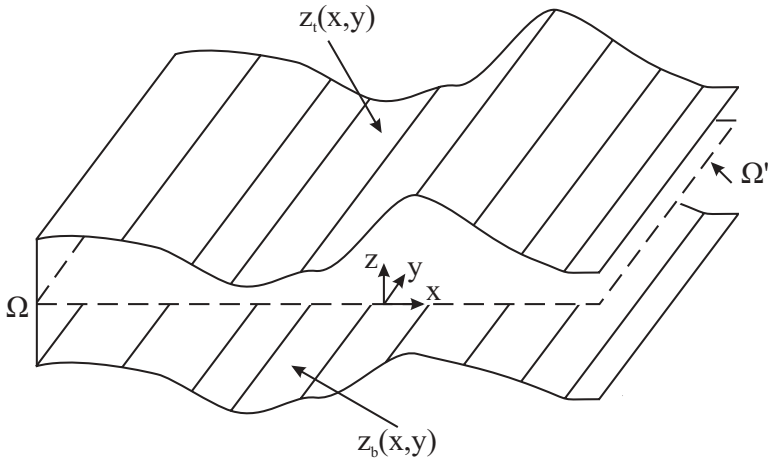


Figure 1.10: Considered domain $\Omega \in \mathbb{R}^3$ with its horizontal plane $\Omega' \in \mathbb{R}^2$

where

$$\frac{\partial \tilde{\theta}(h)}{\partial h} = \begin{cases} E_l & \text{if } h \le z_t \\ E_s e & \text{if } h \ge z_t \end{cases}$$

and

$$\tilde{\mathbf{K}}(h) = \begin{cases} \mathbf{K}_s(h - z_b) & \text{if } h \le z_t \\ \mathbf{K}_s e & \text{if } h \ge z_t \end{cases}$$

and finally

$$Q_d(h) = \begin{cases} 0 & \text{if } h \le z_t \\ \mathbf{K}_d(h - z_t) & \text{if } h \ge z_t \end{cases} .$$

The problem (1.85a)–(1.85d) is two-dimensional, all the variables and in particular the unknown piezometric head $h$ ([L]), $h = p + z$, are only functions of the horizontal coordinates $x, y$, and the gradient and divergence operators are also only two-dimensional. The storativity $E_l$ ([-]) is related to the water content $\theta$ by $E_l = \theta_s - \theta_r$. The specific storativity $E_s$ ([$\mathrm{L}^{-1}$]) is given by the water compressibility and is usually very small in comparison with $E_l/e$. The tensor $\mathbf{K}_s$ ([$\mathrm{LT}^{-1}$]) expresses the hydraulic conductivity in the saturated state. The discharge $Q_d$ ([$\mathrm{LT}^{-1}$]) depends on the hydraulic conductance $\mathbf{K}_d$ ([$\mathrm{T}^{-1}$]). In analogy with the Darcy law, we define

$$\tilde{\mathbf{v}} := -\tilde{\mathbf{K}}(h)\nabla h\,. \tag{1.86}$$

Notice that $\tilde{\mathbf{v}}$ is a two-dimensional vector in $\Omega'$ with the units of [$\mathrm{L}^2\mathrm{T}^{-1}$]. The flux of $\tilde{\mathbf{v}}$ through a segment $\mathbf{b} \in \Omega'$, $\int_{\mathbf{b}} \mathbf{v}(\mathbf{x}, t) \cdot \mathbf{n}_{\mathbf{b}}\, \mathrm{d}\gamma(\mathbf{x})$ ([$\mathrm{L}^3\mathrm{T}^{-1}$]), approximates the flux of groundwater over a vertical face in $\Omega$, whose intersection with the horizontal plane $\Omega'$ is the segment $\mathbf{b}$.

We make similar approximations in the contaminant transport problem (1.79a)–(1.79c). We namely suppose that the concentration $c$ does not vary with $z$ and that the diffusion and convection are only two-dimensional in the horizontal plane $\Omega'$ of $\Omega$. By formally integrating the three-dimensional convection–reaction–diffusion equation in $\Omega$ over $e$ and adding the discharge, we replace the functions $\theta$, $q_{\mathrm{in}}$, and $q_{\mathrm{out}}$ defined in $\Omega$ by the functions $\tilde{\theta}$, $\tilde{q}_{\mathrm{in}}$, and $\tilde{q}_{\mathrm{out}} - Q_d(h)$ defined in $\Omega'$. We finally use $\tilde{\mathbf{v}}$ instead of $\mathbf{v}$ in the convection term and in the definition of the diffusion–dispersion tensor $\mathbf{S}$ and consider the gradient and divergence operators only in $\Omega'$. Notice that we have to replace the molecular diffusion coefficient $\sigma$ by $\tilde{\sigma} = \sigma e$. Hence the final transport problem is, as the flow problem, two-dimensional in the plane $\Omega'$, with the three-dimensional units (namely, the concentration is measured in [$\mathrm{ML}^{-3}$]).

With the assumptions of the previous paragraph, the transport scheme is constructed as follows. We consider a (nonmatching locally refined) square grid $\mathcal{D}_h$ of $\Omega'$ and its dual triangular grid $\mathcal{T}_h$, as that in Figure 1.7. We associate with each $D \in \mathcal{D}_h$ an aperture $e_D$, given for instance as the mean of $e$ over $D$. We seek the values $c_D^n$, $D \in \mathcal{D}_h$, $n \in \{1, 2, \ldots, N\}$, such that

$$\frac{\tilde{\theta}_D^n c_D^n - \tilde{\theta}_D^{n-1} c_D^{n-1}}{\triangle t_n}|D| + (\rho_b)_D \frac{w(c_D^n) - w(c_D^{n-1})}{\triangle t_n}\,|D|e_D - \sum_{V_E \in \mathcal{M}(V_D)} \tilde{\mathbb{S}}_{D,E}^n (c_E^n - c_D^n)$$

$$+ \sum_{E \in \mathcal{N}(D)} \tilde{\mathbf{v}}_{D,E}^n \, \overline{c_{D,E}^n} + \lambda[\tilde{\theta}_D^n c_D^n + (\rho_b)_D w(c_D^n) e_D]|D| - [\tilde{q}_{\text{out}} - Q_d(h)]_D^n c_D^n |D| = (\tilde{q}_{\text{in}} c_s)_D^n |D|$$

$$D \in \mathcal{D}_h\,,\ n \in \{1, 2, \ldots, N\}$$

with appropriately prescribed initial and boundary conditions. Here $\tilde{\theta}_D^n$, $D \in \mathcal{D}_h$, $n \in \{0, 1, \ldots, N\}$, are the approximations of $\tilde{\theta}$ from (1.85a), given by a flow numerical scheme. In a similar manner, $\tilde{\mathbf{v}}_{D,E}^n$ are the approximations of the flux of $\tilde{\mathbf{v}}$ given by (1.86) through the interface between the control volumes $D \in \mathcal{D}_h$, $E \in \mathcal{N}(D)$ at time $t_n$. Note that from (1.85a) and using a locally conservative flow numerical scheme (such as a finite volume one), $\tilde{\mathbf{v}}_{D,E}^n = -\tilde{\mathbf{v}}_{E,D}^n$. We define $(\rho_b)_D$ e.g. as the mean of the bulk density $\rho_b$ over the cube $D \times e_D$. The transmissibilities $\tilde{\mathbb{S}}_{D,E}^n$ are defined by (1.83), while employing $\tilde{\mathbf{v}}$ and $\tilde{\sigma}$ in the definition of the diffusion–dispersion tensor $\mathbf{S}$ instead of $\mathbf{v}$ and $\sigma$. Note finally that again for non-negative transmissibilities, the scheme verifies the discrete maximum principle, which is in particular the consequence of $\nabla \cdot \tilde{\mathbf{v}} = \tilde{q}_{\text{out}} + \tilde{q}_{\text{in}} - Q_d(h) - \partial\tilde{\theta}/\partial t$ following from (1.85a) and (1.86).

The parameters of the given aquifer are visualized in Figure 1.11. Its horizontal plane $\Omega'$ fits into a rectangle 1500 × 2400 meters. Its aperture $e$ is smaller than 9 meters and the above sea level of its top ranges between 137 and 146 meters. There is a small valley in the western part of the region, going in the northsouthern direction. The given aquifer consists predominantly of sands with saturated hydraulic conductivity $\mathbf{K}_s$ in orders of $10^{-3}$ m s$^{-1}$, but there is an important clay barrier with $\mathbf{K}_s$ as low as $10^{-6}$ m s$^{-1}$ along the eastern boundary and in the southeastern part of the aquifer. There is no discharge in the entire aquifer except of the valley, where the hydraulic conductance $\mathbf{K}_d$ equals to 0.01 s$^{-1}$. We suppose that the storativity $E_l$ and the specific storativity $E_s$ are constant throughout the aquifer and equal respectively to 0.1 and $10^{-4}$ m$^{-1}$ and that the saturated water content $\theta_s$ (porosity) equals to 0.3. The aquifer is receiving a constant effective recharge of 11 cm per year and there are 88 point sources of $10^{-9}$ m$^3$s$^{-1}$ distributed in the domain. Dirichlet boundary conditions are prescribed (fixed piezometric head imposed on the boundary of $\Omega'$). The initial piezometric head is given also in Figure 1.11. The horizontal plane $\Omega'$ of the aquifer is divided into 8759 identical squares of 15 × 15 meters and the simulation period of one year is divided into 10 equidistant time steps.

The task is, given the hydrodynamical parameters specified in the previous paragraph, to simulate the propagation of a contaminant entering the aquifer at a concentration of 10 kg m$^{-3}$ through a new source of a constant yield of $10^{-3}$ m$^3$s$^{-1}$. This source is located in the southeastern part of the domain near the clay barrier. We suppose that the bulk density $\rho_b$ of the porous medium is constant throughout the aquifer and equals to 1600 kg m$^{-3}$. Also the longitudinal and transverse dispersivities $\alpha_L$ and $\alpha_T$, as well as the molecular diffusion coefficient $\sigma$, are supposed constant and equal to, respectively, 10 m, 1 m, and $10^{-9}$ m$^2$s$^{-1}$. We consider the Langmuir adsorption isotherm with in particular $\nu_1 = 10^{-8}$ and $\nu_2 = 10^5$ m$^3$kg$^{-1}$. Finally, first-order irreversible hydrolysis is supposed to take place so that the reaction rate

constant $\lambda$ equals to $10^{-7}$ s$^{-1}$. The polluted region will be sufficiently far away from the boundary, so that Robin boundary conditions for the transport problem are prescribed (zero total concentration flux through the boundary of $\Omega'$).

First the flow problem was solved. We give in Figure 1.12 the flow field near the pollution source at the end of the simulated period. The absolute majority of the groundwater flows around the clay barrier because of its low conductivity. Then, using the water content and Darcy velocity values on each simulated period, the transport problem was dealt with. This problem is not convection-dominated; its complexity lies rather in the high ratio of the longitudinal and transverse dispersivities and in the complex flow field. Since the molecular diffusion coefficient is very small, the concentration should mainly follow the flow field and can in fact only enter the clay barrier due to the dispersion. The simulations were first performed on an unrefined grid and then, to justify the results, the mesh was refined. It again turned out that the refinement of the most exposed parts is sufficient. We give in particular in Figure 1.13 an example of a still very coarse grid that nevertheless already yields an accurate result. Although the combined scheme in the given case theoretically does not guarantee the discrete maximum principle, there were virtually no negative concentrations.

### 1.9.6 Concluding remarks

The code TALISMAN was originally a finite volume code working with regular cartesian grids. There was an interest in enabling a local refinement in this code, while subdividing the computational cells independently (as in Figure 1.7). The first attempt was to maintain the pure cell-centered finite volume scheme on square cells, while neglecting the orthogonality condition (i.e. to use the same scheme as that proposed in [36]). This violating of consistency while refining the grid however showed to produce an error rather than to decrease it. Another problem was how to discretize the inhomogeneous and anisotropic diffusion–dispersion tensor, especially on locally refined grids.

It was the implementation of the combined finite volume–finite element scheme in this code that overcame all the above difficulties. By constructing the dual triangular grid as in Figure 1.7, the combined scheme completely falls into the theoretical frame of Sections 1.9.3 and 1.9.4. The numerical experiments in Section 1.9.5 confirm that with this scheme, the local refinement does not produce any errors but substantially improves the results, and this without any considerable increase of the number of unknowns. In addition, inhomogeneous and anisotropic diffusion–dispersion tensors are easily incorporated. These results may serve as an example of the efficiency of the ideas proposed in this appendix.

A local refinement of the computational grid fixed throughout the calculation cannot of course lead to satisfactory results namely in the convection-dominated case, as it was illustrated in Section 1.9.5. We intend to use in the future an adaptive local mesh refinement. The idea is to refine the mesh automatically in the regions where the precision is not sufficient and to derefine it again as the precision gets sufficient. The derivation of a posteriori error estimates and development of a local refinement indicator such as that proposed in [95, 96] is a challenging task for a future work.

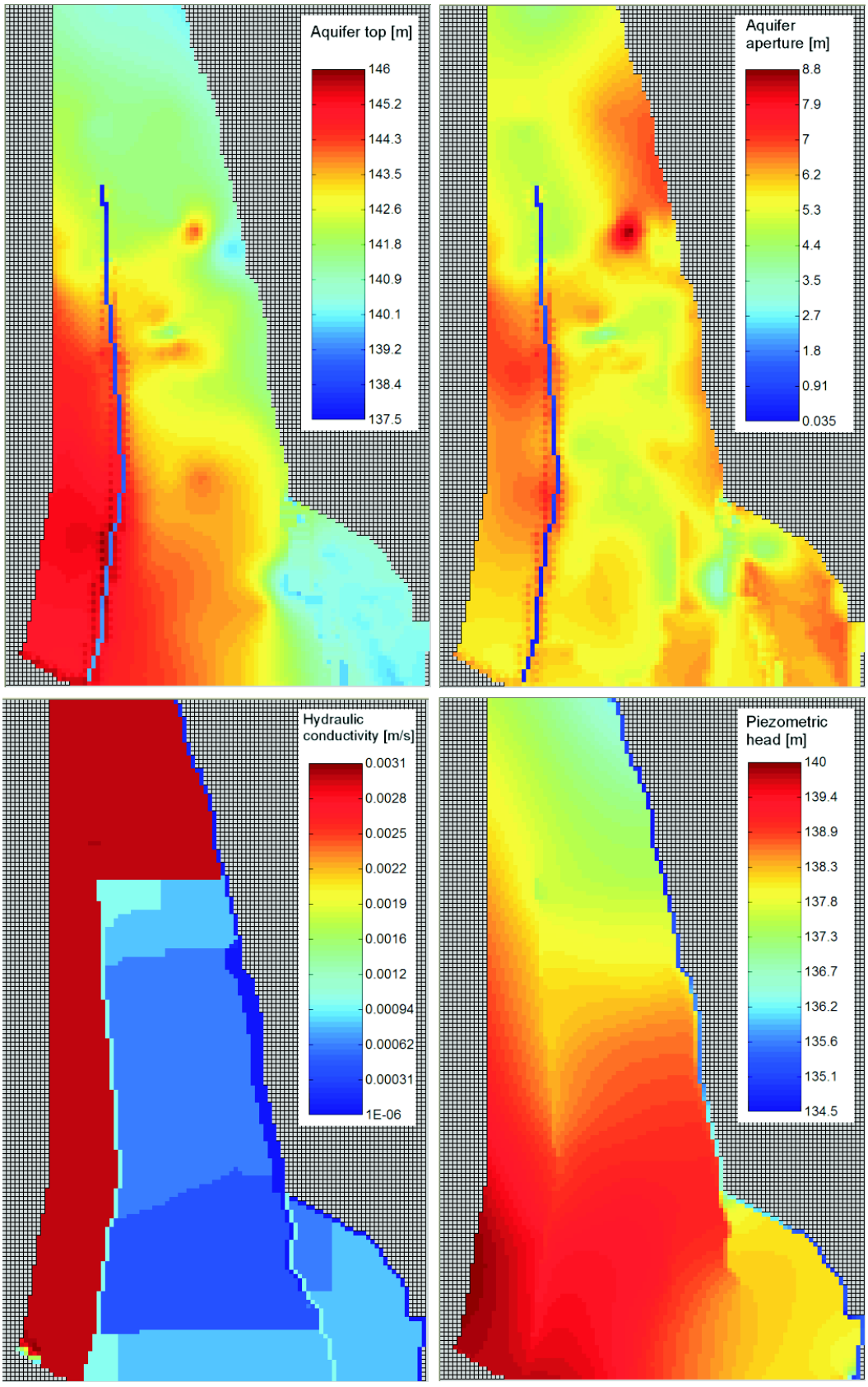


Figure 1.11: Simulated aquifer properties

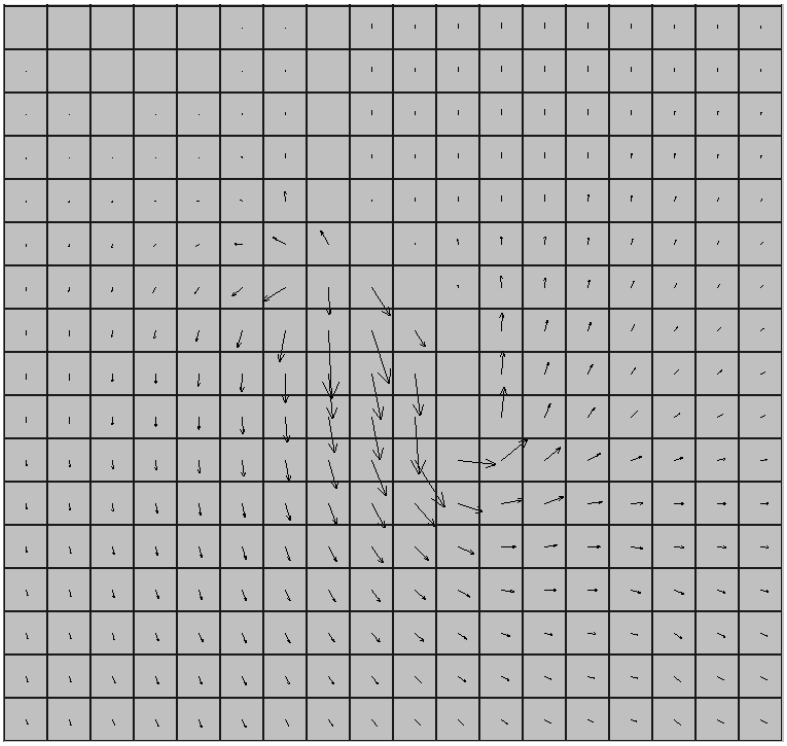

Figure 1.12: Flow field at the end of the simulated period

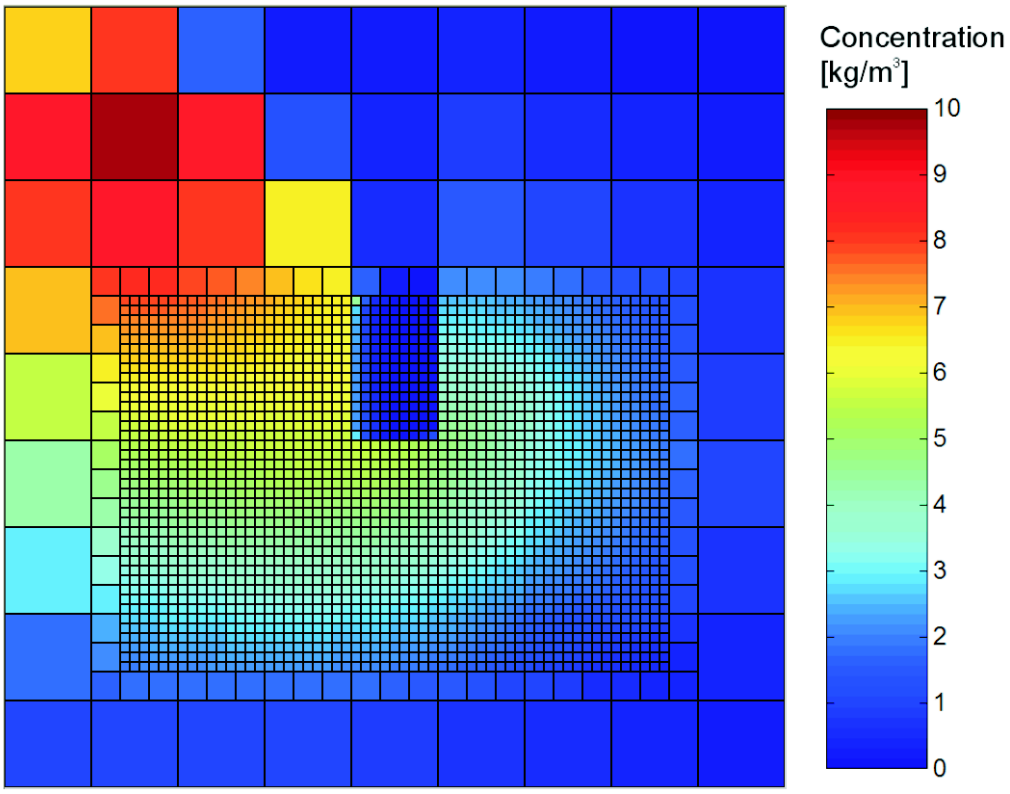


Figure 1.13: Concentration at the end of the simulated period, locally refined mesh

# Chapter 2

# Discrete Poincaré–Friedrichs inequalities

We present in this chapter a direct proof of the discrete Poincaré–Friedrichs inequalities for a class of nonconforming approximations of the Sobolev space $H^1(\Omega)$, indicate optimal values of the constants in these inequalities, and extend the discrete Friedrichs inequality onto domains only bounded in one direction. We consider a polygonal domain $\Omega$ in two or three space dimensions and its shape-regular simplicial triangulation. The nonconforming approximations of $H^1(\Omega)$ consist of functions from $H^1$ on each element such that the mean values of their traces on interelement boundaries coincide. The key idea is to extend the proof of the discrete Poincaré–Friedrichs inequalities for piecewise constant functions used in the finite volume method. The results have applications in the analysis of nonconforming numerical methods, such as nonconforming finite element or discontinuous Galerkin methods.

## 2.1 Introduction

The Friedrichs (also called Poincaré) inequality

$$\int_\Omega g^2(\mathbf{x})\,\mathrm{d}\mathbf{x} \le c_F \int_\Omega |\nabla g(\mathbf{x})|^2\,\mathrm{d}\mathbf{x} \qquad \forall g \in H_0^1(\Omega) \tag{2.1}$$

and the Poincaré (also called mean Poincaré) inequality

$$\int_\Omega g^2(\mathbf{x})\,\mathrm{d}\mathbf{x} \le c_P \int_\Omega |\nabla g(\mathbf{x})|^2\,\mathrm{d}\mathbf{x} + \tilde{c}_P\Big(\int_\Omega g(\mathbf{x})\,\mathrm{d}\mathbf{x}\Big)^2 \qquad \forall g \in H^1(\Omega) \tag{2.2}$$

(cf. [91]) play an important role in the theory of partial differential equations. We consider here a bounded polygonal domain (open and connected set) $\Omega \subset \mathbb{R}^d$, $d = 2, 3$, $H^1(\Omega)$ is the Sobolev space of $L^2(\Omega)$ functions with square-integrable generalized derivatives, and $H_0^1(\Omega)$ is the subspace of $H^1(\Omega)$ of functions with zero trace on the boundary $\partial\Omega$ of $\Omega$. We refer for instance to [4] for details on the spaces $H^1(\Omega)$, $H_0^1(\Omega)$.

Let $\{\mathcal{T}_h\}_h$ be a family of simplicial triangulations of $\Omega$ (consisting of triangles in space dimension two and of tetrahedra in space dimension three). Let the spaces $W(\mathcal{T}_h)$ be formed by functions locally in $H^1(K)$ on each $K \in \mathcal{T}_h$ such that the mean values of their traces on interior sides (edges if $d = 2$, faces if $d = 3$) coincide. Finally, let $W_0(\mathcal{T}_h) \subset W(\mathcal{T}_h)$ be such that the mean values of the traces on exterior sides of functions from $W_0(\mathcal{T}_h)$ are equal to zero (precise definitions are given in the next section). These spaces are nonconforming approximations of the continuous ones, i.e. $W_0(\mathcal{T}_h) \not\subset H_0^1(\Omega)$ and $W(\mathcal{T}_h) \not\subset H^1(\Omega)$. We investigate in this chapter analogies of (2.1) and (2.2) in the forms

$$\int_\Omega g^2(\mathbf{x})\,\mathrm{d}\mathbf{x} \le C_F \sum_{K\in\mathcal{T}_h} \int_K |\nabla g(\mathbf{x})|^2\,\mathrm{d}\mathbf{x} \qquad \forall g \in W_0(\mathcal{T}_h)\,,\ \forall h > 0\,, \tag{2.3}$$

$$\int_\Omega g^2(\mathbf{x})\,\mathrm{d}\mathbf{x} \le C_P \sum_{K\in\mathcal{T}_h} \int_K |\nabla g(\mathbf{x})|^2\,\mathrm{d}\mathbf{x} + \tilde{C}_P\Big(\int_\Omega g(\mathbf{x})\,\mathrm{d}\mathbf{x}\Big)^2 \qquad \forall g \in W(\mathcal{T}_h)\,,\ \forall h > 0\,. \tag{2.4}$$

The validity of (2.3) for $W_0(\mathcal{T}_h)$ consisting of piecewise linear functions (used e.g. in the Crouzeix–Raviart finite element method) has been established in [116, Proposition 4.13] provided that $\Omega$ is convex and in [51] for a generally nonconvex $\Omega$ but with triangulations that are not locally refined. These results have been later extended in [84] onto $\mathcal{T}_h$ only satisfying the shape regularity (minimal angle) assumption and onto spaces that include $W_0(\mathcal{T}_h)$. Another proof of this last result is presented in [28]. This paper also shows how to extend the discrete Friedrichs and Poincaré inequalities to general polygonal (nonmatching) partitions of $\Omega$ and to functions that do not satisfy the equality of the means of traces on interior sides, provided that (2.3), (2.4) are satisfied.

It was shown in [84] and in [28] that the constants $C_F$, $C_P$ only depend on the domain $\Omega$ and on the shape regularity of the meshes. We establish in this chapter the exact dependence of $C_F$, $C_P$ on these parameters. We show that in space dimension two $C_F$ only depends on the area of $\Omega$ and that in space dimension two or three $C_F$ only depends on the square of the infimum of the diameters of $\Omega$ in one direction. For convex domains, $C_P$ only depends on the square of the diameter of $\Omega$ and on the ratio between the area of the circumscribed ball and the area of $\Omega$. For nonconvex domains, our results involve a more complicated dependence of $C_P$ on $\Omega$. The above-mentioned dependencies are optimal in the sense that they coincide with the dependencies of $c_F$, $c_P$ on $\Omega$ in the continuous case. The dependence of $C_F$ on $\Omega$ also allows for

the extension of the discrete Friedrichs inequality to domains only bounded in one direction. We finally show that $C_F$ depends, in space dimension two and provided that it is expressed using the area of $\Omega$, on the square of a parameter describing the shape regularity of the meshes given in the next section. This dependence still holds true for $C_F$ in space dimension two or three and expressed using the square of the infimum of the diameters of $\Omega$ in one direction and also for $C_P$, provided that the mesh is not locally refined. We present an example showing that this dependence is optimal. For locally refined meshes, our results involve a more complicated dependence on the shape regularity parameter. The established constants are necessary in the analysis of nonconforming numerical methods, such as nonconforming finite element or discontinuous Galerkin methods.

Our proof of the discrete Friedrichs and Poincaré inequalities on the spaces $W_0(\mathcal{T}_h)$, $W(\mathcal{T}_h)$ respectively is more direct than those presented in [84] and in [28]; in particular, all the necessary intermediate results are proved here. In [84] the author uses a Clément-type interpolation operator (cf. [43]) mapping the space $W_0(\mathcal{T}_h)$ to $H_0^1(\Omega)$. In [28] the key idea is to construct nonconforming $P_1$ interpolants of functions from $W(\mathcal{T}_h)$ and to connect the nonconforming $P_1$ finite elements and conforming $P_2$ finite elements (in space dimension two) or conforming $P_3$ finite elements (in space dimension three). In both cases one finally makes use of the continuous inequalities (2.1), (2.2). Our main idea is to construct a piecewise constant interpolant and to extend the discrete Poincaré–Friedrichs inequalities for piecewise constant functions known from finite volume methods, see [59, 61]. In particular, we do not make use of the continuous inequalities; since $H_0^1(\Omega) \subset W_0(\mathcal{T}_h)$ and $H^1(\Omega) \subset W(\mathcal{T}_h)$, we rather prove them.

The rest of the chapter is organized as follows. In Section 2.2 we describe the assumptions on $\mathcal{T}_h$, define a dual mesh $\mathcal{D}_h$ where the dual elements are associated with the sides of $\mathcal{T}_h$, define the function spaces used in the sequel, and introduce the interpolation operator. In Section 2.3 we give the discrete Friedrichs inequality for piecewise constant functions on $\mathcal{D}_h$. In Section 2.4 we prove some interpolation estimates on functions from $H^1(K)$, where $K$ is a simplex in two or three space dimensions. In Section 2.5 we prove the discrete Friedrichs inequality for functions from $W_0(\mathcal{T}_h)$, using their interpolation by piecewise constant functions on $\mathcal{D}_h$. In Section 2.6 we show how this proof simplifies for Crouzeix–Raviart finite elements in two space dimensions. Finally, Section 2.7 is devoted to the proof of the discrete Poincaré inequality for piecewise constant functions on $\mathcal{D}_h$ and Section 2.8 to the extension of this result to functions from $W(\mathcal{T}_h)$.

## 2.2 Notation and assumptions

Throughout this chapter, we shall mean by "segment" a segment of a straight line. Let us consider a domain $K \subset \mathbb{R}^d$, $d = 2, 3$. We denote by $\|\cdot\|_{0,K}$ the norm on $L^2(K)$, $\|g\|_{0,K}^2 = \int_K g^2(\mathbf{x})\,\mathrm{d}\mathbf{x}$, by $|K|$ is the $d$-dimensional Lebesgue measure of $K$, by $|\sigma|$ the $(d-1)$-dimensional Lebesgue measure of $\sigma$, a part of a hyperplane in $\mathbb{R}^d$, and by $|\mathbf{s}|$ the length of a segment $\mathbf{s}$. Let $\mathbf{b}$ be a vector. We shall mean by the diameter of $K$ in the direction of $\mathbf{b}$, denoted by $\mathrm{diam}_{\mathbf{b}}(K)$, the supremum of the lengths of segments $\mathbf{s}$ with the direction vector $\mathbf{b}$ such that $\mathbf{s} \subset K$. The diameter of $K$ is the supremum of the lengths of all the segments $\mathbf{s}$ such that $\mathbf{s} \subset K$.

### Triangulation

We suppose that $\mathcal{T}_h$ for all $h > 0$ consists of closed simplices such that $\overline{\Omega} = \bigcup_{K \in \mathcal{T}_h} K$ and such that if $K, L \in \mathcal{T}_h$, $K \neq L$, then $K \cap L$ is either an empty set or a common face, edge, or

vertex of $K$ and $L$. The parameter $h$ is defined by $h := \max_{K\in\mathcal{T}_h} \operatorname{diam}(K)$. We denote by $\mathcal{E}_h$ the set of all sides, by $\mathcal{E}_h^{\rm int}$ the set of all interior sides, by $\mathcal{E}_h^{\rm ext}$ the set of all exterior sides, and by $\mathcal{E}_K$ the set of all the sides of an element $K \in \mathcal{T}_h$. We make the following shape regularity assumption on $\{\mathcal{T}_h\}_h$:

*Assumption (A) (Shape regularity assumption)*

*There exists a constant* $\kappa_{\mathcal{T}} > 0$ *such that*

$$\min_{K\in\mathcal{T}_h} \frac{|K|}{\operatorname{diam}(K)^d} \geq \kappa_{\mathcal{T}} \qquad \forall h > 0\,.$$

Assumption *(A)* is equivalent to the existence of a constant $\theta_{\mathcal{T}} > 0$ such that

$$\max_{K\in\mathcal{T}_h} \frac{\operatorname{diam}(K)}{\rho_K} \leq \theta_{\mathcal{T}} \qquad \forall h > 0\,, \tag{2.5}$$

where $\rho_K$ is the diameter of the largest ball inscribed in the simplex $K$. Finally, Assumption *(A)* is equivalent to the existence of a constant $\phi_{\mathcal{T}} > 0$ such that

$$\min_{K\in\mathcal{T}_h} \phi_K \geq \phi_{\mathcal{T}} \qquad \forall h > 0\,. \tag{2.6}$$

Here $\phi_K$ is the smallest angle of the simplex $K$ (plain angle in radians if $d = 2$ and spheric angle in steradians if $d = 3$).

In the sequel we shall consider apart triangulations that may not be locally refined, i.e. the case where the following assumption holds:

*Assumption (B) (Inverse assumption)*

*There exists a constant* $\zeta_{\mathcal{T}} > 0$ *such that*

$$\max_{K\in\mathcal{T}_h} \frac{h}{\operatorname{diam}(K)} \leq \zeta_{\mathcal{T}} \qquad \forall h > 0\,.$$

Assumptions *(A)* and *(B)* imply

$$\min_{K\in\mathcal{T}_h} \frac{|K|}{h^d} \geq \tilde{\kappa}_{\mathcal{T}} \qquad \forall h > 0\,, \tag{2.7}$$

where $\tilde{\kappa}_{\mathcal{T}} := \kappa_{\mathcal{T}}/\zeta_{\mathcal{T}}^d$.

### Dual mesh

In the sequel we will use a dual mesh $\mathcal{D}_h$ to $\mathcal{T}_h$ such that $\overline{\Omega} = \bigcup_{D\in\mathcal{D}_h} D$. There is one dual element $D$ associated with each side $\sigma_D \in \mathcal{E}_h$. We construct it by connecting the barycentres of every $K \in \mathcal{T}_h$ that contains $\sigma_D$ through the vertices of $\sigma_D$. For $\sigma_D \in \mathcal{E}_h^{\rm ext}$, the contour of $D$ is completed by the side $\sigma_D$ itself. We refer to Fig. 2.1 for the two-dimensional case. We denote by $\mathcal{D}_h^{\rm int}$ the set of all interior and by $\mathcal{D}_h^{\rm ext}$ the set of all boundary dual elements. As for the primal mesh, we set $\mathcal{F}_h$, $\mathcal{F}_h^{\rm int}$, $\mathcal{F}_h^{\rm ext}$, and $\mathcal{F}_D$ for the dual mesh sides. We denote by $Q_D$ the barycentre of a side $\sigma_D$ and for two adjacent elements $D, E \in \mathcal{D}_h$, we set $\sigma_{D,E} := \partial D \cap \partial E$, $d_{D,E} := |Q_E - Q_D|$, and $K_{D,E}$ the element of $\mathcal{T}_h$ such that $\sigma_{D,E} \subset K_{D,E}$. We remark that

$$|K \cap D| = \frac{|K|}{d+1} \tag{2.8}$$

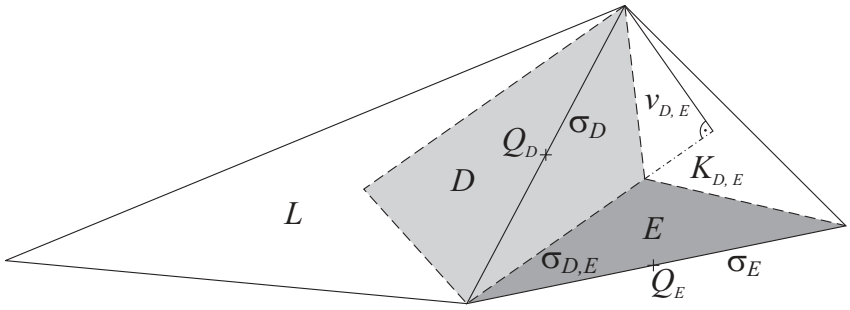


Figure 2.1: Triangles $K, L \in \mathcal{T}_h$ and dual elements $D, E \in \mathcal{D}_h$ with edges $\sigma_D, \sigma_E \in \mathcal{E}_h$

for each $K \in \mathcal{T}_h$ and $D \in \mathcal{D}_h$ such that $\sigma_D \in \mathcal{E}_K$. Let us now consider $\sigma_{D,E} \in \mathcal{F}_h^{\rm int}$, $\sigma_{D,E} = \partial D \cap \partial E$ in the two-dimensional case. Let $K_{D,E} \cap D$ be in the clockwise direction from $K_{D,E} \cap E$. We then define $v_{D,E}$ as the height of the triangle $|K_{D,E} \cap D|$ with respect to its base $\sigma_{D,E}$ and have (see Fig. 2.1)

$$|K_{D,E} \cap D| = \frac{|\sigma_{D,E}| v_{D,E}}{2} \,. \tag{2.9}$$

### Function spaces

We define the space $W(\mathcal{T}_h)$ by

$$\begin{aligned} W(\mathcal{T}_h) \;:=\; \Big\{ & g \in L^2(\Omega)\,;\, g|_K \in H^1(K) \qquad \forall K \in \mathcal{T}_h\,, \\ & \int_{\sigma_{K,L}} g|_K(\mathbf{x})\,\mathrm{d}\gamma(\mathbf{x}) = \int_{\sigma_{K,L}} g|_L(\mathbf{x})\,\mathrm{d}\gamma(\mathbf{x}) \\ & \qquad \forall \sigma_{K,L} \in \mathcal{E}_h^{\rm int}\,,\ \sigma_{K,L} = \partial K \cap \partial L \Big\}\,. \end{aligned} \tag{2.10}$$

We keep the same notation for the function $g$ and its trace and denote $\mathrm{d}\gamma(\mathbf{x})$ the integration symbol for the Lebesgue measure on a hyperplane of $\Omega$. The space $W_0(\mathcal{T}_h)$ is defined by

$$W_0(\mathcal{T}_h) := \Big\{ g \in W(\mathcal{T}_h)\,;\, \int_\sigma g(\mathbf{x})\,\mathrm{d}\gamma(\mathbf{x}) = 0 \qquad \forall \sigma \in \mathcal{E}_h^{\rm ext} \Big\}\,. \tag{2.11}$$

We finally define

$$|g|_{1,\mathcal{T}} := \Big( \sum_{K \in \mathcal{T}_h} \int_K |\nabla g(\mathbf{x})|^2\,\mathrm{d}\mathbf{x} \Big)^{\frac{1}{2}}\,,$$

which is a seminorm on $W(\mathcal{T}_h)$ and a norm on $W_0(\mathcal{T}_h)$. The spaces $X(\mathcal{T}_h) \subset W(\mathcal{T}_h)$ and $X_0(\mathcal{T}_h) \subset W_0(\mathcal{T}_h)$ are defined by piecewise linear functions on $\mathcal{T}_h$. Note that the functions from $X(\mathcal{T}_h)$ are continuous in barycentres of interior sides and that the functions from $X_0(\mathcal{T}_h)$ are moreover equal to zero in barycentres of exterior sides.

The space $Y(\mathcal{D}_h)$ is the space of piecewise constant functions on $\mathcal{D}_h$,

$$Y(\mathcal{D}_h) := \big\{ c \in L^2(\Omega)\,;\, c|_D \text{ is constant } \forall D \in \mathcal{D}_h \big\}\,,$$

and $Y_0(\mathcal{D}_h)$ is its subspace of functions equal to zero on all $D \in \mathcal{D}_h^{\rm ext}$,

$$Y_0(\mathcal{D}_h) := \big\{ c \in Y(\mathcal{D}_h)\,;\, c|_D = 0 \quad \forall D \in \mathcal{D}_h^{\rm ext} \big\}\,.$$

For $c \in Y(\mathcal{D}_h)$ given by the values $c_D$ on $D \in \mathcal{D}_h$, we define

$$|c|_{1,\mathcal{T},*} := \Big( \sum_{\sigma_{D,E} \in \mathcal{F}_h^{\rm int}} \frac{|\sigma_{D,E}|}{v_{D,E}} (c_E - c_D)^2 \Big)^{\frac{1}{2}},$$

$$|c|_{1,\mathcal{T},\dagger} := \Big( \sum_{\sigma_{D,E} \in \mathcal{F}_h^{\rm int}} \frac{|\sigma_{D,E}|}{\mathrm{diam}(K_{D,E})} (c_E - c_D)^2 \Big)^{\frac{1}{2}},$$

$$|c|_{1,\mathcal{T},\ddagger} := \Big( \sum_{\sigma_{D,E} \in \mathcal{F}_h^{\rm int}} \frac{|\sigma_{D,E}|}{d_{D,E}} (c_E - c_D)^2 \Big)^{\frac{1}{2}};$$

$|\cdot|_{1,\mathcal{T},*}$, $|\cdot|_{1,\mathcal{T},\dagger}$, and $|\cdot|_{1,\mathcal{T},\dagger}$ are seminorms on $Y(\mathcal{D}_h)$ and norms on $Y_0(\mathcal{D}_h)$.

### Interpolation operator

The interpolation operator $I$ associates to a function $g \in W(\mathcal{T}_h)$ a function $I(g) \in Y(\mathcal{D}_h)$ such that

$$I(g)|_D = g_D := \frac{1}{|\sigma_D|} \int_{\sigma_D} g|_K(\mathbf{x})\, \mathrm{d}\gamma(\mathbf{x}) \qquad \forall D \in \mathcal{D}_h\,,$$

where $K \in \mathcal{T}_h$ is such that $\sigma_D \in \mathcal{E}_K$. Note that by (2.10), if $\sigma_D \in \mathcal{E}_K$ and $\sigma_D \in \mathcal{E}_L$, $K \neq L$, the choice between $K$ and $L$ does not matter. We recall that $\sigma_D \in \mathcal{E}_h$ is the side associated with the dual element $D \in \mathcal{D}_h$. Note that for $g \in W_0(\mathcal{T}_h)$, $I(g) \in Y_0(\mathcal{D}_h)$.

## 2.3 Discrete Friedrichs inequality for piecewise constant functions

In finite volume methods (cf. [61]) one can prove the discrete Friedrichs inequality for piecewise constant functions for meshes that satisfy the following orthogonality property: there exists a point associated with each element of the mesh such that the straight line connecting these points for two neighboring elements is orthogonal to the common side of these two elements. The proofs in [59, 61] rely on this property of the meshes. We present in this section analogies of Lemma 9.5 and consequent Remark 9.13 and of Lemma 9.1 of [61] for the mesh $\mathcal{D}_h$, where the orthogonality property is not necessarily satisfied.

**Theorem 2.3.1. (Discrete Friedrichs inequality for piecewise constant functions in two space dimensions)** *Let $d = 2$. Then for all $c \in Y_0(\mathcal{D}_h)$,*

$$\|c\|_{0,\Omega}^2 \leq \frac{|\Omega|}{2} |c|_{1,\mathcal{T},*}^2\,.$$

Proof:

Let $\mathbf{b}_1 = (1,0)$ and $\mathbf{b}_2 = (0,1)$ be two fixed unit vectors in the axis directions. For all $\mathbf{x} \in \Omega$, let $\mathcal{B}_{\mathbf{x}}^1$ and $\mathcal{B}_{\mathbf{x}}^2$ be the straight lines going through $\mathbf{x}$ and defined by the vectors $\mathbf{b}_1$, $\mathbf{b}_2$ respectively. Let the functions $\chi_\sigma^{(i)}(\mathbf{x})$, $i = 1, 2$, for each $\sigma \in \mathcal{F}_h^{\rm int}$ be defined by

$$\chi_\sigma^{(i)}(\mathbf{x}) := \begin{cases} 1 & \text{if } \sigma \cap \mathcal{B}_{\mathbf{x}}^i \neq \emptyset \\ 0 & \text{if } \sigma \cap \mathcal{B}_{\mathbf{x}}^i = \emptyset \end{cases}.$$

Let finally $D \in \mathcal{D}_h^{\rm int}$ be fixed. Then for a.e. $\mathbf{x} \in D$, $\mathcal{B}_{\mathbf{x}}^i$, $i = 1, 2$, do not contain any vertex of the dual mesh and $\mathcal{B}_{\mathbf{x}}^i \cap \sigma$, $i = 1, 2$, contain at most one point of all $\sigma \in \mathcal{F}_h$. This implies

that for a.e. $\mathbf{x} \in D$, $\mathcal{B}^i_{\mathbf{x}}$, $i = 1, 2$, always have to intersect the interior of some $E \in \mathcal{D}_h^{\mathrm{ext}}$ before "leaving" or after "entering" $\Omega$ (we recall that $\Omega$ may be nonconvex). Using this, the fact that $c_E = 0$ for all $E \in \mathcal{D}_h^{\mathrm{ext}}$, and the triangle inequality, we have

$$2|c_D| \le \sum_{\sigma_{F,G} \in \mathcal{F}_h^{\mathrm{int}}} |c_G - c_F| \chi^{(i)}_{\sigma_{F,G}}(\mathbf{x}) \quad \text{for a.e. } \mathbf{x} \in D\,,\ i = 1, 2\,.$$

This gives

$$|c_D|^2 \le \frac{1}{4} \sum_{\sigma_{F,G} \in \mathcal{F}_h^{\mathrm{int}}} |c_G - c_F| \chi^{(1)}_{\sigma_{F,G}}(\mathbf{x}) \sum_{\sigma_{F,G} \in \mathcal{F}_h^{\mathrm{int}}} |c_G - c_F| \chi^{(2)}_{\sigma_{F,G}}(\mathbf{x}) \quad \text{for a.e. } \mathbf{x} \in D\,,$$

which is obviously valid also for $D \in \mathcal{D}_h^{\mathrm{ext}}$, considering that $c_D = 0$ on $D \in \mathcal{D}_h^{\mathrm{ext}}$. Integrating the above inequality over $D$ and summing over $D \in \mathcal{D}_h$ yields

$$\sum_{D \in \mathcal{D}_h} c_D^2 |D| \le \frac{1}{4} \int_\Omega \Big( \sum_{\sigma_{D,E} \in \mathcal{F}_h^{\mathrm{int}}} |c_E - c_D| \chi^{(1)}_{\sigma_{D,E}}(\mathbf{x}) \sum_{\sigma_{D,E} \in \mathcal{F}_h^{\mathrm{int}}} |c_E - c_D| \chi^{(2)}_{\sigma_{D,E}}(\mathbf{x}) \Big) \,\mathrm{d}\mathbf{x}\,.$$

Let $\alpha = \inf\{x_1; (x_1, x_2) \in \Omega\}$ and $\beta = \sup\{x_1; (x_1, x_2) \in \Omega\}$. For each $x_1 \in (\alpha, \beta)$, we denote by $J(x_1)$ the set of $x_2$ such that $\mathbf{x} = (x_1, x_2) \in \Omega$. We now notice that $\chi^{(1)}_\sigma(\mathbf{x})$ only depends on $x_2$ and that $\chi^{(2)}_\sigma(\mathbf{x})$ only depends on $x_1$. Thus

$$\begin{aligned}
&\int_\alpha^\beta \int_{J(x_1)} \Big( \sum_{\sigma_{D,E} \in \mathcal{F}_h^{\mathrm{int}}} |c_E - c_D| \chi^{(1)}_{\sigma_{D,E}}(x_2) \sum_{\sigma_{D,E} \in \mathcal{F}_h^{\mathrm{int}}} |c_E - c_D| \chi^{(2)}_{\sigma_{D,E}}(x_1) \Big) \,\mathrm{d}x_2 \,\mathrm{d}x_1 \\
&= \int_\alpha^\beta \sum_{\sigma_{D,E} \in \mathcal{F}_h^{\mathrm{int}}} |c_E - c_D| \chi^{(2)}_{\sigma_{D,E}}(x_1) \sum_{\sigma_{D,E} \in \mathcal{F}_h^{\mathrm{int}}} |c_E - c_D| \int_{J(x_1)} \chi^{(1)}_{\sigma_{D,E}}(x_2) \,\mathrm{d}x_2 \,\mathrm{d}x_1 \\
&\le \sum_{\sigma_{D,E} \in \mathcal{F}_h^{\mathrm{int}}} |c_E - c_D| |\sigma_{D,E}| \int_\alpha^\beta \sum_{\sigma_{D,E} \in \mathcal{F}_h^{\mathrm{int}}} |c_E - c_D| \chi^{(2)}_{\sigma_{D,E}}(x_1) \,\mathrm{d}x_1\,,
\end{aligned}$$

where we have used $\int_{J(x_1)} \chi^{(1)}_{\sigma_{D,E}}(x_2) \,\mathrm{d}x_2 \le |\sigma_{D,E}|$. Using analogously $\int_\alpha^\beta \chi^{(2)}_{\sigma_{D,E}}(x_1) \,\mathrm{d}x_1 \le |\sigma_{D,E}|$, we come to

$$\sum_{D \in \mathcal{D}_h} c_D^2 |D| \le \frac{1}{4} \Big( \sum_{\sigma_{D,E} \in \mathcal{F}_h^{\mathrm{int}}} |\sigma_{D,E}| |c_E - c_D| \Big)^2\,.$$

Finally, using the Cauchy–Schwarz inequality, we have

$$\sum_{D \in \mathcal{D}_h} c_D^2 |D| \le \frac{1}{4} \sum_{\sigma_{D,E} \in \mathcal{F}_h^{\mathrm{int}}} |\sigma_{D,E}| v_{D,E} \sum_{\sigma_{D,E} \in \mathcal{F}_h^{\mathrm{int}}} \frac{|\sigma_{D,E}|}{v_{D,E}} (c_E - c_D)^2\,.$$

The equality $\sum_{\sigma_{D,E} \in \mathcal{F}_h^{\mathrm{int}}} |\sigma_{D,E}| v_{D,E} = 2|\Omega|$, which follows from (2.9), concludes the proof. □

**Remark 2.3.2. (Discrete Friedrichs inequality for piecewise constant functions on equilateral simplices)** *Let $\mathbf{b} \in \mathbb{R}^d$ be a fixed vector and let $\mathcal{T}_h$ consist of equilateral simplices. Then for all $c \in Y_0(\mathcal{D}_h)$,*

$$\|c\|^2_{0,\Omega} \le [\mathrm{diam}_{\mathbf{b}}(\Omega) + 2h]^2 |c|^2_{1,\mathcal{T},\ddagger}\,.$$

*This follows from [61, Lemma 9.1] (cf. alternatively [59, Lemma 1]), since the dual mesh $\mathcal{D}_h$ satisfies in this case the orthogonality property.*

**Lemma 2.3.3.** *Let Assumption (B) be satisfied and let* $\mathbf{b} \subset \Omega$ *be a segment that does not contain any vertex of the dual mesh* $\mathcal{D}_h$*. Then*

$$A := \sum_{\sigma_{D,E} \in \mathcal{F}_h^{\mathrm{int}},\, \sigma_{D,E} \cap \mathbf{b} \neq \emptyset} \mathrm{diam}(K_{D,E}) \leq C_{d,\mathcal{T}}\, \mathrm{diam}_{\mathbf{b}}(\Omega)\,,$$

*where*

$$C_{d,\mathcal{T}} = \frac{2^d(d-1)}{\tilde{\kappa}_{\mathcal{T}}}(1 + 2\theta_{\mathcal{T}})\,. \tag{2.12}$$

Proof:

The number of nonzero terms of $A$ is equal to the number of interior dual sides intersected by $\mathbf{b}$. In view of the fact that $\mathbf{b}$ does not contain any vertex of the dual mesh, this number is bounded by $2(d-1)$-times the number of simplices $K \in \mathcal{T}_h$ whose interior is intersected by $\mathbf{b}$. All intersected simplices have to be entirely in the rectangle/rectangular parallelepiped constructed around $\mathbf{b}$, with the distance between $\mathbf{b}$ and its boundary equal to $h$. Considering the consequence (2.7) of Assumptions *(A)* and *(B)*, we can estimate the number of intersected elements by

$$\frac{(2h)^{d-1}(|\mathbf{b}| + 2h)}{\tilde{\kappa}_{\mathcal{T}} h^d}\,.$$

Using in addition $\mathrm{diam}(K_{D,E}) \leq h$ and $|\mathbf{b}| \leq \mathrm{diam}_{\mathbf{b}}(\Omega)$, we have

$$A \leq \frac{2^d(d-1)}{\tilde{\kappa}_{\mathcal{T}}}(\mathrm{diam}_{\mathbf{b}}(\Omega) + 2h)\,.$$

Noticing that

$$h \leq \theta_{\mathcal{T}} \mathrm{diam}_{\mathbf{b}}(\Omega) \tag{2.13}$$

by the consequence (2.5) of Assumption *(A)* concludes the proof. □

**Lemma 2.3.4.** *Let* $\mathbf{b} \subset \Omega$ *be a segment that does not contain any vertex of the dual mesh* $\mathcal{D}_h$*. Then*

$$A := \sum_{\sigma_{D,E} \in \mathcal{F}_h^{\mathrm{int}},\, \sigma_{D,E} \cap \mathbf{b} \neq \emptyset} \mathrm{diam}(K_{D,E}) \leq C_{d,\mathcal{T}}\, \mathrm{diam}_{\mathbf{b}}(\Omega)\,, \tag{2.14}$$

*where*

$$C_{d,\mathcal{T}} = 4N(d-1)\theta_{\mathcal{T}}^{2N}\,, \quad N = \frac{2^{d-1}\pi}{\phi_{\mathcal{T}}}\,. \tag{2.15}$$

Proof:

The number of nonzero terms of $A$ is equal to the number of interior dual sides intersected by $\mathbf{b}$. In view of the fact that $\mathbf{b}$ does not contain any vertex of the dual mesh, this number is bounded by $2(d-1)$-times the number of simplices $K \in \mathcal{T}_h$ whose interior is intersected by $\mathbf{b}$. We consider two different cases.

If the segment $\mathbf{b}$ intersects at most $N$ simplices, where $N$ is given by (2.15), we estimate

$$\mathrm{diam}(K) \leq \theta_{\mathcal{T}} \rho_K \leq \theta_{\mathcal{T}} \mathrm{diam}_{\mathbf{b}}(\Omega) \qquad \forall K \in \mathcal{T}_h\,,$$

which follows from the consequence (2.5) of Assumption *(A)*, to see that

$$A \leq 2(d-1)N\theta_{\mathcal{T}} \mathrm{diam}_{\mathbf{b}}(\Omega)\,.$$

This in view of $N \geq 1$ and $\theta_{\mathcal{T}} > 1$ implies (2.14) with $C_{d,\mathcal{T}}$ given by (2.15).

We next consider the case where the segment $\mathbf{b}$ intersects at least $N+1$ simplices. We divide it into a system of nonoverlapping segments $\{\mathbf{b}_k\}_{k=1}^M$ such that $\mathbf{b} = \cup_{k=1}^M \mathbf{b}_k$. We further require that each $\mathbf{b}_k$ intersects at least $N$ and at most $2N$ simplices and that no simplex has an intersection with a positive 1-dimensional Lebesgue measure with two different segments. We then have

$$A \le 2(d-1) \sum_{k=1}^{M} \sum_{K\in\mathcal{T}_h;\, K^\circ\cap\mathbf{b}_k\neq\emptyset} \operatorname{diam}(K)\,.$$

Next it follows from the consequence (2.5) of Assumption *(A)* that $\rho_K \le \theta_{\mathcal{T}} \rho_L$ if $K, L \in \mathcal{T}_h$ are neighboring elements. Recall that $\rho_K$ is the diameter of the largest ball inscribed in the simplex $K$. Thus we come to

$$\frac{\max\limits_{K\in\mathcal{T}_h;\, K^\circ\cap\mathbf{b}_k\neq\emptyset} \rho_K}{\min\limits_{K\in\mathcal{T}_h;\, K^\circ\cap\mathbf{b}_k\neq\emptyset} \rho_L} \le \theta_{\mathcal{T}}^{2N-1} \qquad \forall k = 1,\dots,M\,.$$

We further claim that

$$\min_{K\in\mathcal{T}_h;\, K^\circ\cap\mathbf{b}_k\neq\emptyset} \rho_K \le |\mathbf{b}_k| \qquad \forall k = 1,\dots,M\,,$$

i.e. if we take $N$ simplices intersected by a straight line, where $N$ is given by (2.15), then the length of the intersection is at least equal to the smallest diameter of the inscribed balls of the simplices. We show this by contradiction. Let us suppose that $N$ simplices are intersected by a segment $\mathbf{l}$ and that the length of the intersection is smaller or equal to the smallest diameter of the inscribed balls of the simplices. By contradiction, the centers of all the inscribed balls lie outside of the segment $\mathbf{l}$. Now with each simplex intersected by $\mathbf{l}$, we add an angle greater or equal to $\phi_{\mathcal{T}}$ by the consequence (2.6) of Assumption *(A)*. Since we have $N$ simplices, their angles fill the whole circle ($2\pi$, $d=2$) or sphere ($4\pi$, $d=3$), which already yields the contradiction.

Using the last two estimates, the fact that each $\mathbf{b}_k$ intersects at most $2N$ simplices, and once more the consequence (2.5) of Assumption *(A)*, we have

$$A \le 2(d-1) \sum_{k=1}^{M} 2N\theta_{\mathcal{T}}^{2N} |\mathbf{b}_k| \le 4N(d-1)\theta_{\mathcal{T}}^{2N} |\mathbf{b}| \le 4N(d-1)\theta_{\mathcal{T}}^{2N} \operatorname{diam}_{\mathbf{b}}(\Omega)\,.$$

This proves (2.14) with $C_{d,\mathcal{T}}$ given by (2.15) for the second case and consequently the whole lemma. □

**Theorem 2.3.5. (Discrete Friedrichs inequality for piecewise constant functions)** *Let $\mathbf{b} \in \mathbb{R}^d$ be a fixed vector. Then for all $c \in Y_0(\mathcal{D}_h)$,*

$$\|c\|_{0,\Omega}^2 \le C_{d,\mathcal{T}} [\operatorname{diam}_{\mathbf{b}}(\Omega)]^2 |c|_{1,\mathcal{T},\dagger}^2\,,$$

*where $C_{d,\mathcal{T}}$ is given by (2.12) when Assumption (B) is satisfied and by (2.15) in the general case.*

Proof:

For all $\mathbf{x} \in \Omega$, we denote by $\mathcal{B}_{\mathbf{x}}$ the straight semi-line defined by the origin $\mathbf{x}$ and the vector $\mathbf{b}$. Let $\mathbf{y}(\mathbf{x}) \in \partial\Omega \cap \mathcal{B}_{\mathbf{x}}$ be the point where $\mathcal{B}_{\mathbf{x}}$ intersects $\partial\Omega$ for the first time. Then $[\mathbf{x}, \mathbf{y}(\mathbf{x})] \subset \overline{\Omega}$. We finally define a function $\chi_\sigma(\mathbf{x})$ for each $\sigma \in \mathcal{F}_h^{\mathrm{int}}$ by

$$\chi_\sigma(\mathbf{x}) := \begin{cases} 1 & \text{if } \sigma \cap [\mathbf{x}, \mathbf{y}(\mathbf{x})] \neq \emptyset \\ 0 & \text{if } \sigma \cap [\mathbf{x}, \mathbf{y}(\mathbf{x})] = \emptyset \end{cases}\,. \tag{2.16}$$

Let $D \in \mathcal{D}_h^{\rm int}$ be fixed. Then for a.e. $\mathbf{x} \in D$, $\mathcal{B}_{\mathbf{x}}$ does not contain any vertex of the dual mesh and $\mathcal{B}_{\mathbf{x}} \cap \sigma$ contains at most one point of all $\sigma \in \mathcal{F}_h$. This implies that for a.e. $\mathbf{x} \in D$, $\mathcal{B}_{\mathbf{x}}$ always has to intersect the interior of some $E \in \mathcal{D}_h^{\rm ext}$ before "leaving" $\Omega$. Using this, the fact that $c_E = 0$ for all $E \in \mathcal{D}_h^{\rm ext}$, and the triangle inequality, we have

$$|c_D| \le \sum_{\sigma_{F,G} \in \mathcal{F}_h^{\rm int}} |c_G - c_F| \chi_{\sigma_{F,G}}(\mathbf{x}) \quad \text{for a.e. } \mathbf{x} \in D\,.$$

The Cauchy–Schwarz inequality yields

$$|c_D|^2 \le \sum_{\sigma_{F,G} \in \mathcal{F}_h^{\rm int}} \chi_{\sigma_{F,G}}(\mathbf{x}) \operatorname{diam}(K_{F,G}) \sum_{\sigma_{F,G} \in \mathcal{F}_h^{\rm int}} \frac{(c_G - c_F)^2}{\operatorname{diam}(K_{F,G})} \chi_{\sigma_{F,G}}(\mathbf{x}) \quad \text{for a.e. } \mathbf{x} \in D\,, \tag{2.17}$$

which is obviously valid also for $D \in \mathcal{D}_h^{\rm ext}$, considering that $c_D = 0$ on $D \in \mathcal{D}_h^{\rm ext}$. Integrating the above inequality over $D$, summing over $D \in \mathcal{D}_h$, and using Lemma 2.3.3 when Assumption *(B)* is satisfied and Lemma 2.3.4 in the general case yields

$$\sum_{D \in \mathcal{D}_h} |c_D|^2 |D| \le C_{d,\mathcal{T}} \operatorname{diam}_{\mathbf{b}}(\Omega) \sum_{\sigma_{D,E} \in \mathcal{F}_h^{\rm int}} \frac{(c_E - c_D)^2}{\operatorname{diam}(K_{D,E})} \int_\Omega \chi_{\sigma_{D,E}}(\mathbf{x}) \,\mathrm{d}\mathbf{x}\,.$$

Now the value $\int_\Omega \chi_{\sigma_{D,E}}(\mathbf{x}) \,\mathrm{d}\mathbf{x}$ is the measure of the set of points of $\Omega$ located inside a cylinder whose basis is $\sigma_{D,E}$ and generator vector is $-\mathbf{b}$. Thus

$$\int_\Omega \chi_{\sigma_{D,E}}(\mathbf{x}) \,\mathrm{d}\mathbf{x} \le |\sigma_{D,E}| \operatorname{diam}_{\mathbf{b}}(\Omega)\,,$$

which leads to the assertion of the lemma. □

## 2.4 Interpolation estimates on functions from $H^1(K)$

**Lemma 2.4.1.** *Let $K$ be a simplex, $\sigma$ its side, and $g \in H^1(K)$. We set*

$$g_K := \frac{1}{|K|} \int_K g(\mathbf{x}) \,\mathrm{d}\mathbf{x}\,, \tag{2.18}$$

$$g_\sigma := \frac{1}{|\sigma|} \int_\sigma g(\mathbf{x}) \,\mathrm{d}\gamma(\mathbf{x})\,. \tag{2.19}$$

*Then*

$$(g_K - g_\sigma)^2 \le c_d \frac{\operatorname{diam}(K)^2}{|K|} \int_K |\nabla g(\mathbf{x})|^2 \,\mathrm{d}\mathbf{x}\,, \tag{2.20}$$

$$\int_K [g(\mathbf{x}) - g_\sigma]^2 \,\mathrm{d}\mathbf{x} \le c_d \operatorname{diam}(K)^2 \int_K |\nabla g(\mathbf{x})|^2 \,\mathrm{d}\mathbf{x}\,, \tag{2.21}$$

*where*

$$c_d = 6 \ \textit{for}\ d = 2\,, \quad c_d = 9 \ \textit{for}\ d = 3\,. \tag{2.22}$$

Proof:

The inequality (2.20) is proved as a part of [61, Lemma 9.4] or [59, Lemma 2] for $d = 2$. In these references a general convex polygonal element $K$ is considered; the fact that $c_d = 6$

follows by considering a triangular element. The inequality (2.21) also follows from these proofs, using the Cauchy–Schwarz inequality. We now give the proof for the three-dimensional case, following the ideas of the proof for $d = 2$.

Let us consider a tetrahedron $K$ and its face $\sigma$. Let us denote the space coordinates by $x_1, x_2, x_3$. We assume, without loss of generality, that $\sigma \subset \{0\} \times \mathbb{R} \times \mathbb{R}^+$, that one vertex of $\sigma$ lies in the origin, that the longest edge of $\sigma$ lies on $x_2^+$, and that $K \subset \mathbb{R}^+ \times \mathbb{R} \times \mathbb{R}$. Let $\mathbf{a} = (\alpha, \beta, \gamma)$ be the vertex that does not lie on $\sigma$. For all $x_1 \in [0, \alpha]$, we set $J(x_1) = \{x_2 \in \mathbb{R}$ such that $(x_1, x_2, x_3) \in K$ for some $x_3 \in \mathbb{R}\}$. For all $x_2 \in J(x_1)$ with $x_1 \in [0, \alpha]$ given, we set $J(x_1, x_2) = \{x_3 \in \mathbb{R}$ such that $(x_1, x_2, x_3) \in K\}$. For a.e. $\mathbf{x} = (x_1, x_2, x_3) \in K$ and a.e. $\mathbf{y} = (0, y_2, y_3) \in \sigma$, we set $\mathbf{z}(\mathbf{x}, \mathbf{y}) = t\mathbf{a} + (1 - t)\mathbf{y}$ with $t = \frac{x_1}{\alpha}$. Since $K$ is convex, $\mathbf{z}(\mathbf{x}, \mathbf{y}) \in K$ and we have $\mathbf{z}(\mathbf{x}, \mathbf{y}) = (x_1, z_2(x_1, y_2), z_3(x_1, y_3))$ with $z_2(x_1, y_2) = \frac{x_1}{\alpha}\beta + (1 - \frac{x_1}{\alpha})y_2$ and $z_3(x_1, y_3) = \frac{x_1}{\alpha}\gamma + (1 - \frac{x_1}{\alpha})y_3$.

Using the Cauchy–Schwarz inequality, we have

$$\begin{aligned}
&\int_K [g(\mathbf{x}) - g_\sigma]^2 \,\mathrm{d}\mathbf{x} = \int_K \Big[\frac{1}{|\sigma|}\int_\sigma g(\mathbf{x})\,\mathrm{d}\gamma(\mathbf{y}) - \frac{1}{|\sigma|}\int_\sigma g(\mathbf{y})\,\mathrm{d}\gamma(\mathbf{y}) \\
&\pm\frac{1}{|\sigma|}\int_\sigma g(\mathbf{z}(\mathbf{x},\mathbf{y}))\,\mathrm{d}\gamma(\mathbf{y})\Big]^2 \mathrm{d}\mathbf{x} \le \frac{2}{|\sigma|^2}\int_K \Big[\int_\sigma \Big(g(\mathbf{x}) - g(\mathbf{z}(\mathbf{x},\mathbf{y}))\Big)\,\mathrm{d}\gamma(\mathbf{y})\Big]^2 \mathrm{d}\mathbf{x} \\
&+\frac{2}{|\sigma|^2}\int_K \Big[\int_\sigma \Big(g(\mathbf{z}(\mathbf{x},\mathbf{y})) - g(\mathbf{y})\Big)\,\mathrm{d}\gamma(\mathbf{y})\Big]^2 \mathrm{d}\mathbf{x} \le \frac{2}{|\sigma|}(A + B)\,,
\end{aligned}$$

where

$$\begin{aligned}
A &:= \int_K \int_\sigma \Big(g(\mathbf{x}) - g(\mathbf{z}(\mathbf{x},\mathbf{y}))\Big)^2 \,\mathrm{d}\gamma(\mathbf{y})\,\mathrm{d}\mathbf{x}\,, \\
B &:= \int_K \int_\sigma \Big(g(\mathbf{z}(\mathbf{x},\mathbf{y})) - g(\mathbf{y})\Big)^2 \,\mathrm{d}\gamma(\mathbf{y})\,\mathrm{d}\mathbf{x}\,.
\end{aligned}$$

Similarly,

$$(g_K - g_\sigma)^2 \le \frac{2}{|K||\sigma|}(A + B)\,.$$

We denote by $D_i g$ the partial derivative of $g$ with respect to $x_i$, $i \in \{1, 2, 3\}$, and estimate $A$ and $B$ separately. For this purpose, we suppose that $g \in C^1(K)$ and use the density of $C^1(K)$ in $H^1(K)$ to extend the estimates to $g \in H^1(K)$.

We first estimate $A$. We have

$$\begin{aligned}
A = \int_0^\alpha \int_{J(x_1)} \int_{J(x_1,x_2)} \int_{J(0)} \int_{J(0,y_2)} \Big(&g(x_1, x_2, x_3) \\
&- g(x_1, z_2(x_1, y_2), z_3(x_1, y_3))\Big)^2 \,\mathrm{d}y_3\,\mathrm{d}y_2\,\mathrm{d}x_3\,\mathrm{d}x_2\,\mathrm{d}x_1\,.
\end{aligned}$$

Let us suppose that $x_3 \ge z_3$. This implies that $[x_1, x_2, z_3(x_1, y_3)] \in K$, since the cross-section of $K$ and the plane $x_1 = const$ is a triangle whose bottom edge is horizontal and the longest of its three edges. We deduce the inequality

$$\begin{aligned}
&\Big(g(x_1, x_2, x_3) - g(x_1, z_2(x_1, y_2), z_3(x_1, y_3))\Big)^2 = \Big(g(x_1, x_2, x_3) - g(x_1, x_2, z_3(x_1, y_3)) \\
&+g(x_1, x_2, z_3(x_1, y_3)) - g(x_1, z_2(x_1, y_2), z_3(x_1, y_3))\Big)^2 = \Big(\int_{z_3(x_1,y_3)}^{x_3} D_3 g(x_1, x_2, s)\,\mathrm{d}s \\
&+\int_{z_2(x_1,y_2)}^{x_2} D_2 g(x_1, s, z_3(x_1, y_3))\,\mathrm{d}s\Big)^2 \le 2\mathrm{diam}(K)\int_{J(x_1,x_2)} [D_3 g(x_1, x_2, s)]^2\,\mathrm{d}s \\
&+2\mathrm{diam}(K)\Big(1 - \frac{x_1}{\alpha}\Big)\int_{z_2(x_1,y_2)}^{x_2} [D_2 g(x_1, s, z_3(x_1, y_3))]^2\,\mathrm{d}s\,,
\end{aligned}$$

where we have used the Newton integration formula and the Cauchy–Schwarz inequality. Defining $D_i g$, $i \in \{1,2,3\}$, by 0 outside of $K$ and considering also $x_3 < z_3$, we come to

$$A \le 2\mathrm{diam}(K)(A_1 + A_2 + A_3 + A_4)$$

with

$$\begin{aligned}
A_1 &:= \int_0^\alpha \int_{J(x_1)} \int_{J(x_1,x_2)} \int_{J(0)} \int_{J(0,y_2)} \int_{J(x_1,x_2)} [D_3 g(x_1,x_2,s)]^2 \,\mathrm{d}s\,\mathrm{d}y_3\,\mathrm{d}y_2\,\mathrm{d}x_3\,\mathrm{d}x_2\,\mathrm{d}x_1\,,\\
A_2 &:= \int_0^\alpha \int_{J(x_1)} \int_{J(x_1,x_2)} \int_{J(0)} \int_{J(0,y_2)} \Big(1-\frac{x_1}{\alpha}\Big)\\
&\qquad\qquad \int_{z_2(x_1,y_2)}^{x_2} [D_2 g(x_1,s,z_3(x_1,y_3))]^2 \,\mathrm{d}s\,\mathrm{d}y_3\,\mathrm{d}y_2\,\mathrm{d}x_3\,\mathrm{d}x_2\,\mathrm{d}x_1\,,\\
A_3 &:= \int_0^\alpha \int_{J(x_1)} \int_{J(x_1,x_2)} \int_{J(0)} \int_{J(0,y_2)} \int_{z_2(x_1,y_2)}^{x_2} [D_2 g(x_1,s,x_3)]^2 \,\mathrm{d}s\,\mathrm{d}y_3\,\mathrm{d}y_2\,\mathrm{d}x_3\,\mathrm{d}x_2\,\mathrm{d}x_1\,,\\
A_4 &:= \int_0^\alpha \int_{J(x_1)} \int_{J(x_1,x_2)} \int_{J(0)} \int_{J(0,y_2)} \Big(1-\frac{x_1}{\alpha}\Big)\\
&\qquad\qquad \int_{z_3(x_1,y_3)}^{x_3} [D_3 g(x_1,z_2(x_1,y_2),s)]^2 \,\mathrm{d}s\,\mathrm{d}y_3\,\mathrm{d}y_2\,\mathrm{d}x_3\,\mathrm{d}x_2\,\mathrm{d}x_1\,.
\end{aligned}$$

We easily see that

$$A_1 \le \mathrm{diam}(K)|\sigma| \int_K [D_3 g(\mathbf{x})]^2 \,\mathrm{d}\mathbf{x}\,.$$

Next, we estimate $A_2$. Using the Fubini theorem and the change of variables $z_3 = z_3(x_1, y_3)$, we have

$$\begin{aligned}
&\int_{J(0,y_2)} \Big(1-\frac{x_1}{\alpha}\Big) \int_{z_2(x_1,y_2)}^{x_2} [D_2 g(x_1,s,z_3(x_1,y_3))]^2 \,\mathrm{d}s\,\mathrm{d}y_3\\
=\ &\int_{z_2(x_1,y_2)}^{x_2} \int_{J(x_1,z_2(x_1,y_2))} [D_2 g(x_1,s,z_3)]^2 \,\mathrm{d}z_3\,\mathrm{d}s\\
\le\ &\int_{J(x_1)} \int_{J(x_1,s)} [D_2 g(x_1,s,z_3)]^2 \,\mathrm{d}z_3\,\mathrm{d}s\,,
\end{aligned}$$

where the estimate follows by extending the integration region. Hence

$$A_2 \le \mathrm{diam}(K)|\sigma| \int_K [D_2 g(\mathbf{x})]^2 \,\mathrm{d}\mathbf{x}\,.$$

Using the Fubini theorem, we similarly estimate $A_3$ and $A_4$,

$$\begin{aligned}
A_3 &\le \mathrm{diam}(K)|\sigma| \int_K [D_2 g(\mathbf{x})]^2 \,\mathrm{d}\mathbf{x}\,,\\
A_4 &\le \mathrm{diam}(K)|\sigma| \int_K [D_3 g(\mathbf{x})]^2 \,\mathrm{d}\mathbf{x}\,,
\end{aligned}$$

which finally yields

$$A \le 4\mathrm{diam}(K)^2|\sigma| \int_K |\nabla g(\mathbf{x})|^2 \,\mathrm{d}\mathbf{x}\,. \tag{2.23}$$

We now turn to the study of $B$. We write it as

$$B = \int_0^\alpha \int_{J(x_1)} \int_{J(x_1,x_2)} \int_{J(0)} \int_{J(0,y_2)} \Big( g(x_1, z_2(x_1,y_2), z_3(x_1,y_3)) - \\ - g(0,y_2,y_3) \Big)^2 \,\mathrm{d}y_3 \,\mathrm{d}y_2 \,\mathrm{d}x_3 \,\mathrm{d}x_2 \,\mathrm{d}x_1 \,.$$

Using the Newton integration formula and the Cauchy–Schwarz and Hölder inequalities, we have

$$\begin{aligned} &\Big( g(x_1, z_2(x_1,y_2), z_3(x_1,y_3)) - g(0,y_2,y_3) \Big)^2 = \Big( \int_0^{x_1} \Big[ D_1 g(s, z_2(s,y_2), z_3(s,y_3)) \\ &+ D_2 g(s, z_2(s,y_2), z_3(s,y_3)) \frac{\beta - y_2}{\alpha} + D_3 g(s, z_2(s,y_2), z_3(s,y_3)) \frac{\gamma - y_3}{\alpha} \Big] \,\mathrm{d}s \Big)^2 \\ \le\ & \alpha \Big( 1 + \Big( \frac{\beta - y_2}{\alpha} \Big)^2 + \Big( \frac{\gamma - y_3}{\alpha} \Big)^2 \Big) \int_0^{x_1} \sum_{i=1}^3 [D_i g(s, z_2(s,y_2), z_3(s,y_3))]^2 \,\mathrm{d}s \,. \end{aligned}$$

Hence

$$B \le \alpha \Big( 1 + \Big( \frac{\beta - y_2}{\alpha} \Big)^2 + \Big( \frac{\gamma - y_3}{\alpha} \Big)^2 \Big) \sum_{i=1}^3 B_i$$

with

$$B_i = \int_0^\alpha \int_{J(x_1)} \int_{J(x_1,x_2)} \int_{J(0)} \int_{J(0,y_2)} \int_0^{x_1} [D_i g(s, z_2(s,y_2), z_3(s,y_3))]^2 \,\mathrm{d}s \,\mathrm{d}y_3 \,\mathrm{d}y_2 \,\mathrm{d}x_3 \,\mathrm{d}x_2 \,\mathrm{d}x_1 \,,$$

$i \in \{1,2,3\}$. Using the Fubini theorem, we have

$$B_i = \int_{J(0)} \int_{J(0,y_2)} \int_0^\alpha [D_i g(s, z_2(s,y_2), z_3(s,y_3))]^2 \int_s^\alpha \int_{J(x_1)} \int_{J(x_1,x_2)} \mathrm{d}x_3 \,\mathrm{d}x_2 \,\mathrm{d}x_1 \,\mathrm{d}s \,\mathrm{d}y_3 \,\mathrm{d}y_2 \,.$$

Hence

$$B_i \le \frac{|\sigma|}{2\alpha} \int_0^\alpha \int_{J(0)} \int_{J(0,y_2)} [D_i g(s, z_2(s,y_2), z_3(s,y_3))]^2 (\alpha - s)^2 \,\mathrm{d}y_3 \,\mathrm{d}y_2 \,\mathrm{d}s \,,$$

where we have used the estimate

$$\int_{J(x_1)} \int_{J(x_1,x_2)} \mathrm{d}x_3 \,\mathrm{d}x_2 \le |\sigma| \Big( 1 - \frac{x_1}{\alpha} \Big)$$

on the area of the cross-section of $K$ and the plane $x_1 = const$. Now using the change of variables $z_3 = z_3(s,y_3)$ and $z_2 = z_2(s,y_2)$ gives

$$\begin{aligned} &\int_{J(0)} \int_{J(0,y_2)} [D_i g(s, z_2(s,y_2), z_3(s,y_3))]^2 (\alpha - s)^2 \,\mathrm{d}y_3 \,\mathrm{d}y_2 \\ =\ & \alpha^2 \int_{J(s)} \int_{J(s,z_2)} [D_i g(s, z_2, z_3)]^2 \,\mathrm{d}z_3 \,\mathrm{d}z_2 \end{aligned}$$

and thus

$$B_i \le \frac{|\sigma|\alpha}{2} \int_K [D_i g(\mathbf{x})]^2 \,\mathrm{d}\mathbf{x} \,,$$

which finally yields, noticing that $\alpha^2 + (\beta - y_2)^2 + (\gamma - y_3)^2 = |\mathbf{a} - \mathbf{y}|^2 \le \mathrm{diam}(K)^2$,

$$B \le \frac{|\sigma|}{2} \mathrm{diam}(K)^2 \int_K |\nabla g(\mathbf{x})|^2 \,\mathrm{d}\mathbf{x} \,. \tag{2.24}$$

Now combining (2.23) and (2.24) leads to the assertion of the lemma for $d = 3$. □

## 2.5 Discrete Friedrichs inequality

We prove in this section the discrete Friedrichs inequality, using the results of the previous sections. We first give several auxiliary lemmas.

**Lemma 2.5.1.** *Let $d = 2$. Then*

$$|I(g)|_{1,\mathcal{T},*}^2 \le \frac{C_d}{\kappa_{\mathcal{T}}^2} |g|_{1,\mathcal{T}}^2 \qquad \forall g \in W(\mathcal{T}_h)\,,$$

*where $C_d$ is given by (2.26) below.*

Proof:
Let $K \in \mathcal{T}_h$ and $\sigma_D, \sigma_E \in \mathcal{E}_K$. We define $g_K$ by (2.18) and deduce from the inequality $(a-b)^2 \le 2a^2 + 2b^2$ and from (2.20) that

$$(g_E - g_D)^2 \le 2(g_E - g_K)^2 + 2(g_D - g_K)^2 \le 4c_d \frac{\mathrm{diam}(K)^2}{|K|} \int_K |\nabla g(\mathbf{x})|^2 \,\mathrm{d}\mathbf{x}\,. \tag{2.25}$$

Using this, the definition of $|\cdot|_{1,\mathcal{T},*}$, $|\sigma_{D,E}| \le 2/3\,\mathrm{diam}(K)$, (2.9) and (2.8), the fact that each $K \in \mathcal{T}_h$ contains exactly three dual edges, and Assumption *(A)*, we have

$$\begin{aligned}
|I(g)|_{1,\mathcal{T},*}^2 &= \sum_{\sigma_{D,E} \in \mathcal{F}_h^{\mathrm{int}}} \frac{|\sigma_{D,E}|}{v_{D,E}} (g_E - g_D)^2 \\
&\le 4c_d \sum_{K \in \mathcal{T}_h} \sum_{\sigma_{D,E} \in \mathcal{F}_h^{\mathrm{int}},\, \sigma_{D,E} \subset K} \frac{|\sigma_{D,E}|^2}{v_{D,E}|\sigma_{D,E}|} \frac{\mathrm{diam}(K)^2}{|K|} \int_K |\nabla g(\mathbf{x})|^2 \,\mathrm{d}\mathbf{x} \\
&\le 8c_d \sum_{K \in \mathcal{T}_h} \Big[\frac{\mathrm{diam}(K)^2}{|K|}\Big]^2 \int_K |\nabla g(\mathbf{x})|^2 \,\mathrm{d}\mathbf{x} \le \frac{8c_d}{\kappa_{\mathcal{T}}^2} \sum_{K \in \mathcal{T}_h} \int_K |\nabla g(\mathbf{x})|^2 \,\mathrm{d}\mathbf{x}\,. \quad \square
\end{aligned}$$

**Lemma 2.5.2.** *There holds*

$$|I(g)|_{1,\mathcal{T},\dagger}^2 \le \frac{C_d}{\kappa_{\mathcal{T}}} |g|_{1,\mathcal{T}}^2 \qquad \forall g \in W(\mathcal{T}_h)\,,$$

*where*

$$C_d = 8c_d \ \text{ for } \ d = 2\,, \quad C_d = \frac{27}{4} c_d \ \text{ for } \ d = 3\,, \tag{2.26}$$

*and $c_d$ is given by (2.22).*

Proof:
Using the definition of $|\cdot|_{1,\mathcal{T},\dagger}$, (2.25), $|\sigma_{D,E}| \le C_d^* \mathrm{diam}(K_{D,E})^{d-1}$ with $C_d^* = 2/3$ if $d = 2$ and $C_d^* = 9/32$ if $d = 3$, the fact that each $K \in \mathcal{T}_h$ contains $\binom{d+1}{2} = \frac{(d+1)d}{2}$ dual sides, and Assumption *(A)*, we have

$$\begin{aligned}
|I(g)|_{1,\mathcal{T},\dagger}^2 &= \sum_{\sigma_{D,E} \in \mathcal{F}_h^{\mathrm{int}}} \frac{|\sigma_{D,E}|}{\mathrm{diam}(K_{D,E})} (g_E - g_D)^2 \\
&\le 4c_d \sum_{K \in \mathcal{T}_h} \sum_{\sigma_{D,E} \in \mathcal{F}_h^{\mathrm{int}},\, \sigma_{D,E} \subset K} \frac{|\sigma_{D,E}| \mathrm{diam}(K)}{|K|} \int_K |\nabla g(\mathbf{x})|^2 \,\mathrm{d}\mathbf{x} \\
&\le 2c_d(d+1)dC_d^* \sum_{K \in \mathcal{T}_h} \frac{\mathrm{diam}(K)^d}{|K|} \int_K |\nabla g(\mathbf{x})|^2 \,\mathrm{d}\mathbf{x} \le \frac{C_d}{\kappa_{\mathcal{T}}} \sum_{K \in \mathcal{T}_h} \int_K |\nabla g(\mathbf{x})|^2 \,\mathrm{d}\mathbf{x}\,. \quad \square
\end{aligned}$$

**Lemma 2.5.3. (Interpolation estimate)** *There holds*

$$\|g - I(g)\|_{0,\Omega}^2 \leq c_d h^2 |g|_{1,\mathcal{T}}^2 \qquad \forall g \in W(\mathcal{T}_h)\,.$$

PROOF:
We have

$$\begin{aligned}\|g - I(g)\|_{0,\Omega}^2 &= \sum_{K\in\mathcal{T}_h}\sum_{\sigma_D\in\mathcal{E}_K}\int_{K\cap D}[g(\mathbf{x}) - g_D]^2\,\mathrm{d}\mathbf{x}\\ &\leq c_d\sum_{K\in\mathcal{T}_h}\sum_{\sigma_D\in\mathcal{E}_K}[\mathrm{diam}(K\cap D)]^2\int_{K\cap D}|\nabla g(\mathbf{x})|^2\,\mathrm{d}\mathbf{x}\\ &\leq c_d h^2\sum_{K\in\mathcal{T}_h}\int_K|\nabla g(\mathbf{x})|^2\,\mathrm{d}\mathbf{x}\,,\end{aligned}$$

using the estimate (2.21) for the simplex $K\cap D$ and $\mathrm{diam}(K\cap D)\leq h$. □

We state below the first of the two main results of this chapter.

**Theorem 2.5.4. (Discrete Friedrichs inequality)** *There holds*

$$\|g\|_{0,\Omega}^2 \leq C_F|g|_{1,\mathcal{T}}^2 \qquad \forall g\in W_0(\mathcal{T}_h)\,,\ \forall h>0$$

*with*

$$C_F = \frac{C_d}{\kappa_{\mathcal{T}}^2}|\Omega| + 2c_d h^2 \ \text{ for } d=2\,,\quad C_F = 2C_d\frac{C_{d,\mathcal{T}}}{\kappa_{\mathcal{T}}}\Big[\inf_{\mathbf{b}\in\mathbb{R}^d}\{\mathrm{diam}_{\mathbf{b}}(\Omega)\}\Big]^2 + 2c_d h^2 \ \text{ for } d=2,3\,,$$

*where $C_{d,\mathcal{T}}$ is given by (2.12) when Assumption (B) is satisfied and by (2.15) in the general case, $c_d$ is given by (2.22), and $C_d$ is given by (2.26).*

PROOF:
One has

$$\|g\|_{0,\Omega}^2 \leq 2\|g - I(g)\|_{0,\Omega}^2 + 2\|I(g)\|_{0,\Omega}^2\,.$$

The error $\|g - I(g)\|_{0,\Omega}^2$ of the approximation follows from Lemma 2.5.3. Note that $I(g)\in Y_0(\mathcal{D}_h)$ and hence the discrete Friedrichs inequality for piecewise constant functions given by Theorem 2.3.1 together with Lemma 2.5.1 yield

$$\|I(g)\|_{0,\Omega}^2 \leq \frac{C_d}{2\kappa_{\mathcal{T}}^2}|\Omega||g|_{1,\mathcal{T}}^2$$

for the case where $d=2$. Similarly, using the discrete Friedrichs inequality for piecewise constant functions given by Theorem 2.3.5 together with Lemma 2.5.2, one has

$$\|I(g)\|_{0,\Omega}^2 \leq C_d\frac{C_{d,\mathcal{T}}}{\kappa_{\mathcal{T}}}[\mathrm{diam}_{\mathbf{b}}(\Omega)]^2|g|_{1,\mathcal{T}}^2$$

for an arbitrary vector $\mathbf{b}\in\mathbb{R}^d$ for the case where $d=2,3$. □

**Remark 2.5.5. (Dependence of $C_F$ on $\Omega$)** *We have $h^2\leq|\Omega|/\kappa_{\mathcal{T}}$ by Assumption (A) and $h\leq\theta_{\mathcal{T}}\mathrm{diam}_{\mathbf{b}}(\Omega)$ by the consequence (2.5) of Assumption (A). Hence the constant in the discrete Friedrichs inequality only depends on the area of $\Omega$ if $d=2$ and on the square of the infimum of the diameters of $\Omega$ in one direction if $d=2,3$. This dependence is optimal: [91, Theorem 1.1] gives the same dependence for the Friedrichs inequality and $H_0^1(\Omega)\subset W_0(\mathcal{T}_h)$.*

**Remark 2.5.6. (Dependence of $C_F$ on the shape regularity parameter)** *One can see that $C_F$ depends on $1/\kappa_{\mathcal{T}}^2$ if $d = 2$ and when it is expressed using $|\Omega|$. We are able to establish the same result also when $C_F$ is expressed using $\inf_{\mathbf{b}\in\mathbb{R}^d} \operatorname{diam}_{\mathbf{b}}(\Omega)$, but only when the meshes are not locally refined (when Assumption (B) is satisfied). Indeed, $C_F$ in this case depends on $C_{d,\mathcal{T}}/\kappa_{\mathcal{T}}$ and the constant $C_{d,\mathcal{T}}$ given by (2.12) is of the form $[2^d(d-1)\zeta_{\mathcal{T}}^d(2C+1)]/\kappa_{\mathcal{T}}$; this follows by replacing the inequality (2.13) by $h \le C\operatorname{diam}_{\mathbf{b}}(\Omega)$ for some suitable constant $C$. Example 2.6.3 below shows that this dependence is optimal. However, in the case where the meshes are only shape-regular, we were only able to establish (2.15).*

**Remark 2.5.7. (Discrete Friedrichs inequality for domains only bounded in one direction)** *We see that the constant $C_F$ only depends on the infimum of the diameters of $\Omega$ in one direction. Thus the discrete Friedrichs inequality may be extended onto domains only bounded in one direction, as it is the case for the Friedrichs inequality (cf. [91, Remark 1.1]).*

**Remark 2.5.8. (Discrete Friedrichs inequality for functions only fixed to zero on a particular part of the boundary)** *Let $\Gamma \subset \partial\Omega$ (given by a set of boundary sides) be such that there exists a vector $\mathbf{b} \in \mathbb{R}^d$ such that the first intersection of $\mathcal{B}_{\mathbf{x}}$ and $\partial\Omega$ lies in $\Gamma$ for all $\mathbf{x} \in \Omega$, where $\mathcal{B}_{\mathbf{x}}$ is a straight semi-line defined by the origin $\mathbf{x}$ and the vector $\mathbf{b}$. We notice that the discrete Friedrichs inequality can be immediately extended onto functions only fixed to zero on $\Gamma$. This follows easily from the proof of Theorem 2.3.5 (the zero condition is only used on boundary sides lying in $\Gamma$). The dependence of $C_F$ on the shape regularity parameter is thus given by $C_{d,\mathcal{T}}/\kappa_{\mathcal{T}}$, cf. Remark 2.5.6. The constant $C_F$ in this case depends on the square of the infimum of $\operatorname{diam}_{\mathbf{b}}(\Omega)$ over suitable vectors $\mathbf{b}$ (compare with the general case treated in the next remark).*

**Remark 2.5.9. (Discrete Friedrichs inequality for functions only fixed to zero on a general part of the boundary)** *The discrete Friedrichs inequality can also be extended onto functions only fixed to zero on an arbitrary set of boundary sides, see Lemma 2.7.2 and Remark 2.7.3 below. Then, for convex domains, $C_F$ depends on the square of the diameter of $\Omega$; for nonconvex domains, the dependence of $C_F$ on $\Omega$ is more complicated. The dependence of $C_F$ on the shape regularity parameter again reveals given by $C_{d,\mathcal{T}}/\kappa_{\mathcal{T}}$.*

## 2.6 Discrete Friedrichs inequality for Crouzeix–Raviart finite elements

We show in this section how the proofs from the previous sections simplify for the case of Crouzeix–Raviart finite elements in two space dimensions. Let us consider the space $X(\mathcal{T}_h)$ introduced in Section 2.2. The basis of this space is spanned by the shape functions $\varphi_D$, $D \in \mathcal{D}_h$, such that $\varphi_D(Q_E) = \delta_{DE}$, $E \in \mathcal{D}_h$, $\delta$ being the Kronecker delta.

**Lemma 2.6.1.** *Let $d = 2$. Then for all $c \in X(\mathcal{T}_h)$,*

$$\|c\|_{0,\Omega} = \|I(c)\|_{0,\Omega}\,.$$

Proof:

Let us write $c = \sum_{D\in\mathcal{D}_h} c_D\varphi_D$. Using that the quadrature formula $\int_K \psi\,\mathrm{d}\mathbf{x} \approx \frac{1}{3}|K| \sum_{\sigma_D\in\mathcal{E}_K} \psi(Q_D)$ is exact for quadratic functions on triangles and (2.8), we have

$$\int_\Omega c^2(\mathbf{x})\,\mathrm{d}\mathbf{x} = \sum_{K\in\mathcal{T}_h} \int_K c^2(\mathbf{x})\,\mathrm{d}\mathbf{x} = \sum_{K\in\mathcal{T}_h} \frac{1}{3}|K| \sum_{\sigma_D\in\mathcal{E}_K} c^2(Q_D) = \sum_{D\in\mathcal{D}_h} c_D^2|D|\,. \quad \square$$

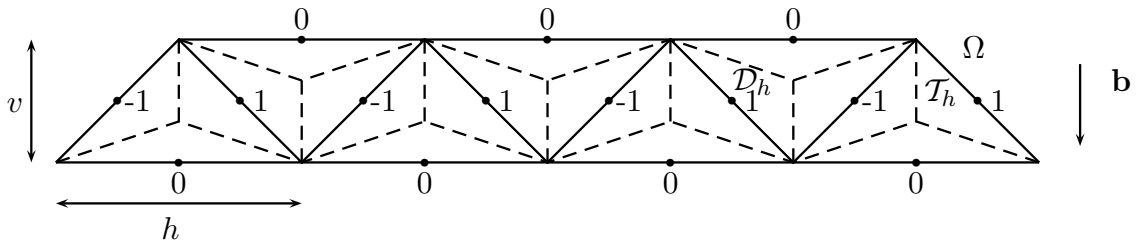


Figure 2.2: Domain $\Omega$, triangulation $\mathcal{T}_h$, dual mesh $\mathcal{D}_h$, and values of a function $c \in X(\mathcal{T}_h)$ for the optimality example

**Lemma 2.6.2. (Discrete Friedrichs inequality for Crouzeix–Raviart finite elements in two space dimensions)** *Let $d = 2$. Then*

$$\|c\|_{0,\Omega}^2 \le C_F |c|_{1,\mathcal{T}}^2 \qquad \forall c \in X_0(\mathcal{T}_h)\,, \forall h > 0\,,$$

*where*

$$C_F = \frac{1}{4\kappa_{\mathcal{T}}^2}|\Omega| \;\; or \;\; C_F = \frac{C_{d,\mathcal{T}}}{2\kappa_{\mathcal{T}}}\Big[\inf_{\mathbf{b}\in\mathbb{R}^d}\{\mathrm{diam}_{\mathbf{b}}(\Omega)\}\Big]^2.$$

Proof:
Let $c \in X_0(\mathcal{T}_h)$, $c = \sum_{D\in\mathcal{D}_h} c_D\varphi_D$. Note that by the definition of $X_0(\mathcal{T}_h)$, $c_D = 0$ for all $D \in \mathcal{D}_h^{\mathrm{ext}}$. Using respectively Lemma 2.6.1 and Theorem 2.3.1 or Theorem 2.3.5, we get

$$\|c\|_{0,\Omega}^2 \le \frac{|\Omega|}{2}|I(c)|_{1,\mathcal{T},*}^2\,, \quad \|c\|_{0,\Omega}^2 \le C_{d,\mathcal{T}}[\mathrm{diam}_{\mathbf{b}}(\Omega)]^2|I(c)|_{1,\mathcal{T},\dagger}^2$$

for an arbitrary vector $\mathbf{b} \in \mathbb{R}^2$. Finally, we deduce that

$$\begin{aligned}
|I(c)|_{1,\mathcal{T},*}^2 &= \sum_{\sigma_{D,E}\in\mathcal{F}_h^{\mathrm{int}}} \frac{|\sigma_{D,E}|^2}{v_{D,E}|\sigma_{D,E}|}\Big(\nabla c|_{K_{D,E}}\cdot(Q_E - Q_D)\Big)^2 \\
&\le \frac{2}{3}\sum_{\sigma_{D,E}\in\mathcal{F}_h^{\mathrm{int}}} \frac{\mathrm{diam}(K_{D,E})^2}{|K_{D,E}|}\Big|\nabla c|_{K_{D,E}}\Big|^2 d_{D,E}^2 \\
&\le \frac{1}{2\kappa_{\mathcal{T}}^2}\sum_{K\in\mathcal{T}_h}\Big|\nabla c|_K\Big|^2|K| = \frac{1}{2\kappa_{\mathcal{T}}^2}|c|_{1,\mathcal{T}}^2\,,
\end{aligned}$$

using (2.9) and (2.8), $|\sigma_{D,E}| \le 2/3\ \mathrm{diam}(K_{D,E})$, the fact that the gradient of $c$ is elementwise constant and that each $K \in \mathcal{T}_h$ contains exactly three dual edges, $d_{D,E} \le \mathrm{diam}(K_{D,E})/2$, and Assumption *(A)*. Similarly, $|I(c)|_{1,\mathcal{T},\dagger}^2 \le 1/(2\kappa_{\mathcal{T}})\,|c|_{1,\mathcal{T}}^2$. □

**Example 2.6.3. (Optimality of the dependence of $C_F$ on the shape regularity parameter)** *Let us consider a domain $\Omega$, its triangulation $\mathcal{T}_h$, a vector $\mathbf{b}$, and a function $c \in X(\mathcal{T}_h)$ given by the values $0, 1, -1$ as depicted in Figure 2.2. Using Lemma 2.6.1, we immediately have*

$$\|c\|_{0,\Omega}^2 = \sum_{K\in\mathcal{T}_h}\frac{1}{3}|K|(0+1+1) = \frac{2}{3}|\Omega|\,.$$

*On each $K \in \mathcal{T}_h$, $|\nabla c|_K| = 4/h$, hence $|c|_{1,\mathcal{T}}^2 = 16/h^2\,|\Omega|$. Using Remark 2.5.8, the discrete Friedrichs inequality given by Lemma 2.6.2 holds true. The term occurring on its right hand*

*side, independent of the shape regularity parameter, is* $1/2[\mathrm{diam}_{\mathbf{b}}(\Omega)]^2|c|_{1,\mathcal{T}}^2 = 8v^2/h^2\,|\Omega|$. *This term can be arbitrarily smaller than* $\|c\|_{0,\Omega}^2$, *letting* $h \to +\infty$ *or* $v \to 0$. *Next,* $\kappa_{\mathcal{T}} = v/(2h)$. *Note that* $\mathcal{T}_h$ *satisfies Assumption (B) and hence* $C_{d,\mathcal{T}} \approx 1/\kappa_{\mathcal{T}}$. *In fact, by a simple estimation of the term A from Lemma 2.3.3, one has* $C_{d,\mathcal{T}} = 1/\kappa_{\mathcal{T}}$ *in this case and thus* $C_{d,\mathcal{T}}/\kappa_{\mathcal{T}} = 1/\kappa_{\mathcal{T}}^2 = 4h^2/v^2$. *One immediately sees that the multiplication by this term is necessary.*

**Corollary 2.6.4. (Discrete Friedrichs inequality for Crouzeix–Raviart finite elements on equilateral triangles)** *Let* $d = 2$ *and let* $\mathcal{T}_h$ *consist of equilateral triangles. Then*

$$\|c\|_{0,\Omega}^2 \le C_F |c|_{1,\mathcal{T}}^2 \qquad \forall c \in X_0(\mathcal{T}_h)\,,\ \forall h > 0\,,$$

*where*

$$C_F = \frac{|\Omega|}{2} \ \text{ or } \ C_F = \Big[\inf_{\mathbf{b}\in\mathbb{R}^d}\{\mathrm{diam}_{\mathbf{b}}(\Omega)\} + 2h\Big]^2.$$

Proof:
Let $c$ be as in the previous lemma. For equilateral triangles, one has $d_{D,E} = v_{D,E}$ and thus the norms $|\cdot|_{1,\mathcal{T},*}$ and $|\cdot|_{1,\mathcal{T},\ddagger}$ coincide. By (2.9) and (2.8), $|\sigma_{D,E}|v_{D,E} = 2/3\,|K|$, $\cos^2(\alpha) + \cos^2(\alpha + \pi/3) + \cos^2(\alpha + 2\pi/3) = 3/2$, so that

$$\sum_{K\in\mathcal{T}_h}\sum_{\sigma_{D,E}\in\mathcal{F}_h^{\mathrm{int}},\,\sigma_{D,E}\subset K}\frac{|\sigma_{D,E}|}{d_{D,E}}\Big|\nabla c|_K\Big|^2 d_{D,E}^2\cos^2(\nabla c|_K, Q_E - Q_D) = \sum_{K\in\mathcal{T}_h}\Big|\nabla c|_K\Big|^2|K|\,.$$

Now using respectively Lemma 2.6.1 and Theorem 2.3.1 or Remark 2.3.2 yields the assertion. □

**Remark 2.6.5. ($C_F$ for Crouzeix–Raviart finite elements on equilateral triangles)** *Let* $d = 2$. *Then the constant in the Friedrichs inequality may be expressed as* $c_F = |\Omega|/2$ *or* $c_F = [\inf_{\mathbf{b}\in\mathbb{R}^d}\{\mathrm{diam}_{\mathbf{b}}(\Omega)\}]^2$, *cf. [91, Theorem 1.1]. Corollary 2.6.4 shows that for Crouzeix–Raviart finite elements and equilateral triangles, we are able to achieve the same result (up to h) also for the constant* $C_F$ *from the discrete Friedrichs inequality. We however remark that there exist sharper estimates in the continuous case, see e.g. [107].*

## 2.7 Discrete Poincaré inequality for piecewise constant functions

As in the case of the discrete Friedrichs inequality, we start with the discrete Poincaré inequality for piecewise constant functions. [61, Lemma 10.2] states the discrete Poincaré inequality for piecewise constant functions on meshes satisfying the orthogonality property. We present in this section an analogy of this lemma for the mesh $\mathcal{D}_h$, where the orthogonality property is not necessarily satisfied.

**Lemma 2.7.1.** *Let* $\omega$ *be an open convex subset of* $\Omega$, $\omega \neq 0$, *and let*

$$m_\omega(c) := \frac{1}{|\omega|}\int_\omega c(\mathbf{x})\,\mathrm{d}\mathbf{x}\,.$$

*Then for all* $c \in Y(\mathcal{D}_h)$,

$$\|c - m_\omega(c)\|_{0,\omega}^2 \le \frac{|B_\Omega|}{|\omega|}C_{d,\mathcal{T}}[\mathrm{diam}(\Omega)]^2|c|_{1,\mathcal{T},\dagger}^2\,,$$

*where* $B_\Omega$ *is the ball of* $\mathbb{R}^d$ *with center* 0 *and radius* $\mathrm{diam}(\Omega)$ *and* $C_{d,\mathcal{T}}$ *is given by (2.12) when Assumption (B) is satisfied and by (2.15) in the general case.*

The proof of this lemma follows the proof of the first step of [61, Lemma 10.2], using the techniques introduced in Section 2.3 for meshes where the orthogonality property is not satisfied.

**Lemma 2.7.2.** *Let $\omega$ be a polygonal open convex subset of $\Omega$ and let $I \subset \partial\omega$ with $|I| > 0$. Let $E \in \mathcal{D}_h$ be such that $I \cap E$ is not an empty set and not just a point (such dual element always exists). Then for all $c \in Y(\mathcal{D}_h)$ with $c_E = 0$,*

$$\|c\|_{0,\omega}^2 \leq C_{d,\mathcal{T}}[\mathrm{diam}(\Omega)]^2 |c|_{1,\mathcal{T},\dagger}^2 ,$$

*where $C_{d,\mathcal{T}}$ is given by (2.12) when Assumption (B) is satisfied and by (2.15) in the general case.*

Proof:

The proof is similar to that of Theorem 2.3.5. There exist a set of vectors $\mathbf{b}_i$ and of nonempty nonoverlapping subsets $\omega_i$ of $\omega$, $i = 1, \ldots, M$ (M may be equal to $+\infty$) with the following properties: (i) $\mathbf{b}_i$ is such that $\mathcal{C}_{\mathbf{b}_i} \cap \omega \neq \emptyset$, where $\mathcal{C}_{\mathbf{b}_i}$ is the cylinder whose basis is $I \cap E$ and generator vector is $-\mathbf{b}_i$; (ii) $\omega_i = \mathcal{C}_{\mathbf{b}_i} \cap \omega \setminus \cup_{j=1}^{i-1} \omega_j$; (iii) $\cup_{i=1}^{M} \omega_i = \omega$. Note that the fact that $\omega$ is convex is important. For all $\mathbf{x} \in \omega_i$, we set $\mathcal{B}_{\mathbf{x}}^i$ as the straight semi-line defined by the origin $\mathbf{x}$ and the vector $\mathbf{b}_i$. Let $\mathbf{y}(\mathbf{x}) = I \cap E \cap \mathcal{B}_{\mathbf{x}}^i$. Let the function $\chi_\sigma(\mathbf{x})$ be given by (2.16) for each $\sigma \in \mathcal{F}_h^{\mathrm{int}}$. Let $D \in \mathcal{D}_h$, $D \cap \omega_i \neq \emptyset$, be fixed. We then have (2.17) for a.e. $\mathbf{x} \in D \cap \omega_i$, as in Theorem 2.3.5. Integrating (2.17) over $D \cap \omega_i$, summing over all $D \in \mathcal{D}_h$ such that $D \cap \omega_i \neq \emptyset$, and using Lemma 2.3.3 when Assumption *(B)* is satisfied and Lemma 2.3.4 in the general case yields

$$\sum_{D \in \mathcal{D}_h} |c_D|^2 |D \cap \omega_i| \leq C_{d,\mathcal{T}} \mathrm{diam}(\Omega) \sum_{\sigma_{D,E} \in \mathcal{F}_h^{\mathrm{int}}} \frac{(c_E - c_D)^2}{\mathrm{diam}(K_{D,E})} \int_{\omega_i} \chi_{\sigma_{D,E}}(\mathbf{x}) \, \mathrm{d}\mathbf{x} .$$

Using the inequality

$$\int_{\omega_i} \chi_{\sigma_{D,E}}(\mathbf{x}) \, \mathrm{d}\mathbf{x} \leq |\sigma_{D,E} \cap \omega_i| \, \mathrm{diam}(\omega) ,$$

$\mathrm{diam}(\omega) \leq \mathrm{diam}(\Omega)$, and summing over all $i$ concludes the proof. □

**Remark 2.7.3.** *Let $\Omega$ be convex. Then taking $\omega = \Omega$ in Lemma 2.7.2, we have an extension of Theorem 2.3.5 onto functions from $Y(\mathcal{D}_h)$ that vanish on only one boundary dual element.*

**Remark 2.7.4.** *Lemma 2.7.2 is an alternative to the second step of the proof of [61, Lemma 10.2].*

**Theorem 2.7.5. (Discrete Poincaré inequality for piecewise constant functions)** *Let*

$$m_\Omega(c) := \frac{1}{|\Omega|} \int_\Omega c(\mathbf{x}) \, \mathrm{d}\mathbf{x} .$$

*Then for all $c \in Y(\mathcal{D}_h)$,*

$$\|c - m_\Omega(c)\|_{0,\Omega}^2 \leq C_\Omega C_{d,\mathcal{T}} [\mathrm{diam}(\Omega)]^2 |c|_{1,\mathcal{T},\dagger}^2 ,$$

*where*

$$C_\Omega = \frac{|B_\Omega|}{|\Omega|} \tag{2.27}$$

*when $\Omega$ is convex and*

$$C_\Omega = 2\sum_{i=1}^{n} \frac{|B_\Omega|}{|\Omega_i|} + 16(n-1)^2 \frac{|\Omega|}{|\Omega_i|_{\min}} \Big( \frac{|B_\Omega|}{|\Omega_i|_{\min}} + 1 \Big) \tag{2.28}$$

*when $\Omega$ is not convex but there exists a finite number of disjoint open convex polygonal sets $\Omega_i$ such that $\overline{\Omega} = \cup_{i=1}^n \overline{\Omega_i}$. Here, $|\Omega_i|_{\min} = \min_{i=1,\ldots,n}\{|\Omega_i|\}$, $B_\Omega$ is the ball of $\mathbb{R}^d$ with center $0$ and radius $\operatorname{diam}(\Omega)$, and $C_{d,\mathcal{T}}$ is given by (2.12) when Assumption (B) is satisfied and by (2.15) in the general case.*

Proof:

When $\Omega$ is convex, the assertion of this theorem coincides with that of Lemma 2.7.1 for $\omega = \Omega$. When $\Omega$ is not convex, we have Lemmas 2.7.1 and 2.7.2 for each $\Omega_i$. Then the third step of the proof of [61, Lemma 10.2] yields the assertion of the theorem. □

**Remark 2.7.6.** *One has*

$$\|c\|_{0,\Omega}^2 \le 2\|c - m_\Omega(c)\|_{0,\Omega}^2 + 2\|m_\Omega(c)\|_{0,\Omega}^2 .$$

*Hence Theorem 2.7.5 implies the discrete Poincaré inequality for piecewise constant functions in the more common form*

$$\|c\|_{0,\Omega}^2 \le 2C_\Omega C_{d,\mathcal{T}} [\operatorname{diam}(\Omega)]^2 |c|_{1,\mathcal{T},\dagger}^2 + \frac{2}{|\Omega|}\Big(\int_\Omega c(\mathbf{x})\,\mathrm{d}\mathbf{x}\Big)^2 \qquad \forall c \in Y(\mathcal{D}_h)\,,\ \forall h > 0\,.$$

## 2.8 Discrete Poincaré inequality

We state below the second of the two main results of this chapter.

**Theorem 2.8.1. (Discrete Poincaré inequality)** *There holds*

$$\|g\|_{0,\Omega}^2 \le C_P |g|_{1,\mathcal{T}}^2 + \frac{4}{|\Omega|}\Big(\int_\Omega g(\mathbf{x})\,\mathrm{d}\mathbf{x}\Big)^2 \qquad \forall g \in W(\mathcal{T}_h)\,,\ \forall h > 0$$

*with*

$$C_P = 4C_d C_\Omega \frac{C_{d,\mathcal{T}}}{\kappa_\mathcal{T}} [\operatorname{diam}(\Omega)]^2 + 8c_d h^2\,,$$

*where $C_\Omega$ is given by (2.27) when $\Omega$ is convex and by (2.28) otherwise, $C_{d,\mathcal{T}}$ is given by (2.12) when Assumption (B) is satisfied and by (2.15) in the general case, $c_d$ is given by (2.22), and $C_d$ is given by (2.26).*

Proof:

One has

$$\|g\|_{0,\Omega}^2 \le 4\|g - I(g)\|_{0,\Omega}^2 + 4\|I(g) - m_\Omega[I(g)]\|_{0,\Omega}^2 + 4\|m_\Omega[I(g)] - m_\Omega(g)\|_{0,\Omega}^2 + 4\|m_\Omega(g)\|_{0,\Omega}^2\,,$$

where $m_\Omega(f) = 1/|\Omega| \int_\Omega f(\mathbf{x})\,\mathrm{d}\mathbf{x}$. The discrete Poincaré inequality for piecewise constant functions given by Theorem 2.7.5 and Lemma 2.5.2 imply

$$\|I(g) - m_\Omega[I(g)]\|_{0,\Omega}^2 \le C_d C_\Omega \frac{C_{d,\mathcal{T}}}{\kappa_\mathcal{T}} [\operatorname{diam}(\Omega)]^2 |g|_{1,\mathcal{T}}^2\,.$$

We have

$$\|m_\Omega[I(g)] - m_\Omega(g)\|_{0,\Omega}^2 \le \|g - I(g)\|_{0,\Omega}^2$$

by the Cauchy–Schwarz inequality. Finally, the error $\|g - I(g)\|_{0,\Omega}^2$ of the approximation follows from Lemma 2.5.3. □

**Remark 2.8.2. (Dependence of $C_P$ on $\Omega$)** *Let $\Omega$ be a cube. We then have $h \leq \operatorname{diam}(\Omega)$ and $C_\Omega \leq \pi\sqrt{3}/2$ and hence the constant in the discrete Poincaré inequality in this case only depends on the square of the diameter of $\Omega$. This dependence is optimal: [91, Theorem 1.3] gives the same dependence for the Poincaré inequality and $H^1(\Omega) \subset W(\mathcal{T}_h)$.*

**Remark 2.8.3. (Dependence of $C_P$ on the shape regularity parameter)** *Our results indicate that the dependence of $C_P$ on the shape regularity parameter is given by $C_{d,\mathcal{T}}/\kappa_{\mathcal{T}}$, cf. Remark 2.5.6.*

# Chapter 3

# Equivalence between lowest-order mixed finite element and multi-point finite volume methods

We consider in this chapter the lowest-order Raviart–Thomas mixed finite element method for elliptic diffusion problems on simplicial meshes in two or three space dimensions. This method produces saddle-point problems for scalar and flux unknowns. We show how to easily eliminate the flux unknowns, which implies equivalence between this method and a particular multi-point finite volume scheme, without any approximate numerical integration. The matrix of the final linear system is sparse, positive definite for a large class of problems, but in general nonsymmetric. We next show that these ideas also apply to mixed and upwind-mixed finite element discretizations of nonlinear parabolic convection–reaction–diffusion problems. We present a set of numerical experiments confirming important computational savings while using the equivalent finite volume form of the lowest-order mixed finite element method and compare it to a finite volume and combined finite volume–finite element schemes.

## 3.1 Introduction

Let us consider the elliptic problem

$$\mathbf{u} = -\mathbf{S}\nabla p \quad \text{in } \Omega\,, \tag{3.1a}$$
$$\nabla\cdot\mathbf{u} = q \quad \text{in } \Omega\,, \tag{3.1b}$$
$$p = p_D \quad \text{on } \Gamma_D\,, \quad \mathbf{u}\cdot\mathbf{n} = u_N \quad \text{on } \Gamma_N\,, \tag{3.1c}$$

where $\Omega\subset\mathbb{R}^d$, $d=2,3$, is a polygonal domain (open, bounded, and connected set), $\mathbf{S}$ is a bounded, symmetric (this is however not necessary), and uniformly positive definite tensor, $p_D\in H^{\frac12}(\Gamma_D)$, $u_N\in H^{-\frac12}(\Gamma_N)$, $q\in L_2(\Omega)$, $\Gamma_D\cap\Gamma_N=\emptyset$, $\overline{\Gamma_D}\cup\overline{\Gamma_N}=\partial\Omega$, and $|\Gamma_D|\neq 0$, where $|\Gamma_D|$ is the measure of the set $\Gamma_D$.

Let $\mathcal{T}_h$ be a simplicial triangulation of $\Omega$ (consisting of triangles if $d=2$ and of tetrahedra if $d=3$) such that each boundary side (edge if $d=2$, face if $d=3$) lies entirely either in $\Gamma_D$ or in $\Gamma_N$. Let us denote by $\mathcal{E}_h$ the set of all non-Neumann sides of $\mathcal{T}_h$. Let finally $\tilde{\mathbf{u}}\in\mathbf{H}(\mathrm{div},\Omega)$ be such that $\tilde{\mathbf{u}}\cdot\mathbf{n}=u_N$ on $\Gamma_N$ in the appropriate sense. The approximation of the problem (3.1a)–(3.1c) by means of the mixed finite element method consists in finding $\mathbf{u}_h=\mathbf{u}_{0,h}+\tilde{\mathbf{u}}$, $\mathbf{u}_{0,h}\in\mathbf{V}(\mathcal{E}_h)$, and $p_h\in\Phi(\mathcal{T}_h)$ such that (see [33, 108])

$$(\mathbf{S}^{-1}\mathbf{u}_{0,h},\mathbf{v}_h)_\Omega - (\nabla\cdot\mathbf{v}_h,p_h)_\Omega = -\langle\mathbf{v}_h\cdot\mathbf{n},p_D\rangle_{\partial\Omega} - (\mathbf{S}^{-1}\tilde{\mathbf{u}},\mathbf{v}_h)_\Omega \qquad \forall\,\mathbf{v}_h\in\mathbf{V}(\mathcal{E}_h)\,, \tag{3.2a}$$
$$-(\nabla\cdot\mathbf{u}_{0,h},\phi_h)_\Omega = -(q,\phi_h)_\Omega + (\nabla\cdot\tilde{\mathbf{u}},\phi_h)_\Omega \qquad \forall\phi_h\in\Phi(\mathcal{T}_h)\,, \tag{3.2b}$$

where $(\mathbf{u}_h,\mathbf{v}_h)_\Omega=\int_\Omega\mathbf{u}_h\cdot\mathbf{v}_h\,\mathrm{d}\mathbf{x}$, $\langle\mathbf{v}_h\cdot\mathbf{n},\varphi\rangle_{\partial\Omega}=\int_{\partial\Omega}\mathbf{v}_h\cdot\mathbf{n}\,\varphi\,\mathrm{d}\gamma(\mathbf{x})$, and $\mathbf{V}(\mathcal{E}_h)$ and $\Phi(\mathcal{T}_h)$ are suitable finite-dimensional spaces defined on $\mathcal{T}_h$. The associated matrix problem is saddle-point and can be written in the form

$$\begin{pmatrix}\mathbb{A} & \mathbb{B}^t\\ \mathbb{B} & 0\end{pmatrix}\begin{pmatrix}U\\P\end{pmatrix}=\begin{pmatrix}F\\G\end{pmatrix}. \tag{3.3}$$

In the lowest-order Raviart–Thomas method [105] and its three-dimensional Nédélec variant [92] the scalar unknowns $P$ are associated with the elements of $\mathcal{T}_h$ and $U$ are the fluxes through the sides of $\mathcal{E}_h$. Using the hybridization technique steaming from the ideas of [69], one can decrease the number of unknowns to the Lagrange multipliers associated with non-Dirichlet sides and obtain a symmetric and positive definite matrix, cf. [15, 33]. In fact, the hybridization is very close to the piecewise linear nonconforming finite element method, cf. [38] or Lemma 1.8.1 or a more detailed study in Section 4.6 of this thesis. The fluxes can then be recovered using the technique first proposed in [88]. Especially in three space dimensions, there are much less elements than sides, and hence the long-standing interest in reducing the unknowns to only the scalar unknowns $P$. This is indeed possible, using approximate numerical integration, see [110] for rectangles and $\mathbf{S}$ diagonal and [8, 18] for rectangles and triangles and $\mathbf{S}$ diagonal and for a limited class of tetrahedra and $\mathbf{S}=Id$. Using the expanded mixed finite element method, these techniques can be extended also onto full-matrix diffusion tensors $\mathbf{S}$ for rectangular parallelepipeds [13] and for "smooth" coefficients and meshes consisting of triangles, quadrilaterals, and hexahedra [12]. To our knowledge, the only technique for reducing the number of unknowns to the number of elements without any numerical integration is proposed and studied in [37, 121, 122]. In two space dimensions, it works on unstructured triangular meshes, but in three space dimensions, it only works on a limited class of structured tetrahedral meshes. One associates here to each element a new unknown.

We present in Section 3.2 of this chapter a new method which permits to exactly and efficiently reduce the system (3.3) to a system for the (original) scalar unknowns $P$ only. We show that, under a condition of the invertibility of some local matrices associated with vertices and only depending on the mesh and on the diffusion tensor, one can express the flux through a given side using the scalar unknowns, sources, and possibly boundary conditions associated with the elements sharing one of the vertices of this side. Recall that expressing the flux through a given side using the scalar unknowns in neighboring elements is the principle of multi-point finite volume schemes, cf. [1, 7, 44, 58, 65]. Hence the lowest-order Raviart–Thomas mixed finite element method is in the given case equivalent to a particular multi-point finite volume scheme, and this without any numerical integration. We call this scheme a *condensed mixed finite element scheme*. We then discuss the modifications of the proposed scheme if the local matrices are not invertible, consisting namely in considering different sets of elements for the expression of the flux through a given side.

The condensation of the lowest-order Raviart–Thomas method leads to linear systems with sparse but in general nonsymmetric matrices, as we show in Section 3.3. The system matrix is positive definite under a condition on the mesh and on the tensor $\mathbf{S}$, which can be reduced to a shape criterion allowing for fairly general elements if $\mathbf{S}$ is piecewise constant and scalar. For example, one can deform a square $(0,1)\times(0,1)$, discretized by regular right-angled triangles, until the triangle elements contain angles greater than 130 degrees, see Example 3.3.8 below. The fulfillment of this condition in particular implies the invertibility of the local matrices from the previous paragraph. Finally, in Section 3.4, we apply the proposed condensation to mixed (cf. [14, 52]) and upwind-mixed (cf. [46, 47, 77]) finite element discretizations of nonlinear parabolic convection–reaction–diffusion problems.

The essential idea of what we propose can be formulated as follows: given a second-order problem, first decompose it into scalar and flux unknowns and guarantee the fulfillment of the inf–sup (Babuška [16]–Brezzi [30]) condition. Then eliminate the added fluxes. One can in this way obtain the precision of the mixed finite element method for the price of the finite volume one. This is confirmed by numerical experiments carried out in Section 3.5. Especially for nonlinear parabolic convection–reaction–diffusion problems, one can reduce the CPU time of standard mixed solution approaches by a factor of 2 to 4. We refer to a more detailed discussion in Section 3.5.4. Finally, the proposed condensation can be easily implemented in a new self-standing code or in existing mixed finite element codes. Extension to higher-order schemes is an ongoing work.

## 3.2 The equivalence

We first define the spaces $\mathbf{V}(\mathcal{E}_h)$ and $\Phi(\mathcal{T}_h)$ in this section. We then establish the equivalence between the lowest-order mixed finite element and a particular multi-point finite volume method.

Let us consider simplices $K, L \in \mathcal{T}_h$ sharing an interior side $\sigma$. Let $V_K$ be the vertex of $K$ opposite to $\sigma$ and $V_L$ the vertex of $L$ opposite to $\sigma$. Then the RTN (Raviart–Thomas–Nédélec) basis function $\mathbf{v}_\sigma \in \mathbf{V}(\mathcal{E}_h)$ associated with the side $\sigma$ can be written in the form $\mathbf{v}_\sigma(\mathbf{x}) = \frac{1}{d|K|}(\mathbf{x} - V_K)$, $\mathbf{x} \in K$, $\mathbf{v}_\sigma(\mathbf{x}) = \frac{1}{d|L|}(V_L - \mathbf{x})$, $\mathbf{x} \in L$, $\mathbf{v}_\sigma(\mathbf{x}) = 0$ otherwise. We refer to Figure 3.1 for a schematic visualization of a RTN basis function in two space dimensions. We fix the orientation of $\mathbf{v}_\sigma$, i.e. the order of $K$ and $L$. For a Dirichlet boundary side $\sigma$, the support of $\mathbf{v}_\sigma$ only consists of $K \in \mathcal{T}_h$ such that $\sigma \in \mathcal{E}_K$, where $\mathcal{E}_K$ stands for the sides of the element $K$. A basis function $\phi_K \in \Phi(\mathcal{T}_h)$ associated with an element $K \in \mathcal{T}_h$ is equal to 1 on $K$ and to 0 otherwise.

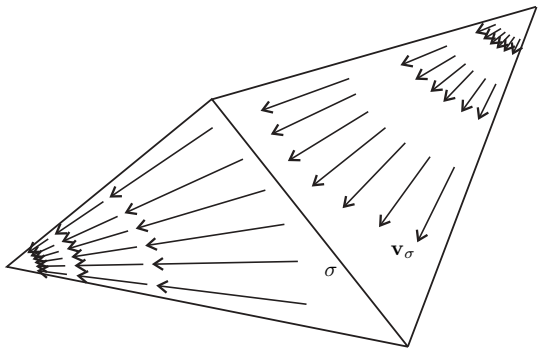


Figure 3.1: RTN basis function $\mathbf{v}_\sigma$ associated with the edge $\sigma$

Let us denote by $\mathcal{V}_h$ the set of all vertices and consider $V \in \mathcal{V}_h$. We call the set of all elements of $\mathcal{T}_h$ sharing this vertex a *cluster* associated with $V$ and denote it by $\mathcal{C}_V$. Let us denote by $\mathcal{E}_{\mathcal{C}_V}$ the set of all non-Neumann sides of $\mathcal{C}_V$, by $\mathcal{F}_{\mathcal{C}_V}$ the set of all non-Neumann sides sharing $V$, and by $\mathcal{G}_{\mathcal{C}_V}$ the set of other non-Neumann sides of $\mathcal{C}_V$. Let finally $\mathcal{C}_V^{\rm el}$ denote the set of elements from the cluster that contain exactly one side from $\mathcal{G}_{\mathcal{C}_V}$. We denote by $\delta_K$ the side from $\mathcal{E}_K \cap \mathcal{G}_{\mathcal{C}_V}$ for $K \in \mathcal{C}_V^{\rm el}$. We have $\mathcal{E}_{\mathcal{C}_V} = \mathcal{F}_{\mathcal{C}_V} \cup \mathcal{G}_{\mathcal{C}_V}$, $\mathcal{F}_{\mathcal{C}_V} \cap \mathcal{G}_{\mathcal{C}_V} = \emptyset$, and $|\mathcal{C}_V^{\rm el}| = |\mathcal{G}_{\mathcal{C}_V}|$, where we denote by $|A|$ the cardinality of a set $A$. An example of a cluster $\mathcal{C}_V$ lying in the interior of the domain $\Omega$ is given in Figure 3.2. In this case, $\mathcal{F}_{\mathcal{C}_V}$ are simply the sides sharing $V$, $\mathcal{G}_{\mathcal{C}_V}$ the other sides of $\mathcal{C}_V$, and $\mathcal{C}_V^{\rm el} = \mathcal{C}_V$. The situation is more delicate near the boundary, especially if there are Neumann boundary conditions, cf. Figure 3.3 below. This is also the reason for the quite complex notation introduced. The basic principle of the condensation will however be clear from Figure 3.2. Finally, we are not interested in the particular and trivial cases where $\mathcal{F}_{\mathcal{C}_V} = \emptyset$ or $\mathcal{G}_{\mathcal{C}_V} = \emptyset$.

Our aim is to express $\mathbf{u}_{0,h}$ with the aid of $p_h$, or, equivalently, the fluxes $U$ with the aid of the scalar unknowns $P$. For this purpose, we consider the equations (3.2a) for the basis functions $\mathbf{v}_\gamma$, $\gamma \in \mathcal{F}_{\mathcal{C}_V}$. We remark that the support of all $\mathbf{v}_\gamma$, $\gamma \in \mathcal{F}_{\mathcal{C}_V}$, is included in $\mathcal{C}_V$ and that $\mathbf{u}_{0,h}|_{\mathcal{C}_V} = \sum_{\sigma \in \mathcal{E}_{\mathcal{C}_V}} U_\sigma \mathbf{v}_\sigma$. This yields, using also that $p_h|_K = P_K$,

$$\sum_{\sigma \in \mathcal{E}_{\mathcal{C}_V}} U_\sigma (\mathbf{v}_\sigma, \mathbf{S}^{-1}\mathbf{v}_\gamma)_{\mathcal{C}_V} - \sum_{K \in \mathcal{C}_V} P_K (\nabla \cdot \mathbf{v}_\gamma, 1)_K = -\langle \mathbf{v}_\gamma \cdot \mathbf{n}, p_D \rangle_{\partial\Omega} - (\mathbf{S}^{-1}\tilde{\mathbf{u}}, \mathbf{v}_\gamma)_{\mathcal{C}_V} \qquad \forall \gamma \in \mathcal{F}_{\mathcal{C}_V}\,, \tag{3.4}$$

i.e. $|\mathcal{F}_{\mathcal{C}_V}|$ equations for the $|\mathcal{E}_{\mathcal{C}_V}|$ unknown fluxes $U_\sigma$, $\sigma \in \mathcal{E}_{\mathcal{C}_V}$, where we consider the scalar unknowns $P_K$, $K \in \mathcal{C}_V$, as parameters. Note that in practice, $p_D|_\sigma \approx \langle p_D, 1\rangle_\sigma / |\sigma|$, $\sigma \subset \Gamma_D$, and $\tilde{\mathbf{u}} \approx \sum_{\sigma \subset \Gamma_N} \langle u_N, 1\rangle_\sigma \mathbf{v}_\sigma$, so that the above system is completely discrete. The remaining $|\mathcal{G}_{\mathcal{C}_V}|$ equations are given by (3.2b) for all $\phi_K$, $K \in \mathcal{C}_V^{\rm el}$,

$$-\sum_{\sigma \in \mathcal{E}_K, \sigma \notin \Gamma_N} U_\sigma (\nabla \cdot \mathbf{v}_\sigma, 1)_K = -(q,1)_K + (\nabla \cdot \tilde{\mathbf{u}}, 1)_K \qquad \forall K \in \mathcal{C}_V^{\rm el}\,. \tag{3.5}$$

The matrix problem associated with the set of equations (3.4)–(3.5) can be written in the form

$$\begin{pmatrix} \mathbb{A}_{1,V} & \mathbb{A}_{2,V} \\ \mathbb{B}_{1,V} & \mathbb{B}_{2,V} \end{pmatrix} \begin{pmatrix} U_V^{\mathcal{F}} \\ U_V^{\mathcal{G}} \end{pmatrix} = \begin{pmatrix} F_V - \mathbb{B}_V^t P_V \\ G_V \end{pmatrix}, \tag{3.6}$$

where $U_V^{\mathcal{F}} = \{U_\sigma\}_{\sigma \in \mathcal{F}_{\mathcal{C}_V}}$, $U_V^{\mathcal{G}} = \{U_\sigma\}_{\sigma \in \mathcal{G}_{\mathcal{C}_V}}$, and $P_V = \{P_K\}_{K \in \mathcal{C}_V}$.

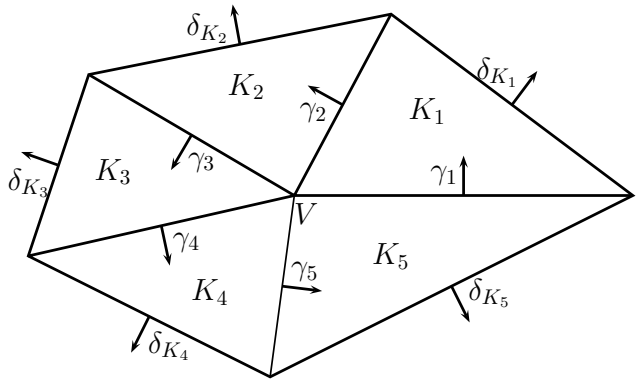


$$\begin{aligned}\mathcal{C}_V &= \{K_i\}_{i=1}^5\\ \mathcal{C}_V^{\mathrm{el}} &= \{K_i\}_{i=1}^5\\ \mathcal{F}_{\mathcal{C}_V} &= \{\gamma_i\}_{i=1}^5\\ \mathcal{G}_{\mathcal{C}_V} &= \{\delta_{K_i}\}_{i=1}^5\end{aligned}$$

Figure 3.2: Example of a cluster $\mathcal{C}_V$ in the interior of $\Omega$

We now notice that the matrix $\mathbb{B}_{2,V}$ is square, diagonal, and its entries are equal to $\pm 1$ (this follows from the fact that each $K \in \mathcal{C}_V^{\mathrm{el}}$ contains exactly one side from $\mathcal{G}_{\mathcal{C}_V}$ and using that $(\nabla \cdot \mathbf{v}_\sigma, 1)_K = \pm 1$ for $\sigma \in \mathcal{E}_K$). Hence we can eliminate the $U_V^{\mathcal{G}}$ unknowns and come to

$$\mathbb{M}_V U_V^{\mathcal{F}} = F_V - \mathbb{B}_V^t P_V - \mathbb{A}_{2,V}\mathbb{B}_{2,V}^{-1} G_V \tag{3.7}$$

for each vertex $V \in \mathcal{V}_h$. Let us call the matrix

$$\mathbb{M}_V := \mathbb{A}_{1,V} - \mathbb{A}_{2,V}\mathbb{B}_{2,V}^{-1}\mathbb{B}_{1,V} \tag{3.8}$$

a *local condensation matrix* associated with the vertex $V$. We now summarize the results in the following theorem:

**Theorem 3.2.1. (Equivalence between MFEM and a particular multi-point FVM)** *Let the matrices $\mathbb{M}_V$ given by (3.8) be invertible for all $V \in \mathcal{V}_h$. Then the lowest-order Raviart–Thomas mixed finite element method on simplicial meshes is equivalent to a multi-point finite volume scheme, where the flux through each side can be expressed using the scalar unknowns, sources, and possibly boundary conditions associated with the elements sharing one of the vertices of this side.*

**Remark 3.2.2. (Comparison with a classical multi-point FVM)** *In "classical" multi-point finite volume schemes, cf. [1, 7, 44, 58, 65], one attempts to express the flux through a given side only using the scalar unknowns associated with the neighboring elements. There are two essential differences between these classical multi-point finite volume schemes and a particular multi-point finite volume scheme—the mixed finite element method. First, in the mixed finite element method, not only the scalar unknowns, but also the sources and possibly boundary conditions associated with the neighboring elements are used to express the flux through a given side. Second, to obtain this expression, one has to solve a local linear problem. In this last feature, the condensed mixed finite element scheme is similar to the "multipoint flux-approximation" scheme proposed and tested in [1, 2].*

Let $V \in \mathcal{V}_h$. Let us define a mapping $\Psi_V : \mathbb{R}^{|\mathcal{F}_{\mathcal{C}_V}|} \to \mathbb{R}^{|\mathcal{E}_h|}$, extending a vector $U_V^{\mathcal{F}} = \{U_\sigma\}_{\sigma \in \mathcal{F}_{\mathcal{C}_V}}$ of values associated with the sides from $\mathcal{F}_{\mathcal{C}_V}$ to a vector of values associated with all non-Neumann sides $\mathcal{E}_h$ by

$$[\Psi_V(U_V^{\mathcal{F}})]_\sigma := \begin{cases} U_\sigma & \text{if } \sigma \in \mathcal{F}_{\mathcal{C}_V} \\ 0 & \text{if } \sigma \notin \mathcal{F}_{\mathcal{C}_V} \end{cases} .$$

Since there is no possibility of confusion, we keep the same notation also for a mapping $\mathbb{R}^{|\mathcal{F}_{\mathcal{C}_V}|\times|\mathcal{F}_{\mathcal{C}_V}|} \to \mathbb{R}^{|\mathcal{E}_h|\times|\mathcal{E}_h|}$, extending a local matrix $\mathbb{M}_V$ to a full-size one by zeros by

$$[\Psi_V(\mathbb{M}_V)]_{\sigma,\gamma} := \begin{cases} (\mathbb{M}_V)_{\sigma,\gamma} & \text{if } \sigma \in \mathcal{F}_{\mathcal{C}_V} \text{ and } \gamma \in \mathcal{F}_{\mathcal{C}_V} \\ 0 & \text{if } \sigma \notin \mathcal{F}_{\mathcal{C}_V} \text{ or } \gamma \notin \mathcal{F}_{\mathcal{C}_V} \end{cases} .$$

We finally in the same fashion define a mapping $\Theta_V : \mathbb{R}^{|\mathcal{F}_{\mathcal{C}_V}|\times|\mathcal{C}_V^{\mathrm{el}}|} \to \mathbb{R}^{|\mathcal{E}_h|\times|\mathcal{T}_h|}$, filling a full-size representation of a matrix $\mathbb{J}_V$ by zeros on the rows associated with the sides that are not from $\mathcal{F}_{\mathcal{C}_V}$ and on the columns associated with the elements that are not from $\mathcal{C}_V^{\mathrm{el}}$,

$$[\Theta_V(\mathbb{J}_V)]_{\sigma,K} := \begin{cases} (\mathbb{J}_V)_{\sigma,K} & \text{if } \sigma \in \mathcal{F}_{\mathcal{C}_V} \text{ and } K \in \mathcal{C}_V^{\mathrm{el}} \\ 0 & \text{if } \sigma \notin \mathcal{F}_{\mathcal{C}_V} \text{ or } K \notin \mathcal{C}_V^{\mathrm{el}} \end{cases} .$$

Let the local condensation matrices $\mathbb{M}_V$ be invertible for all $V \in \mathcal{V}_h$. Let us define $\mathbb{J}_V$ by $\mathbb{J}_V := \mathbb{M}_V^{-1}\mathbb{A}_{2,V}\mathbb{B}_{2,V}^{-1}$. We then can rewrite (3.7) as

$$\Psi_V(U_V^{\mathcal{F}}) = \Psi_V(\mathbb{M}_V^{-1})(F - \mathbb{B}^t P) - \Theta_V(\mathbb{J}_V)G\,. \tag{3.9}$$

We now notice that

$$\sum_{V\in\mathcal{V}_h} \frac{1}{d}\Psi_V(U_V^{\mathcal{F}}) = U\,, \tag{3.10}$$

which expresses that if we go through all $V \in \mathcal{V}_h$ and observe the sides in the sets $\mathcal{F}_{\mathcal{C}_V}$, each $\sigma \in \mathcal{E}_h$ appears just $d$-times (each side has $d$ vertices). Hence we can sum (3.9) over all vertices and divide it by $d$ to find that

$$U = \tilde{\mathbb{A}}^{-1}(F - \mathbb{B}^t P) - \mathbb{J}G\,, \tag{3.11}$$

where

$$\tilde{\mathbb{A}}^{-1} := \frac{1}{d}\sum_{V\in\mathcal{V}_h} \Psi_V(\mathbb{M}_V^{-1})\,, \quad \mathbb{J} := \frac{1}{d}\sum_{V\in\mathcal{V}_h} \Theta_V(\mathbb{J}_V)\,. \tag{3.12}$$

Finally, inserting this expression into the second equation of (3.3), we obtain a system for only the scalar unknowns

$$-\mathbb{B}\tilde{\mathbb{A}}^{-1}\mathbb{B}^t P = G - \mathbb{B}\tilde{\mathbb{A}}^{-1}F + \mathbb{B}\mathbb{J}G\,. \tag{3.13}$$

We now give two remarks.

**Remark 3.2.3. (Comparison with the direct elimination of the fluxes)** *From (3.3), $U = \mathbb{A}^{-1}(F - \mathbb{B}^t P)$. There are two essential differences in comparison with (3.11). First, the matrix $\tilde{\mathbb{A}}^{-1}$ is sparse, whereas $\mathbb{A}^{-1}$ tends to be full. Second, $\tilde{\mathbb{A}}^{-1}$ is obtained for the price of the inverse of $|\mathcal{V}_h|$ local matrices, whereas obtaining $\mathbb{A}^{-1}$ is in general very expensive.*

**Remark 3.2.4. (Implementation into existing mixed finite element codes)** *The local problems (3.6) correspond to the rows of (3.3) associated with the sides from $\mathcal{F}_{\mathcal{C}_V}$ and elements from $\mathcal{C}_V^{\mathrm{el}}$. Hence obtaining the final problem (3.13) from (3.3) is immediate.*

It appears that in some particular cases, the matrix $\mathbb{M}_V$ is not invertible, cf. Example 3.3.10 below. We give sufficient conditions on the mesh $\mathcal{T}_h$ and on the diffusion tensor $\mathbf{S}$ ensuring that $\mathbb{M}_V$ are invertible for all $V \in \mathcal{V}_h$ below as byproducts of Lemmas 3.3.6 and 3.3.9. Finally, we discuss in Section 3.3.3 the approaches how to modify the proposed technique in order to overcome this difficulty.

## 3.3 Properties of the condensed mixed finite element scheme

We study in this section the properties of the system matrix of the condensed mixed finite element scheme important from the computational point of view, namely its sparsity pattern, symmetry, and positive definiteness. It shows that all these properties are closely related to the properties of the local condensation matrices, which we shall study hereafter. We finally discuss variants and extensions of the proposed technique and open questions.

### 3.3.1 Properties of the system matrix

**Theorem 3.3.1. (Stencil of the system matrix)** *Let $\mathbb{M}_V$ be invertible for all $V \in \mathcal{V}_h$. Then on a row of the final system matrix $\mathbb{B}\tilde{\mathbb{A}}^{-1}\mathbb{B}^t$ corresponding to an element $K \in \mathcal{T}_h$, the only possible nonzero entries are on columns corresponding to $L \in \mathcal{T}_h$ such that $K$ and $L$ share a common vertex.*

Proof:

The assertion of this theorem follows from the fact that by (3.7), the flux through a side $\sigma$ is expressed only using the scalar unknowns of the elements $K \in \mathcal{T}_h$ such that $K$ and $\sigma$ share a common vertex. □

**Theorem 3.3.2. (Positive definiteness of the system matrix)** *Let $\mathbb{M}_V$ be positive definite for all $V \in \mathcal{V}_h$. Then the final system matrix $\mathbb{B}\tilde{\mathbb{A}}^{-1}\mathbb{B}^t$ is also positive definite.*

Proof:

Since $\mathbb{B}$ has a full row rank, $\mathbb{B}\tilde{\mathbb{A}}^{-1}\mathbb{B}^t$ is positive definite as soon as $\tilde{\mathbb{A}}^{-1}$ is positive definite, i.e. when

$$X^t\tilde{\mathbb{A}}^{-1}X > 0 \quad \text{for all } X \in \mathbb{R}^{|\mathcal{T}_h|}\,,\ X \neq 0\,.$$

Let $V \in \mathcal{V}_h$. We define a mapping $\Pi_V : \mathbb{R}^{|\mathcal{E}_h|} \to \mathbb{R}^{|\mathcal{F}_{\mathcal{C}_V}|}$, restricting a vector of values associated with all non-Neumann sides to a vector of values associated with the sides from $\mathcal{F}_{\mathcal{C}_V}$. Let $X \in \mathbb{R}^{|\mathcal{E}_h|}$, $X \neq 0$. Then

$$X^t\tilde{\mathbb{A}}^{-1}X = \frac{1}{d}\sum_{V\in\mathcal{V}_h} X^t\Psi_V(\mathbb{M}_V^{-1})X = \frac{1}{d}\sum_{V\in\mathcal{V}_h} [\Pi_V(X)]^t\mathbb{M}_V^{-1}\Pi_V(X) > 0\,,$$

using the positive definiteness of the local condensation matrices $\mathbb{M}_V$ and consequently of $\mathbb{M}_V^{-1}$ for all $V \in \mathcal{V}_h$ and the fact that in the above sum, all the terms are non-negative and at least $d$ of them are positive. □

**Theorem 3.3.3. (Symmetry of the system matrix)** *Let $\mathbb{M}_V$ be invertible and symmetric for all $V \in \mathcal{V}_h$. Then the final system matrix $\mathbb{B}\tilde{\mathbb{A}}^{-1}\mathbb{B}^t$ is also symmetric.*

Proof:

If $\mathbb{M}_V$ and consequently $\mathbb{M}_V^{-1}$ are symmetric for all $V \in \mathcal{V}_h$, their extensions $\Psi_V(\mathbb{M}_V^{-1})$ are symmetric as well. Hence $\tilde{\mathbb{A}}^{-1}$, a sum of symmetric matrices by (3.12), is symmetric. Finally, if $\tilde{\mathbb{A}}^{-1}$ is symmetric, $\mathbb{B}\tilde{\mathbb{A}}^{-1}\mathbb{B}^t$ is symmetric as well. □

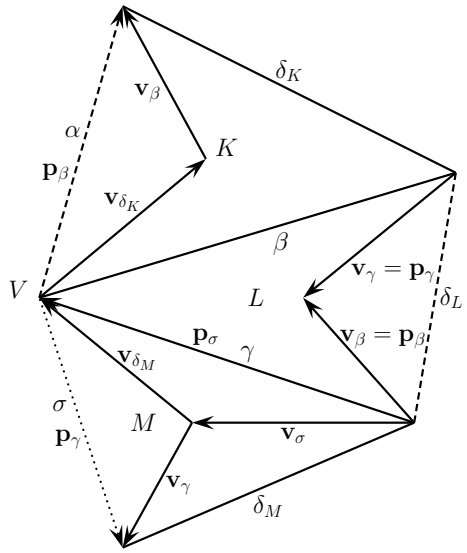


$$
\begin{aligned}
\mathcal{C}_V &= \{K, L, M\} \\
\mathcal{C}_V^{\mathrm{el}} &= \{K, M\} \\
\mathcal{F}_{\mathcal{C}_V} &= \{\beta, \gamma, \sigma\} \\
\mathcal{G}_{\mathcal{C}_V} &= \{\delta_K, \delta_M\} \\
\Gamma_N &\supset \alpha, \delta_L \\
\Gamma_D &\supset \sigma \\
\mathbf{V}(\mathcal{F}_{\mathcal{C}_V}) &= \mathrm{span}\{\mathbf{v}_\beta, \mathbf{v}_\gamma, \mathbf{v}_\sigma\} \\
\mathbf{V}(\mathrm{div}, \mathcal{E}_{\mathcal{C}_V}) &= \mathrm{span}\{\mathbf{p}_\beta, \mathbf{p}_\gamma, \mathbf{p}_\sigma\}
\end{aligned}
$$

Figure 3.3: Example of a boundary cluster $\mathcal{C}_V$ and schematic representation of the basis functions of the spaces $\mathbf{V}(\mathcal{F}_{\mathcal{C}_V})$ and $\mathbf{V}(\mathrm{div}, \mathcal{E}_{\mathcal{C}_V})$

### 3.3.2 Properties of the local condensation matrices

The local condensation matrix $\mathbb{M}_V$ (3.8) for $V \in \mathcal{V}_h$ steams from the equations (3.4)–(3.5). It does not depend on the right-hand side, and hence it is connected with the following problem: find $\mathbf{u} \in \mathbf{V}(\mathcal{E}_{\mathcal{C}_V})$ such that

$$
\begin{aligned}
(\mathbf{u}, \mathbf{S}^{-1}\mathbf{v})_{\mathcal{C}_V} &= 0 \qquad \forall \mathbf{v} \in \mathbf{V}(\mathcal{F}_{\mathcal{C}_V}), && \text{(3.14a)} \\
(\nabla \cdot \mathbf{u}, \phi_K)_K &= 0 \qquad \forall K \in \mathcal{C}_V^{\mathrm{el}}. && \text{(3.14b)}
\end{aligned}
$$

Here, $\mathbf{V}(\mathcal{E}_{\mathcal{C}_V})$ is the space spanned by the RTN basis functions $\mathbf{v}_\sigma$ associated with the non-Neumann sides $\mathcal{E}_{\mathcal{C}_V}$ of the cluster $\mathcal{C}_V$ and $\mathbf{V}(\mathcal{F}_{\mathcal{C}_V})$ is its restriction with the basis functions $\mathbf{v}_\sigma$ associated with the sides from $\mathcal{F}_{\mathcal{C}_V}$. The problem (3.14a)–(3.14b) is further equivalent to the following Petrov–Galerkin problem: find $\mathbf{u} \in \mathbf{V}(\mathrm{div}, \mathcal{E}_{\mathcal{C}_V})$ such that

$$
(\mathbf{u}, \mathbf{S}^{-1}\mathbf{v})_{\mathcal{C}_V} = 0 \qquad \forall \mathbf{v} \in \mathbf{V}(\mathcal{F}_{\mathcal{C}_V}),
$$

where $\mathbf{V}(\mathrm{div}, \mathcal{E}_{\mathcal{C}_V})$ is the subspace of $\mathbf{V}(\mathcal{E}_{\mathcal{C}_V})$ of the functions whose divergence is equal to 0 on all elements $K \in \mathcal{C}_V^{\mathrm{el}}$. The space $\mathbf{V}(\mathrm{div}, \mathcal{E}_{\mathcal{C}_V})$ is spanned by basis functions $\mathbf{p}_\sigma$ associated with the sides from $\mathcal{F}_{\mathcal{C}_V}$, which have the same support as the RTN basis functions $\mathbf{v}_\sigma$ and whose fluxes through the associated sides equal to those of $\mathbf{v}_\sigma$ (this namely fixes their orientation). In particular, for $K \in \mathcal{C}_V^{\mathrm{el}}$ and $\sigma \in \mathcal{E}_K \cap \mathcal{F}_{\mathcal{C}_V}$, $\mathbf{p}_\sigma|_K = \mathbf{v}_\sigma - \frac{(\nabla \cdot \mathbf{v}_\sigma, 1)_K}{(\nabla \cdot \mathbf{v}_{\delta_K}, 1)_K} \mathbf{v}_{\delta_K}$. Note that this is a constant function given by $\frac{1}{d|K|}\mathbf{q}_\sigma|_K$, where $\mathbf{q}_\sigma|_K$ is the vector of the edge of $K$ that is not included in the sides $\sigma$ and $\delta_K$. For $K \in \mathcal{C}_V \setminus \mathcal{C}_V^{\mathrm{el}}$, $\mathbf{p}_\sigma|_K = \mathbf{v}_\sigma|_K$. We refer to Figure 3.3 for a schematic visualization for $d = 2$.

**Lemma 3.3.4. (Form of the local condensation matrices)** *The local condensation matrix $\mathbb{M}_V$ for $V \in \mathcal{V}_h$ is given by*

$$
(\mathbb{M}_V)_{\gamma,\sigma} = (\mathbf{p}_\sigma, \mathbf{S}^{-1}\mathbf{v}_\gamma)_{\mathcal{C}_V},
$$

*where $\mathbf{p}_\sigma$ and $\mathbf{v}_\sigma$, $\sigma \in \mathcal{F}_{\mathcal{C}_V}$, are the basis functions of the spaces $\mathbf{V}(\mathrm{div}, \mathcal{E}_{\mathcal{C}_V})$ and $\mathbf{V}(\mathcal{F}_{\mathcal{C}_V})$, respectively, defined above.*

PROOF:

We can rewrite (3.14a)–(3.14b) as

$$\sum_{\sigma\in\mathcal{E}_{\mathcal{C}_V}} U_\sigma(\mathbf{v}_\sigma,\mathbf{S}^{-1}\mathbf{v}_\gamma)_{\mathcal{C}_V} = 0 \qquad \forall\gamma\in\mathcal{F}_{\mathcal{C}_V}\,, \tag{3.15a}$$

$$\sum_{\sigma\in\mathcal{E}_K,\sigma\not\subset\Gamma_N} U_\sigma(\nabla\cdot\mathbf{v}_\sigma,1)_K = 0 \qquad \forall K\in\mathcal{C}_V^{\mathrm{el}}\,, \tag{3.15b}$$

where $\mathbf{u}=\sum_{\sigma\in\mathcal{E}_{\mathcal{C}_V}} U_\sigma\mathbf{v}_\sigma$. Expressing $U_{\delta_K}$ from (3.15b) gives

$$U_{\delta_K} = \frac{-\sum_{\sigma\in\mathcal{E}_K\cap\mathcal{F}_{\mathcal{C}_V}} U_\sigma(\nabla\cdot\mathbf{v}_\sigma,1)_K}{(\nabla\cdot\mathbf{v}_{\delta_K},1)_K}\,.$$

Inserting this into (3.15a), we have

$$\begin{aligned}\sum_{\sigma\in\mathcal{E}_{\mathcal{C}_V}} U_\sigma(\mathbf{v}_\sigma,\mathbf{S}^{-1}\mathbf{v}_\gamma)_{\mathcal{C}_V} &= \sum_{K\in\mathrm{supp}(\mathbf{v}_\gamma)}\Big\{\sum_{\sigma\in\mathcal{E}_K\cap\mathcal{F}_{\mathcal{C}_V}} U_\sigma(\mathbf{v}_\sigma,\mathbf{S}^{-1}\mathbf{v}_\gamma)_K + U_{\delta_K}(\mathbf{v}_{\delta_K},\mathbf{S}^{-1}\mathbf{v}_\gamma)_K\Big\}\\ &= \sum_{K\in\mathrm{supp}(\mathbf{v}_\gamma)}\sum_{\sigma\in\mathcal{E}_K\cap\mathcal{F}_{\mathcal{C}_V}} U_\sigma\Big(\mathbf{v}_\sigma-\frac{(\nabla\cdot\mathbf{v}_\sigma,1)_K}{(\nabla\cdot\mathbf{v}_{\delta_K},1)_K}\mathbf{v}_{\delta_K},\mathbf{S}^{-1}\mathbf{v}_\gamma\Big)_K\,,\end{aligned}$$

where we have defined for simplification $\mathbf{v}_{\delta_K}=0$ if $K\in\mathcal{C}_V\setminus\mathcal{C}_V^{\mathrm{el}}$ (i.e. if $\mathcal{E}_K\cap\mathcal{G}_{\mathcal{C}_V}=\emptyset$). Hence, using the definition of the basis functions of the spaces $\mathbf{V}(\mathrm{div},\mathcal{E}_{\mathcal{C}_V})$ and $\mathbf{V}(\mathcal{F}_{\mathcal{C}_V})$, the assertion of the lemma follows. □

**Remark 3.3.5. (Implementation)** *Let* $\mathbf{S}$ *be piecewise constant and let* $\Gamma_N=\emptyset$. *Then*

$$\begin{aligned}(\mathbb{M}_V)_{\gamma,\sigma} &= \sum_{K\in\mathcal{C}_V;\,\sigma,\gamma\in\mathcal{E}_K}(\mathbf{p}_\sigma,\mathbf{S}^{-1}\mathbf{v}_\gamma)_K = \sum_{K\in\mathcal{C}_V;\,\sigma,\gamma\in\mathcal{E}_K}\frac{(\nabla\cdot\mathbf{v}_\gamma,1)_K}{d^2|K|^2}(\mathbf{S}^{-1}\mathbf{q}_\sigma,\mathbf{x}-V_{\gamma,K})_K\\ &= \sum_{K\in\mathcal{C}_V;\,\sigma,\gamma\in\mathcal{E}_K}\frac{1}{d^2|K|}\mathbf{S}|_K^{-1}\mathbf{q}_\sigma|_K\cdot\mathbf{w}_\gamma|_K\,,\end{aligned}$$

*where* $\sigma,\gamma\in\mathcal{F}_{\mathcal{C}_V}$ *and* $\mathbf{w}_\gamma|_K := (\nabla\cdot\mathbf{v}_\gamma,1)_K(\mathbf{x}_K-V_{\gamma,K})$ *with* $\mathbf{x}_K$ *the barycentre of* $K$ *and* $V_{\gamma,K}$ *the vertex of* $K$ *opposite to the side* $\gamma$, *cf. Figure 3.4. We have used the facts that* $\{K\in\mathcal{C}_V;\,\sigma,\gamma\in\mathcal{E}_K\}=\mathrm{supp}(\mathbf{p}_\sigma)\cap\mathrm{supp}(\mathbf{v}_\gamma)$ *and that* $\mathbf{x}_K=(\mathbf{x},1)_K/|K|$. *Hence, to implement the condensed mixed finite element scheme when in addition* $q=0$, *everything we need are the edge and vertex–barycentre vectors in each simplex and the measure of each simplex.*

We now give two lemmas that guarantee the positive definiteness of the local condensation matrices, the assumption of Theorem 3.3.2. Since positive definiteness implies invertibility, the local condensation matrices are under the following conditions namely invertible, which guarantees the feasibility of the condensation in the proposed form. The given conditions are sufficient but not necessary to ensure the positive definiteness—they can be used as a simple elementwise or sidewise criterion, in order to avoid the direct checking of the positive definiteness of the local condensation matrices.

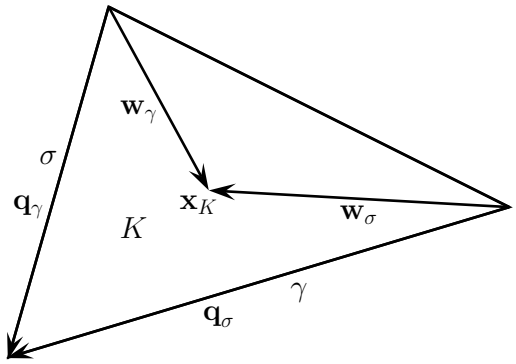


Figure 3.4: Triangle $K$ for the simplified elementwise positive definiteness criterion

**Lemma 3.3.6. (Positive definiteness of the local condensation matrices—elementwise criterion)** *Let the matrices* $\mathbb{E}_{V,K} \in \mathbb{R}^{|\mathcal{E}_K \cap \mathcal{F}_{\mathcal{C}_V}| \times |\mathcal{E}_K \cap \mathcal{F}_{\mathcal{C}_V}|}$ *given by*

$$(\mathbb{E}_{V,K})_{\gamma,\sigma} := (\mathbf{p}_\sigma, \mathbf{S}^{-1}\mathbf{v}_\gamma)_K \,,$$

*where* $\mathbf{p}_\sigma$ *and* $\mathbf{v}_\sigma$, $\sigma \in \mathcal{E}_K \cap \mathcal{F}_{\mathcal{C}_V}$, *are the basis functions of the spaces* $\mathbf{V}(\mathrm{div}, \mathcal{E}_{\mathcal{C}_V})$ *and* $\mathbf{V}(\mathcal{F}_{\mathcal{C}_V})$, *respectively, be positive definite for all* $K \in \mathcal{T}_h$ *and for all vertices* $V$ *of* $K$. *Then the local condensation matrices* $\mathbb{M}_V$ *are positive definite for all* $V \in \mathcal{V}_h$.

Proof:
Let $V \in \mathcal{V}_h$ and let $X \in \mathbb{R}^{|\mathcal{F}_{\mathcal{C}_V}|}$, $X \neq 0$. We then have, with $\mathbf{p} = \sum_{\sigma \in \mathcal{F}_{\mathcal{C}_V}} X_\sigma \mathbf{p}_\sigma$, $\mathbf{v} = \sum_{\sigma \in \mathcal{F}_{\mathcal{C}_V}} X_\sigma \mathbf{v}_\sigma$,

$$\begin{aligned} X^t \mathbb{M}_V X &= (\mathbf{p}, \mathbf{S}^{-1}\mathbf{v})_{\mathcal{C}_V} = \sum_{K \in \mathcal{C}_V^{\mathrm{el}}} (\mathbf{p}, \mathbf{S}^{-1}\mathbf{v})_K + \sum_{K \in \mathcal{C}_V \setminus \mathcal{C}_V^{\mathrm{el}}} (\mathbf{p}, \mathbf{S}^{-1}\mathbf{v})_K \\ &= \sum_{K \in \mathcal{C}_V^{\mathrm{el}}} [\Pi_{V,K}(X)]^t \mathbb{E}_{V,K} \Pi_{V,K}(X) + \sum_{K \in \mathcal{C}_V \setminus \mathcal{C}_V^{\mathrm{el}}} (\mathbf{v}, \mathbf{S}^{-1}\mathbf{v})_K > 0 \,, \end{aligned}$$

where the mapping $\Pi_{V,K} : \mathbb{R}^{|\mathcal{F}_{\mathcal{C}_V}|} \to \mathbb{R}^{|\mathcal{E}_K \cap \mathcal{F}_{\mathcal{C}_V}|}$ restricts a vector of values associated with the sides from $\mathcal{F}_{\mathcal{C}_V}$ to a vector of values associated with the sides from $\mathcal{E}_K \cap \mathcal{F}_{\mathcal{C}_V}$, and using that the two last terms are non-negative and at least one of them is positive. □

**Remark 3.3.7. (Simplified elementwise positive definiteness criterion in two space dimensions)** *Let* $d = 2$ *and let* $\mathbf{S}$ *be piecewise constant. Let* $\mathbf{q}_\sigma, \mathbf{q}_\gamma, \mathbf{w}_\sigma, \mathbf{w}_\gamma$ *be the constant edge and vertex–barycentre vectors of a triangle* $K$ *as in Figure 3.4. Then a simplified criterion for the positive definiteness of the local condensation matrices is*

$$\left| \mathbf{S}|_K^{-1} \mathbf{q}_\sigma \cdot \mathbf{w}_\gamma + \mathbf{S}|_K^{-1} \mathbf{q}_\gamma \cdot \mathbf{w}_\sigma \right|^2 < 4 (\mathbf{S}|_K^{-1} \mathbf{q}_\sigma \cdot \mathbf{w}_\sigma)(\mathbf{S}|_K^{-1} \mathbf{q}_\gamma \cdot \mathbf{w}_\gamma)$$

*for all* $K \in \mathcal{T}_h$ *and for all denotation* $\sigma, \gamma$ *of two edges of* $K$. *Notice that* $\mathbf{q}_\sigma \cdot \mathbf{w}_\gamma = 0$ *for an equilateral triangle and that this quantity grows in the absolute value while deforming the triangle. On the contrary,* $\mathbf{q}_\sigma \cdot \mathbf{w}_\sigma$ *decreases with the angle between* $\mathbf{q}_\sigma$ *and* $\mathbf{w}_\sigma$ *and it is positive only if this angle is less than* $\pi/2$. *This criterion is a consequence of Remark 3.3.5 and of Lemma 3.3.6 with a tighten up criterion for triangles with Neumann edges.*

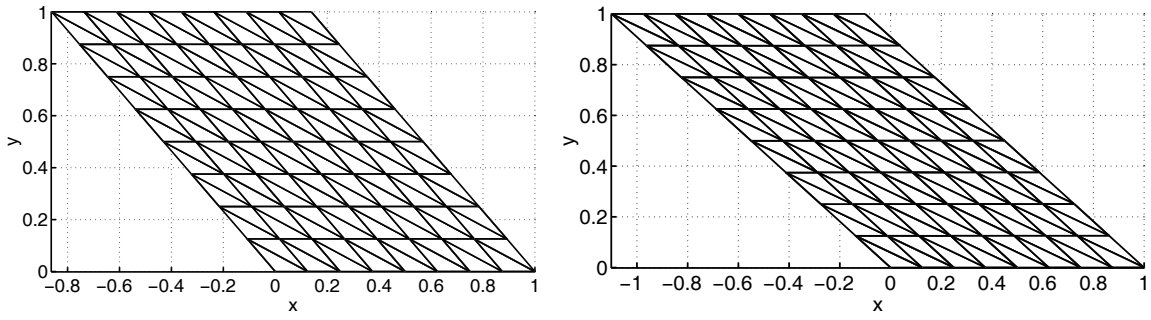


Figure 3.5: Theoretical (left) and experimental (right) limit mesh for the positive definiteness of the system matrix for a deformed square and $\mathbf{S} = Id$

**Example 3.3.8. (Positive definiteness for a triangulation of a deformed square)** *Let $\mathbf{S} = Id$, let $\Omega$ be a square $(0,1) \times (0,1)$, and let $\mathcal{T}_h$ be its triangulation by regular right-angled triangles. Let us deform the domain and the mesh by shifting horizontally the upper edge of the square. Remark 3.3.7 gives that the local condensation matrices (and consequently the system matrix) are positive definite up to the mesh given in Figure 3.5 on the left-hand side. The experimental limit mesh is still a bit less restrictive and is given in Figure 3.5 on the right-hand side.*

**Lemma 3.3.9. (Positive definiteness of the local condensation matrices—sidewise criterion)** *Let $\mathbf{S}$ be piecewise constant and let $\Gamma_N = \emptyset$. Let for all $\gamma \in \mathcal{E}_h$ and for all vertices $V$ of $\gamma$,*

$$\sum_{K \in \mathrm{supp}(\mathbf{v}_\gamma)} \frac{1}{d^2|K|} \mathbf{S}|_K^{-1} \mathbf{q}_\gamma|_K \cdot \mathbf{w}_\gamma|_K \quad > \quad \sum_{K \in \mathrm{supp}(\mathbf{v}_\gamma)} \frac{1}{d^2|K|} \sum_{\sigma \in \mathcal{E}_K \cap \mathcal{F}_{\mathcal{C}_V}, \sigma \neq \gamma} \left| \frac{1}{2} \mathbf{S}|_K^{-1} (\mathbf{q}_\sigma|_K \cdot \mathbf{w}_\gamma|_K + \mathbf{q}_\gamma|_K \cdot \mathbf{w}_\sigma|_K) \right|,$$

*where the constant edge and vertex–barycentre vectors $\mathbf{q}_\sigma|_K$, $\mathbf{w}_\sigma|_K$, respectively, are derived from the basis functions of the spaces $\mathbf{V}(\mathrm{div}, \mathcal{E}_{\mathcal{C}_V})$ and $\mathbf{V}(\mathcal{F}_{\mathcal{C}_V})$ $\mathbf{p}_\sigma$ and $\mathbf{v}_\sigma$ as in Remark 3.3.5. Then the local condensation matrices $\mathbb{M}_V$ are positive definite for all $V \in \mathcal{V}_h$.*

Proof:

The assumption of the lemma ensures that the matrices $\frac{1}{2}(\mathbb{M}_V + \mathbb{M}_V^t)$ for all $V \in \mathcal{V}_h$ have positive diagonal entries and are strictly diagonally dominant and hence they are positive definite. To conclude, it suffices to note that the matrix $\mathbb{M}_V$ is positive definite if and only if its symmetric part $\frac{1}{2}(\mathbb{M}_V + \mathbb{M}_V^t)$ is positive definite. □

**Example 3.3.10. (Singular local condensation matrix)** *We give in Figure 3.6 an example of a mesh where the local condensation matrix $\mathbb{M}_V$ is singular for $\mathbf{S} = Id$. All the triangles sharing the vertex $V$ have exactly one edge $\sigma$ such that $\mathbf{q}_\sigma \cdot \mathbf{w}_\sigma = 0$ with the notation of Figure 3.4. Hence, in particular, the assumptions of Lemma 3.3.6 are not verified. This singularity is not local—it suffices to modify the coordinates of one point to make $\mathbb{M}_V$ invertible.*

We now state under which conditions the assumption of Theorem 3.3.3 is satisfied.

**Lemma 3.3.11. (Symmetry of the local condensation matrices)** *Let $\mathcal{T}_h$ consist of equilateral simplices and let $\mathbf{S}$ be a piecewise constant scalar function. Then $\mathbb{M}_V$ are symmetric for all $V \in \mathcal{V}_h$.*

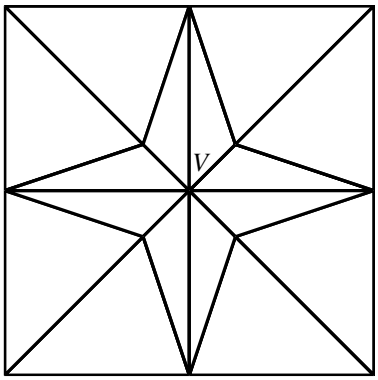


Figure 3.6: A mesh where the local condensation matrix $\mathbb{M}_V$ is singular

PROOF:
We have

$$(\mathbb{M}_V)_{\gamma,\sigma} = \left(\mathbf{v}_\sigma - \frac{(\nabla\cdot\mathbf{v}_\sigma,1)_K}{(\nabla\cdot\mathbf{v}_{\delta_K},1)_K}\mathbf{v}_{\delta_K}, \mathbf{S}^{-1}\mathbf{v}_\gamma\right)_K,$$

where $K \in \mathrm{supp}(\mathbf{p}_\sigma) \cap \mathrm{supp}(\mathbf{v}_\gamma)$, $\sigma,\gamma \in \mathcal{F}_{\mathcal{C}_V}$, $\sigma \neq \gamma$. If $K \in \mathcal{C}_V \setminus \mathcal{C}_V^{\mathrm{el}}$ and thus $\mathbf{v}_{\delta_K} = 0$ by the definition, $(\mathbb{M}_V)_{\gamma,\sigma}$ clearly equals to $(\mathbb{M}_V)_{\sigma,\gamma}$ for a general $\mathbf{S}$ by its symmetry. If $K \in \mathcal{C}_V^{\mathrm{el}}$, $(\mathbb{M}_V)_{\gamma,\sigma} = (\mathbb{M}_V)_{\sigma,\gamma}$ as soon as

$$\left(\mathbf{S}^{-1}\mathbf{v}_{\delta_K}, \mathbf{v}_\gamma(\nabla\cdot\mathbf{v}_\gamma,1)_K\right)_K = \left(\mathbf{S}^{-1}\mathbf{v}_{\delta_K}, \mathbf{v}_\sigma(\nabla\cdot\mathbf{v}_\sigma,1)_K\right)_K,$$

which is the case of an equilateral simplex and $\mathbf{S}$ a piecewise constant scalar function. □

**Remark 3.3.12. (Equilateral simplices and a piecewise constant scalar diffusion tensor)** *Let $\mathcal{T}_h$ consist of equilateral simplices, let $\mathbf{S}$ be a piecewise constant scalar function, and let $\Gamma_N = \emptyset$. Then it follows from Remark 3.3.5 that $(\mathbb{M}_V)_{\gamma,\sigma} = 0$ if $\sigma \neq \gamma$ (since the vectors $\mathbf{q}_\sigma|_K$ and $\mathbf{w}_\gamma|_K$ are orthogonal), and hence the local condensation matrices are diagonal. Thus to express the flux though an interior side $\gamma$ in this case, we only need the scalar unknowns associated with the two elements that share this side. As a consequence, the final system matrix has only a 4-point stencil in two space dimensions and a 5-point stencil in three space dimensions and is moreover symmetric and positive definite. A simple computation gives that this matrix is equivalent to that of the standard finite volume scheme [61] when $\mathbf{S} = Id$. Note however that the right-hand side is generally different in a presence of a source term!*

### 3.3.3 Variants, extensions, and open problems

The essential idea of the proposed elimination, briefly said, consists in considering such sets of elements that it is possible to eliminate the fluxes through the exterior sides of these sets by the divergence equations on the exterior elements. The clusters defined by all elements sharing a given vertex represent just the most basic possibility. We now precise on this point.

Let $\mathcal{C}$ be a set of elements of $\mathcal{T}_h$ and let $\mathcal{G}_\mathcal{C}$ be the set of sides of $\mathcal{C}$ between an element $K \in \mathcal{C}$ and $L \notin \mathcal{C}$. Let each $K \in \mathcal{C}$ contain at most one $\sigma \in \mathcal{G}_\mathcal{C}$ and let us denote the subset of $\mathcal{C}$ of elements containing a $\sigma \in \mathcal{G}_\mathcal{C}$ by $\mathcal{C}^{\mathrm{el}}$. Clearly, $|\mathcal{C}^{\mathrm{el}}| = |\mathcal{G}_\mathcal{C}|$, and we denote by $\delta_K$ the side of $K \in \mathcal{C}^{\mathrm{el}}$ such that $\delta_K \in \mathcal{G}_\mathcal{C}$. Finally, let $\mathcal{E}_\mathcal{C}$ stand for all non-Neumann sides of $\mathcal{C}$ and $\mathcal{F}_\mathcal{C}$ for $\mathcal{E}_\mathcal{C} \setminus \mathcal{G}_\mathcal{C}$. A particular example is the cluster $\mathcal{C}_V$ associated with a vertex $V$. We have the spaces $\mathbf{V}(\mathcal{F}_{\mathcal{C}_V})$ and $\mathbf{V}(\mathrm{div}, \mathcal{E}_{\mathcal{C}_V})$ as in Section 3.3.2 and the following generalization of Lemma 3.3.6:

**Lemma 3.3.13. (Positive definiteness of local condensation matrices on general clusters)** *Let the matrices* $\mathbb{E}_{\mathcal{C},K} \in \mathbb{R}^{|\mathcal{E}_K \cap \mathcal{F}_\mathcal{C}| \times |\mathcal{E}_K \cap \mathcal{F}_\mathcal{C}|}$ *given by*

$$(\mathbb{E}_{\mathcal{C},K})_{\gamma,\sigma} := (\mathbf{p}_\sigma, \mathbf{S}^{-1}\mathbf{v}_\gamma)_K \,,$$

*where* $\mathbf{p}_\sigma$ *and* $\mathbf{v}_\sigma$, $\sigma \in \mathcal{E}_K \cap \mathcal{F}_\mathcal{C}$, *are the basis functions of the spaces* $\mathbf{V}(\mathrm{div}, \mathcal{E}_\mathcal{C})$ *and* $\mathbf{V}(\mathcal{F}_\mathcal{C})$, *respectively, be positive definite for all* $K \in \mathcal{C}^{\mathrm{el}}$. *Then the local condensation matrix* $\mathbb{M}_\mathcal{C}$ *associated with the cluster* $\mathcal{C}$, $(\mathbb{M}_\mathcal{C})_{\gamma,\sigma} = (\mathbf{p}_\sigma, \mathbf{S}^{-1}\mathbf{v}_\gamma)_\mathcal{C}$, *is positive definite.*

Proof:
Let $X \in \mathbb{R}^{|\mathcal{F}_\mathcal{C}|}$, $X \neq 0$. We then have, with $\mathbf{p} = \sum_{\sigma \in \mathcal{F}_\mathcal{C}} X_\sigma \mathbf{p}_\sigma$, $\mathbf{v} = \sum_{\sigma \in \mathcal{F}_\mathcal{C}} X_\sigma \mathbf{v}_\sigma$,

$$\begin{aligned} X^t \mathbb{M}_\mathcal{C} X &= (\mathbf{p}, \mathbf{S}^{-1}\mathbf{v})_\mathcal{C} = \sum_{K \in \mathcal{C}^{\mathrm{el}}} (\mathbf{p}, \mathbf{S}^{-1}\mathbf{v})_K + \sum_{K \in \mathcal{C} \setminus \mathcal{C}^{\mathrm{el}}} (\mathbf{p}, \mathbf{S}^{-1}\mathbf{v})_K \\ &= \sum_{K \in \mathcal{C}^{\mathrm{el}}} [\Pi_{\mathcal{C},K}(X)]^t \mathbb{E}_{\mathcal{C},K} \Pi_{\mathcal{C},K}(X) + \sum_{K \in \mathcal{C} \setminus \mathcal{C}^{\mathrm{el}}} (\mathbf{v}, \mathbf{S}^{-1}\mathbf{v})_K > 0 \,, \end{aligned}$$

where the mapping $\Pi_{\mathcal{C},K} : \mathbb{R}^{|\mathcal{F}_\mathcal{C}|} \to \mathbb{R}^{|\mathcal{E}_K \cap \mathcal{F}_\mathcal{C}|}$ restricts a vector of values associated with the sides from $\mathcal{F}_\mathcal{C}$ to a vector of values associated with the sides from $\mathcal{E}_K \cap \mathcal{F}_\mathcal{C}$, and using that the two last terms are non-negative and at least one of them is positive. □

The above lemma shows that the positive definiteness of local condensation matrices only depends on the elements from $\mathcal{C}^{\mathrm{el}}$. Hence, in particular, shall the local condensation matrix associated with a cluster of a vertex $V$ be singular, we can resort to a wider cluster. This namely functions in the case of Example 3.3.10. Finally, to expose the problem in its full complexity, it appears that it is not necessary to consider the divergence equations on the elements of $\mathcal{C}$ sharing a side with an element $L \notin \mathcal{C}$. Let again $\mathcal{C}$ be a set of elements of $\mathcal{T}_h$ and let $\mathcal{G}_\mathcal{C}$ be the set of sides of $\mathcal{C}$ between an element $K \in \mathcal{C}$ and $L \notin \mathcal{C}$. Let $\mathcal{E}_\mathcal{C}$ stand for all non-Neumann sides of $\mathcal{C}$ and $\mathcal{F}_\mathcal{C}$ for $\mathcal{E}_\mathcal{C} \setminus \mathcal{G}_\mathcal{C}$. We notice that on the rows of the submatrix $\mathbb{A}$ of (3.3) associated with the sides from $\mathcal{F}_\mathcal{C}$ and on the rows of the submatrix $\mathbb{B}$ associated with the elements from $\mathcal{C}$, the only nonzero entries are on the columns associated with the sides from $\mathcal{E}_\mathcal{C}$. Hence, to carry out the condensation, it is sufficient if the submatrix consisting of the above rows has a rank equal to $|\mathcal{E}_\mathcal{C}|$. The main open problem, which resembles the existence of "singular triangles" in [37, 121], is whether there always has to exist a system of clusters covering $\mathcal{T}_h$ with the above property. Next, in the case of clusters associated with vertices, we have the simple expression (3.10) for the fluxes through all non-Neumann sides. For general clusters, however, we have to associate a weight $\alpha_\sigma^i$ to each side $\sigma \in \mathcal{E}_h$ and $i$-th out of $b$ clusters $\mathcal{C}$ where $\sigma$ belongs to $\mathcal{F}_\mathcal{C}$, such that $\sum_{i=1}^b \alpha_\sigma^i = 1$, in order to have $\sum_{i=1}^b \alpha_\sigma^i U_\sigma^i = U_\sigma$, where $U_\sigma^i$ is the expression of the flux through $\sigma$ from the $i$-th cluster. Another interesting open problem is whether one could influence the stencil, symmetry, and positive definiteness of the system matrix by a suitable choice of these weights. For the moment, we have only focused on the basic case. Throughout all the tests presented in Section 3.5, which involve general meshes and inhomogeneous and anisotropic (nonconstant full-matrix) diffusion tensors, we have used the local condensation matrices associated with vertices. These were always invertible, although not always positive definite.

In the lowest-order Raviart–Thomas mixed finite element method on rectangular meshes or in the lowest-order Brezzi–Douglas–Marini mixed finite element method [31, 32] on simplicial meshes, it is either not possible to create subsets $\mathcal{C}$ of $\mathcal{T}_h$ such that each element of $\mathcal{C}$ shares at

most one side with an element $L \notin \mathcal{C}$, or the number of degrees of freedom of vector unknowns per side is greater than the number of degrees of freedom of scalar unknowns per element. Hence the basic form of the condensation with clusters around vertices does not apply. On the other hand, for both Raviart–Thomas and Brezzi–Douglas–Marini mixed finite elements of second order on simplicial meshes, the two above properties are satisfied. The extension of the basic condensation to this case, which may lead to an interesting relation between these second-order mixed finite element methods and the discontinuous Galerkin method, is an ongoing work.

## 3.4 Application to nonlinear parabolic problems

We show in this section that the above ideas easily apply also to the discretization of nonlinear parabolic convection–reaction–diffusion problems. We consider in particular the problem

$$\begin{aligned}
\frac{\partial \beta(p)}{\partial t} + \nabla \cdot \mathbf{u} + F(p) &= q \quad \text{in } \Omega \times (0,T)\,, && \text{(3.16a)}\\
\mathbf{u} &= -\mathbf{S}\nabla p + \psi(p)\mathbf{w} \quad \text{in } \Omega \times (0,T)\,, && \text{(3.16b)}\\
p(\cdot,0) &= p_0 \quad \text{in } \Omega\,, && \text{(3.16c)}\\
p &= p_D \quad \text{on } \Gamma_D \times (0,T)\,, && \text{(3.16d)}\\
\mathbf{u}\cdot\mathbf{n} &= u_N \quad \text{on } \Gamma_N \times (0,T)\,, && \text{(3.16e)}
\end{aligned}$$

where $\beta$, $\psi$, and $F$ are nonlinear functions, $\mathbf{S}$ is again a bounded, symmetric, and uniformly positive definite tensor, $\mathbf{w}$ is a velocity field, and $q$ represents a source term.

Let again $\tilde{\mathbf{u}}$ be such that $\tilde{\mathbf{u}}\cdot\mathbf{n} = u_N$ on $\Gamma_N$ in the appropriate sense. We split up the time interval $(0,T)$ such that $0 = t_0 < \ldots < t_n < \ldots < t_N = T$ and define $\triangle t_n := t_n - t_{n-1}$, $n \in \{1,2,\ldots,N\}$, and $p_h^0|_K$ by $(p_0,1)_K/|K|$ for all $K \in \mathcal{T}_h$. The fully implicit lowest-order Raviart–Thomas mixed finite element approximation of the problem (3.16a)–(3.16e), cf. [14], consists in finding on each time level $t_n$, $n \in \{1,2,\ldots,N\}$, the functions $\mathbf{u}_h^n = \mathbf{u}_{0,h}^n + \tilde{\mathbf{u}}^n$, $\mathbf{u}_{0,h}^n \in \mathbf{V}(\mathcal{E}_h)$, and $p_h^n \in \Phi(\mathcal{T}_h)$ such that

$$\begin{aligned}
(\mathbf{S}^{-n}\mathbf{u}_{0,h}^n, \mathbf{v}_h)_\Omega - (\nabla\cdot\mathbf{v}_h, p_h^n)_\Omega - (\psi(p_h^n)\mathbf{w}^n, \mathbf{S}^{-n}\mathbf{v}_h)_\Omega &= -\langle \mathbf{v}_h\cdot\mathbf{n}, p_D^n\rangle_{\partial\Omega}\\
&\quad -(\mathbf{S}^{-n}\tilde{\mathbf{u}}^n, \mathbf{v}_h)_\Omega \qquad \forall\, \mathbf{v}_h \in \mathbf{V}(\mathcal{E}_h)\,, && \text{(3.17a)}\\
\Big(\frac{\beta(p_h^n) - \beta(p_h^{n-1})}{\triangle t_n}, \phi_h\Big)_\Omega + (\nabla\cdot\mathbf{u}_{0,h}^n, \phi_h)_\Omega + (F(p_h^n), \phi_h)_\Omega &= (q,\phi_h)_\Omega\\
&\quad -(\nabla\cdot\tilde{\mathbf{u}}^n, \phi_h)_\Omega \qquad \forall \phi_h \in \Phi(\mathcal{T}_h)\,, && \text{(3.17b)}
\end{aligned}$$

where

$$\mathbf{S}^{-n} := \frac{1}{\triangle t_n}\int_{t_{n-1}}^{t_n} \mathbf{S}^{-1}(\cdot,t)\,\mathrm{d}t\,, \quad \mathbf{w}^n := \frac{1}{\triangle t_n}\int_{t_{n-1}}^{t_n} \mathbf{w}(\cdot,t)\,\mathrm{d}t\,,$$
$$p_D^n := \frac{1}{\triangle t_n}\int_{t_{n-1}}^{t_n} p_D(\cdot,t)\,\mathrm{d}t\,, \quad \tilde{\mathbf{u}}^n := \frac{1}{\triangle t_n}\int_{t_{n-1}}^{t_n} \tilde{\mathbf{u}}(\cdot,t)\,\mathrm{d}t \qquad n \in \{1,2,\ldots,N\}\,.$$

Note that if $\beta = F = \psi = 0$, the matrix form of the problem (3.17a)–(3.17b) is given by (3.3), where the second equation is multiplied by $-1$. Such system matrix is not symmetric, but is positive definite, which is a favorable starting form for (3.17a)–(3.17b).

Everything we have to say about the application of the proposed condensation to the system (3.17a)–(3.17b) is that the terms where the unknown discrete velocity function $\mathbf{u}_{0,h}^n$

appears are exactly the same as in the linear elliptic diffusion case, see (3.2a)–(3.2b). Hence one can eliminate $\mathbf{u}_{0,h}^n$ on each discrete time level as in Section 3.2. This time, the flux unknowns are *nonlinear* functions of the scalar unknowns, convection velocity field, sources, and boundary conditions. The system (3.17a)–(3.17b), linearized by e.g. the Newton method, can be written in the matrix form as

$$\begin{pmatrix} \mathbb{A} & \mathbb{C} \\ \mathbb{B} & \mathbb{D} \end{pmatrix} \begin{pmatrix} U \\ P \end{pmatrix} = \begin{pmatrix} F \\ G \end{pmatrix}. \tag{3.18}$$

Let $V \in \mathcal{V}_h$ be a vertex and $\mathcal{C}_V$ the associated cluster and let us consider the linearized equations (3.17a) for the basis functions $\mathbf{v}_\gamma$, $\gamma \in \mathcal{F}_{\mathcal{C}_V}$, and the linearized equations (3.17b) for all $\phi_K$, $K \in \mathcal{C}_V^{\mathrm{el}}$. This gives

$$\begin{pmatrix} \mathbb{A}_{1,V} & \mathbb{A}_{2,V} \\ \mathbb{B}_{1,V} & \mathbb{B}_{2,V} \end{pmatrix} \begin{pmatrix} U_V^{\mathcal{F}} \\ U_V^{\mathcal{G}} \end{pmatrix} = \begin{pmatrix} F_V - \mathbb{C}_V P_{1,V} \\ G_V - \mathbb{D}_V P_{2,V} \end{pmatrix}. \tag{3.19}$$

In fact, in the present case, $P_{1,V} = P_{2,V} = \{P_K\}_{K \in \mathcal{C}_V}$. We shall need the form (3.19) below for the upwind-mixed method. The matrix $\mathbb{B}_{2,V}$ is still diagonal, and hence we easily have

$$\mathbb{M}_V U_V^{\mathcal{F}} = F_V - \mathbb{C}_V P_{1,V} - \mathbb{A}_{2,V}\mathbb{B}_{2,V}^{-1}(G_V - \mathbb{D}_V P_{2,V}), \tag{3.20}$$

where the local condensation matrix associated with the vertex $V$, $\mathbb{M}_V = \mathbb{A}_{1,V} - \mathbb{A}_{2,V}\mathbb{B}_{2,V}^{-1}\mathbb{B}_{1,V}$, is the same as in the linear elliptic diffusion case. Hence its invertibility and the feasibility of the condensation in this form is determined by the rules studied in Section 3.3. Shall $\mathbb{M}_V$ be invertible for all $V \in \mathcal{V}_h$, we have

$$U = \tilde{\mathbb{A}}^{-1}(F - \mathbb{C}P) - \mathbb{J}(G - \mathbb{D}P),$$

using (3.10). Here $\tilde{\mathbb{A}}^{-1}$ and $\mathbb{J}$ are given by (3.12). It now suffices to insert this expression for $U$ into the second equation of (3.18) to obtain the final system for the scalar unknowns $P$ only,

$$(-\mathbb{B}\tilde{\mathbb{A}}^{-1}\mathbb{C} + \mathbb{B}\mathbb{J}\mathbb{D} + \mathbb{D})P = G - \mathbb{B}\tilde{\mathbb{A}}^{-1}F + \mathbb{B}\mathbb{J}G. \tag{3.21}$$

This transcription enables in particular a straightforward implementation of the proposed condensation in any mixed finite element code.

**Remark 3.4.1. (Assemblage of $\tilde{\mathbb{A}}^{-1}$ and $\mathbb{J}$)** *We note that the matrices $\tilde{\mathbb{A}}^{-1}$ and $\mathbb{J}$ only depend on the matrices $\mathbb{A}, \mathbb{B}$ of (3.18). Hence, if these matrices do not change (i.e. when the diffusion tensor $\mathbf{S}$ is constant with respect to time), the assemblage of $\tilde{\mathbb{A}}^{-1}$ and $\mathbb{J}$ can be done only once before the start of the calculation. On each time and linearization step, one then needs only $\mathbb{C}$, $\mathbb{D}$, $F$, and $G$ from (3.18) to assemble the final linear system (3.21).*

We now finally turn to the upwind-mixed lowest-order Raviart–Thomas method, cf. [46, 47, 77]. For this purpose, we first rewrite (3.16a)–(3.16b) as

$$\begin{aligned} \frac{\partial \beta(p)}{\partial t} + \nabla \cdot \mathbf{r} + \nabla \cdot (\psi(p)\mathbf{w}) + F(p) &= q \quad \text{in } \Omega \times (0,T), \\ \mathbf{r} &= -\mathbf{S}\nabla p \quad \text{in } \Omega \times (0,T). \end{aligned}$$

Whereas the initial and Dirichlet boundary conditions (3.16c) and (3.16d) stay the same, we rewrite the Robin boundary condition (3.16e) as a Neumann one,

$$\mathbf{r} \cdot \mathbf{n} = v_N \quad \text{on } \Gamma_N \times (0,T).$$

Let again $\tilde{\mathbf{r}}$ be such that $\tilde{\mathbf{r}} \cdot \mathbf{n} = v_N$ on $\Gamma_N$ in the appropriate sense and define $\tilde{\mathbf{r}}^n := \frac{1}{\triangle t_n} \int_{t_{n-1}}^{t_n} \tilde{\mathbf{r}}(\cdot, t)\, \mathrm{d}t$, $n \in \{1, 2, \ldots, N\}$. The fully implicit upwind-mixed finite element method then reads: on each time level $t_n$, $n \in \{1, 2, \ldots, N\}$, find the functions $\mathbf{r}_h^n = \mathbf{r}_{0,h}^n + \tilde{\mathbf{r}}^n$, $\mathbf{r}_{0,h}^n \in \mathbf{V}(\mathcal{E}_h)$, and $p_h^n \in \Phi(\mathcal{T}_h)$ such that

$$(\mathbf{S}^{-n}\mathbf{r}_{0,h}^n, \mathbf{v}_h)_\Omega - (\nabla \cdot \mathbf{v}_h, p_h^n)_\Omega = -\langle \mathbf{v}_h \cdot \mathbf{n}, p_D^n \rangle_{\partial\Omega} - (\mathbf{S}^{-n}\tilde{\mathbf{r}}^n, \mathbf{v}_h)_\Omega \qquad \forall\, \mathbf{v}_h \in \mathbf{V}(\mathcal{E}_h)\,, \tag{3.23a}$$

$$\Big(\frac{\beta(P_K^n) - \beta(P_K^{n-1})}{\triangle t_n}, \phi_K\Big)_K + (\nabla \cdot \mathbf{r}_{0,h}^n, \phi_K)_K + \sum_{\sigma \in \mathcal{E}_K} \psi(\widehat{p_\sigma^n}) \mathbf{w}_{K,\sigma}^n + (F(P_K^n), \phi_K)_K = (q, \phi_K)_K - (\nabla \cdot \tilde{\mathbf{r}}^n, \phi_K)_K \qquad \forall K \in \mathcal{T}_h\,, \tag{3.23b}$$

where $\mathbf{w}_{K,\sigma}^n = \langle \mathbf{w}^n \cdot \mathbf{n}, 1 \rangle_\sigma$ and $\widehat{p_\sigma^n}$ is the upwind value defined by

$$\widehat{p_\sigma^n} := \begin{cases} P_K^n & \text{if } \mathbf{w}_{K,\sigma}^n \geq 0 \\ P_L^n & \text{if } \mathbf{w}_{K,\sigma}^n < 0 \end{cases}$$

if $\sigma$ is an interior side between the elements $K$ and $L$,

$$\widehat{p_\sigma^n} := \begin{cases} P_K^n & \text{if } \mathbf{w}_{K,\sigma}^n \geq 0 \\ \langle p_D^n, 1 \rangle_\sigma / |\sigma| & \text{if } \mathbf{w}_{K,\sigma}^n < 0 \end{cases}$$

if $\sigma$ is a Dirichlet boundary side, and $\widehat{p_\sigma^n} := P_K^n$ if $\sigma$ is a Neumann boundary side. The linearization of the system (3.23a)–(3.23b) has again the form (3.18), with this time $\mathbb{C} = -\mathbb{B}^t$. The condensation applies again directly and in particular the final system has the form (3.21). The only difference is that because of the upstream weighting, $P_{1,V} \neq P_{2,V}$ in (3.19). In the expression for the fluxes through the $\mathcal{F}_{\mathcal{C}_V}$ sides, all the scalar unknowns associated with the elements sharing a side with an element from the cluster $\mathcal{C}_V$ may appear. Hence also the stencil of the final matrix is in this case wider: on a row of the final matrix corresponding to an element $K \in \mathcal{T}_h$, the only possible nonzero entries are on columns corresponding to $L \in \mathcal{T}_h$ such that $L$ shares a common side with an element $M \in \mathcal{T}_h$ such that $M$ and $K$ share a common vertex. Finally, a similar observation to Remark 3.4.1 holds also in this case. Shall $\mathbb{A}$ and $\mathbb{B}$ be constant, we only need to upload $\mathbb{D}$, $F$, and $G$ on each time and linearization step, as in the finite volume method.

## 3.5 Numerical experiments

We give the results of several numerical experiments in two space dimensions in this section. We first compare the computational cost of the proposed condensation of the lowest-order mixed finite element method with standard mixed solution approaches for elliptic and parabolic problems. We then present a comparison of precision and efficiency between the condensed mixed finite element, finite volume, and combined finite volume–finite element methods for a nonlinear parabolic problem. We use the basic local condensation matrices associated with vertices; these are not always positive definite, but are always invertible.

We perform the simulations on unstructured triangular meshes, given as regular refinements (each triangle is refined into four triangles by joining its edges midpoints) of some mesh from Figure 3.7. In the mesh A, the minimal and maximal angles are equal to 29.1 and 82.7 degrees, in the mesh B to 29.1 and 84.8 degrees, in the mesh C to 15.3 and 135 degrees, and in the mesh D to 15.3 and 142 degrees, respectively. We denote the number of refinements by $r$ ($r = 0$

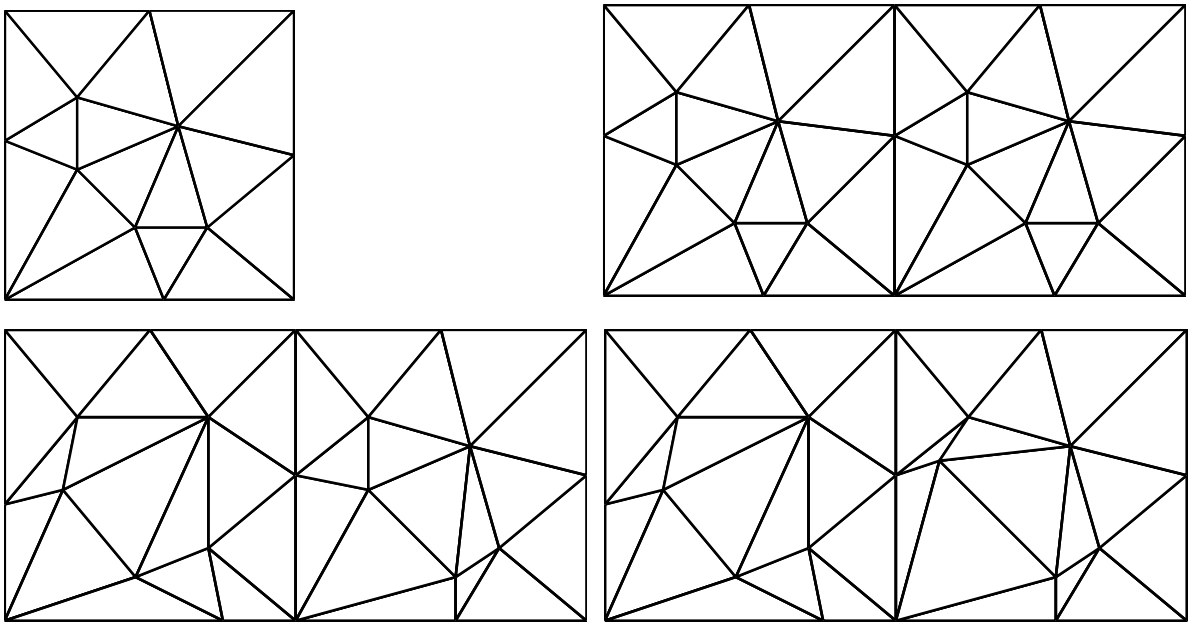

Figure 3.7: Initial meshes A (top left), B (top right), C (bottom left), and D (bottom right)

corresponds to the initial mesh). For a parabolic problem on a time interval $(0, T)$, the initial time step is equal to $T/2$ and is divided by two each time the space mesh is refined. Since the discrete maximum principle is not necessarily satisfied by the considered numerical schemes, we prolong each function $\beta(p)$ only defined for positive values also for negative values by $\beta(-p) = -\beta(p)$. In the tables with results, we shall use the abbreviation SPD for a symmetric positive definite matrix, NPD for a nonsymmetric but positive definite matrix (recall that a real matrix $\mathbb{M} \in \mathbb{R}^{M\times M}$ is positive definite if $X^t\mathbb{M}X > 0$ for all $X \in \mathbb{R}^M$, $X \neq 0$), and NID for a nonsymmetric indefinite matrix. We further use st. for the stencil, i.e. for the maximum number of nonzero entries on each matrix row, and cond. for the 2-norm condition number (defined for a matrix $\mathbb{M}$ by $\|\mathbb{M}\|_2\|\mathbb{M}^{-1}\|_2$, or equivalently by the ratio of its largest and smallest singular value).

We employ two iterative methods for the solution of systems of linear equations with sparse matrices. If the matrix is symmetric and positive definite, we use the conjugate gradients (CG) method [73, 103]. For nonsymmetric matrices, we employ the bi-conjugate gradients stabilized (Bi-CGStab, in tables abbreviated as Bi-CGS) method [103, 117]. In all considered cases, the nonsymmetric matrices are negative-stable (all their eigenvalues have positive real parts, which is in particular the case when the system matrix is positive definite), which is an essential requirement for a reasonably fast convergence of the Bi-CGStab method. To accelerate the convergence of these methods, we use incomplete Cholesky (IC) or incomplete LU (ILU) factorizations with a specified drop tolerance, cf. [111]. We denote the preconditioned methods by PCG and PBi-CGStab (PBi-CGS), respectively. In order to stop the iterative process, we monitor the relative residual $\|Y - \mathbb{M}\tilde{X}\|_2/\|Y\|_2$, where $\tilde{X}$ is the approximate solution to the system $\mathbb{M}X = Y$. We focus on iterative solvers since they permit an efficient solution of nonlinear problems, combined with the Newton method and a suitable preconditioning.

All the computations were done in a C++ code in double precision on a notebook with Intel Pentium 4-M 1.8 GHz processor and MS Windows XP operating system. Machine precision was in power of $10^{-16}$. All the matrix operations were done with the help of MATLAB 6.1.

| | Ref. | Unkn. | Matr. | St. | Cond. | Bi-CGS | Iter. | CG | Iter. |
|---|---|---|---|---|---|---|---|---|---|
| CMFE | 3 | 1024 | NPD | 14 | 721 | 0.20 | 76.5 | | |
| | 4 | 4096 | NPD | 14 | 2882 | 1.43 | 147.5 | | |
| | 5 | 16384 | NPD | 14 | 11523 | 12.55 | 295.5 | | |
| | 6 | 65536 | NPD | 14 | 46093 | 117.58 | 555.5 | | |
| MHFE | 3 | 1504 | SPD | 5 | 1397 | 0.31 | 118.0 | 0.22 | 157 |
| | 4 | 6080 | SPD | 5 | 5616 | 2.43 | 230.5 | 1.75 | 316 |
| | 5 | 24448 | SPD | 5 | 22499 | 23.40 | 449.5 | 16.87 | 623 |
| | 6 | 98048 | SPD | 5 | 89995 | 227.04 | 864.0 | 162.09 | 1226 |

Table 3.1: Comparison of the computational cost of the condensed and hybridized mixed finite element methods, problem (3.24), mesh A

### 3.5.1 Condensed mixed finite element method for elliptic problems

For $\Omega = (0,1) \times (0,1)$, we consider the problem

$$-\triangle p = -2e^x e^y \tag{3.24}$$

with a Dirichlet boundary condition given by the exact solution $p(x,y) = e^x e^y$ and the initial mesh A from Figure 3.7. We compare the computational cost of the condensation of the mixed finite element method proposed in this chapter and of the hybridization of the mixed finite element method onto the Lagrange multipliers associated with the edges.

We compare the number of unknowns (number of triangles for the condensed and number of edges for the hybridized mixed finite element method), symmetry, positive definiteness, stencil, and the condition number of the system matrices in Table 3.1. Recall that the system matrix of the mixed-hybrid method is in the given case equivalent to that of the nonconforming finite element method, cf. [38], Lemma 1.8.1, or a more detailed study in Section 4.6 of this thesis. We further give the CPU time in seconds and the number of iterations necessary to decrease the relative residual below 1e-10. We have used a zero start vector.

One needs about 1.35-times less CPU time for the condensed version than for the hybridized version of the mixed finite element method. If the system matrix may become nonsymmetric (convection–diffusion problems, nonsymmetric diffusion tensors), then e.g. the Bi-CGStab method will be necessary also for the mixed-hybrid method. One may expect more important computational savings in this case, as it is indicated by the use of this method in the present case (up to 2-times less the CPU time). Essential computational savings are however confirmed in the next section for (nonlinear) parabolic problems, where also a detailed study of the influence of the coefficients of the equation at hand, of the shapes of the elements of the mesh, and of the preconditioning is performed.

### 3.5.2 Condensed mixed finite element method for nonlinear parabolic problems

We compare in this section the condensed and standard mixed finite element methods for several nonlinear parabolic (convection–)reaction–diffusion problems, which may involve discontinuous coefficients and inhomogeneous and anisotropic diffusion tensors.

| | Unkn. | Matr. | St. | Cond. | Bi-CGS | Iter. | CPU | ILU | PBi-CGS | Iter. |
|---|---|---|---|---|---|---|---|---|---|---|
| CMFE | 128 | NPD | 14 | 37 | 0.02 | 29.5 | 0.02 | 0.01 | 0.01 | 2.0 |
| | 512 | NPD | 14 | 109 | 0.06 | 50.0 | 0.02 | 0.01 | 0.01 | 2.5 |
| | 2048 | NPD | 14 | 298 | 0.37 | 80.5 | 0.10 | 0.06 | 0.04 | 3.0 |
| | 8192 | NPD | 14 | 747 | 2.45 | 122.5 | 0.68 | 0.38 | 0.30 | 5.0 |
| | 32768 | NPD | 14 | 1753 | 14.24 | 175.0 | 4.75 | 2.95 | 1.80 | 7.0 |
| | | | | | CG | | | IC | PCG | |
| MFE | 204 | SPD | 5 | 290 | 0.05 | 110 | 0.02 | 0.01 | 0.01 | 5 |
| | 792 | SPD | 5 | 764 | 0.14 | 206 | 0.04 | 0.02 | 0.02 | 7 |
| | 3120 | SPD | 5 | 1770 | 0.95 | 333 | 0.18 | 0.08 | 0.10 | 11 |
| | 12384 | SPD | 5 | 3820 | 5.36 | 508 | 1.21 | 0.58 | 0.63 | 14 |
| | 49344 | SPD | 5 | 7974 | 34.45 | 743 | 8.17 | 3.83 | 4.34 | 18 |

Table 3.2: Comparison of the computational cost of the condensed and standard mixed finite element methods, first time and linearization step, problem (3.25), tensor (3.26), mesh B

### A reaction–diffusion problem

For $\Omega = (0,2) \times (0,1)$ and a time interval $(0,1)$, we consider the nonlinear reaction–diffusion problem

$$\frac{\partial (p + p^\alpha)}{\partial t} - \nabla \cdot (\mathbf{S} \nabla p) + 3p + \alpha p^\alpha = 0 \tag{3.25}$$

with $\alpha = 0.5$ and either

$$\mathbf{S} = \begin{pmatrix} 1 & 0 \\ 0 & 1 \end{pmatrix} \text{ in } \Omega \tag{3.26}$$

or

$$\mathbf{S} = \begin{pmatrix} 1 & 0 \\ 0 & 1 \end{pmatrix} \text{ for } x < 1\,, \quad \mathbf{S} = \begin{pmatrix} 2 & -1 \\ -1 & 2 \end{pmatrix} \text{ for } x > 1\,. \tag{3.27}$$

Initial and Dirichlet boundary conditions are given by the exact solution $p(x,y,t) = e^x e^y e^{-t}/e^3$. Notice that the flux of the solution given by $-\mathbf{S}\nabla p$ has a continuous normal trace across the discontinuity line $x = 1$ for the diffusion tensor (3.27). The derivative of the function $p^\alpha$, $\alpha = 0.5$, blows up in 0 but the problem is not really degenerate parabolic, since the exact solution does not take the value of 0. We perform the simulations starting from the meshes B and C from Figure 3.7. We consider the condensation of the mixed finite element method (3.21) and the mixed finite element method (3.17a)–(3.17b). We notice that the system of equations of the mixed method has on each time and linearization step the form (3.18), where $\mathbb{D}$ is a diagonal matrix. Hence a standard solution approach is to inverse $\mathbb{D}$, then solve for $U$ the system $(\mathbb{A} - \mathbb{C}\mathbb{D}^{-1}\mathbb{B})U = F - \mathbb{C}\mathbb{D}^{-1}G$, and finally recover $P$ from $P = \mathbb{D}^{-1}(G - \mathbb{B}U)$. In fact, in the present case, $\mathbb{C} = \mathbb{B}^t$, and thus the final system matrix is symmetric. It is noted in [74] that this approach is not suitable when the term occurring in the time derivative and the reaction term are too small in comparison with the other terms, which is however not the present case. On the contrary, according to [74], such solution approach is more reliable than the hybridization of the mixed finite element method for general diffusion tensors.

We compare the properties of the system matrices on the first time and Newton linearization steps in Table 3.2, considering the tensor (3.26) and the initial mesh B. We further give

| | Unkn. | Matr. | St. | Cond. | Bi-CGS | Iter. | CPU | ILU | PBi-CGS | Iter. |
|---|---|---|---|---|---|---|---|---|---|---|
| CMFE | 128 | NPD | 14 | 61 | 0.02 | 31.0 | 0.02 | 0.01 | 0.01 | 2.0 |
| | 512 | NPD | 14 | 225 | 0.07 | 62.0 | 0.02 | 0.01 | 0.01 | 2.5 |
| | 2048 | NPD | 14 | 676 | 0.49 | 119.0 | 0.12 | 0.07 | 0.05 | 3.5 |
| | 8192 | NPD | 14 | 1814 | 3.76 | 212.0 | 0.75 | 0.39 | 0.36 | 6.0 |
| | 32768 | NPD | 14 | 4603 | 26.62 | 335.5 | 5.31 | 3.02 | 2.29 | 8.0 |
| | | | | | CG | | | IC | PCG | |
| MFE | 204 | SPD | 5 | 1358 | 0.07 | 170 | 0.02 | 0.01 | 0.01 | 6 |
| | 792 | SPD | 5 | 4314 | 0.36 | 409 | 0.04 | 0.02 | 0.02 | 10 |
| | 3120 | SPD | 5 | 11506 | 2.23 | 836 | 0.28 | 0.12 | 0.16 | 16 |
| | 12384 | SPD | 5 | 28188 | 15.93 | 1456 | 1.61 | 0.68 | 0.93 | 20 |
| | 49344 | SPD | 5 | 65024 | 108.51 | 2279 | 11.75 | 5.76 | 5.99 | 27 |

Table 3.3: Comparison of the computational cost of the condensed and standard mixed finite element methods, first time and linearization step, problem (3.25), tensor (3.27), mesh C

the CPU time in seconds and the number of iterations necessary to decrease the relative residual below 1e-8 by the Bi-CGStab and CG methods, respectively, without any preconditioning. We then use the incomplete LU and Cholesky factorizations, respectively, as preconditioners. The drop tolerance is chosen in such way that the sum of CPU times for the preconditioning and the solution of the preconditioned system was minimal. We give in Table 3.2 the separate times as well as their sum (CPU) and the number of iterations of the preconditioned method. We have always used a zero start vector. We report finally in Table 3.3 the same values for the case of the tensor (3.27) and the initial mesh C.

The CPU time of the condensed mixed finite element method is about 2-times shorter than the CPU time of the standard approach in the case of the tensor (3.26) and the initial mesh B. When full-matrix and discontinuous diffusion tensor (3.27) and a less regular mesh C are used, then the CPU time of the condensed version is more than 4-times shorter when no preconditioning is used and more than 2-times shorter with preconditioning. Note the important increase of the condition number of the system matrix of the standard mixed finite element method for the tensor (3.27).

### A convection–reaction–diffusion problem

For $\Omega = (0,2)\times(0,1)$ and a time interval $(0,1)$, we consider the nonlinear convection–reaction–diffusion problem

$$\frac{\partial(p+p^\alpha)}{\partial t} - \nabla\cdot(\mathbf{S}\nabla p) + \nabla\cdot(p\mathbf{w}) + \alpha p^\alpha = 0 \tag{3.28}$$

with $\alpha = 0.5$ and either

$$\mathbf{S} = \begin{pmatrix} 1 & 0 \\ 0 & 1 \end{pmatrix} \text{ in } \Omega\,, \quad \mathbf{w} = (3,0) \text{ in } \Omega \tag{3.29}$$

or

$$\mathbf{S} = \begin{pmatrix} 1 & 0 \\ 0 & 1 \end{pmatrix} \text{ for } x<1\,, \quad \mathbf{S} = \begin{pmatrix} 8 & -7 \\ -7 & 20 \end{pmatrix} \text{ for } x>1\,,$$
$$\mathbf{w} = (3,0) \text{ for } x<1\,, \quad \mathbf{w} = (3,12) \text{ for } x>1\,. \tag{3.30}$$

| | Unkn. | Matr. | St. | Cond. | Bi-CGS | Iter. | CPU | ILU | PBi-CGS | Iter. |
|---|---|---|---|---|---|---|---|---|---|---|
| CMFE | 128 | NPD | 14 | 39 | 0.02 | 27.0 | 0.02 | 0.01 | 0.01 | 2.0 |
| | 512 | NPD | 14 | 116 | 0.07 | 56.5 | 0.02 | 0.01 | 0.01 | 2.5 |
| | 2048 | NPD | 14 | 311 | 0.38 | 82.5 | 0.11 | 0.06 | 0.05 | 3.5 |
| | 8192 | NPD | 14 | 768 | 2.65 | 139.0 | 0.75 | 0.41 | 0.34 | 5.5 |
| | 32768 | NPD | 14 | 1782 | 17.14 | 191.5 | 4.85 | 2.95 | 1.90 | 7.0 |
| MFE | 204 | NPD | 5 | 405 | 0.06 | 95.5 | 0.02 | 0.01 | 0.01 | 2.0 |
| | 792 | NPD | 5 | 917 | 0.22 | 153.0 | 0.07 | 0.03 | 0.04 | 3.0 |
| | 3120 | NPD | 5 | 1949 | 1.36 | 282.0 | 0.34 | 0.14 | 0.20 | 4.0 |
| | 12384 | NPD | 5 | 4016 | 8.47 | 406.5 | 2.57 | 0.94 | 1.63 | 5.0 |
| | 49344 | NPD | 5 | 8181 | 51.18 | 553.0 | 17.63 | 6.94 | 10.69 | 6.0 |

Table 3.4: Comparison of the computational cost of the condensed and standard mixed finite element methods, first time and linearization step, problem (3.28), coefficients (3.29), mesh B

Initial and Dirichlet boundary conditions are again given by the exact solution $p(x, y, t) = e^x e^y e^{-t}/e^3$. Notice that in the case of the coefficients given by (3.30), the velocity field $\mathbf{w}$ as well as the flux of the solution given by $-\mathbf{S}\nabla p + (p\mathbf{w})$ have a continuous normal trace across the discontinuity line $x = 1$. We perform the simulations on refinements of the meshes B, C, and D from Figure 3.7. The problem is not convection-dominated, and hence we can use the mixed finite element method (3.17a)–(3.17b). Notice that the associated linear system on each time and linearization step has again the form (3.18) with $\mathbb{D}$ a diagonal matrix. Hence the same solution approach as in the previous section can be used. In this case however $\mathbb{C} \neq \mathbb{B}^t$, and thus the final system for $U$ is nonsymmetric.

We compare the properties of the linear systems on the first time and Newton linearization steps for different combinations of coefficients and meshes in Tables 3.4, 3.5, and 3.6. The settings are the same as in the previous section, except for the fact that we have to use the Bi-CGStab method and the LU incomplete factorization also for the standard mixed approach in view of the nonsymmetry of its system matrices.

One can observe that the increase of the condition number of the system matrix of the condensed mixed finite element method with less regular coefficients and meshes in much less important than that of the standard mixed finite element method. Hence the CPU time of the unpreconditioned Bi-CGStab method for the condensed version is about 3-times shorter for the coefficients (3.29) and mesh B, but about 10-times shorter for the coefficients (3.30) and meshes C and D. Using the preconditioning by the LU incomplete factorization considerably smears the difference. The CPU time of the condensed version is then about 3.5-times shorter for the coefficients (3.29) and mesh B and 4-times shorter for the coefficients (3.30) and mesh C. The system matrix of the condensed mixed finite element method looses the positive definiteness property while changing from the mesh C to the mesh D when the coefficients (3.30) are considered. It appears that this transition is connected with a remarkable 50% increase in the CPU time in the case where the preconditioning is used. The system matrix of the standard mixed finite element method stays positive definite and the increase in the CPU time while changing from mesh C to mesh D with the coefficients (3.30) is about 10%. Hence the CPU time of the condensed version is about 3-times shorter for the coefficients (3.30) and mesh D, while using the preconditioning.

| | Unkn. | Matr. | St. | Cond. | Bi-CGS | Iter. | CPU | ILU | PBi-CGS | Iter. |
|---|---|---|---|---|---|---|---|---|---|---|
| CMFE | 128 | NPD | 14 | 470 | 0.04 | 70.0 | 0.02 | 0.01 | 0.01 | 2.0 |
| | 512 | NPD | 14 | 1665 | 0.21 | 149.5 | 0.03 | 0.01 | 0.02 | 2.5 |
| | 2048 | NPD | 14 | 4824 | 1.47 | 322.5 | 0.12 | 0.07 | 0.05 | 3.5 |
| | 8192 | NPD | 14 | 12523 | 8.66 | 474.5 | 0.88 | 0.56 | 0.32 | 5.0 |
| | 32768 | NPD | 14 | 31368 | 61.53 | 787.5 | 7.47 | 5.46 | 2.01 | 5.5 |
| MFE | 204 | NPD | 5 | 13849 | 0.23 | 412.5 | 0.02 | 0.01 | 0.01 | 2.0 |
| | 792 | NPD | 5 | 39935 | 1.38 | 1105.5 | 0.04 | 0.02 | 0.02 | 2.5 |
| | 3120 | NPD | 5 | 103342 | 12.12 | 2419.5 | 0.41 | 0.18 | 0.23 | 3.0 |
| | 12384 | NPD | 5 | 250923 | 103.42 | 5390.5 | 3.06 | 1.32 | 1.74 | 3.5 |
| | 49344 | NPD | 5 | 586375 | 617.26 | 7145.5 | 29.88 | 14.96 | 14.92 | 4.0 |

Table 3.5: Comparison of the computational cost of the condensed and standard mixed finite element methods, first time and linearization step, problem (3.28), coefficients (3.30), mesh C

| | Unkn. | Matr. | St. | Cond. | Bi-CGS | Iter. | CPU | ILU | PBi-CGS | Iter. |
|---|---|---|---|---|---|---|---|---|---|---|
| CMFE | 128 | NID | 14 | 613 | 0.03 | 74.0 | 0.02 | 0.01 | 0.01 | 2.0 |
| | 512 | NID | 14 | 2232 | 0.26 | 185.5 | 0.03 | 0.01 | 0.02 | 2.5 |
| | 2048 | NID | 14 | 6512 | 1.57 | 326.5 | 0.19 | 0.09 | 0.10 | 3.5 |
| | 8192 | NID | 14 | 16755 | 9.41 | 521.5 | 1.37 | 0.61 | 0.76 | 4.0 |
| | 32768 | NID | 14 | 41716 | 73.20 | 903.5 | 11.89 | 5.36 | 6.53 | 5.5 |
| MFE | 204 | NPD | 5 | 17156 | 0.25 | 441.5 | 0.02 | 0.01 | 0.01 | 2.0 |
| | 792 | NPD | 5 | 49995 | 1.32 | 1063.5 | 0.05 | 0.02 | 0.03 | 2.5 |
| | 3120 | NPD | 5 | 131073 | 13.62 | 2691.5 | 0.47 | 0.20 | 0.27 | 3.0 |
| | 12384 | NPD | 5 | 319842 | 87.93 | 4222.5 | 3.36 | 1.62 | 1.74 | 3.5 |
| | 49344 | NPD | 5 | 750271 | 686.64 | 7248.0 | 32.68 | 15.77 | 16.91 | 4.5 |

Table 3.6: Comparison of the computational cost of the condensed and standard mixed finite element methods, first time and linearization step, problem (3.28), coefficients (3.30), mesh D

| | Unkn. | Matr. | St. | Cond. | Bi-CGS | Iter. | CPU | Per. | ILU | PBi-CGS | Iter. |
|---|---|---|---|---|---|---|---|---|---|---|---|
| CU-MFE | 128 | NPD | 19 | 42 | 0.02 | 25.5 | 0.02 | | 0.01 | 0.01 | 2.0 |
| | 512 | NPD | 19 | 120 | 0.09 | 57.0 | 0.02 | | 0.01 | 0.01 | 2.5 |
| | 2048 | NPD | 19 | 318 | 0.46 | 88.0 | 0.11 | | 0.06 | 0.05 | 3.0 |
| | 8192 | NPD | 19 | 777 | 2.99 | 138.5 | 0.68 | | 0.36 | 0.32 | 5.0 |
| | 32768 | NPD | 19 | 1792 | 18.86 | 210.5 | 4.89 | | 2.87 | 2.02 | 7.5 |
| U-MFE | 332 | NPD | 7 | 17 | 0.18 | 235.5 | 0.03 | 0.01 | 0.01 | 0.01 | 2.0 |
| | 1304 | NPD | 7 | 29 | 1.17 | 549.5 | 0.09 | 0.01 | 0.03 | 0.05 | 2.5 |
| | 5168 | NPD | 7 | 67 | 13.01 | 1540.5 | 0.48 | 0.03 | 0.15 | 0.30 | 3.5 |
| | 20576 | NPD | 7 | 168 | 124.06 | 3561.5 | 2.83 | 0.32 | 0.98 | 1.53 | 4.0 |
| | 82112 | NPD | 7 | 393 | 3233.05 | 16763.5 | 15.70 | 1.35 | 4.92 | 9.43 | 6.0 |

Table 3.7: Comparison of the computational cost of the condensed and standard upwind-mixed finite element methods, first time and linearization step, problem (3.28), coefficients (3.29), mesh B

#### A convection–reaction–diffusion problem and the upwind-mixed method

We consider here once more the problem (3.28) with coefficients (3.29) and mesh B. This time, we employ the upwind-mixed finite element method (3.23a)–(3.23b) and the corresponding condensed version.

We compare the properties of the linear systems on the first time and Newton linearization steps in Table 3.7. Although there is an increase in the stencil of the condensed upwind-mixed finite element method, the system matrix condition number and CPU times are very much like for the condensed mixed finite element method, cf. Table 3.4. The system for the upwind-mixed finite element method on each time and linearization step has again the form (3.18). The matrix $\mathbb{D}$ is however in this case not diagonal, and hence we cannot easily eliminate the scalar unknowns $P$. We thus consider the whole matrix for the unknowns $U$ and $P$. This matrix is very well conditioned, nonsymmetric, positive definite, and negative-stable, but the direct application of the Bi-CGStab method does not lead to satisfactory results, cf. Table 3.7. Also the direct LU incomplete factorization is almost impossible, since the LU factors tend to considerably increase the fill-in. A suitable solution approach however seems to be to first perform the column minimum degree permutation [70]. The matrix with permuted columns then has sparser LU incomplete factors, which can in turn be successfully used as preconditioners. We report in Table 3.7 the CPU times necessary for finding the column minimum degree permutation, LU incomplete factorization of the matrix with permuted columns, and for the solution of the preconditioned systems by the Bi-CGStab method, as well as the sum of these times (CPU). In the present case, the condensation reduces the CPU time by a factor better than 3.

### 3.5.3 Comparison of the condensed mixed finite element, finite volume, and combined finite volume–finite element methods

We compare in this section the precision and efficiency of the discretization schemes studied in this thesis for a nonlinear convection–reaction–diffusion problem.

| Method | Unkn. | Matr. | St. | Cond. |
|---|---|---|---|---|
| FV | 8192 | NPD | 4 | 1704 |
| CMFE | 8192 | NPD | 14 | 768 |
| FV–FE | 4001 | NPD | 8 | 281 |
| FV–NCFE | 12192 | NPD | 5 | 1501 |

Table 3.8: Characteristics of the system matrices on the first time and linearization steps, problem (3.28), coefficients (3.29), Dirichlet boundary conditions, mesh B, $r = 4$

| Method | Unkn. | Matr. | St. | Cond. |
|---|---|---|---|---|
| CMFE | 8192 | NID | 14 | 19589 |
| FV–FE | 4032 | NPD | 8 | 12965 |
| FV–NCFE | 12224 | NPD | 5 | 59029 |

Table 3.9: Characteristics of the system matrices on the first time and linearization steps, problem (3.28), coefficients (3.30), Dirichlet–Robin boundary conditions, mesh D, $r = 4$

The first considered scheme is the condensed mixed finite element (CMFE) scheme studied in this chapter. The second scheme is the combined finite volume–nonconforming finite element (FV–NCFE) scheme studied in Chapter 1. Since we will only consider piecewise constant diffusion tensors, this scheme coincides with the combined finite volume–mixed-hybrid finite element one, see Remark 1.3.5. The third scheme is the combined finite volume–finite element (FV–FE) scheme studied in Appendix 1.9 of Chapter 1. In fact, in contrast to Appendix 1.9, we shall start here from the triangular mesh and then construct the dual mesh by joining triangle barycentres with edge midpoints, as originally proposed in [67, 90]. Finally, for triangulations with acute angles and for scalar diffusion tensors, we will also consider the cell-centered finite volume (FV) scheme, cf. [61, 72]. Recall that in the FV and CMFE schemes, the degrees of freedom are associated with triangles, in the FV–FE scheme with vertices, and in the FV–NCFE scheme with edges.

We consider the problem (3.28) with various coefficients, meshes, and boundary conditions. For the FV, FV–FE, and FV–NCFE schemes, we use the local Péclet upstream weighting defined by (1.10), (1.11). Since the problem is not convection-dominated, we employ the CMFE scheme starting from the mixed finite element method (3.17a)–(3.17b). The system matrices properties on the first time and Newton linearization steps for the different methods and 4-times refined original meshes are listed in Tables 3.8 and 3.9. Initial conditions for the CMFE and FV methods are given by the mean values of the known exact solution over the triangles at time $t = 0$. For the FV–FE and FV–NCFE methods, we consider instead the point values of the exact solution at vertices and edge midpoints, respectively, at $t = 0$. The boundary conditions for the FV–FE method are given by the point values of the exact solution at the vertices lying on the boundary. For the other methods, we consider the point values in the boundary edges midpoints. A quintic (7-point) numerical integration formulae on triangles is used to evaluate the initial conditions for CMFE and FV methods, as well for error computation. It has no influence on the considered order of precision of the results.

Tables 3.10 and 3.11 give discrete relative and projection relative errors for all the compared schemes and up to five refinements of the original space-time grid, considering coefficients (3.29), mesh B, and Dirichlet boundary conditions. The discrete $L^\infty(0,T;L^2(\Omega))$

| Method \ $r$ | 0 | 1 | 2 | 3 | 4 | 5 |
|---|---|---|---|---|---|---|
| FV | 0.15130 | 0.07538 | 0.03768 | 0.01884 | 0.00942 | 0.00471 |
| PFV | 0.02914 | 0.01159 | 0.00551 | 0.00276 | 0.00140 | 0.00070 |
| CMFE | 0.14519 | 0.07221 | 0.03607 | 0.01804 | 0.00902 | 0.00451 |
| PCMFE | 0.03480 | 0.01249 | 0.00558 | 0.00276 | 0.00139 | 0.00069 |
| FV–FE | 0.04892 | 0.01665 | 0.00693 | 0.00314 | 0.00149 | 0.00073 |
| FV–NCFE | 0.02642 | 0.01146 | 0.00554 | 0.00278 | 0.00140 | 0.00070 |

Table 3.10: Discrete $L^\infty(0,T;L^2(\Omega))$ relative errors, problem (3.28), coefficients (3.29), mesh B

| Method \ $r$ | 0 | 1 | 2 | 3 | 4 | 5 |
|---|---|---|---|---|---|---|
| FV | 0.04957 | 0.02428 | 0.01215 | 0.00608 | 0.00304 | 0.00152 |
| CMFE | 0.02542 | 0.01099 | 0.00539 | 0.00273 | 0.00138 | 0.00070 |
| FV–FE | 0.13859 | 0.04922 | 0.01771 | 0.00655 | 0.00252 | 0.00102 |
| FV–NCFE | 0.03595 | 0.01495 | 0.00658 | 0.00306 | 0.00147 | 0.00072 |

Table 3.11: Discrete $L^\infty(0,T;L^2(\Omega))$ projection relative errors, problem (3.28), coefficients (3.29), mesh B

relative error is defined by

$$\max_{n\in\{1,2,\dots,N\}} \frac{\|p_h^n(\cdot)-p(\cdot,t_n)\|_{0,\Omega}}{\|p(\cdot,t_n)\|_{0,\Omega}},$$

where $p_h^n$ is the approximate solution at time $t_n$. For the FV–FE and FV–NCFE schemes, we consider piecewise linear approximations, whereas for the FV and CMFE schemes, only a piecewise constant solution is originally at disposal. Hence we use the following postprocessing technique to construct also piecewise linear approximations. In both the FV and CMFE schemes, one can easily evaluate the discrete diffusive fluxes $\{U^{\mathrm{dif}}_{K,\sigma}\}_{\sigma\in\mathcal{E}_K}$ through the edges of each triangle. In the FV scheme, $U^{\mathrm{dif}}_{K,\sigma}=(P_K-P_L)|\sigma|/d_{K,L}$, where $K$ and $L$ are the triangles sharing an interior edge $\sigma$ and $d_{K,L}$ is the distance between $\mathbf{x}_K$ and $\mathbf{x}_L$, the circumscribed circles centers (intersections of the edge orthogonal bisectors) of $K$ and $L$. This follows naturally from the definition of the scheme, cf. [61, 72]. In the considered CMFE scheme, the established unknowns $U_\sigma$, $\sigma\in\mathcal{E}_h$, represent full (the sum of convective and diffusive) fluxes through the triangle edges (in the orientation of the RTN basis functions). To obtain only diffusive fluxes, we thus subtract the convective ones, which we approximate by $U^{\mathrm{conv}}_{K,\sigma}\approx(P_K+P_L)\mathbf{w}_\sigma/2$, where again $K$ and $L$ are the triangles sharing the edge $\sigma$ and $\mathbf{w}_\sigma=\langle\mathbf{w}\cdot\mathbf{n},1\rangle_\sigma$, $\mathbf{n}$ being the unit normal vector of the edge $\sigma$, outward to $K$. Under the same principles, there are slight modifications on the boundary. Then the three fluxes on each triangle define a linear vector function, the diffusive flux, $\mathbf{u}_h^{\mathrm{dif}}|_K:=\sum_{\sigma\in\mathcal{E}_K}U^{\mathrm{dif}}_{K,\sigma}\mathbf{v}_\sigma$, where $\mathbf{v}_\sigma$ is the RTN basis function associated with the side $\sigma$, oriented outward from $K$. Note that for the elliptic diffusion problem (3.1a)–(3.1c), this would be the solution $\mathbf{u}_h$, approximation of $-\mathbf{S}\nabla p$, for the mixed finite element method. Similar approximation holds in the finite volume method, see [60]. We evaluate the function $\mathbf{u}_h^{\mathrm{dif}}$ in triangle barycentres, so as to make it a constant vector on each $K$. Now disposing by the approximation of the gradient and by one value per triangle, it is straightforward to reconstruct a linear approximation: we fix it in $\mathbf{x}_K$ by the known value $P_K$ for the finite volume method and by its mean value $P_K$ over $K$ for the mixed finite element method. Note that this approximation is elementwise linear but generally completely discon-

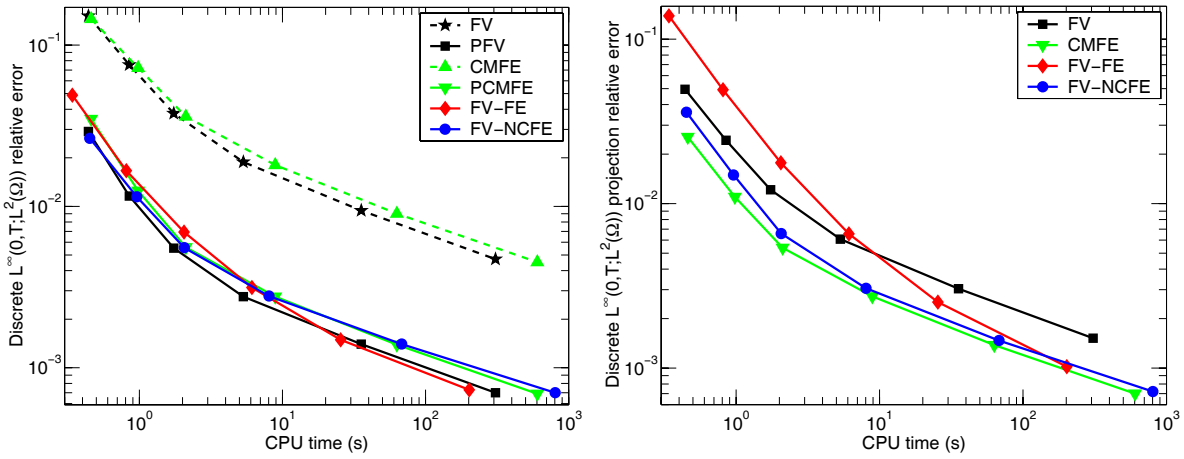


Figure 3.8: Efficiency comparison, problem (3.28), coefficients (3.29), mesh B

tinuous and that the price for its obtaining is negligible, since we do it locally. We denote by PFV and PCMFE the FV and CMFE schemes with these postprocessed solutions.

We define a discrete $L^\infty(0,T;L^2(\Omega))$ projection relative error by

$$\max_{n\in\{1,2,\dots,N\}} \frac{\|\tilde{p}_h^n(\cdot)-\tilde{p}(\cdot,t_n)\|_{0,\Omega}}{\|p(\cdot,t_n)\|_{0,\Omega}},$$

where $\tilde{p}_h^n$ is the piecewise constant approximate solution at time $t_n$. For the FV–FE and FV–NCFE schemes, we consider the solutions piecewise constant on the dual volumes, whereas for the FV and CMFE scheme, we use the original elementwise constant results. The function $\tilde{p}$ is given by the mean values of the exact solution $p$ on the dual volumes for the combined schemes and on the triangles for the FV and CMFE schemes. We finally give "efficiency comparisons" in Figure 3.8. We plot the approximation errors against the CPU times of the whole calculations. We have used the inexact Newton method, where on each linearization step, a limited number (three to four) of Bi-CGStab iterations, started from the previous linearization values, was performed. The LU incomplete factorization for preconditioning was done at the beginning of each linearization cycle. The drop tolerance was chosen in order to decrease the relative residual on the first linearization step after the limit number of iterations to about 1e-5 (the stopping criterion was 1e-8). The Newton linearization was initiated by the previous time step (initial) values and terminated whenever

$$\Big(\sum_{i=1}^{M}\big(X_i^{n,k}-X_i^{n,k-1}\big)^2\Big)^{\frac{1}{2}}\Big/\Big(\sum_{i=1}^{M}\big(X_i^{n,k}\big)^2\Big)^{\frac{1}{2}} \le \text{1e-8}\,,$$

where $X^{n,k}$ is the vector of approximation values on time and linearization steps $n$ and $k$, respectively. Three or four linearization steps on each time level were necessary.

As the FV–FE and FV–NCFE schemes produce piecewise linear approximations, their discrete $L^\infty(0,T;L^2(\Omega))$ relative errors are smaller than those of the FV and CMFE schemes that we obtain while employing the original elementwise solutions. Using instead the postprocessed values however completely eliminates this difference and on the finest mesh, all schemes give comparable results. This implies the highest efficiency for the FV–FE scheme because its lowest computational cost (for $r = 5$ and 64 time steps, the CPU times of the whole calculations were 202 seconds for the FV–FE scheme, 308 seconds for the FV scheme, 604 seconds for the CMFE scheme, and 804 seconds for the FV–NCFE scheme). The lowest discrete

| Method \ $r$ | 0 | 1 | 2 | 3 | 4 | 5 |
|---|---|---|---|---|---|---|
| CMFE | 0.14313 | 0.07135 | 0.03564 | 0.01782 | 0.00891 | 0.00446 |
| PCMFE | 0.02608 | 0.00761 | 0.00259 | 0.00110 | 0.00053 | 0.00026 |
| FV–FE | 0.03961 | 0.01345 | 0.00537 | 0.00238 | 0.00111 | 0.00054 |
| FV–NCFE | 0.01990 | 0.00680 | 0.00293 | 0.00143 | 0.00072 | 0.00036 |

Table 3.12: Discrete $L^\infty(0,T;L^2(\Omega))$ relative errors, problem (3.28), coefficients (3.30), mesh D

| Method \ $r$ | 0 | 1 | 2 | 3 | 4 | 5 |
|---|---|---|---|---|---|---|
| CMFE | 0.00821 | 0.00389 | 0.00199 | 0.00102 | 0.00052 | 0.00027 |
| FV–FE | 0.13895 | 0.04848 | 0.01713 | 0.00619 | 0.00230 | 0.00089 |
| FV–NCFE | 0.03122 | 0.01210 | 0.00475 | 0.00197 | 0.00087 | 0.00040 |

Table 3.13: Discrete $L^\infty(0,T;L^2(\Omega))$ projection relative errors, problem (3.28), coefficients (3.30), mesh D

$L^\infty(0,T;L^2(\Omega))$ projection relative error is produced by the mixed finite element method and the highest by the finite volume method. The differences are important enough to persist to the efficiency graph. The experimental order of convergence for fine meshes is $O(h,\triangle t)$, a little bit better for coarser meshes.

Tables 3.12 and 3.13 give the discrete relative and projection relative errors for the coefficients (3.30), mesh D, and Robin boundary conditions on $x = 0$ and Dirichlet boundary conditions otherwise. In the present case, the FV–FE scheme gives worse results than the FV–NCFE scheme, which is in turn outperformed by the elementwise linear postprocessed solution of the CMFE scheme. In a similar manner, the projection error of the mixed finite element method is very low, in spite of the discontinuous coefficients and inhomogeneous and anisotropic diffusion tensor. It can be seen from Table 3.9 that the conditioning of the system matrices is in this case considerably increased. However, this increase in conditioning is much more important for the FV–FE and FV–NCFE schemes than for the CMFE scheme. We have purposely chosen the mesh D, where the system matrix of the CMFE scheme fails to be positive definite. The results from Section 3.5.2 indicate that this may considerably increase the CPU time of the CMFE scheme in comparison with the mesh C, where the CMFE system matrix would be positive definite. Nevertheless, the CMFE scheme shows to be superior in this case also in terms of efficiency, followed by the two other schemes, cf. Figure 3.9. These differences are more important for the $L^\infty(0,T;L^2(\Omega))$ projection error. For the sake of completeness, we indicate that for $r = 5$ and 64 time steps, the CPU times were 242 seconds for the FV–FE scheme, 1017 seconds for the CMFE scheme, and 1153 seconds for the FV–NCFE scheme.

To conclude, we mention that we have only considered the discretization of not convection-dominated problems on fixed grids. When the problem at hand approaches the hyperbolic case, the presented schemes reduce to a finite volume scheme stabilized by an upstream weighting. They then only differ by the definition of the control volumes. A comparative study of the influence of the definition of the control volumes is given in [97]. It follows from this study that the most efficient choice is represented by triangular control volumes, then by control volumes associated with vertices, and finally by control volumes associated with edges. Finally, for a precise and efficient solution of convection-dominated problems, either local mesh refinement or the use of higher-order schemes would be necessary.

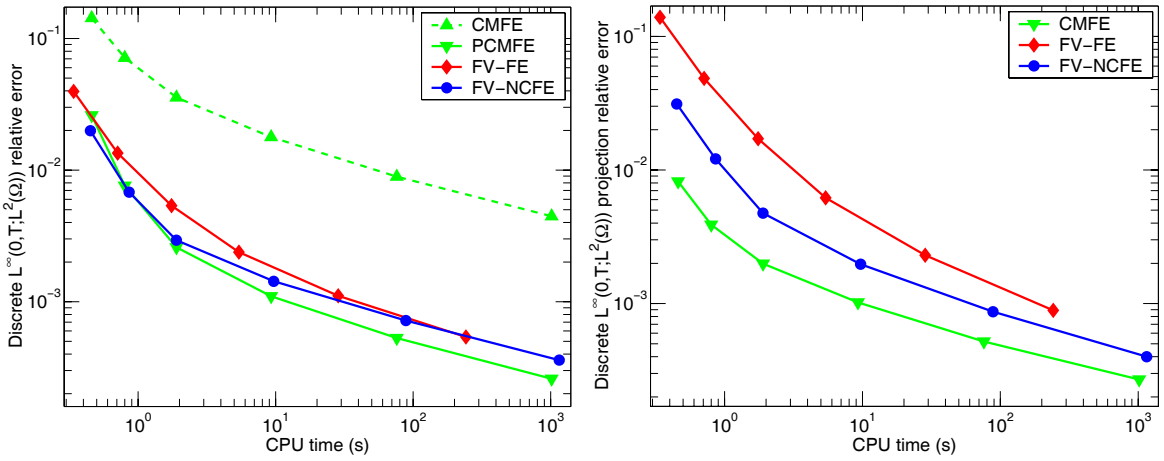


Figure 3.9: Efficiency comparison, problem (3.28), coefficients (3.30), mesh D

### 3.5.4 Conclusions

We have studied in this section the computational cost of the proposed condensation of the mixed finite element method for elliptic and (nonlinear) parabolic problems.

For elliptic diffusion problems in two space dimensions, the standard hybridization leads to systems for the number of edges unknowns with symmetric positive definite matrices with a 5-point stencil. In the proposed condensation, the number of unknowns is reduced to the number of elements (which is approximately 2/3 of the number of edges), but the system matrices are in general nonsymmetric, have a wider (about 13-point) stencil, and are positive definite only under a condition on the mesh and the diffusion tensor. This condition however allows for quite deformed triangles in the case of a piecewise constant scalar diffusion tensor. The CPU time speed-up for the test case was about 1.35. The finite volume reformulation of the mixed finite element method proposed and studied in [37, 121, 122] leads to symmetric matrices with the number of elements unknowns and a 4-point stencil. The matrices are positive definite for Delaunay triangulations and constant scalar diffusion tensors but indefinite otherwise. Hence the computational savings of the reformulation will be very probably more important than those of the condensation for Delaunay triangulations and constant scalar diffusion tensors. The situation should be much more favorable for the condensation when the mesh is not Delaunay or when the diffusion tensor is inhomogeneous and anisotropic. In three space dimensions, the finite volume reformulation is in general not possible, see [121]. In contrast, the condensation applies directly as in two space dimensions. Moreover, the number of unknowns is in this case only about 1/2 of that of the hybridization. Hence one can expect even more important computational savings than in the two-dimensional case.

We believe that the main importance of the proposed condensation lies in its application to mixed finite element discretizations of (nonlinear) parabolic convection–reaction–diffusion problems. The resulting matrices are still sparse, positive definite for a large class of meshes and diffusion tensors, nonsymmetric, and seem to be very well conditioned. Moreover, if the diffusion tensor is constant with respect to time, one can assemble and invert the local condensation matrices only once before the start of the calculation and then only work with the scalar unknowns as in the finite volume method, which still reduces the computational complexity. In two space dimensions, the number of unknowns is equal to approximately 2/3 of that of standard solution approaches in the mixed finite element method and to approximately 2/5 of

that of the upwind-mixed method. The CPU times necessary for the solution of the associated linear systems in the presented test cases were reduced by a factor 2 for parabolic reaction–diffusion problems. When convection is present, nonsymmetric matrices arise naturally also in the mixed and upwind-mixed schemes. The speed-up was in this case comprised between 3 and 4. The finite volume reformulation of the mixed finite element method is possible for parabolic reaction–diffusion problems, but leads in general to indefinite nonsymmetric systems with a limited gain in the terms of the computational cost, cf. [37, 122]. Hence the condensation seems to be much more attractive in this case. This is still emphasized by the fact that it can be very easily implemented into existing mixed finite element codes. Finally, the speed-up should be even more important in three space dimensions, where the number of unknowns of the condensation is about 1/2 of that of the mixed and 1/3 of that of the upwind-mixed schemes.

We have finally compared the condensed mixed finite element scheme with a finite volume and combined finite volume–finite element ones for nonlinear parabolic equations. For problems with discontinuous coefficients and inhomogeneous and anisotropic diffusion tensors, the mixed finite element method clearly gives better results. This, taking into account the gain in the CPU time due to the proposed condensation, makes it both more precise and efficient than the combined schemes. Also, for such problems, the combined finite volume–nonconforming/mixed-hybrid finite element scheme seems to be superior to the combined finite volume–finite element one, one of the possible reasons being that the latter scheme employs the arithmetic average of the heterogeneities. When no essential heterogeneities and discontinuities are present, the combined finite volume–finite element scheme may be the most efficient due to its low computational cost. Finally, when the diffusion operator is only a Laplacian and for Delaunay meshes, the finite volume method represents another cheap and efficient solution technique.

# Chapter 4

# Mixed and nonconforming finite element methods on a fracture network

We investigate in this chapter the lowest-order Raviart–Thomas mixed finite element method for second-order elliptic problems posed over a system of intersecting two-dimensional polygons placed in three-dimensional Euclidean space. The domain is characteristic by the presence of intersection lines shared by three or more polygons. We first construct continuous and discrete function spaces ensuring the continuity of scalar functions and an appropriate continuity of the normal trace of vector functions across such intersection lines. We then propose a variant of the lowest-order Raviart–Thomas mixed finite element method for the given problem with the domain discretized into a triangular mesh and prove its well-posedness. We finally investigate the relation of the hybridization of the considered mixed finite element method to the piecewise linear nonconforming finite element method. We extend the results known in this direction onto networks of polygons, general diffusion tensors, and general boundary conditions. This enables us in particular to efficiently implement the mixed finite element method. We verify the theoretical results on a model problem with a known analytical solution and show the application of the proposed method to the simulation of underground water flow through a system of polygons representing a network of fractures that perturbs a rock massif.

## 4.1 Introduction

The motivation of this chapter is the need to simulate water flow through underground rock massifs. Such massifs are proposed as e.g. nuclear waste repositories and they are always disrupted by a system of geological faults, *fractures*. One of the possible modeling approaches is to approximate the fractures by a network of planar polygonal disks and to consider two-dimensional Darcy flow through such network, see e.g. [5, 24, 119]. This problem is mathematically a second-order elliptic problem posed over a system of intersecting two-dimensional polygons placed in three-dimensional Euclidean space. An example of such system is given in Figure 4.1. The system in this figure is already discretized into a triangular mesh (the colors represent various values of hydraulic conductivity associated with the elements). We can easily notice an essential property of a domain created by a system of polygons that is impossible in classical planar domains: there exist interelement edges in the triangulation which belong to three or more triangular elements.

We propose and investigate in this chapter a variant of the lowest-order Raviart–Thomas mixed finite element method [105] (cf. also [33, 108]) for systems of polygons. It turns out that the essential step is the definition of appropriate continuous and discrete function spaces: we have to ensure the continuity of the scalar primary unknown (pressure) across the intersection lines between polygons and an appropriate continuity of the normal trace of the flux of the primary unknown (the hydraulic conductivity tensor times the negative of the gradient of the pressure, i.e. the Darcy velocity) across these intersection lines. The well-posedness of the weak mixed formulation is then implied by the well-posedness of the weak primal formulation, which is easy to show. To demonstrate the existence and uniqueness of the mixed approximation, we define a global interpolation operator on the discrete velocity space and prove the commuting diagram property, which implies the discrete inf–sup (Babuška [16]–Brezzi [30]) condition.

We next investigate the relation of the hybridization of the lowest-order Raviart–Thomas mixed finite element method to the piecewise linear nonconforming finite element method. It is known that the matrices of these two methods coincide for an elliptic problem with an elementwise constant diffusion tensor and a homogeneous Dirichlet boundary condition, see [15] or a detailed study given in [38]. We extend these results onto systems of polygons, nonconstant diffusion tensors, and inhomogeneous mixed Dirichlet/Neumann boundary conditions. The implementation of the considered mixed finite element method via the nonconforming method is on the one hand very efficient and on the other hand, since a polygonal domain is a trivial instance of a system of polygons, is naturally valid also for standard planar domains. Such implementation in particular avoids the inverting of local matrices (cf. [33, Section V.1.2]), usually used when the relation with the nonconforming method is not known. Recall that inverting of local matrices is a potential source of significant numerical errors, cf. [74].

The outline of this chapter is as follows. In Section 4.2 we formulate the second-order elliptic problem on a system of polygons and in Section 4.3 we define continuous and discrete function spaces on such system. We state the weak primal formulation and the nonconforming finite element approximation in Section 4.4. Section 4.5 is devoted to the lowest-order Raviart–Thomas mixed finite element method: we state and show the existence and uniqueness of the weak mixed solution and of the mixed approximation, introduce the hybridization of the mixed approximation, and give error estimates. Finally, in Section 4.6 we investigate the relation between mixed and nonconforming methods and in the first part of Section 4.7 we present the results of a numerical experiment on a model problem with a known analytical solution. We refer to the second part of Section 4.7 for the description of the application of the proposed method to the simulation of fracture flow and for a comparison with other methods.

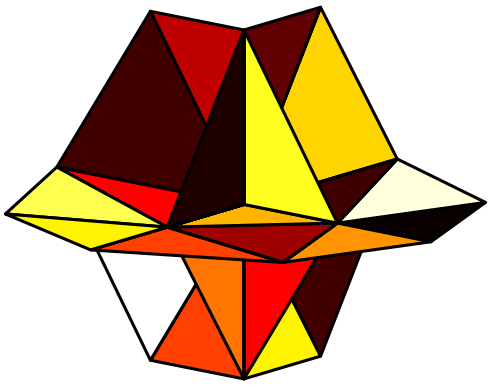

Figure 4.1: Example of a simple system of polygons (discretized into a triangular mesh)

## 4.2 Second-order elliptic problem on a system of polygons

We define the system of polygons $\mathcal{S}$ and the second-order elliptic problem on this system in this section. We set

$$\mathcal{S} := \left\{ \bigcup_{\ell \in L} \overline{\alpha_\ell} \setminus \partial\mathcal{S} \right\}, \tag{4.1}$$

where $\alpha_\ell$ is an open two-dimensional polygon placed in three-dimensional space and $L$ is the index set of polygons. We suppose that the closures $\overline{\alpha_\ell}$ of polygons are all connected into the system; the connection is only possible through an edge, not through a point. For the purpose of the mathematical description, we require that $\alpha_i \cap \alpha_j = \emptyset$ if $i \neq j$ and that $\overline{\alpha_i} \cap \overline{\alpha_j}$, $i \neq j$, is either an edge or a point or an empty set. In order to fulfill this property it is enough to divide each polygon from a general system of polygons as that of Figure 4.1 into subpolygons along each intersection line that it contains. Finally, $\partial\mathcal{S}$ is the set of those boundary points of $\alpha_\ell$, $\ell \in L$, which do not create the connection with other polygons. We suppose that there is a two-dimensional orthogonal coordinate system given in each polygon. The system of the model problem from Section 4.7 viewed in Figure 4.3 below may serve as an example. In this case $\mathcal{S}$ consists of three rectangles, denoted as four polygons $\alpha_1$–$\alpha_4$, and $\partial\mathcal{S}$ consists of twelve edges $\Gamma_1$–$\Gamma_{12}$.

We seek $p$ (a scalar function in each $\overline{\alpha_\ell}$) and $\mathbf{u}$ (a two-dimensional vector in each $\overline{\alpha_\ell}$) which are the solutions of the problem

$$\mathbf{u} = -\mathbf{K}(\nabla p + \nabla z) \quad \text{in } \alpha_\ell\,,\ \ell \in L\,, \tag{4.2a}$$

$$\nabla \cdot \mathbf{u} = q \quad \text{in } \alpha_\ell\,,\ \ell \in L\,, \tag{4.2b}$$

$$p = p_D \quad \text{on } \Gamma_D\,, \quad \mathbf{u}\cdot\mathbf{n} = u_N \quad \text{on } \Gamma_N\,, \tag{4.2c}$$

where all the variables are expressed in local coordinates of the appropriate $\alpha_\ell$ and also the differentiation is always done with respect to these local coordinates. In the context of groundwater flow the variable $p$ denotes the pressure head, $p = \tilde{p}/\varrho g$, where $\tilde{p}$ is the fluid pressure, $g$ is the gravitational acceleration constant and $\varrho$ is the fluid density, $\mathbf{u}$ is the flow velocity, $q$ represents stationary sources or sinks, $z$ is the elevation, i.e. the upward vertical three-dimensional coordinate, and $\mathbf{K}$ is the tensor of hydraulic conductivity. The equation (4.2a) is then the Darcy law, (4.2b) is the mass balance equation, and (4.2c) prescribes Dirichlet and Neumann boundary conditions. We suppose that $\Gamma_D \cap \Gamma_N = \emptyset$, $\overline{\Gamma_D} \cup \overline{\Gamma_N} = \partial\mathcal{S}$, and that the measure of $\Gamma_D$ is nonzero. Note that $\mathbf{n}$ in (4.2c) is the unit outward normal vector of the appropriate $\alpha_\ell$.

Let $f$ be an edge such that there exist polygons $\alpha_i$ and $\alpha_j$, $i \neq j$, such that $f = \overline{\alpha_i} \cap \overline{\alpha_j}$. We denote the set of such edges by $\mathcal{E}^{\text{int}}$ and the set of all $i \in L$ such that $f \subset \partial\alpha_i$ by $I_f$. The system (4.2a)–(4.2c) is completed by requiring

$$p|_{\overline{\alpha_i}} = p|_{\overline{\alpha_j}} \quad \text{on } f \qquad \forall f \in \mathcal{E}^{\text{int}}\,, \forall i,j \in I_f\,, \tag{4.3a}$$

$$\sum_{i\in I_f} \mathbf{u}|_{\overline{\alpha_i}} \cdot \mathbf{n}_{f,\alpha_i} = 0 \quad \text{on } f \qquad \forall f \in \mathcal{E}^{\text{int}}\,, \tag{4.3b}$$

where $\mathbf{n}_{f,\alpha_i}$ is the unit outward normal vector of the edge $f$ with respect to the polygon $\alpha_i$. The equations (4.3a)–(4.3b) express the continuity of $p$ across the interpolygon boundaries and the mass balance of $\mathbf{u}$ across these boundaries (what is the outflow from one polygon has to be the inflow into the neighboring ones). We finally suppose that the second rank tensor $\mathbf{K}$ is symmetric and uniformly positive definite in each $\alpha_\ell$, i.e.

$$\mathbf{K}(\mathbf{x})\boldsymbol{\eta}\cdot\boldsymbol{\eta} \geq c_{\mathbf{K}}\boldsymbol{\eta}\cdot\boldsymbol{\eta}\,, \quad c_{\mathbf{K}} > 0 \tag{4.4}$$

for any $\boldsymbol{\eta} \in \mathbb{R}^2$ and almost all $\mathbf{x} \in \alpha_\ell$, for all $\ell \in L$.

## 4.3 Function spaces for nonconforming and mixed finite elements

We give in this section the definitions of function spaces used in the sequel. We will use the spaces $H^1(\alpha_\ell)$ and $\mathbf{H}(\mathrm{div},\alpha_\ell)$ on separate polygons with certain matching conditions on the interpolygon boundaries in order to define the spaces $H^1(\mathcal{S})$ and $\mathbf{H}(\mathrm{div},\mathcal{S})$ on the whole system $\mathcal{S}$. We introduce also the discrete counterparts of these spaces.

### 4.3.1 Continuous function spaces

We use the product of the spaces $L^p$, $1 \leq p \leq \infty$, on separate polygons in order to define the spaces $L^p(\mathcal{S})$ and $\mathbf{L}^p(S)$ on the system $\mathcal{S}$,

$$L^p(\mathcal{S}) := \prod_{\ell\in L} L^p(\alpha_\ell)\,, \quad \mathbf{L}^p(\mathcal{S}) := L^p(\mathcal{S}) \times L^p(\mathcal{S})\,. \tag{4.5}$$

For each polygon $\alpha_\ell$, we denote by $H^1(\alpha_\ell)$ the Sobolev space of scalar functions with square-integrable weak derivatives, $H^1(\alpha_\ell) = \{\varphi \in L^2(\alpha_\ell)\,;\, \nabla\varphi \in \mathbf{L}^2(\alpha_\ell)\}$. We define $H^1(\mathcal{S})$ as the space of functions whose restrictions to each $\alpha_\ell$ are from $H^1(\alpha_\ell)$ and that coincide on the interpolygon boundaries in the sense of traces,

$$\begin{aligned} H^1(\mathcal{S}) := \big\{ & v \in L^2(\mathcal{S})\,;\, v|_{\alpha_\ell} \in H^1(\alpha_\ell) \quad \forall \ell \in L\ , \\ & (v|_{\alpha_i})|_f = (v|_{\alpha_j})|_f \quad \forall f \in \mathcal{E}^{\text{int}}\,, \forall i,j \in I_f \big\}\ . \end{aligned} \tag{4.6}$$

We then have the space $H^1_D(\mathcal{S})$ of the functions from $H^1(\mathcal{S})$ vanishing on $\Gamma_D$ and the spaces $H^{\frac12}(\partial\mathcal{S})$, $H^{-\frac12}(\partial\mathcal{S})$, $H^{\frac12}(\Gamma_D)$, and $H^{-\frac12}(\Gamma_N)$ as in the standard planar case.

For each polygon $\alpha_\ell$, we denote by $\mathbf{H}(\mathrm{div},\alpha_\ell)$ the space of vector functions with square-integrable weak divergences, $\mathbf{H}(\mathrm{div},\alpha_\ell) = \{\mathbf{v} \in \mathbf{L}^2(\alpha_\ell)\,;\, \nabla\cdot\mathbf{v} \in L^2(\alpha_\ell)\}$. We define $\mathbf{H}(\mathrm{div},\mathcal{S})$ as the space of functions whose restrictions to each $\alpha_\ell$ are from $\mathbf{H}(\mathrm{div},\alpha_\ell)$ and whose sum of normal traces over all polygons sharing a given edge $f \in \mathcal{E}^{\text{int}}$ is zero in the appropriate sense,

$$\begin{aligned} \mathbf{H}(\mathrm{div},\mathcal{S}) := \Big\{ & \mathbf{v} \in \mathbf{L}^2(\mathcal{S})\,;\, \mathbf{v}|_{\alpha_\ell} \in \mathbf{H}(\mathrm{div},\alpha_\ell) \quad \forall \ell \in L\,, \sum_{i\in I_f} \langle \mathbf{v}|_{\alpha_i}\cdot\mathbf{n}_{\partial\alpha_i}, \varphi_i\rangle_{\partial\alpha_i} = 0 \\ & \forall \varphi_i \in H^1_{\partial\alpha_i\setminus f}(\alpha_i)\,,\ \varphi_i|_f = \varphi_j|_f\ \forall i,j \in I_f\,, \forall f \in \mathcal{E}^{\text{int}} \Big\}\,. \end{aligned} \tag{4.7}$$

Finally, we denote

$$\mathbf{H}_{0,N}(\mathrm{div},\mathcal{S}) := \left\{ \mathbf{v} \in \mathbf{H}(\mathrm{div},\mathcal{S})\,;\, \langle \mathbf{v}\cdot\mathbf{n},\varphi\rangle_{\partial\mathcal{S}} = 0 \quad \forall \varphi \in H^1_D(\mathcal{S}) \right\}$$

as the space of functions from $\mathbf{H}(\mathrm{div},\mathcal{S})$ such that their normal trace on $\Gamma_N$ is equal to zero in the appropriate sense.

We use $(\cdot,\cdot)_{0,\alpha_\ell}$ to denote the $L^2$ scalar product, $\|\cdot\|_{0,\alpha_\ell}$ to denote the associated $L^2$ norm, $\|\cdot\|_{1,\alpha_\ell}$ to denote the $H^1(\alpha_\ell)$ norm, and $\|\cdot\|_{\mathbf{H}(\mathrm{div},\alpha_\ell)}$ to denote the $\mathbf{H}(\mathrm{div},\alpha_\ell)$ norm given by $\|\mathbf{v}\|^2_{\mathbf{H}(\mathrm{div},\alpha_\ell)} = \|\mathbf{v}\|^2_{0,\alpha_\ell} + \|\nabla\cdot\mathbf{v}\|^2_{0,\alpha_\ell}$. The bracket $\langle \mathbf{v}\cdot\mathbf{n},\varphi\rangle_{\partial\mathcal{S}}$ denotes the duality pairing between $H^{-\frac{1}{2}}(\partial\mathcal{S})$ and $H^{\frac{1}{2}}(\partial\mathcal{S})$ and may be written formally as $\int_{\partial\mathcal{S}} \mathbf{v}\cdot\mathbf{n}\,\varphi\,\mathrm{d}\gamma(\mathbf{x})$. The norms on the spaces defined by (4.5), (4.6), and (4.7) are given by

$$\|\cdot\|^2_{\cdot,\mathcal{S}} := \sum_{\ell\in L} \|\cdot\|^2_{\cdot,\alpha_\ell}\,. \tag{4.8}$$

**Remark 4.3.1. (Continuity across the interpolygon boundaries)** *The definitions (4.6) and (4.7) express weakly the conditions (4.3a) and (4.3b). Let $\Omega\subset\mathbb{R}^2$ be a polygonal domain and let $\mathcal{S}$ be its polygonal partition. Then the definitions (4.6) and (4.7) coincide with the standard characterizations of the spaces $H^1(\Omega)$ and $\mathbf{H}(\mathrm{div},\Omega)$ (cf. [33, Propositions III.1.1 and III.1.2] or [108, Theorem 1.3]).*

Throughout this chapter, we shall suppose that $\mathbf{K}_{ij}\in L^\infty(\mathcal{S})$, $q\in L_2(\mathcal{S})$, $p_D\in H^{\frac{1}{2}}(\Gamma_D)$, and $u_N\in H^{-\frac{1}{2}}(\Gamma_N)$.

### 4.3.2 Discrete function spaces

Let us suppose a triangulation $\mathcal{T}_h$ of the system $\mathcal{S}$ such that the boundary edges lie entirely either in $\Gamma_D$ or in $\Gamma_N$. We set

$$M^0_{-1}(\mathcal{T}_h) := \left\{ \phi\in L^2(\mathcal{S})\,;\, \phi|_e \text{ is constant } \forall e\in\mathcal{T}_h \right\}.$$

We denote the set of all edges of $\mathcal{T}_h$ by $\mathcal{E}_h$, the set of all edges of $\mathcal{T}_h$ except those from $\Gamma_D$ by $\mathcal{E}_{h,D}$, and the set of all interior edges of $\mathcal{T}_h$ by $\mathcal{E}_h^{\mathrm{int}}$. We set

$$\begin{aligned} M^0_{-1}(\mathcal{E}_{h,D}) \;:=\; & \{\mu:\mathcal{E}_h\to\mathbb{R}\,;\, \mu|_f \text{ is constant } \forall f\in\mathcal{E}_h\,,\\ & \mu|_f = 0 \quad \forall f\subset\Gamma_D\}\,. \end{aligned}$$

For the nonconforming approximation, we set

$$X^1_0(\mathcal{E}_h) := \left\{\varphi\in L^2(\mathcal{S});\ \varphi|_e \text{ is linear } \forall e\in\mathcal{T}_h\,,\ \varphi \text{ is continuous in } Q_f, f\in\mathcal{E}_h^{\mathrm{int}}\right\},$$

where $Q_f$ is the midpoint of the edge $f$. The basis of $X^1_0(\mathcal{E}_h)$ is spanned by shape functions $\varphi_f$, $f\in\mathcal{E}_h$, such that $\varphi_f(Q_g)=\delta_{fg}$, $g\in\mathcal{E}_h$, $\delta$ being the Kronecker delta. A simple computation gives

$$\nabla\varphi_f|_e = \frac{|f|}{|e|}\mathbf{n}_f \qquad e\in\mathcal{T}_h\,,\ f\subset\partial e\,, \tag{4.9}$$

where $|e|$ is the area of the element $e$, $|f|$ is the length of the edge $f$, and $\mathbf{n}_f$ is the unit normal vector of the edge $f$, outward to $e$. We finally set

$$X^1_0(\mathcal{E}_{h,D}) := \left\{\varphi\in X^1_0(\mathcal{E}_h);\ \varphi(Q_f)=0 \quad \forall f\subset\Gamma_D\right\}.$$

For a given triangular element $e \in \mathcal{T}_h$, we define $\mathbf{RT}^0(e)$ as the space of linear vector functions with the basis $\mathbf{v}_i^e$, $i = 1, 2, 3$,

$$\mathbf{v}_i^e(\mathbf{x}) := \frac{1}{2|e|} \begin{pmatrix} x - x_i \\ y - y_i \end{pmatrix} \text{ if } \mathbf{x} = (x, y)^t \in e\,, \quad \mathbf{v}_i^e(\mathbf{x}) := \begin{pmatrix} 0 \\ 0 \end{pmatrix} \text{ if } \mathbf{x} \notin e\,, \tag{4.10}$$

where $(x_i, y_i)^t$ are the coordinates of the $i$-th vertex of $e$. Note that $\mathbf{v}_i^e \cdot \mathbf{n}_f$ is constant over each edge $f \subset \partial e$. The Raviart–Thomas space $\mathbf{RT}^0_{-1}(\mathcal{T}_h)$ of elementwise linear vector functions without any continuity requirement is defined by

$$\mathbf{RT}^0_{-1}(\mathcal{T}_h) := \left\{ \mathbf{v} \in \mathbf{L}^2(\mathcal{S})\,;\, \mathbf{v}|_e \in \mathbf{RT}^0(e) \quad \forall e \in \mathcal{T}_h \right\}. \tag{4.11}$$

We set the space $\mathbf{RT}^0_0(\mathcal{T}_h)$ of functions ensuring the normal trace continuity as

$$\begin{aligned} \mathbf{RT}^0_0(\mathcal{T}_h) &:= \left\{ \mathbf{v} \in \mathbf{RT}^0_{-1}(\mathcal{T}_h)\,;\, \sum_{e \in \mathcal{T}_h\,;\, f \subset \partial e} \mathbf{v}|_e \cdot \mathbf{n}_{f,e} = 0 \text{ on } f \quad \forall f \in \mathcal{E}_h^{\text{int}} \right\} \\ &= \mathbf{RT}^0_{-1}(\mathcal{T}_h) \cap \mathbf{H}(\mathrm{div}, \mathcal{S})\,. \end{aligned} \tag{4.12}$$

To characterize the discrete functions with zero normal trace on $\Gamma_N$, we finally set

$$\mathbf{RT}^0_{0,N}(\mathcal{T}_h) := \left\{ \mathbf{v} \in \mathbf{RT}^0_0(\mathcal{T}_h)\,;\, \mathbf{v} \cdot \mathbf{n} = 0 \text{ on } \Gamma_N \right\} = \mathbf{RT}^0_{-1}(\mathcal{T}_h) \cap \mathbf{H}_{0,N}(\mathrm{div}, \mathcal{S})\,.$$

## 4.4 Nonconforming finite element method

We introduce in this section a weak primal solution of the problem (4.2a)–(4.3b). We next define its piecewise linear nonconforming finite element approximation.

### 4.4.1 Weak primal solution

Let $\tilde{p} \in H^1(\mathcal{S})$ be such that $\tilde{p} = p_D$ on $\Gamma_D$ in the sense of traces. We then define:

**Definition 4.4.1. (Weak primal solution)** *As the weak primal solution of the problem (4.2a)–(4.3b), we understand a function $p = p_0 + \tilde{p}$, $p_0 \in H^1_D(\mathcal{S})$, satisfying*

$$\begin{aligned} (\mathbf{K}\nabla p_0, \nabla\varphi)_{0,\mathcal{S}} &= (q, \varphi)_{0,\mathcal{S}} - \langle u_N, \varphi\rangle_{\partial\mathcal{S}} - (\mathbf{K}\nabla z, \nabla\varphi)_{0,\mathcal{S}} \\ &\quad -(\mathbf{K}\nabla\tilde{p}, \nabla\varphi)_{0,\mathcal{S}} \qquad \forall\varphi \in H^1_D(\mathcal{S})\,. \end{aligned} \tag{4.13}$$

Existence and uniqueness of the weak primal solution follow from (4.4) and from the definition of the norms on $\mathcal{S}$ given by (4.8) using the Lax–Milgram lemma.

### 4.4.2 Nonconforming finite element approximation

We define:

**Definition 4.4.2. (Nonconforming finite element approximation)** *As the piecewise linear nonconforming finite element approximation of the problem (4.13), we understand a function $p_h = p_{0,h} + \tilde{p}$, $p_{0,h} \in X^1_0(\mathcal{E}_{h,D})$, satisfying*

$$\begin{aligned} \sum_{e \in \mathcal{T}_h} (\mathbf{K}\nabla p_{0,h}, \nabla\varphi_h)_{0,e} &= \sum_{e \in \mathcal{T}_h} \{(q, \varphi_h)_{0,e} - \langle u_N, \varphi_h\rangle_{\partial e \cap \partial\mathcal{S}} - (\mathbf{K}\nabla z, \nabla\varphi_h)_{0,e} \\ &\quad - (\mathbf{K}\nabla\tilde{p}, \nabla\varphi_h)_{0,e}\} \qquad \forall\varphi_h \in X^1_0(\mathcal{E}_{h,D})\,. \end{aligned} \tag{4.14}$$

Existence and uniqueness of the nonconforming approximation follow by the same arguments as above.

## 4.5 Raviart–Thomas mixed finite element method

We first define in this section a weak mixed solution of the problem (4.2a)–(4.3b) and show its existence and uniqueness. We then study its lowest-order Raviart–Thomas mixed finite element approximation. We finally introduce its hybridization.

### 4.5.1 Weak mixed solution

Let $\tilde{\mathbf{u}} \in \mathbf{H}(\mathrm{div}, \mathcal{S})$ be such that $\tilde{\mathbf{u}} \cdot \mathbf{n} = u_N$ on $\Gamma_N$ in the appropriate sense. We then define:

**Definition 4.5.1. (Weak mixed solution)** *As the weak mixed solution of the problem (4.2a)–(4.3b), we understand functions* $\mathbf{u} = \mathbf{u}_0 + \tilde{\mathbf{u}}$, $\mathbf{u}_0 \in \mathbf{H}_{0,N}(\mathrm{div}, \mathcal{S})$, *and* $p \in L^2(\mathcal{S})$ *such that*

$$\begin{aligned}(\mathbf{K}^{-1}\mathbf{u}_0, \mathbf{v})_{0,\mathcal{S}} - (\nabla \cdot \mathbf{v}, p)_{0,\mathcal{S}} &= -\langle \mathbf{v} \cdot \mathbf{n}, p_D \rangle_{\partial\mathcal{S}} + (\nabla \cdot \mathbf{v}, z)_{0,\mathcal{S}} \\ -\langle \mathbf{v} \cdot \mathbf{n}, z \rangle_{\partial\mathcal{S}} - (\mathbf{K}^{-1}\tilde{\mathbf{u}}, \mathbf{v})_{0,\mathcal{S}} \qquad &\forall \mathbf{v} \in \mathbf{H}_{0,N}(\mathrm{div}, \mathcal{S}) \,,\end{aligned} \tag{4.15a}$$

$$-(\nabla \cdot \mathbf{u}_0, \phi)_{0,\mathcal{S}} = -(q, \phi)_{0,\mathcal{S}} + (\nabla \cdot \tilde{\mathbf{u}}, \phi)_{0,\mathcal{S}} \qquad \forall \phi \in L^2(\mathcal{S}) \,. \tag{4.15b}$$

**Theorem 4.5.2. (Existence and uniqueness of the weak mixed solution)** *The problem (4.15a)–(4.15b) has a unique solution.*

Proof:

The coercivity of the bilinear form $(\mathbf{K}^{-1}\mathbf{u}, \mathbf{v})_{0,\mathcal{S}}$, $\mathbf{u}, \mathbf{v} \in \mathbf{H}_{0,N}(\mathrm{div}, \mathcal{S})$, on the space $\mathbf{W} = \{\mathbf{v} \in \mathbf{H}_{0,N}(\mathrm{div}, \mathcal{S}) \,;\, (\nabla \cdot \mathbf{v}, \phi)_{0,\mathcal{S}} = 0 \quad \forall \phi \in L^2(\mathcal{S})\}$ is the consequence of the uniform positive definiteness of the tensor $\mathbf{K}$ on each $\alpha_\ell$ given by (4.4). We next show that for all $q \in L^2(\mathcal{S})$ there exists $\mathbf{v} \in \mathbf{H}_{0,N}(\mathrm{div}, \mathcal{S})$ such that $(\nabla \cdot \mathbf{v}, \phi)_{0,\mathcal{S}} = (q, \phi)_{0,\mathcal{S}}$ for all $\phi \in L^2(\mathcal{S})$. This will guarantee that the divergence operator from $\mathbf{H}_{0,N}(\mathrm{div}, \mathcal{S})$ to $L^2(\mathcal{S})$ is surjective (and hence the inf–sup condition). To show this, consider for given $q \in L^2(\mathcal{S})$ the problem of finding $p \in H^1_D(\mathcal{S})$ such that

$$(\nabla p, \nabla \varphi)_{0,\mathcal{S}} = (q, \varphi)_{0,\mathcal{S}} \qquad \forall \varphi \in H^1_D(\mathcal{S}) \,. \tag{4.16}$$

The existence and uniqueness of such $p$ follow by the well-posedness of the weak primal formulation given in Section 4.4.1. We shall pose $\mathbf{v} = -\nabla p$. To justify such choice, we have to show that $\nabla p \in \mathbf{H}_{0,N}(\mathrm{div}, \mathcal{S})$ and that $-\nabla \cdot \nabla p = q$ in the appropriate sense. The second assertion is a simple consequence of (4.16), considering $\varphi \in H^1_0(\alpha_\ell)$, $\ell \in L$, as test functions in (4.16). We now proceed to show the first assertion. Let us consider an edge $f \in \mathcal{E}^{\mathrm{int}}$. We take $\varphi \in H^1_D(\mathcal{S})$ such that $\varphi$ only has as a support the polygons sharing the edge $f$ and such that $\varphi$ is zero on $\partial\alpha_i \setminus f$ for all $i \in I_f$ in the sense of traces. The second assertion gives $\nabla p|_{\alpha_\ell} \in \mathbf{H}(\mathrm{div}, \alpha_\ell)$, $\ell \in L$, and $-\sum_{i \in I_f} (\nabla \cdot \nabla p, \varphi)_{0,\alpha_i} = (q, \varphi)_{0,\mathcal{S}}$. Hence, using the Green theorem on each polygon in (4.16) with the considered $\varphi$ as the test function,

$$\begin{aligned} 0 \;=\; &\sum_{i \in I_f} (\nabla p, \nabla \varphi)_{0,\alpha_i} - (q, \varphi)_{0,\mathcal{S}} = \sum_{i \in I_f} \langle \nabla p|_{\alpha_i} \cdot \mathbf{n}_{\partial\alpha_i}, \varphi \rangle_{\partial\alpha_i} \\ &- \sum_{i \in I_f} (\nabla \cdot \nabla p, \varphi)_{0,\alpha_i} - (q, \varphi)_{0,\mathcal{S}} = \sum_{i \in I_f} \langle \nabla p|_{\alpha_i} \cdot \mathbf{n}_{\partial\alpha_i}, \varphi \rangle_{\partial\alpha_i} \,, \end{aligned}$$

which by the fact that $\varphi \in H^1(\mathcal{S})$ implies that $\nabla p \in \mathbf{H}(\mathrm{div}, \mathcal{S})$, cf. the definition (4.7). Finally, $\nabla p \in \mathbf{H}_{0,N}(\mathrm{div}, \mathcal{S})$ follows by the above technique applied to (4.16). The existence and uniqueness of the weak mixed solution follow by [33, Theorem II.1.1] or [108, Theorem 10.1]. □

### 4.5.2 Properties of the discrete velocity space

We begin with the space $\mathbf{RT}^0(e)$ for a given $e \in \mathcal{T}_h$. Its basis is given by (4.10). The dual basis to this basis is given by the functionals $N_j^e$, $j = 1, 2, 3$, where

$$N_j^e(\mathbf{u}) = \int_{f_j^e} \mathbf{u} \cdot \mathbf{n}_{\partial e} \, \mathrm{d}\gamma(\mathbf{x}) \qquad \mathbf{u} \in \mathbf{RT}^0(e)\,.$$

Each $N_j^e$ expresses the flux of $\mathbf{u}$ through one edge $f_j^e$ of $e$. The local interpolation operator is then given by

$$\pi_e(\mathbf{u}) = \sum_{i=1}^{3} N_i^e(\mathbf{u})\mathbf{v}_i^e \qquad \mathbf{u} \in (H^1(e))^2\,. \tag{4.17}$$

We now turn to the problem of finding the basis and the dual basis of $\mathbf{RT}_0^0(\mathcal{T}_h)$. Let us consider $\mathbf{u} \in \mathbf{RT}_0^0(\mathcal{T}_h)$. We set $\mathcal{N}_h = \{N_1, N_2, \ldots, N_{|I_{\mathcal{N}_h}|}\}$, where for each boundary edge $f$ such that $f \subset \partial e$, we define one functional $N_f$ by

$$N_f(\mathbf{u}) := \int_f \mathbf{u}|_e \cdot \mathbf{n}_{\partial e} \, \mathrm{d}\gamma(\mathbf{x})\,,$$

and for each interior edge $f$ shared by the elements $e_1, e_2, \ldots, e_{|I_f|}$, we define $|I_f|-1$ functionals by

$$N_{f,j}(\mathbf{u}) := \frac{1}{|I_f|}\int_f \mathbf{u}|_{e_1} \cdot \mathbf{n}_{\partial e_1} \, \mathrm{d}\gamma(\mathbf{x}) - \frac{1}{|I_f|}\int_f \mathbf{u}|_{e_{j+1}} \cdot \mathbf{n}_{\partial e_{j+1}} \, \mathrm{d}\gamma(\mathbf{x})\,, \quad j = 1, \ldots, |I_f| - 1\,.$$

We use the same denotation $I_f$ for the index set of polygons sharing a given edge $f \in \mathcal{E}^{\mathrm{int}}$ in the continuous case and for the index set of elements sharing a given edge $f \in \mathcal{E}_h^{\mathrm{int}}$ in the discrete case. We have the following lemma:

**Lemma 4.5.3. (Basis of the dual space to $\mathbf{RT}_0^0(\mathcal{T}_h)$)** *$\mathcal{N}_h$ is a basis of the dual space to $\mathbf{RT}_0^0(\mathcal{T}_h)$.*

Proof:
To prove the lemma it suffices to show that for all $\mathbf{u} \in \mathbf{RT}_0^0(\mathcal{T}_h)$, from $N_j(\mathbf{u}) = 0 \;\forall\, j = 1, \ldots, |I_{\mathcal{N}_h}|$, it follows that $\mathbf{u} = 0$. Let us suppose that $N_j(\mathbf{u}) = 0 \;\forall\, j = 1, \ldots, |I_{\mathcal{N}_h}|$. From the definition of the functionals $N_f$ on boundary edges, we have $\int_f \mathbf{u}|_e \cdot \mathbf{n}_{\partial e} \, \mathrm{d}\gamma(\mathbf{x}) = 0$ for all boundary edges $f$. Using the definition of the functionals $N_{f,j}$ on interior edges, we have $\int_f \mathbf{u}|_{e_1} \cdot \mathbf{n}_{\partial e_1} \, \mathrm{d}\gamma(\mathbf{x}) = \int_f \mathbf{u}|_{e_j} \cdot \mathbf{n}_{\partial e_j} \, \mathrm{d}\gamma(\mathbf{x})$ for all $j = 2, \ldots, |I_f|$. Considering the equality $\sum_{i \in I_f} \int_f \mathbf{u}|_{e_i} \cdot \mathbf{n}_{\partial e_i} \, \mathrm{d}\gamma(\mathbf{x}) = 0$ characterizing the continuity of the normal trace of the functions from $\mathbf{RT}_0^0(\mathcal{T}_h)$, cf. the definition (4.12), we come to $\int_f \mathbf{u}|_e \cdot \mathbf{n}_{\partial e} \, \mathrm{d}\gamma(\mathbf{x}) = 0$ for all $f \in \mathcal{E}_h$ and all $e$, $f \subset \partial e$. Since $\mathbf{RT}_0^0(\mathcal{T}_h) \subset \mathbf{RT}_{-1}^0(\mathcal{T}_h)$, $\mathbf{u} = 0$ follows. □

We set $\mathcal{V}_h = \{\mathbf{v}_1, \mathbf{v}_2, \ldots, \mathbf{v}_{|I_{\mathcal{N}_h}|}\}$, the basis of $\mathbf{RT}_0^0(\mathcal{T}_h)$, in the following way: we define one basis function $\mathbf{v}_f$ by $\mathbf{v}_f := \mathbf{v}_f^e$ for each boundary edge $f$. Here $\mathbf{v}_f^e$ is the local basis function associated with the element $e$ and its edge $f$. For each interior edge $f$ shared by the elements $e_1, e_2, \ldots, e_{|I_f|}$, we define $|I_f| - 1$ basis functions by

$$\mathbf{v}_{f,i} := \sum_{k=1,\, k \neq i+1}^{|I_f|} \mathbf{v}_f^{e_k} - (|I_f| - 1)\mathbf{v}_f^{e_{i+1}}\,, \quad i = 1, \ldots, |I_f| - 1\,.$$

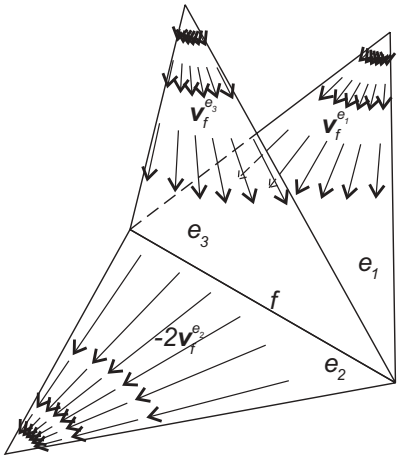


Figure 4.2: Velocity basis function for three elements sharing the same edge

Note that by the definition (4.12) of $\mathbf{RT}_0^0(\mathcal{T}_h)$, there is one condition imposed on each interior edge, so that the number of basis functions of $\mathbf{RT}_{-1}^0(\mathcal{T}_h)$ is decreased by one on each interior edge to obtain the appropriate continuity of the normal trace. When $|I_f| = 2$, we have the classical basis function. An example of one of the two basis functions for three elements with the same edge is given in Figure 4.2. We have the following lemma:

**Lemma 4.5.4. (Duality)** *$\mathcal{V}_h$ is the dual basis to $\mathcal{N}_h$.*

Proof:

We have to show that $N_j(\mathbf{v}_i) = \delta_{ij}$, $i, j = 1, \ldots, |I_{\mathcal{N}_h}|$. We have from the definition of the basis functions of $\mathbf{RT}^0(e)$ that $N_f(\mathbf{v}_f) = 1$ for all boundary edges $f$, and simply $N_f(\mathbf{v}) = 0$ for all $\mathbf{v} \in \mathcal{V}_h$, $\mathbf{v} \neq \mathbf{v}_f$. Concerning the interior edges, we easily come to $N_{f,j}(\mathbf{v}_g) = 0$ for all $j = 1, \ldots, |I_f| - 1$, $f$ an interior edge, $g$ a boundary edge, and to $N_{f,j}(\mathbf{v}_{g,i}) = 0$ for all $j = 1, \ldots, |I_f| - 1$, $i = 1, \ldots, |I_g| - 1$, $f$ an interior edge, $g$ another interior edge. We have

$$N_{f,j}(\mathbf{v}_{f,i}) = \frac{1}{|I_f|} \int_f \mathbf{v}_f^{e_1} \cdot \mathbf{n}_{\partial e_1} \, \mathrm{d}\gamma(\mathbf{x}) - \frac{1}{|I_f|} \int_f \mathbf{v}_f^{e_{j+1}} \cdot \mathbf{n}_{\partial e_{j+1}} \, \mathrm{d}\gamma(\mathbf{x}) = \frac{1}{|I_f|} - \frac{1}{|I_f|} = 0$$

for $i \neq j$ and

$$\begin{aligned} N_{f,i}(\mathbf{v}_{f,i}) &= \frac{1}{|I_f|} \int_f \mathbf{v}_f^{e_1} \cdot \mathbf{n}_{\partial e_1} \, \mathrm{d}\gamma(\mathbf{x}) - \frac{1}{|I_f|} \int_f -(|I_f| - 1) \mathbf{v}_f^{e_{i+1}} \cdot \mathbf{n}_{\partial e_{i+1}} \, \mathrm{d}\gamma(\mathbf{x}) \\ &= \frac{1}{|I_f|} + \frac{1}{|I_f|}(|I_f| - 1) = 1 \end{aligned}$$

for $i = 1, \ldots, |I_f| - 1$, $f$ an interior edge. Thus the proof is completed. □

We are now ready to define the global interpolation operator. We introduce first a space smoother than $\mathbf{H}(\mathrm{div}, \mathcal{S})$,

$$\begin{aligned} \mathbf{H}(\mathrm{grad}, \mathcal{S}) := \Big\{ & v \in \mathbf{L}^2(\mathcal{S}) \, ; \, \mathbf{v}|_{\alpha_\ell} \in (H^1(\alpha_\ell))^2 \quad \forall \ell \in L \, , \\ & \sum_{i \in I_f} \mathbf{v}|_{\alpha_i} \cdot \mathbf{n}_{f,\alpha_i} = 0 \ \text{ on } f \quad \forall f \in \mathcal{E}^{\mathrm{int}} \Big\} . \end{aligned} \tag{4.18}$$

We then define the global interpolation operator $\pi_h$ by

$$\pi_h(\mathbf{u}) := \sum_{i=1}^{|I_{\mathcal{N}_h}|} N_i(\mathbf{u})\mathbf{v}_i \qquad \mathbf{u} \in \mathbf{H}(\mathrm{grad}, \mathcal{S})\,. \tag{4.19}$$

We have the following relation between $\pi_e$ and $\pi_h$:

**Lemma 4.5.5. (Equality between local and global interpolation operators)** *The local and global interpolation operators defined by (4.17) and (4.19), respectively, equal on each element, i.e.*

$$\pi_h(\mathbf{u})|_e = \pi_e(\mathbf{u}|_e) \qquad \forall e \in \mathcal{T}_h,\, \forall\, \mathbf{u} \in \mathbf{H}(\mathrm{grad}, \mathcal{S})\,.$$

Proof:

As the basis functions $\mathbf{v}_i$, $i = 1, \ldots, |I_{\mathcal{N}_h}|$, of $\mathbf{RT}_0^0(\mathcal{T}_h)$ are combined from the local basis functions $\mathbf{v}_j^e$ on each element, we only have to verify that the coefficients of $\mathbf{v}_j^e$ are the same. For boundary edges, the coefficients for both local and global interpolation operators are equally given by $\int_f \mathbf{u}|_e \cdot \mathbf{n}_{\partial e}\, \mathrm{d}\gamma(\mathbf{x})$. For an interior edge $f$, we have for the global interpolation operator

$$\begin{aligned}
&\Big\{ \sum_{i=1}^{|I_f|-1} N_{f,i}(\mathbf{u})\mathbf{v}_{f,i} \Big\}\Big|_{e_j} = \Big\{ \sum_{i=1}^{|I_f|-1} \Big( \frac{1}{|I_f|} \int_f \mathbf{u}|_{e_1} \cdot \mathbf{n}_{\partial e_1}\, \mathrm{d}\gamma(\mathbf{x}) \\
&-\frac{1}{|I_f|} \int_f \mathbf{u}|_{e_{i+1}} \cdot \mathbf{n}_{\partial e_{i+1}}\, \mathrm{d}\gamma(\mathbf{x}) \Big) \Big( \sum_{k=1,\, k\neq i+1}^{|I_f|} \mathbf{v}_f^{e_k} - (|I_f|-1)\mathbf{v}_f^{e_{i+1}} \Big) \Big\} \Big|_{e_j} \\
= \quad & \sum_{i=1,\, i\neq j-1}^{|I_f|-1} \Big( \frac{1}{|I_f|} \int_f \mathbf{u}|_{e_1} \cdot \mathbf{n}_{\partial e_1}\, \mathrm{d}\gamma(\mathbf{x}) - \frac{1}{|I_f|} \int_f \mathbf{u}|_{e_{i+1}} \cdot \mathbf{n}_{\partial e_{i+1}}\, \mathrm{d}\gamma(\mathbf{x}) \Big) \mathbf{v}_f^{e_j} \\
&-(1-\delta_{j1}) \Big( \frac{1}{|I_f|} \int_f \mathbf{u}|_{e_1} \cdot \mathbf{n}_{\partial e_1}\, \mathrm{d}\gamma(\mathbf{x}) - \frac{1}{|I_f|} \int_f \mathbf{u}|_{e_j} \cdot \mathbf{n}_{\partial e_j}\, \mathrm{d}\gamma(\mathbf{x}) \Big) (|I_f|-1)\mathbf{v}_f^{e_j}
\end{aligned}$$

using the definition of $N_{f,i}$ and $\mathbf{v}_{f,i}$, $i = 1, \ldots, |I_f|-1$, $j = 1, \ldots, |I_f|$. Considering now only the coefficients of $\mathbf{v}_f^{e_j}$, we come to

$$\begin{aligned}
&\sum_{i=1}^{|I_f|-1} \frac{1}{|I_f|} \int_f \mathbf{u}|_{e_1} \cdot \mathbf{n}_{\partial e_1}\, \mathrm{d}\gamma(\mathbf{x}) - \sum_{i=1}^{|I_f|-1} \frac{1}{|I_f|} \int_f \mathbf{u}|_{e_{i+1}} \cdot \mathbf{n}_{\partial e_{i+1}}\, \mathrm{d}\gamma(\mathbf{x}) \\
= \quad & \Big( (|I_f|-1)\frac{1}{|I_f|} + \frac{1}{|I_f|} \Big) \int_f \mathbf{u}|_{e_1} \cdot \mathbf{n}_{\partial e_1}\, \mathrm{d}\gamma(\mathbf{x}) = \int_f \mathbf{u}|_{e_1} \cdot \mathbf{n}_{\partial e_1}\, \mathrm{d}\gamma(\mathbf{x})
\end{aligned}$$

for $j = 1$, using the normal trace continuity of $\mathbf{u}$, which is expressed by $\sum_{i=1}^{|I_f|} \int_f \mathbf{u}|_{e_i} \cdot \mathbf{n}_{\partial e_i}\, \mathrm{d}\gamma(\mathbf{x}) = 0$. Similarly,

$$\begin{aligned}
&(|I_f|-2)\frac{1}{|I_f|} \int_f \mathbf{u}|_{e_1} \cdot \mathbf{n}_{\partial e_1}\, \mathrm{d}\gamma(\mathbf{x}) + \frac{1}{|I_f|} \int_f \mathbf{u}|_{e_1} \cdot \mathbf{n}_{\partial e_1}\, \mathrm{d}\gamma(\mathbf{x}) \\
&+\frac{1}{|I_f|} \int_f \mathbf{u}|_{e_j} \cdot \mathbf{n}_{\partial e_j}\, \mathrm{d}\gamma(\mathbf{x}) - (|I_f|-1)\frac{1}{|I_f|} \int_f \mathbf{u}|_{e_1} \cdot \mathbf{n}_{\partial e_1}\, \mathrm{d}\gamma(\mathbf{x}) \\
&+(|I_f|-1)\frac{1}{|I_f|} \int_f \mathbf{u}|_{e_j} \cdot \mathbf{n}_{\partial e_j}\, \mathrm{d}\gamma(\mathbf{x}) = \int_f \mathbf{u}|_{e_j} \cdot \mathbf{n}_{\partial e_j}\, \mathrm{d}\gamma(\mathbf{x})
\end{aligned}$$

for $j \geq 2$, and thus the proof is completed. □

We conclude this section by the following theorem:

**Theorem 4.5.6. (Commuting diagram property)** *The commuting diagram property holds, i.e.*

$$\begin{array}{ccc} \mathbf{H}(\mathrm{grad},\mathcal{S}) & \xrightarrow{\mathrm{div}} & L^2(\mathcal{S}) \\ \big\downarrow \pi_h & & \big\downarrow P_h \\ \mathbf{RT}_0^0(\mathcal{T}_h) & \xrightarrow{\mathrm{div}} & M_{-1}^0(\mathcal{T}_h) \end{array} ,$$

*where $\pi_h$ is the global interpolation operator defined by (4.19) and $P_h$ is the $L^2(\mathcal{S})$-orthogonal projection onto $M_{-1}^0(\mathcal{T}_h)$.*

Proof:
The proof is immediate using the previous lemma and the validity of the commuting diagram property for the local interpolation operator, see e.g. [33, Proposition III.3.7] or [103, Section 3.4.2]. □

### 4.5.3 Mixed finite element approximation

We are ready to define the mixed approximation:

**Definition 4.5.7. (Mixed finite element approximation)** *As the lowest-order Raviart–Thomas mixed finite element approximation of the problem (4.15a)–(4.15b), we understand functions $\mathbf{u}_h = \mathbf{u}_{0,h} + \tilde{\mathbf{u}}$, $\mathbf{u}_{0,h} \in \mathbf{RT}_{0,N}^0(\mathcal{T}_h)$, and $p_h \in M_{-1}^0(\mathcal{T}_h)$ satisfying*

$$\begin{aligned} (\mathbf{K}^{-1}\mathbf{u}_{0,h}, \mathbf{v}_h)_{0,\mathcal{S}} - (\nabla\cdot\mathbf{v}_h, p_h)_{0,\mathcal{S}} &= -\langle \mathbf{v}_h\cdot\mathbf{n}, p_D\rangle_{\partial\mathcal{S}} + (\nabla\cdot\mathbf{v}_h, z)_{0,\mathcal{S}} \\ -\langle \mathbf{v}_h\cdot\mathbf{n}, z\rangle_{\partial\mathcal{S}} - (\mathbf{K}^{-1}\tilde{\mathbf{u}}, \mathbf{v}_h)_{0,\mathcal{S}} \qquad & \forall\, \mathbf{v}_h \in \mathbf{RT}_{0,N}^0(\mathcal{T}_h)\,, \end{aligned} \tag{4.20a}$$

$$-(\nabla\cdot\mathbf{u}_{0,h}, \phi_h)_{0,\mathcal{S}} = -(q,\phi_h)_{0,\mathcal{S}} + (\nabla\cdot\tilde{\mathbf{u}}, \phi_h)_{0,\mathcal{S}} \qquad \forall \phi_h \in M_{-1}^0(\mathcal{T}_h)\,. \tag{4.20b}$$

The commuting diagram property expressed by Theorem 4.5.6 implies the discrete inf–sup condition, which in turn ensures that the problem (4.20a)–(4.20b) has a unique solution.

### 4.5.4 Hybridization of the mixed approximation

We will now introduce the hybridization of the mixed approximation:

**Definition 4.5.8. (Hybridization of the mixed approximation)** *As the hybridization of the lowest-order Raviart–Thomas mixed finite element approximation of the problem (4.15a)–(4.15b), we understand functions $\mathbf{u}_h = \mathbf{u}_{0,h} + \tilde{\mathbf{u}}$, $\mathbf{u}_{0,h} \in \mathbf{RT}_{-1}^0(\mathcal{T}_h)$, $p_h \in M_{-1}^0(\mathcal{T}_h)$, and $\lambda_h \in M_{-1}^0(\mathcal{E}_{h,D})$ satisfying*

$$\begin{aligned} &\sum_{e\in\mathcal{T}_h} \left\{ (\mathbf{K}^{-1}\mathbf{u}_{0,h}, \mathbf{v}_h)_{0,e} - (\nabla\cdot\mathbf{v}_h, p_h)_{0,e} + \langle \mathbf{v}_h\cdot\mathbf{n}, \lambda_h\rangle_{\partial e} \right\} \\ &= \sum_{e\in\mathcal{T}_h} \left\{ -\langle \mathbf{v}_h\cdot\mathbf{n}, p_D\rangle_{\partial e\cap\Gamma_D} + (\nabla\cdot\mathbf{v}_h, z)_{0,e} - \langle \mathbf{v}_h\cdot\mathbf{n}, z\rangle_{\partial e} - (\mathbf{K}^{-1}\tilde{\mathbf{u}}, \mathbf{v}_h)_{0,e} \right\} \\ &\qquad \forall\, \mathbf{v}_h \in \mathbf{RT}_{-1}^0(\mathcal{T}_h)\,, \end{aligned} \tag{4.21a}$$

$$\begin{aligned} -\sum_{e\in\mathcal{T}_h} (\nabla\cdot\mathbf{u}_{0,h}, \phi_h)_{0,e} &= -\sum_{e\in\mathcal{T}_h} \left\{ (q,\phi_h)_{0,e} - (\nabla\cdot\tilde{\mathbf{u}}, \phi_h)_{0,e} \right\} \\ &\forall \phi_h \in M_{-1}^0(\mathcal{T}_h)\,, \end{aligned} \tag{4.21b}$$

$$\sum_{e\in\mathcal{T}_h}\langle \mathbf{u}_{0,h}\cdot\mathbf{n},\mu_h\rangle_{\partial e}=0 \qquad \forall \mu_h\in M^0_{-1}(\mathcal{E}_{h,D})\,. \tag{4.21c}$$

It is immediate that if $\mathbf{v}_h\in\mathbf{RT}^0_{-1}(\mathcal{T}_h)$, then $\mathbf{v}_h\in\mathbf{RT}^0_{0,N}(\mathcal{T}_h)$ if and only if

$$\sum_{e\in\mathcal{T}_h}\langle \mathbf{v}_h\cdot\mathbf{n},\lambda_h\rangle_{\partial e}=0 \qquad \forall \lambda_h\in M^0_{-1}(\mathcal{E}_{h,D})\,.$$

This ensures that the triple $\mathbf{u}_{0,h}$, $p_h$, $\lambda_h$ exists and is unique and that $\mathbf{u}_{0,h}$ and $p_h$ are at the same time the unique solutions of (4.20a)–(4.20b). We summarize the previous developments in the following theorem:

**Theorem 4.5.9. (Existence and uniqueness of the mixed-hybrid approximation)** *The problem (4.21a)–(4.21c) has a unique solution.*

### 4.5.5 Error estimates

We now give two error estimates, following from the classical interpolation theory. If the solution $(\mathbf{u},p)$ of (4.15a)–(4.15b) is smooth enough and if $(\mathbf{u}_h,p_h,\lambda_h)$ is the solution of (4.21a)–(4.21c), we have

$$\|\mathbf{u}-\mathbf{u}_h\|_{\mathbf{H}(\mathrm{div},\mathcal{S})}+\|p-p_h\|_{0,\mathcal{S}}\le Ch(\|p\|_{1,\mathcal{S}}+\|\mathbf{u}\|_{1,\mathcal{S}}+\|q\|_{1,\mathcal{S}})\,,$$

where the constant $C$ does not depend on $h$ (see [33, Proposition IV.1.2]).

Using the piecewise linear but nonconforming approximation $\tilde\lambda_h\in X^1_0(\mathcal{E}_h)$ given by the values of the Lagrange multiplier $\lambda_h$ at the midpoints of the edges, we have (see [33, Theorem V.3.1])

$$\|p-\tilde\lambda_h\|_{0,\mathcal{S}}\le Ch^2(\|p\|_{1,\mathcal{S}}+\|\mathbf{u}\|_{1,\mathcal{S}}+\|q\|_{1,\mathcal{S}})\,.$$

## 4.6 Relation between mixed and nonconforming methods

We study in this section the relation between the hybridization of the lowest-order Raviart–Thomas mixed finite element method and the nonconforming method. We extend the results of [38] onto systems of polygons, general diffusion tensors, and general boundary conditions. This also enables us to efficiently implement the mixed finite element method in the considered case.

### 4.6.1 Algebraic condensation of the mixed-hybrid approximation

Let us denote, for all $e\in\mathcal{T}_h$,

$$\mathbf{u}_{0,h}|_e=\begin{pmatrix}a_e+c_ex\\ b_e+c_ey\end{pmatrix}\,,\quad p_h|_e=p_e$$

and similarly, for all $f\in\mathcal{E}_h$,

$$\lambda_h|_f=\lambda_f\,.$$

We now follow the ideas of [38]. Let $e\in\mathcal{T}_h$ be fixed. Consider in (4.21b) a test function $\phi_h$ equal to 1 on $e$ and zero otherwise. This gives $c_e=q_e/2-\tilde{\mathbf{u}}_e/2$ with

$$q_e:=\frac{\int_e q\,\mathrm{d}\mathbf{x}}{|e|}\,,\quad \tilde{\mathbf{u}}_e:=\frac{\int_e\nabla\cdot\tilde{\mathbf{u}}\,\mathrm{d}\mathbf{x}}{|e|}\,. \tag{4.22}$$

Next consider in (4.21a) two test functions, $\mathbf{v}_h = (1,0)^t$, $\mathbf{v}_h = (0,1)^t$ on $e$ and zero otherwise, whose divergence is apparently zero. This gives

$$\int_e \mathbf{K}^{-1}\mathbf{u}_{0,h}\,\mathrm{d}\mathbf{x} + \int_{\partial e} \lambda_h\,\mathbf{n}\,\mathrm{d}\gamma(\mathbf{x}) = \mathbf{r}_e$$

with

$$\mathbf{r}_e := -\int_{\partial e\cap\Gamma_D} p_D\,\mathbf{n}\,\mathrm{d}\gamma(\mathbf{x}) - \int_{\partial e} z\,\mathbf{n}\,\mathrm{d}\gamma(\mathbf{x}) - \int_e \mathbf{K}^{-1}\tilde{\mathbf{u}}\,\mathrm{d}\mathbf{x}\,.$$

Let $\tilde\lambda_h \in X_0^1(\mathcal{E}_{h,D})$ be given by

$$\tilde\lambda_h := \sum_{f\in\mathcal{E}_h} \lambda_f\varphi_f\,.$$

Then using (4.9), we have

$$\int_{\partial e} \lambda_h\,\mathbf{n}\,\mathrm{d}\gamma(\mathbf{x}) = \sum_{f\subset\partial e} \lambda_f|f|\mathbf{n}_f = |e|\sum_{f\in\partial e}\lambda_f\nabla\varphi_f|_e = |e|\,\nabla\tilde\lambda_h|_e\,.$$

Next,

$$\int_e \mathbf{K}^{-1}\mathbf{u}_{0,h}\,\mathrm{d}\mathbf{x} = \int_e \mathbf{K}^{-1}\,\mathrm{d}\mathbf{x}\begin{pmatrix} a_e\\ b_e\end{pmatrix} + c_e\int_e \mathbf{K}^{-1}\begin{pmatrix} x\\ y\end{pmatrix}\mathrm{d}\mathbf{x}\,.$$

Let us denote

$$\mathbf{K}_e := \Big(\frac{1}{|e|}\int_e \mathbf{K}^{-1}\,\mathrm{d}\mathbf{x}\Big)^{-1} \qquad e\in\mathcal{T}_h\,. \tag{4.23}$$

Then the above equations give

$$\begin{pmatrix} a_e\\ b_e\end{pmatrix} + c_e\frac{\mathbf{K}_e}{|e|}\int_e \mathbf{K}^{-1}\begin{pmatrix} x\\ y\end{pmatrix}\mathrm{d}\mathbf{x} + \mathbf{K}_e\nabla\tilde\lambda_h|_e = \mathbf{K}_e\frac{\mathbf{r}_e}{|e|}$$

and consequently

$$\begin{aligned}\mathbf{u}_{0,h}|_e \;=\; & -\mathbf{K}_e\nabla\tilde\lambda_h|_e + \Big[\frac{q_e}{2} - \frac{\tilde{\mathbf{u}}_e}{2}\Big]\Big[\begin{pmatrix} x\\ y\end{pmatrix}\\ & - \frac{\mathbf{K}_e}{|e|}\int_e \mathbf{K}^{-1}\begin{pmatrix} x\\ y\end{pmatrix}\mathrm{d}\mathbf{x}\Big] + \mathbf{K}_e\frac{\mathbf{r}_e}{|e|}\,.\end{aligned} \tag{4.24}$$

We finally substitute (4.24) into (4.21c). This gives the following system of linear equations with the only unknowns the Lagrange multipliers $\lambda_h$:

$$\begin{aligned}\sum_{e\in\mathcal{T}_h}(\mathbf{K}_e\nabla\tilde\lambda_h, \nabla\tilde\mu_h)_{0,e} = \sum_{e\in\mathcal{T}_h}\Big\langle\Big\{\Big[\frac{q_e}{2} - \frac{\tilde{\mathbf{u}}_e}{2}\Big]\Big[\begin{pmatrix} x\\ y\end{pmatrix}\\ -\frac{\mathbf{K}_e}{|e|}\int_e \mathbf{K}^{-1}\begin{pmatrix} x\\ y\end{pmatrix}\mathrm{d}\mathbf{x}\Big] + \mathbf{K}_e\frac{\mathbf{r}_e}{|e|}\Big\}\cdot\mathbf{n}, \mu_h\Big\rangle_{\partial e} \qquad \forall\mu_h\in M_{-1}^0(\mathcal{E}_{h,D})\,,\end{aligned} \tag{4.25}$$

where $\tilde\mu_h \in X_0^1(\mathcal{E}_{h,D})$ is given by

$$\tilde\mu_h := \sum_{f\in\mathcal{E}_h}\mu_f\varphi_f\,.$$

The left-hand side of (4.25) follows by

$$\langle\mathbf{K}_e\nabla\tilde\lambda_h|_e\cdot\mathbf{n}, \mu_h\rangle_{\partial e} = \langle\mathbf{K}_e\nabla\tilde\lambda_h|_e\cdot\mathbf{n}, \tilde\mu_h\rangle_{\partial e} = (\mathbf{K}_e\nabla\tilde\lambda_h, \nabla\tilde\mu_h)_{0,e} \qquad \forall e\in\mathcal{T}_h\,.$$

Here, we have used the fact that $\mathbf{K}_e\nabla\tilde{\lambda}_h|_e\cdot\mathbf{n}\,\mu_h$ is constant over each edge and hence its integral over this edge equals to that of $\mathbf{K}_e\nabla\tilde{\lambda}_h|_e\cdot\mathbf{n}\,\tilde{\mu}_h$, which is a linear function with the same value at the edge midpoint by the definition of $\tilde{\mu}_h$, and finally the Green theorem in $e$ (notice that $\mathbf{K}_e\nabla\tilde{\lambda}_h|_e$ is a constant vector in $e$ and hence its divergence is zero).

The system given by (4.25), in the sequel called (algebraically) *condensed mixed-hybrid method*, enables a very efficient implementation of the scheme (4.21a)–(4.21c). In particular, its system matrix is symmetric and positive definite and the number of unknowns equals to the number of interior and Neumann boundary edges; remark that this number does not increase with the number of triangles sharing the given edge. Moreover, this matrix is assembled directly and one thus can avoid the inverting of local matrices, which is necessary in the traditional static condensation approach (cf. [33, Section V.1.2]). It is pointed out in [74] that the inverting of local matrices is a potential source of significant numerical errors. Finally, note that the velocity $\mathbf{u}_{0,h}\in\mathbf{RT}^0_{0,N}(\mathcal{T}_h)$ is easily obtained from the knowledge of $\tilde{\lambda}_h$ by (4.24). It is easily seen that the system (4.25) is very close to that given by the nonconforming finite element approximation (4.14). We give detailed comments on the relation between these two systems in the next section.

### 4.6.2 Comparison of condensed mixed-hybrid and nonconforming methods

We consider in this section the detailed relation between the condensed mixed-hybrid finite element method given by (4.25) and the nonconforming finite element method given by (4.14). We consider the matrices of the problems and the different parts of the right-hand sides separately.

#### System matrix

It is easily seen from (4.25), (4.14), and (4.23) that the system matrix of the condensed mixed-hybrid method is the system matrix of the nonconforming method with a piecewise constant diffusion tensor, given as the inverse of the elementwise average of the inverse of the original one. In particular, for elementwise constant diffusion tensors, these matrices coincide, as it was already shown in [38]. Simply, the mixed-hybrid method employs the harmonic average of the hydraulic conductivity tensor, whereas the nonconforming method uses instead the arithmetic average.

#### Sources term

Using the simple trick of replacing $\mu_h$ by $\tilde{\mu}_h$ and the Green theorem in each $e\in\mathcal{T}_h$ as at the end of Section 4.6.1, we have for the sources term of the condensed mixed-hybrid method the expression

$$\sum_{e\in\mathcal{T}_h}(q_e,\tilde{\mu}_h)_{0,e}+\sum_{e\in\mathcal{T}_h}\frac{q_e}{2}\left(\begin{pmatrix}x_e\\y_e\end{pmatrix}-\frac{\mathbf{K}_e}{|e|}\int_e\mathbf{K}^{-1}\begin{pmatrix}x\\y\end{pmatrix}\mathrm{d}\mathbf{x},\nabla\tilde{\mu}_h\right)_{0,e},$$

where $(x_e,y_e)^t$ are the coordinates of the barycentre of the triangle $e$. In particular, if $\mathbf{K}$ is elementwise constant, the second term of the above expression vanishes. Hence the essential difference with the source term of the nonconforming method is the employment of the elementwise average of $q$ given by (4.22) rather than taking $q$ directly.

### Dirichlet boundary condition term

Let $p_D$ be smooth enough and let us consider the usual approximation $\tilde{p} \approx \sum_{f\subset\Gamma_D} p_D(Q_f)\varphi_f$. Then the Dirichlet boundary condition term in the nonconforming method becomes

$$-\sum_{e\in\mathcal{T}_h}(\mathbf{K}\nabla\tilde{p},\nabla\tilde{\mu}_h)_{0,e} \approx -\sum_{e\in\mathcal{T}_h}\left(\mathbf{K}\sum_{f\subset\partial e\cap\Gamma_D} p_D(Q_f)\frac{|f|}{|e|}\mathbf{n}_f,\nabla\tilde{\mu}_h\right)_{0,e},$$

where $\tilde{\mu}_h \in X_0^1(\mathcal{E}_{h,D})$ and where we have employed the relation (4.9). This is obviously equivalent, up to replacing $\mathbf{K}$ by $\mathbf{K}_e$, to the expression for this term from the condensed mixed-hybrid method

$$-\sum_{e\in\mathcal{T}_h}\left(\frac{\mathbf{K}_e}{|e|}\int_{\partial e\cap\Gamma_D} p_D\,\mathbf{n}\,\mathrm{d}\gamma(\mathbf{x}),\nabla\tilde{\mu}_h\right)_{0,e} \approx -\sum_{e\in\mathcal{T}_h}\left(\frac{\mathbf{K}_e}{|e|}\sum_{f\subset\partial e\cap\Gamma_D} p_D(Q_f)|f|\mathbf{n}_f,\nabla\tilde{\mu}_h\right)_{0,e}.$$

### Neumann boundary condition term

Let us for simplicity consider just one edge $f$ where the Neumann boundary condition is prescribed, i.e. $\Gamma_N = f$. Then the Neumann boundary condition term in the nonconforming method, with the usual approximation supposing that $u_N$ is smooth enough and for the test function $\varphi_f$, is

$$-\int_f u_N\varphi_f\,\mathrm{d}\gamma(\mathbf{x}) \approx -\int_f u_N(Q_f)\varphi_f\,\mathrm{d}\gamma(\mathbf{x}) = -u_N(Q_f)|f|\,.$$

Recall that this term equals to zero for all other test functions $\varphi_g$, $g\in\mathcal{E}_{h,D}$, $g\neq f$.

Using the same techniques as in the above paragraphs, we can express the Neumann boundary condition term in the condensed mixed-hybrid method as

$$-\sum_{e\in\mathcal{T}_h}(\tilde{\mathbf{u}}_e,\tilde{\mu}_h)_{0,e} - \sum_{e\in\mathcal{T}_h}\frac{\tilde{\mathbf{u}}_e}{2}\left(\begin{pmatrix}x_e\\y_e\end{pmatrix} - \frac{\mathbf{K}_e}{|e|}\int_e\mathbf{K}^{-1}\begin{pmatrix}x\\y\end{pmatrix}\mathrm{d}\mathbf{x},\nabla\tilde{\mu}_h\right)_{0,e}$$
$$-\sum_{e\in\mathcal{T}_h}\left\langle\left\{\frac{\mathbf{K}_e}{|e|}\int_e\mathbf{K}^{-1}\tilde{\mathbf{u}}\,\mathrm{d}\mathbf{x}\right\}\cdot\mathbf{n},\mu_h\right\rangle_{\partial e}.$$

Let $\mathbf{K}$ be elementwise constant; then the second term of the above expression vanishes and its third term simplifies. Let $e\in\mathcal{T}_h$ be such that $f\subset\partial e$ and let us finally consider the usual approximation $\tilde{\mathbf{u}} \approx u_N(Q_f)|f|\mathbf{v}_f^e$, where $\mathbf{v}_f^e\in\mathbf{RT}^0(e)$ is the local velocity basis function associated with the element $e$ and its edge $f$. Then this term is a priori nonzero only for $e$ and for the three test functions $\varphi_g$, $g\subset\partial e$, and has the form

$$-\frac{u_N(Q_f)|f|}{|e|}\Big(\int_e\nabla\cdot\mathbf{v}_f^e\,\mathrm{d}\mathbf{x},\varphi_g\Big)_{0,e} - \frac{u_N(Q_f)|f|}{|e|}\Big\langle\Big\{\int_e\mathbf{v}_f^e\,\mathrm{d}\mathbf{x}\Big\}\cdot\mathbf{n},\varphi_g\Big\rangle_{\partial e}.$$

A simple computation gives

$$\int_e\nabla\cdot\mathbf{v}_f^e\,\mathrm{d}\mathbf{x} = 1\,,\quad \int_e\mathbf{v}_f^e\,\mathrm{d}\mathbf{x} = \frac{1}{2}\mathbf{w}\,,$$

where $\mathbf{w} = (x_e,y_e)^t - (x_f,y_f)^t$ with $(x_f,y_f)^t$ being the coordinates of the vertex of $e$ opposite to $f$. This finally gives for the Neumann boundary condition term in the condensed mixed-hybrid method, using simple geometrical properties of a triangle,

$$-\frac{u_N(Q_f)|f|}{3} - \frac{u_N(Q_f)|f||g|}{2|e|}\mathbf{w}\cdot\mathbf{n}_g = -u_N(Q_f)|f|\delta_{f,g}\,,$$

which coincides with the expression from the nonconforming method.

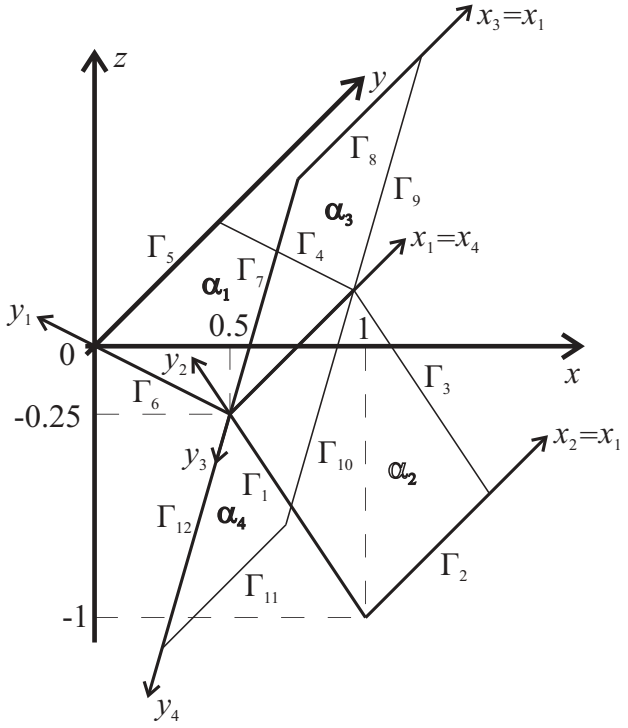


Figure 4.3: System $\mathcal{S}$ for the model problems

**Gravity term**

Using that the gradient of $z$ is piecewise constant, a development similar to that for the Dirichlet boundary condition gives that the expressions for the gravity term from the nonconforming and condensed mixed-hybrid methods differ just by the employment of $\mathbf{K}$, $\mathbf{K}_e$, respectively.

## 4.7 Numerical simulations

We present in this section the results of a numerical experiment on a model problem with a known analytical solution. We then describe the application of the proposed method to the simulation of fracture flow and compare it with other methods.

### 4.7.1 Model problem with a known analytical solution

We consider two simple model problems in this section. The first model problem corresponds to the system $\mathcal{S}$ created by four rectangles as viewed in Figure 4.3. We verify on this problem the theoretical error estimates for the situation where the central edge is shared by four polygons. The second model problem is a simplification of the previous one, with just the rectangles $\alpha_1$ and $\alpha_2$ creating the system; there is no multiply shared edge in this case. Both model problems have the same known analytical solution in $\alpha_1$ and $\alpha_2$. We consider the second model problem in order to investigate the changes of the approximation error implied by the presence of a multiply shared edge. All the computations presented in this section were done in double precision on a personal computer with machine precision being in power of $10^{-16}$. The resulting systems of linear equations were solved by the preconditioned conjugate gradients method, cf. [73, 103, 111].

The first model problem is given by:

$$\mathcal{S} = \overline{\alpha_1} \cup \overline{\alpha_2} \cup \overline{\alpha_3} \cup \overline{\alpha_4} \setminus \partial\mathcal{S}\,,$$

$$\begin{aligned} \mathbf{u} &= -(\nabla p + \nabla z) \quad \text{in } \alpha_i\,, i = 1,2,3,4\,, \\ \nabla \cdot \mathbf{u} &= 0 \quad \text{in } \alpha_i\,, i = 1,2,3,4\,, \end{aligned}$$

$$\begin{gathered} p = 0 \quad \text{on } \Gamma_1\,, \quad p = 0 \quad \text{on } \Gamma_2\,, \\ \mathbf{u}\cdot\mathbf{n} = 0 \quad \text{on } \Gamma_3\,, \quad \mathbf{u}\cdot\mathbf{n} = 0 \quad \text{on } \Gamma_4\,, \\ p = \sin\Big(\frac{\pi x_1}{2X}\Big)\sinh\Big(\frac{\pi(A+B)}{2X}\Big) + S\,A \quad \text{on } \Gamma_5\,, \quad p = S\,y_1 \quad \text{on } \Gamma_6\,, \\ p = 0 \quad \text{on } \Gamma_7\,, \quad p = 0 \quad \text{on } \Gamma_8\,, \\ \mathbf{u}\cdot\mathbf{n} = 0 \quad \text{on } \Gamma_9\,, \quad \mathbf{u}\cdot\mathbf{n} = 0 \quad \text{on } \Gamma_{10}\,, \\ p = \sin\Big(\frac{\pi x_4}{2X}\Big)\sinh\Big(\frac{\pi(B+B)}{2X}\Big) \quad \text{on } \Gamma_{11}\,, \quad p = 0 \quad \text{on } \Gamma_{12}\,, \end{aligned}$$

where $A = |\Gamma_4| = \sqrt{5}/4$, $X = |\Gamma_2| = 1$, $B = |\Gamma_3| = |\Gamma_9| = |\Gamma_{10}| = \sqrt{13}/4$, and $S = \partial z/\partial y_2 - \partial z/\partial y_1$. The geometry of this model problem is viewed in Figure 4.3. The exact solution can be found as

$$\begin{aligned} p|_{\alpha_1} &= \sin\Big(\frac{\pi x_1}{2X}\Big)\sinh\Big(\frac{\pi(y_1+B)}{2X}\Big) + S\,y_1\,, \\ \mathbf{u}|_{\alpha_1} &= \Big(-\frac{\pi}{2X}\cos\Big(\frac{\pi x_1}{2X}\Big)\sinh\Big(\frac{\pi(y_1+B)}{2X}\Big), \\ &\quad -\frac{\pi}{2X}\sin\Big(\frac{\pi x_1}{2X}\Big)\cosh\Big(\frac{\pi(y_1+B)}{2X}\Big) - S - \frac{\partial z}{\partial y_1}\Big)\,, \\ p|_{\alpha_2} &= \sin\Big(\frac{\pi x_2}{2X}\Big)\sinh\Big(\frac{\pi y_2}{2X}\Big)\,, \\ \mathbf{u}|_{\alpha_2} &= \Big(-\frac{\pi}{2X}\cos\Big(\frac{\pi x_2}{2X}\Big)\sinh\Big(\frac{\pi y_2}{2X}\Big), -\frac{\pi}{2X}\sin\Big(\frac{\pi x_2}{2X}\Big)\cosh\Big(\frac{\pi y_2}{2X}\Big) - \frac{\partial z}{\partial y_2}\Big)\,, \\ p|_{\alpha_3} &= \sin\Big(\frac{\pi x_3}{2X}\Big)\sinh\Big(\frac{\pi y_3}{2X}\Big)\,, \\ \mathbf{u}|_{\alpha_3} &= \Big(-\frac{\pi}{2X}\cos\Big(\frac{\pi x_3}{2X}\Big)\sinh\Big(\frac{\pi y_3}{2X}\Big), -\frac{\pi}{2X}\sin\Big(\frac{\pi x_3}{2X}\Big)\cosh\Big(\frac{\pi y_3}{2X}\Big) - \frac{\partial z}{\partial y_3}\Big)\,, \\ p|_{\alpha_4} &= \sin\Big(\frac{\pi x_4}{2X}\Big)\sinh\Big(\frac{\pi(y_4+B)}{2X}\Big)\,, \\ \mathbf{u}|_{\alpha_4} &= \Big(-\frac{\pi}{2X}\cos\Big(\frac{\pi x_4}{2X}\Big)\sinh\Big(\frac{\pi(y_4+B)}{2X}\Big), \\ &\quad -\frac{\pi}{2X}\sin\Big(\frac{\pi x_4}{2X}\Big)\cosh\Big(\frac{\pi(y_4+B)}{2X}\Big) - \frac{\partial z}{\partial y_4}\Big)\,. \end{aligned}$$

Note that the gradients of $z$ in $\alpha_1$ and $\alpha_2$ are different. Hence the occurrence of the term $S$, which ensures the continuity of the normal trace of the velocity field. Table 4.1 gives the approximation errors in the first rectangle $\alpha_1$. The system $\mathcal{S}$ is discretized into $4 \times 2N^2$ regular triangular elements, $h \approx 1/N$. There is the expected $O(h)$ convergence of $\mathbf{u}_h$, $O(h)$ convergence of the elementwise constant $p_h$, and $O(h^2)$ convergence of the piecewise linear but discontinuous $\tilde{\lambda}_h$.

| N | Triangles | $\|p - p_h\|_{0,\mathcal{S}}$ | $\|p - \tilde{\lambda}_h\|_{0,\mathcal{S}}$ | $\|\mathbf{u} - \mathbf{u}_h\|_{\mathbf{H}(\mathrm{div},\mathcal{S})}$ |
|---|---|---|---|---|
| 2 | 8×4 | 0.4445 | 0.1481 | 1.2247 |
| 4 | 32×4 | 0.2212 | 0.0389 | 0.6263 |
| 8 | 128×4 | 0.1102 | 0.0098 | 0.3150 |
| 16 | 512×4 | 0.0550 | 0.0025 | 0.1577 |
| 32 | 2048×4 | 0.0275 | $6.18{\cdot}10^{-4}$ | 0.0789 |
| 64 | 8192×4 | 0.0138 | $1.54{\cdot}10^{-4}$ | 0.0394 |
| 128 | 32768×4 | 0.0069 | $3.87{\cdot}10^{-5}$ | 0.0197 |
| 256 | 131072×4 | 0.0034 | $9.73{\cdot}10^{-6}$ | 0.0099 |

Table 4.1: Approximation errors in $\alpha_1$, the first model problem

| N | Triangles | $\|p - p_h\|_{0,\mathcal{S}}$ | $\|p - \tilde{\lambda}_h\|_{0,\mathcal{S}}$ | $\|\mathbf{u} - \mathbf{u}_h\|_{\mathbf{H}(\mathrm{div},\mathcal{S})}$ |
|---|---|---|---|---|
| 2 | 8×2 | 0.4481 | 0.1496 | 1.2236 |
| 4 | 32×2 | 0.2212 | 0.0393 | 0.6262 |
| 8 | 128×2 | 0.1102 | 0.0099 | 0.3150 |
| 16 | 512×2 | 0.0550 | 0.0025 | 0.1577 |
| 32 | 2048×2 | 0.0275 | $6.24{\cdot}10^{-4}$ | 0.0789 |
| 64 | 8192×2 | 0.0138 | $1.56{\cdot}10^{-4}$ | 0.0394 |
| 128 | 32768×2 | 0.0069 | $3.90{\cdot}10^{-5}$ | 0.0197 |
| 256 | 131072×2 | 0.0034 | $9.76{\cdot}10^{-6}$ | 0.0099 |

Table 4.2: Approximation errors in $\alpha_1$, the second model problem

The second model problem is given by

$$\mathcal{S} = \overline{\alpha_1} \cup \overline{\alpha_2} \setminus \partial\mathcal{S}\,,$$

$$\begin{aligned} \mathbf{u} &= -(\nabla p + \nabla z) \quad \text{in } \alpha_i\,, i = 1,2\,, \\ \nabla \cdot \mathbf{u} &= 0 \quad \text{in } \alpha_i\,, i = 1,2\,. \end{aligned}$$

The boundary conditions on $\Gamma_1$–$\Gamma_6$ are given as in the previous case. Also the exact solution in $\alpha_1$ and $\alpha_2$ stays unchanged. Table 4.2 gives the approximation errors in the first rectangle $\alpha_1$ for this model problem. As the exact solution in $\alpha_1$ coincides with that of the first model problem, we can compare these results with that of Table 4.1. The difference in approximation error is very small even for rough triangulations and disappears for increasing $N$. Hence a confirmation of the conclusions outlined by the theory: the presence of multiply shared interpolygon boundaries does not influence the approximation properties of the lowest-order Raviart–Thomas mixed finite element method.

### 4.7.2 Real problem

We give an example of fracture flow around the explorational drill hole Ptp-3 in the granitoid massif of Potůčky, Western Bohemia in this section. There exists a large variety of approaches to modeling the flow through a network of polygonal disks representing the rock fractures. In [34, 50, 87] the networks of polygonal disks are replaced by networks of one-dimensional pipes. This allows for fast calculations with large networks, but the precision is compromised.

The models proposed in [9, 21, 54, 85, 113] discretize the polygonal networks into triangular or quadrilateral meshes. Because of a very complex geometry, the number of mesh elements is often sizably increased. Finite difference, finite volume, finite element, or boundary element methods are used for the discretization. We refer e.g. to [27] for a more detailed survey.

Our intention was twofold. First, we have constructed a very accurate mesh of the fracture network, which had at the same time as few elements as possible. Second, we have used the mixed finite element method studied in this chapter for the discretization of the fracture flow problem. We have approximated the original three-dimensional fractures by planar polygonal disks whose frequency, size, orientation, assigned aperture, wall roughness, and filling were statistically described from field measurements (core-log evaluation, acoustic camera scanning, ...), given in [89]. We have next computed the intersections of the polygons. In order to simplify the system of intersections in each polygon, these were slightly moved and stretched in the polygon planes. This allows a significant decrease of the number of triangular elements necessary to discretize each polygon and an improvement of their shapes. The triangular mesh has to respect the system of intersections in each polygon, but the interpolygon geometrical correspondence vanishes. This was replaced with an element edges correspondence, sufficient for the mixed finite element method. Briefly, the corresponding edges do not necessarily match geometrically—only what is the outflow from one triangular element through a given edge has to be the inflow into the neighboring ones through the edges that are associated with the given one. Finally, based on the assigned aperture, fracture wall roughness, and filling, the hydraulic permeability of each element was set. The classical parallel plate model was thus avoided.

The optimized triangulation of the fracture network and the model allowing for variable permeability inside the fractures together with the mixed finite element method ensuring the mass balance in each element even for meshes with no real geometrical correspondence have proved a good correspondence between observed phenomena and the numerical approximation. The model gave an accurate velocity field within fracture planes and thus in the whole simulated network. Namely, the channeling effect was successfully simulated both in fracture planes and in the entire network. This effect is given by the fact that the natural three-dimensional fractures have varying apertures and consequently the flow is not evenly distributed within the fracture planes. An example of the distribution of the piezometric head in a fracture network is given in Figure 4.4. These results are summarized in a paper written in collaboration with J. Maryška and O. Severýn which has been published in *Computational Geosciences*.

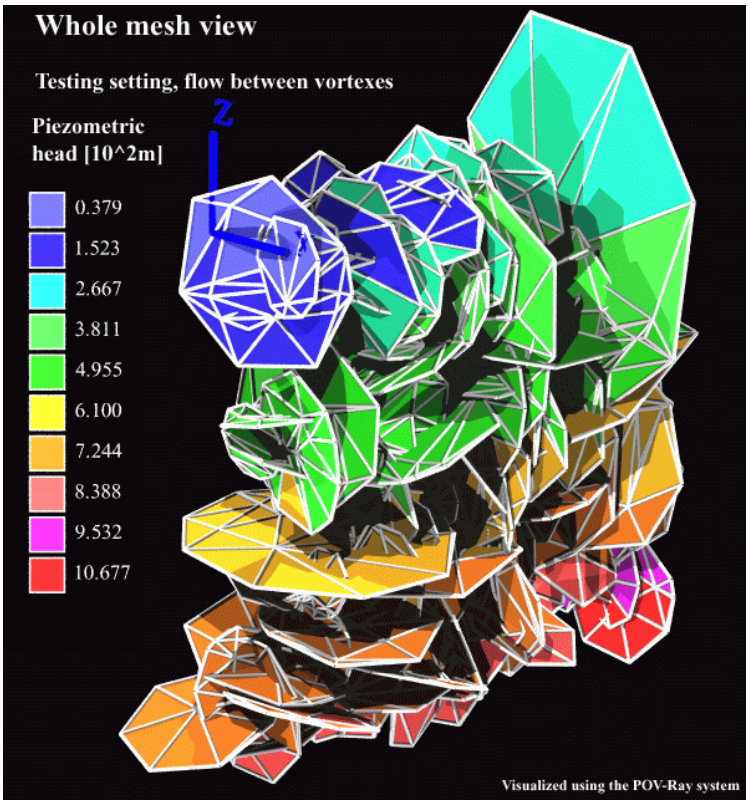


Figure 4.4: Distribution of the piezometric head in a fracture network

# Bibliography


[1] Aavatsmark I., Barkve T., Bøe Ø., Mannseth T., Discretization on unstructured grids for inhomogeneous, anisotropic media. Part I: Derivation of the methods, *SIAM J. Sci. Comput.* **19** (1998), 1700–1716.

[2] Aavatsmark I., Barkve T., Bøe Ø., Mannseth T., Discretization on unstructured grids for inhomogeneous, anisotropic media. Part II: Discussion and numerical results, *SIAM J. Sci. Comput.* **19** (1998), 1717–1736.

[3] Achdou Y., Japhet C., Maday Y., Nataf F., A new cement to glue non-conforming grids with Robin interface conditions: The finite volume case, *Numer. Math.* **92** (2002), 593–620.

[4] Adams R.A., *Sobolev Spaces*, Academic Press, New York, 1975.

[5] Adler P.M., Thovert J.-F., *Fractures and Fracture Networks*, Kluwer, Dordrecht, 1999.

[6] Afif M., Amaziane B., Convergence of finite volume schemes for a degenerate convection–diffusion equation arising in flow in porous media, *Comput. Methods Appl. Mech. Engrg.* **191** (2002), 5265–5286.

[7] Aftosmis M., Gaitonde D., Sean Tavares T., On the accuracy, stability and monotonicity of various reconstruction algorithms for unstructured meshes, *AIAA* (1994), paper No. 94-0415.

[8] Agouzal A., Baranger J., Maître J.-F., Oudin F., Connection between finite volume and mixed finite element methods for a diffusion problem with nonconstant coefficients. Application to a convection diffusion problem, *East-West J. Numer. Math.* **3** (1995), 237–254.

[9] Andersson J., Dverstorp B., Conditional simulations of fluid flow in three-dimensional networks of discrete fractures, *Water Resour. Res.* **23** (1987), 1876–1886.

[10] Angot A., Dolejší V., Feistauer M., Felcman J., Analysis of a combined barycentric finite volume–nonconforming finite element method for nonlinear convection–diffusion problems, *Appl. Math.* **43** (1998), 263–310.

[11] Arbogast T., Cowsar L.C., Wheeler M.F., Yotov I., Mixed finite element methods on nonmatching multiblock grids, *SIAM J. Numer. Anal.* **37** (2000), 1295–1315.

[12] Arbogast T., Dawson C.N., Keenan P.T., Wheeler M.F., Yotov I., Enhanced cell-centered finite differences for elliptic equations on general geometry, *SIAM J. Sci. Comput.* **19** (1998), 404–425.

[13] Arbogast T., Wheeler M.F., Yotov I., Mixed finite elements for elliptic problems with tensor coefficients as cell-centered finite differences, *SIAM J. Numer. Anal.* **34** (1997), 828–852.

[14] Arbogast T., Wheeler M.F., Zhang N., A nonlinear mixed finite element method for a degenerate parabolic equation arising in flow in porous media, *SIAM J. Numer. Anal.* **33** (1996), 1669–1687.

[15] Arnold D.N., Brezzi F., Mixed and nonconforming finite element methods: Implementation, postprocessing and error estimates, *RAIRO Modél. Math. Anal. Numér.* **19** (1985), 7–32.

[16] Babuška I., Error-bounds for finite element method, *Numer. Math.* **16** (1971), 322–333.

[17] Bank R.E., Rose D.J., Some error estimates for the box method, *SIAM J. Numer. Anal.* **24** (1987), 777–787.

[18] Baranger J., Maître J.-F., Oudin F., Connection between finite volume and mixed finite element methods, *M2AN Math. Model. Numer. Anal.* **30** (1996), 445–465.

[19] Barrett J.W., Knabner P., Finite element approximation of transport of reactive solutes in porous media. Part I: Error estimates for non-equilibrium adsorption processes, *SIAM J. Numer. Anal.* **34** (1997), 201–227.

[20] Barrett J.W., Knabner P., Finite element approximation of transport of reactive solutes in porous media. Part II: Error estimates for the equilibrium adsorption processes, *SIAM J. Numer. Anal.* **34** (1997), 455–479.

[21] Bastian P., Chen Z., Ewing R.E., Helmig R., Jakobs H., Reichenberger V., Numerical simulation of multiphase flow in fractured porous media, in Chen Z., Ewing R.E., Shi Z.C. eds., *Numerical Treatmenet of Multiphase Flows in Porous Media*, pp. 50–68, Springer-Verlag, Berlin, 2000.

[22] Baughman L.A., Walkington N.J., Co-volume methods for degenerate parabolic problems, *Numer. Math.* **64** (1993), 45–67.

[23] Bear J., *Dynamics of Fluids in Porous Media*, American Elsevier, New York, 1972.

[24] Bear J., Modeling flow and contaminant transport in fractured rocks, in Bear J., Tsang C.F., de Marsily G. eds., *Flow and Contaminant Transport in Fractured Rock*, pp. 1–38, USA: Academic Press, 1993.

[25] Bear J., Verruijt A., *Modelling Groundwater Flow and Pollution*, Reidel, Dordrecht, 1987.

[26] Bernardi C., Maday Y., Patera A., A new nonconforming approach to domain decomposition: The mortar element method, in Brezis H., Lions J.L. eds., *Nonlinear Partial Differential Equations and their Applications*, pp. 13–51, Pitman, London, 1994.

[27] Bogdanov I.I., Mourzenko V.V., Thovert J.-F., Adler P.M., Effective permeability of fractured porous media in insteady state flow, *Water Resour. Res.* **39** (2003), 1023, doi:10.1029/2001WR000756.

[28] Brenner S.C., Poincaré–Friedrichs inequalities for piecewise $H^1$ functions, *SIAM J. Numer. Anal.* **41** (2003), 306–324.

[29] Brezis H., *Analyse Fonctionnelle, Théorie et Applications*, Masson, Paris, 1983.

[30] Brezzi F., On the existence, uniqueness and approximation of saddle point problems arising from Lagrangian multipliers, *RAIRO Modél. Math. Anal. Numér.* **8** (1974), 129–151.

[31] Brezzi F., Douglas J. Jr., Duran R., Fortin M., Mixed finite elements for second order elliptic problems in three variables, *Numer. Math.* **51** (1987), 237–250.

[32] Brezzi F., Douglas J. Jr., Marini L.D., Two families of mixed finite elements for second order elliptic problems, *Numer. Math.* **47** (1985), 217–235.

[33] Brezzi F., Fortin M., *Mixed and Hybrid Finite Element Methods*, Springer-Verlag, New York, 1991.

[34] Cacas M.C., Ledoux E., de Marsily G., Tillie B., Barbreau A., Durand E., Feuga B., Peaudecerf P., Modeling fracture flow with a stochastic discrete fracture network: Calibration and validation 1. The flow model, *Water Resour. Res.* **26** (1990), 479–489.

[35] Cai Z., Mandel J., McCormick S., The finite volume element method for diffusion equations on general triangulations, *SIAM J. Numer. Anal.* **28** (1991), 392–402.

[36] Cautrès R., Herbin R., Hubert F., The Lions domain decomposition algorithm on non matching cell-centered finite volume meshes, to appear in *IMA J. Numer. Anal.*

[37] Chavent G., Younès A., Ackerer Ph., On the finite volume reformulation of the mixed finite element method for elliptic and parabolic PDE on triangles, *Comput. Methods Appl. Mech. Engrg.* **192** (2003), 655–682.

[38] Chen Z., Equivalence between and multigrid algorithms for nonconforming and mixed methods for second-order elliptic problems, *East-West J. Numer. Math.* **4** (1996), 1–33.

[39] Chen Z., Ewing R.E., Degenerate two-phase incompressible flow III: Sharp error estimates, *Numer. Math.* **90** (2001), 215–240.

[40] Chen Z., Ewing R.E., Jiang Q., Spagnuolo A.M., Error analysis for characteristic-based methods for degenerate parabolic problems, *SIAM J. Numer. Anal.* **40** (2002), 1491–1515.

[41] Ciarlet P.G., Basic error estimates for elliptic problems, in Ciarlet P.G., Lions J.L. eds., *Handbook of Numerical Analysis*, vol. 2, pp. 17–351, Elsevier Science B.V., Amsterdam, 1991.

[42] Ciarlet P.G., *The Finite Element Method for Elliptic Problems*, North-Holland Publishing Company, Amsterdam, 1978.

[43] Clément Ph., Approximation by finite element functions using local regularization, *RAIRO Modél. Math. Anal. Numér.* **9** (1975), 77–84.

[44] Coudière Y., Vila J.-P., Villedieu Ph., Convergence rate of a finite volume scheme for a two dimensional convection–diffusion problem, *M2AN Math. Model. Numer. Anal.* **33** (1999), 493–516.

[45] Crouziex M., Raviart P.-A., Conforming and nonconforming methods for solving the stationary Stokes equations I, *RAIRO Modél. Math. Anal. Numér.* **7** (1973), 33–76.

[46] Dawson C., Analysis of an upwind-mixed finite element method for nonlinear contaminnat transport equations, *SIAM J. Numer. Anal.* **35** (1998), 1709–1724.

[47] Dawson C., Aizinger V., Upwind-mixed methods for transport equations, *Comput. Geosci.* **3** (1999), 93–110.

[48] Debiez C., Dervieux A., Mer K., Nkonga B., Computation of unsteady flows with mixed finite-volume/finite-element upwind methods, *Internat. J. Numer. Methods Fluids* **27** (1998), 193–206.

[49] Deimling K., *Nonlinear Functional Analysis*, Springer-Verlag, Berlin-Heidelberg, 1985.

[50] Dershowitz W.S., Fidelibus C., Derivation of equivalent pipe network analogues for three-dimensional discrete fracture networks by the boundary element method, *Water Resour. Res.* **35** (1999), 2685–2691.

[51] Dolejší V., Feistauer M., Felcman J., On the discrete Friedrichs inequality for nonconforming finite elements, *Numer. Funct. Anal. Optim.* **20** (1999), 437–447.

[52] Douglas J. Jr., Roberts J.E., Global estimates for mixed methods for second order elliptic equations, *Math. Comp.* **44** (1985), 39–52.

[53] Ebmeyer C., Error estimates for a class of degenerate parabolic equations, *SIAM J. Numer. Anal.* **35** (1998), 1095–1112.

[54] Elsworth D., A hybrid boundary element-finite element analysis procedure for fluid flow simulation in fractured rock masses, *Int. J. Numer. Anal. Methods Geomech.* **10** (1986), 569–584.

[55] Ewing R.E., Lazarov R.D., Lin T., Lin Y., Mortar finite volume element approximations of second-order elliptic problems, *East-West J. Numer. Math.* **8** (2000), 93–110.

[56] Ewing R.E., Lin T., Lin Y., On the accuracy of the finite volume element method based on piecewise linear polynomials, *SIAM J. Numer. Anal.* **39** (2002), 1865–1888.

[57] Eymard R., Gallouët T., Convergence d'un schéma de type éléments finis - volumes finis pour un système couplé elliptique - hyperbolique, *RAIRO Modél. Math. Anal. Numér.* **27** (1993), 843–861.

[58] Eymard R., Gallouët T., Herbin R., A finite volume scheme for anisotropic diffusion problems, submitted to *C. R. Acad. Sci. Paris., Ser. I*, 2004.

[59] Eymard R., Gallouët T., Herbin R., Convergence of finite volume schemes for semilinear convection diffusion equations, *Numer. Math.* **82** (1999), 91–116.

[60] Eymard R., Gallouët T., Herbin R., Finite volume approximation of elliptic problems and convergence of an approximate gradient, *Appl. Numer. Math.* **37** (2001), 31–53.

[61] Eymard R., Gallouët T., Herbin R., Finite volume methods, in Ciarlet P.G., Lions J.L. eds., *Handbook of Numerical Analysis*, vol. 7, pp. 713–1020, Elsevier Science B.V., Amsterdam, 2000.

[62] Eymard R., Gallouët T., Herbin R., Michel A., Convergence of a finite volume scheme for nonlinear degenerate parabolic equations, *Numer. Math.* **92** (2002), 41–82.

[63] Eymard R., Gallouët T., Hilhorst D., Naït Slimane Y., Finite volumes and nonlinear diffusion equations, *M2AN Math. Model. Numer. Anal.* **32** (1998), 747–761.

[64] Eymard R., Gutnic M., Hilhorst D., The finite volume method for the Richards equation, *Comput. Geosci.* **3** (2000), 259–294.

[65] Faille I., A control volume method to solve an elliptic equation on a two-dimensional irregular mesh, *Comput. Methods Appl. Mech. Engrg.* **100** (1992), 275–290.

[66] Faille I., Nataf F., Saas L., Willien F., Finite volume methods on non-matching grids with arbitrary interface conditions and highly heterogeneous media, in Kornhuber R., Hoppe R., Périaux J., Pironneau O., Widlund O., Xu J. eds., *Domain Decomposition Methods in Science and Engineering*, Lect. Notes Comput. Sci. Eng. 40, pp. 50–68, Springer-Verlag, Berlin, 2000.

[67] Feistauer M., Felcman J., Medviďová-Lukáčová M., On the convergence of a combined finite volume–finite element method for nonlinear convection–diffusion problems, *Numer. Methods Partial Differential Equations* **13** (1997), 1–28.

[68] Forsyth P.A., A control volume finite element approach to NAPL groundwater contamination, *SIAM J. Sci. Stat. Comput.* **12** (1991), 1029–1057.

[69] Fraejis de Veubeke B., Displacement and equilibrium models in the finite element method, in Zienkiewicz O.C., Holister G. eds., *Stress Analysis*, Wiley, New York, 1965.

[70] Gilbert J.R., Moler C., Schreiber R., Sparse matrices in MATLAB: Design and implementation, *SIAM J. Matrix Anal. Appl.* **13** (1992), 333–356.

[71] Hackbusch W., On first and second order box schemes, *Computing* **41** (1989), 277–296.

[72] Herbin R., An error estimate for a finite volume scheme for a diffusion–convection problem on a triangular mesh, *Numer. Methods Partial Differential Equations* **11** (1995), 165–173.

[73] Hestenes M.R., Stiefel E., Methods of conjugate gradients for solving linear systems, *J. Res. Nat. Bur. Stand.* **49** (1952), 409–436.

[74] Hoteit H., Erhel J., Mosé R., Philippe B., Ackerer Ph., Numerical reliability for mixed methods applied to flow problems in porous media, *Comput. Geosci.* **6** (2002), 161–194.

[75] Hughes T.J.R., Engel G., Mazzei L., Larson M.G., The continuous Galerkin method is locally conservative, *J. Comput. Phys.* **163** (2000), 467–488.

[76] Idelsohn S., Onate E., Finite volumes and finite elements: Two "good friends", *Internat. J. Numer. Methods Engrg.* **37** (1994), 3323–3341.

[77] Jaffré J., Eléments finis mixtes et décentrage pour les équations de diffusion–convection, *Calcolo* **23** (1984), 171–197.

[78] Jäger W., Kačur J., Solution of doubly nonlinear and degenerate parabolic problems by relaxation schemes, *M2AN Math. Model. Numer. Anal.* **29** (1995), 605–627.

[79] Javandel I., Doughty C., Tsang C.F., *Groundwater Transport: Handbook of Mathematical Models*, American Geophysical Union Water Resources Monograph Series, Volume 10, 1984.

[80] Joe B., Delaunay triangular meshes in convex polygons, *SIAM J. Sci. Stat. Comput.* **7** (1986), 514–539.

[81] Kačur J., Solution of degenerate convection–diffusion problems by the method of characteristics, *SIAM J. Numer. Anal.* **39** (2001), 858–879.

[82] Karlsen K.H., Risebro N.H., Towers J.D., Upwind difference approximations for degenerate parabolic convection–diffusion equations with a discontinuous coefficient, *IMA J. Numer. Anal.* **22** (2002), 623–664.

[83] Knabner P., Otto F., Solute transport in porous media with equilibrium and nonequilibrium multiple-site adsorption: Uniqueness of weak solutions, *Nonlinear Anal.* **42** (2000), 381–403.

[84] Knobloch P., Uniform validity of discrete Friedrich's inequality for general nonconforming finite element spaces, *Numer. Funct. Anal. Optim.* **22** (2001), 107–126.

[85] Koudina N., Gonzalez Garcia R., Thovert J.-F., Adler P.M., Permeability of three-dimensional fracture networks, *Phys. Rev. E* **57** (1998), 4466–4479.

[86] Letniowski F.W., Three-dimensional Delaunay triangulations for finite element approximations to a second-order diffusion operator, *SIAM J. Sci. Stat. Comput.* **13** (1992), 765–770.

[87] Long J.C.S., Gilmour P., Witherspoon P.A., A model for steady state flow in random three dimensional networks of disc-shaped fractures, *Water Resour. Res.* **21** (1985), 1105–1115.

[88] Marini L.D., An inexpensive method for the evaluation of the solution of the lowest order Raviart–Thomas mixed method, *SIAM J. Numer. Anal.* **22** (1985), 493–496.

[89] Maros G., Palotás K., Koroknai B., Sallay E., Szongoth G., Kasza Z., Zilahi-Sebess L., Core log evaluation of borehole Ptp-3 in the Krušné hory mts, MS Geological Institute of Hungary, Budapest, 2001.

[90] Medviďová-Lukáčová M., Combined finite element–finite volume method (convergence analysis), *Comment. Math. Univ. Carolinae* **38** (1997), 717–741.

[91] Nečas J., *Les Méthodes Directes en Théorie des Equations Elliptiques*, Masson, Paris, 1967.

[92] Nédélec J.C., Mixed finite elements in $\mathbb{R}^3$, *Numer. Math.* **35** (1980), 315–341.

[93] Nochetto R.H., Schmidt A., Verdi C., A posteriori error estimation and adaptivity for degenerate parabolic problems, *Math. Comp.* **69** (1999), 1–24.

[94] Nochetto R.H., Verdi C., Approximation of degenerate parabolic problems using numerical integration, *SIAM J. Numer. Anal.* **25** (1988), 784–814.

[95] Ohlberger M., A posteriori error estimates and adaptive methods for convection dominated transport processes, Ph.D. thesis, Albert–Ludwigs–Universität Freiburg, Germany, 2001.

[96] Ohlberger M., A posteriori error estimates for vertex centered finite volume approximations of convection–diffusion–reaction equations, *M2AN Math. Model. Numer. Anal.* **35** (2001), 355–387.

[97] Pascal F., Sur des méthodes d'approximation effectives et d'analyse mumérique pour les équations de la mécanique des fluides, Habilatation thesis, Université de Paris-Sud, Orsay, France, 2002.

[98] Pop I.S., Regularization methods in the numerical analysis of some degenerate parabolic equations, Ph.D. thesis, Faculty of Mathematics and Informatics, University Cluj Napoca, Romania, 1998.

[99] Pop I.S., Yong W.-A., A numerical approach to degenerate parabolic equations, *Numer. Math.* **92** (2002), 357–381.

[100] Putti M., Cordes C., Finite element approximation of the diffusion operator on tetrahedra, *SIAM J. Sci. Comput.* **19** (1998), 1154–1168.

[101] Quarteroni A., Sacco R., Saleri F., *Numerical Mathematics*, Springer-Verlag, New York, 2000.

[102] Quarteroni A., Valli A., *Domain Decomposition Methods for Partial Differential Equations*, Oxford University Press, New York, 1999.

[103] Quarteroni A., Valli A., *Numerical Approximation of Partial Differential Equations*, Springer-Verlag, Berlin, 1994.

[104] Ramarosy N., TALISMAN, guide d'utilisation, société HydroExpert, 2001. HydroExpert, 53 rue Charles Frérot, 94 250 Gentilly, France, `www.hydroexpert.com`.

[105] Raviart P.-A., Thomas J.-M., A mixed finite element method for 2-nd order elliptic problems, in Galligani I., Magenes E. eds., *Mathematical Aspects of Finite Element Methods*, Lecture Notes in Math. 606, pp. 292–315, Springer, Berlin, 1977.

[106] Reddy J.N., Oden J.T., Mathematical theory of mixed finite element approximations, *Q. Appl. Math.* **33** (1975), 255–280.

[107] Rektorys K., *Variational Methods in Mathematics, Science, and Engineering*, Kluwer, Dordrecht, 1982.

[108] Roberts J.E., Thomas J.-M., Mixed and hybrid methods, in Ciarlet P.G., Lions J.L. eds., *Handbook of Numerical Analysis*, vol. 2, pp. 523–639, Elsevier Science B.V., Amsterdam, 1991.

[109] Rulla J., Walkington N.J., Optimal rates of convergence for degenerate parabolic problems in two dimensions, *SIAM J. Numer. Anal.* **33** (1996), 56–67.

[110] Russell T.F., Wheeler M.F., Finite element and finite difference methods for continuous flows in porous media, in Ewing R.E. ed., *The Mathematics of Reservoir Simulation*, pp. 35–106, SIAM, Philadelphia, 1983.

[111] Saad Y., *Iterative Methods for Sparse Linear Systems*, PWS Publishing Company, 1996.

[112] Selmin V., The node-centered finite volume approach: Bridge between finite differences and finite elements, *Comput. Methods Appl. Mech. Engrg.* **102** (1993), 107–138.

[113] Slough K.J., Sudicky E.A., Forsyth P.A., Numerical simulations of multiphase flow and phase partitioning in discretely fractured geological media, *J. Contam. Hydrol.* **40** (1999), 107–136.

[114] Sonier F., Eymard R., Mathematical and numerical properties of control-volume finite element scheme for reservoir simulation, *SPE Reservoir Engineering* (November 1994), 283–289.

[115] Strang G., Fix G.J., *An Analysis of the Finite Element Method*, Prentice-Hall, Englewood Cliffs, 1973.

[116] Temam R., *Navier–Stokes Equations*, North-Holland, Amsterdam, 1979.

[117] van der Vorst H.A., Bi-CGSTAB: A fast and smoothly converging variant of Bi-CG for the solution of non-symmetric linear systems, *SIAM J. Sci. Stat. Comput.* **13** (1992), 631–644.

[118] van Genuchten M., A closed form for predicting the hydraulic conductivity of unsaturated soils, *Soil Sci. Soc. Amer. J.* **44** (1980), 892–898.

[119] Wanfang Z., Wheater H.S., Johnston P.M., State of the art of modelling two-phase flow in fractured rock, *Envir. Geol.* **31** (1997), 157–166.

[120] Yotov I., Mixed finite element methods for flow in porous media, Ph.D. thesis, Rice University, Houston, Texas, 1996.

[121] Younès A., Ackerer Ph., Chavent G., From mixed finite elements to finite volumes for elliptic PDEs in two and three dimensions, *Internat. J. Numer. Methods Engrg.* **59** (2004), 365–388.

[122] Younès A., Mose R., Ackerer Ph., Chavent G., A new formulation of the mixed finite element method for solving elliptic and parabolic PDE with triangular elements, *J. Comput. Phys.* **149** (1999), 148–167.

[123] Zheng C., Bennett G.D., *Applied Contaminant Transport Modeling*, Van Nostrand Reinhold, New York, 1995.

[124] Zienkiewicz O.C., *The Finite Element Method*, McGraw-Hill, London, 1977.